



HAL
open science

Synthesis of new [1111]metacyclophane ligands for the formation of molecular coordination networks

Ekaterina Chernova

► **To cite this version:**

Ekaterina Chernova. Synthesis of new [1111]metacyclophane ligands for the formation of molecular coordination networks. Other. Université de Strasbourg; Kazanskiy gosudarstvennyj universitet im. V. I. Ul'janova (Kazan), 2018. English. NNT : 2018STRAF043 . tel-02086002

HAL Id: tel-02086002

<https://theses.hal.science/tel-02086002>

Submitted on 1 Apr 2019

HAL is a multi-disciplinary open access archive for the deposit and dissemination of scientific research documents, whether they are published or not. The documents may come from teaching and research institutions in France or abroad, or from public or private research centers.

L'archive ouverte pluridisciplinaire **HAL**, est destinée au dépôt et à la diffusion de documents scientifiques de niveau recherche, publiés ou non, émanant des établissements d'enseignement et de recherche français ou étrangers, des laboratoires publics ou privés.

ÉCOLE DOCTORALE DES SCIENCES CHIMIQUES ED 222

UMR CNRS n°7140

THÈSE présentée par :

Ekaterina CHERNOVA

soutenue le : **17 octobre 2018**

pour obtenir le grade de : **Docteur de l'université de Strasbourg**

Discipline/ Spécialité : Sciences Chimiques

**Synthèse de nouveaux ligands à base de [1111]
metacyclophane pour la formation de réseaux de
coordination moléculaires**

THÈSE dirigée par :

Pr. HOSSEINI Mir Wais, Université de Strasbourg
Pr. FERLAY Sylvie, Université de Strasbourg
Pr. ANTIPIIN Igor, Université de Kazan, Arbuzov Institut de Chimie
Physique et Organique de Kazan
Pr. SOLOVIEVA Svetlana, Arbuzov Institut de Chimie
Physique et Organique de Kazan

RAPPORTEURS :

Pr. REGNOUF DE VAINS Jean-Bernard, Université de Nancy
Dr. BIBAL Brigitte, Université de Bordeaux.

AUTRES MEMBRES DU JURY :

Dr. SEMERIL David, Université de Strasbourg

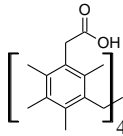
List of abbreviations

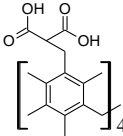
- **Å**: angstrom
- **Ac** : acetyl
- **Ag**: argentum (silver)
- **AgNO₃** : silver nitrate
- **AgPF₆**: silver hexafluorophosphate
- **CHCl₃**: chloroform
- **CH₂Cl₂** : dichloromethane
- **Co**: cobalt
- **Co(NO₃)₂** : cobalt nitrate
- **Co(OAc)₂**: cobalt acetate
- **Cu**: copper
- **CuCl₂**: copper chloride
- **DMF**: dimethylformamide
- **DMSO**: dimethylsulfoxide
- **EDTA**: ethylenediaminetetraacetic acid
- **Eq** : equivalent
- **Et₃N**: triethylamine
- **Et₂O** : diethyl ether
- **EtNO₂** : nitroethane
- **EtOH**: ethanol
- **Hg**: mercury
- **HgCl₂**: mercury chloride
- **Hz** : Hertz
- **L**: ligand
- **M** : metal
- **Me** : methyl
- **MeOH** : methanol
- **MgSO₄** : magnesium sulfate
- **ML**: metal-ligand

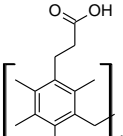
- **mmol** : millimole
- **Mn(NO₃)₂**: manganese nitrate
- **Mn(OAc)₂**: manganese acetate
- **MOF**: metal-organic framework
- **SMM**: single molecule magnet
- **NaH**: sodium hydride
- **NaOH** : sodium hydroxyde
- **OAc** – acetate
- **PDI**: polydispersity index
- **Pd**: palladium
- **Ph** : phenyl
- **NMR**: nuclear magnetic resonance
- **SnCl₄** : tin chloride
- **THF**:tetrahydrofuran
- **W** : Watt
- **Zn**: zinc

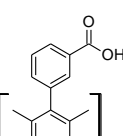
List of synthesized ligands

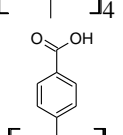
- **L1:** 4,11,18,25-tetra(2-(carboxyl)-methylene)-3,5,7,10,12,14,17,19,21,24,26,28-dodecamethyl-[1.1.1.1]metacyclophane

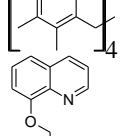

- **L2:** 4,11,18,25-tetra((malonate)-methylene)-3,5,7,10,12,14,17,19,21,24,26,28-dodecamethyl-[1.1.1.1]metacyclophane

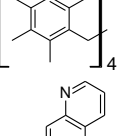

- **L3:** 4,11,18,25-tetra(2-(carboxyl)-ethylene)-3,5,7,10,12,14,17,19,21,24,26,28-dodecamethyl-[1.1.1.1]metacyclophane

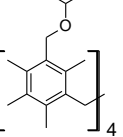

- **L4:** 4,11,18,25-tetra(3-(carboxyl)phenyl)-3,5,7,10,12,14,17,19,21,24,26,28-dodecamethyl-[1.1.1.1]metacyclophane

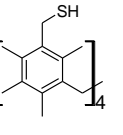

- **L5:** 4,11,18,25-tetra(4-(carboxyl)phenyl)-3,5,7,10,12,14,17,19,21,24,26,28-dodecamethyl-[1.1.1.1]metacyclophane

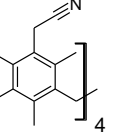

- **L6:** 4,11,18,25-Tetra-8-quinolinomethyl-3,5,7,10,12,14,17,19,21,24,26,28-dodecamethyl[1.1.1.1]metacyclophane


- **L7:** 4,11,18,25-Tetra-6-quinolinomethyl-3,5,7,10,12,14,17,19,21,24,26,28-dodecamethyl[1.1.1.1]metacyclophane


- **L8:** 4,11,18,25-Tetramercaptomethyl-3,5,7,10,12,14,17,19,21,24,26,28-dodecamethyl[1.1.1.1]metacyclophane


- **L8:** 4,11,18,25-Tetramercaptomethyl-3,5,7,10,12,14,17,19,21,24,26,28-dodecamethyl[1.1.1.1]metacyclophane


- **L10:** 4,11,18,25-Tetraphosphonomethyl-3,5,7,10,12,14,17,19,21,24,26,28-dodecamethyl[1.1.1.1]metacyclophane



SYNTHÈSE DE NOUVEAUX LIGANDS À BASE DE [1111] METACYCLOPHANE POUR LA FORMATION DE RÉSEAUX DE COORDINATION MOLÉCULAIRES

Resumé en français

I Introduction

L'objectif de ce projet est la conception de nouveaux ligands organiques et leur combinaison avec des cations métalliques pour la formation de structures supramoléculaires appelées réseaux de coordination. Le projet repose sur les principes développés en chimie supramoléculaire¹ et en ingénierie cristalline.²

Alors que la chimie supramoléculaire contrôle la construction d'assemblages supramoléculaires hautement ordonnés, dotés de propriétés programmées pour la reconnaissance moléculaire, à l'état solide et en solution, l'Ingénierie Cristalline est concentrée sur l'auto-assemblage à l'état solide et en particulier dans la phase cristalline ordonnée.³ Le principe de base de la chimie supramoléculaire repose sur des interactions intermoléculaires faibles: liaisons hydrogène⁴, interactions électrostatiques⁵, forces hydrophobes⁶, ou la combinaison de plusieurs de ces interactions. Le domaine des MOFs (« Metal-Organic Framework », structures métalliques-organiques composées d'ions métalliques liés par des liaisons de coordination à des ligands organiques), repose sur l'utilisation de liaisons de coordination pour la construction de réseaux moléculaires. La stratégie synthétique utilisée aboutit à la formation de chaînes mono-dimensionnelles, de réseaux bidimensionnels (2D) ou de composés tridimensionnels (3D) en reposant sur les principes de reconnaissance moléculaire. Un grand nombre de polymères de coordination, présentant des propriétés de porosité, d'adsorption⁷, de catalyse⁸, de luminescence⁹, magnétiques,¹⁰ ou de propriétés comme matériaux pour l'énergie¹¹ ont ainsi été obtenus.

Concernant notre projet, nous nous sommes concentrés sur la formation de Polymères de Coordination (CP). Des polymères de coordination infinis¹² existent en raison de la liaison de coordination relativement faible et réversible qui permet des processus autoréparables lors de la synthèse. Pour la formation de polymères de coordination, en plus de l'utilisation de ligands organiques simples portant des groupements de coordination classiques, les ligands macrocycliques présentent un réel intérêt: des familles de ligands macrocycliques pour la formation de polymères de coordination sont les résorcinarènes¹³, les éthers couronnes¹⁴, les porphyrines¹⁵, les cyclodextrines¹⁶, cyclophanes¹⁷ et cyclacènes¹⁸ etc...

Dans ce travail, nous avons choisi d'utiliser une famille de ligands macrocycliques rarement explorée: les [1111] métacyclophanes (figure 1). Ces macrocycles, appartenant à la famille plus générale des métacyclophanes, ont été explorés au cours des dernières décennies, en raison de la diversité de leurs structures et les nombreuses possibilités de fonctionnalisation, ce qui autorise la formation d'un grand nombre de complexes et polymères de coordination. Les calix[4]arènes¹⁹ sont des composés bien connus appartenant également à la famille des métacyclophanes. Alors que les calix[4]arènes peuvent adopter quatre conformations stables thermodynamiquement (*Cône*, *Cône partiel*, *1,2-Alternée* et *1,3-Alternée*), la plateforme [1111]métacyclophane n'adopte qu'une

conformation stable (*1,3-Alternée*) sur une large plage de températures,²⁰ ceci étant dû à la gêne causée par les substituants méthyle en position *mé*ta (Figure 1).

Ce dernier point présente un intérêt particulier pour notre projet de construction d'architectures supramoléculaires infinies et rigides.

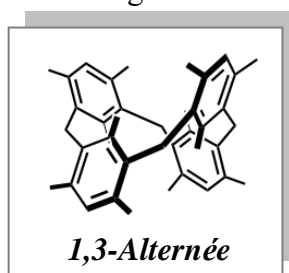


Figure 1. Squelette de [1111] métacyclophane adoptant une conformation stable en *1,3-Alternée*.

En même temps, la présence de quatre cycles benzéniques et de ponts méthylène sont des points communs entre les calix[4]arènes et les [1111] métacyclophanes, mais ces derniers présentent un comportement conformationnel différent. Dans le même ordre d'idées, il convient de noter qu'il doit exister de nombreuses propriétés communes entre les calix[4]arènes et [1111] métacyclophanes dans les domaines de chimie supramoléculaire et ingénierie cristalline; en effet, les calix[4]arènes présentent des propriétés de chiralité,²¹ porosité²² et de formation d'assemblées avec d'autres familles macrocycliques.²³ Concernant les composés de coordination, la formation de clusters²⁴ est largement étudiée. Il existe également de nombreux exemples de polymères de coordination à base de dérivés de calix[4]arène,²⁵ fonctionnalisés par des groupements coordinants du type carboxylato, cyano, phosphonato ou mercapto. Quelques exemples sont donnés ci-dessous.

Par exemple, Burrows *et al.* a rapporté un dérivé de calix[4]arène difonctionnalisé au « bord supérieur » par des groupements carboxylato et qui a été utilisé pour la préparation d'un MOF à base de Pb(II).²⁶ D'autre part, Dalgarno *et al.* a montré la formation de polymère de coordination 1D ou 3D ainsi que des capsules par combinaison d'un dérivé de calix[4]arène en conformation cône, disubstitué par des groupements carboxylato avec Cd(II) et la 1,10-phénanthroline.²⁷ Dans le même temps, Park *et al.* a reporté un calix[4]arène en conformation *1,3-Alternée* fonctionnalisé par des groupements carboxylato sur le « bord inférieur » ainsi que sa capacité à former des polymères de coordination 3D lorsqu'il est combiné avec Pb(NO₃)₂ dans des conditions solvothermales.²⁸ Dans la littérature, il existe de nombreux autres exemples de polymères de coordination à base de dérivés carboxylato de calix[4]arène.²⁹ Les propriétés d'adsorption de gaz de telles assemblées ont été étudiées, révélant souvent une faible surface spécifique, mais une bonne sélectivité pour les mélanges de gaz.³⁰

Les capacités de coordination (essentiellement avec Ag⁺) des dérivés calix[4]arène portant des groupement coordinants de type cyano ont également été étudiées.³¹ Par exemple, Atwood *et al.* a reporté un dérivé de tetracyanocalix[4]arène fonctionnalisé *via* des esters benzyliques au bord inférieur, et adoptant une conformation *Cône*. En présence d'AgPF₆, ce dernier forme un polymère de coordination 1D présentant une stoechiométrie ligand:metal de 1:1.³² Un autre exemple a été fourni par Hosseini *et al.*, où un dérivé

tétracyanocalix[4]arène en conformation *1,3-Alternée* forme également des chaînes non-tubulaires en présence de sels d'argent.^{31a}

En ce qui concerne les calixarène portant des groupements dérivés du phosphore, plusieurs exemples de réseaux de coordination basés sur le calix[4]arène ont été publiés.³³ Raston *et al.* a montré la complexation du dérivé calix[4]arène *p*-phosphoné en conformation *Cône* par des cations sodium. Tous les dérivés phosphonates des calix[4]arène adoptent une conformation *Cône*, tandis que dans notre projet, il est prévu de créer des phosphonato-métacyclophanes en conformation *1,3-Alternée* afin d'obtenir des réseaux de coordination de haute dimensionnalité. Selon la théorie HSAB³⁴, le groupement coordinant phosphonate, devrait être bien adapté à la coordination des cations tels que les lanthanides.

Pour la formation de composés de coordination, le groupement thiol a également été utilisé sur la plateforme calix[4]arene. Hosseini *et al.* a montré la formation d'un complexe binucléaire de *p-tert-butyl-tétramercaptocalix[4]arène* en conformation *1,3-Alternée* avec les cations mercure(II).³⁵

Ces études sont inspirantes pour la conception de nouveaux ligands basés sur le squelette [1111]métacyclophane, pour la génération de polymères de coordination étendus et de réseaux supramoléculaires. Actuellement, de très nombreux polymères de coordination ont été obtenus à partir de calix[4]arènes,²⁵ alors que peu de résultats ont été reportés à partir des [1111]métacyclophanes. Examinons ce type de macrocycle en détail.

Le [1111]métacyclophane (Figure 1) a été synthétisé il y a plusieurs décennies par une réaction de condensation lors de laquelle quatre fragments mésitylène sont liés par des ponts méthylène.³⁶ Pour un tel composé, l'introduction de substituants méthyle perturbe le processus de rotation des ligands macrocycliques et bloque ainsi sa conformation en *1,3-Alternée*. Le métacyclophane classique non substitué peut également être obtenu par condensation du mésitylène et de l'éther de méthyle en présence de chlorure d'étain dans du chlorure de méthylène.³⁷ Le spectre ¹H-RMN (CDCl₃) du métacyclophane est caractérisé par: un singulet pour substituants en position ortho et para des groupements méthyle (respectivement 2,34 ppm et 1,19 ppm) et également un singulet pour les protons des cycles aromatiques et des ponts méthylène (respectivement 6,80 ppm et 3,89 ppm). La conformation *1,3-Alternée* peut ainsi être immédiatement déduite par les données de ¹H-RMN.

Pour la formation de dérivés du [1111]métacyclophane tétrasubstitués par des groupements de coordination, deux intermédiaires importants du [1111] métacyclophane ont été utilisés: les composés tétrabromés et tétrachlorométhylés. Avant de commencer la conception et la synthèse de nouveaux dérivés à base de [1111]métacyclophane, nous avons effectué une revue de la littérature des composés de coordination obtenus avec cette plateforme macrocyclique. La majorité des publications ont été publiées par l'équipe Hosseini. Ce groupe a rapporté plusieurs exemples de [1111]métacyclophanes porteurs de sites de coordination donneurs (N, O) et de leurs combinaisons avec des cations métalliques conduisant à la formation de polymères de coordination ou de complexes. Dans cette revue, Ferlay et Hosseini ont montré qu'au cours des 20 dernières années, la plate-forme de [1111]métacyclophane a été modifiée chimiquement³⁸ afin d'obtenir des ligands de

coordination macrocycliques pouvant être combinés à divers métaux d. Les ligands tétrasubstitués présentés portent des groupements de type carboxylato³⁹, nitro,³⁹ thiométhyl,³⁹ aldéhyde,³⁹ amino,³⁹ diphénylphosphoryl,³⁹ diphénylphosphanyl,³⁸ bipyridyl⁴⁰ et quinolinyl,⁴⁰ ou thiol.⁴¹ Avec ces composés, aucun réseau de coordination n'a été signalé. D'autres groupements de coordination N-donneurs (Pyridyl, pyrazolyl, imidazolyl, cyano) ont été utilisés, formant des ligands di et tétra-substitués à base de [1111]métacyclophane⁴² conduisant à la formation de polymères de coordination ou de complexes de coordination. Divers procédés peuvent être utilisés pour générer des polymères de coordination, tels que la synthèse solvothermale, la diffusion liquide ou en phase vapeur et l'évaporation lente. Ainsi, de nombreuses architectures étendues et périodiques différentes, représentées schématiquement par des polyèdres (figure 2), ont été obtenues.

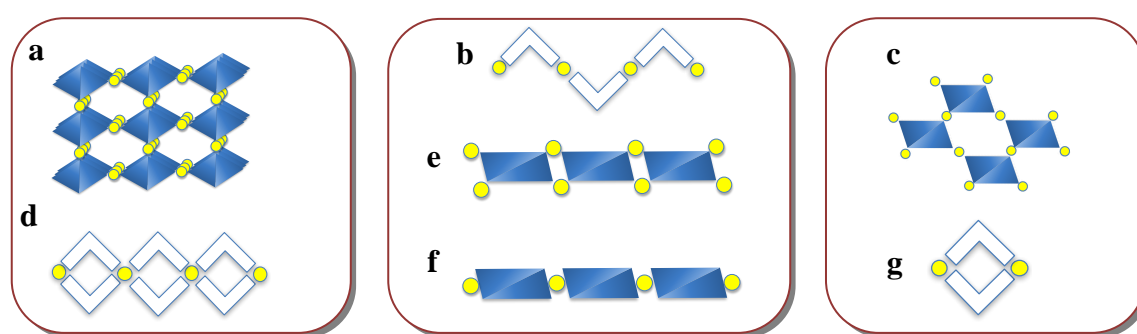
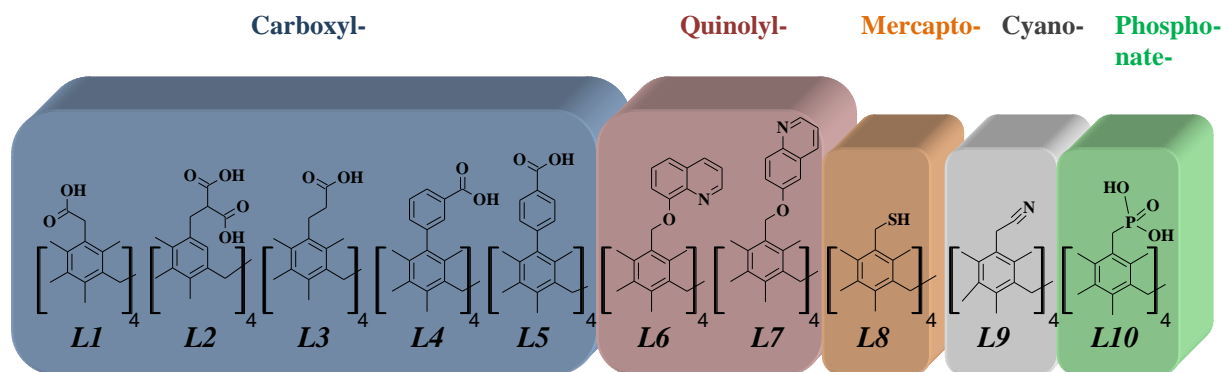


Figure 2: Représentation schématique polyédrique de la dimensionnalité et du type de réseaux de coordination obtenus lors de la combinaison de ligands macrocycliques possédant des groupements coordinants du type N-donneur avec des sels métalliques MX_2 ($\text{M} = \text{Cu}, \text{Co}, \text{Zn}, \text{Hg}$ et $\text{X} = \text{Cl}, \text{Br}$ ou I) ou des sels d'argent MX_2 . Les formes bleues représentent le ligand et les cercles jaunes représentent le centre métallique.³⁸

Des structures cristallines mono-dimensionnelles (Figure 2; b, d, e et f), ainsi que des polymères de coordination bi- (Figure 2; c) et tridimensionnels (Figure 2, a) basés sur la plate-forme de métacyclophane [1111] adoptant une conformation 1,3-Alternée stable ont été obtenus et caractérisés par diffraction de RX sur monocristaux. De plus, des complexes discrets (métallamacrocycles mono et bi-nucléaires, figure 2; g) ont également été obtenus.

Dans le cadre de ce projet, nous nous proposons d'étudier la capacité de coordination de dérivés du [1111]métacyclophane portant des sites d'interaction spécifiques pour la formation d'architectures polymériques. Comme de nombreux groupes N-donneurs monodentates ont été greffés sur le squelette du [1111]métacyclophane et ses analogues de calix[4]arène, nous nous sommes concentrés sur les groupements de coordination du type carboxylato, quinoleyle, mercapto, methylcyano et phosphonato : les ligands cible sont présentés Schéma 1.

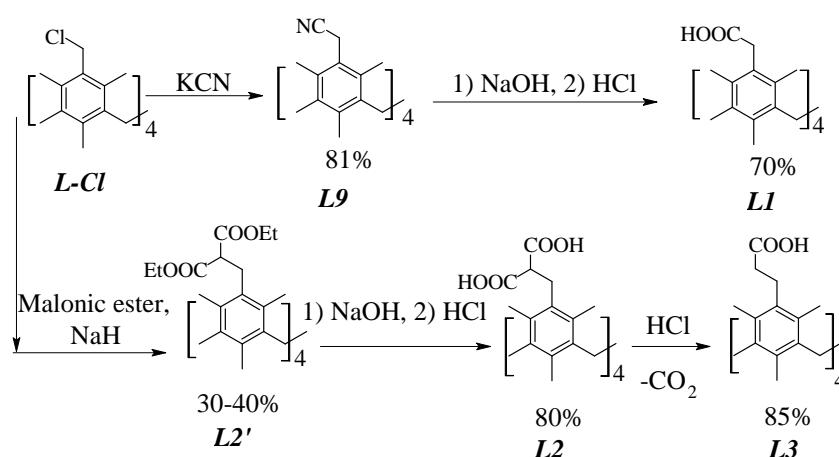


II Synthèse et structure de ligands cibles à base de [1.1.1.1] métacyclophane

a) Synthèse de dérivés carboxylato du [1.1.1.1]métacyclophane *L1-L5*.

Il est bien connu que le groupement carboxylate est un site de coordination efficace pour former les complexes et composés de coordination stables du fait d'interactions électrostatiques lorsqu'il est associé à des cations métalliques, ce qui permet son utilisation intense pour la formation de MOFs. Dans ce travail, la synthèse de nouveaux dérivés carboxylates (*L1-L5*, figure 1) à base de [1.1.1.1] métacyclophane, qui diffèrent par la nature et la longueur du groupe espaceur (aromatique ou aliphatique) utilisé entre le groupement coordinant et le macrocycle, a été réalisée.

Deux voies de synthèse générales ont été choisies pour la synthèse de ces ligands. Les dérivés carboxylates à espaceurs aliphatiques du métacyclophane (*L1-L3*) ont été synthétisés par fonctionnalisation de dérivé tétrachlorométhyle^{42a} (ici *L-Cl*) en utilisant la réaction classique de substitution nucléophile, d'hydrolyse de dérivés esters et de décarboxylation de la fonction acide malonique, comme montré Schéma 2.



La synthèse de dérivés tétracarboxyliques du métacyclophane contenant l'espaceur phényle (**L4-L5**) a été réalisée en utilisant le couplage de Suzuki entre le dérivé tétrabromo initial³⁹ (ici **L-Br**) et l'ester pinacolylique de l'acide phénylboronique portant un groupement ester carboxylique, suivi de l'hydrolyse des intermédiaires portant des fonctions ester, selon le schéma 3.

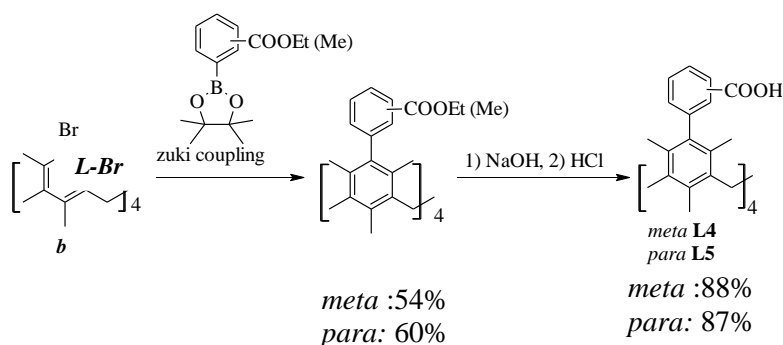


Schéma 3

Ainsi, 5 nouveaux dérivés portant des groupements acide carboxylique de [1.1.1.1]métacyclophane (**L1-L5**) ont été synthétisés avec des rendements élevés.⁴³ La structure des composés obtenus a été étudiée et caractérisée à la fois en solution et à l'état solide. Les expériences de diffraction des rayons X sur les monocristaux obtenus ont révélé que les composés **L2-L5** présentent, comme prévu, une conformation 1,3-Alternée à l'état solide (Figure 3), ce qui est en accord avec les données spectroscopiques RMN ¹H et ¹³C et les données MALDI TOF obtenues pour ces composés en solution.

À l'état solide, les groupements carboxyliques de **L2-L5** forment des liaisons hydrogène avec les molécules de solvants (DMF ou pyridine). Dans certains cas (pour **L3** et **L5**), des liaisons hydrogène intramoléculaires résultant de la reconnaissance des groupements carboxyliques vicinaux est mise en évidence ($d_{O-O} = 2,3 \text{ \AA}$ et $1,8 \text{ \AA}$, pour **L3** et **L5**, respectivement). Des liaisons hydrogènes entre les groupements acide carboxyliques appartenant à deux molécules différentes ne sont pas observées pour **L2-L5**.

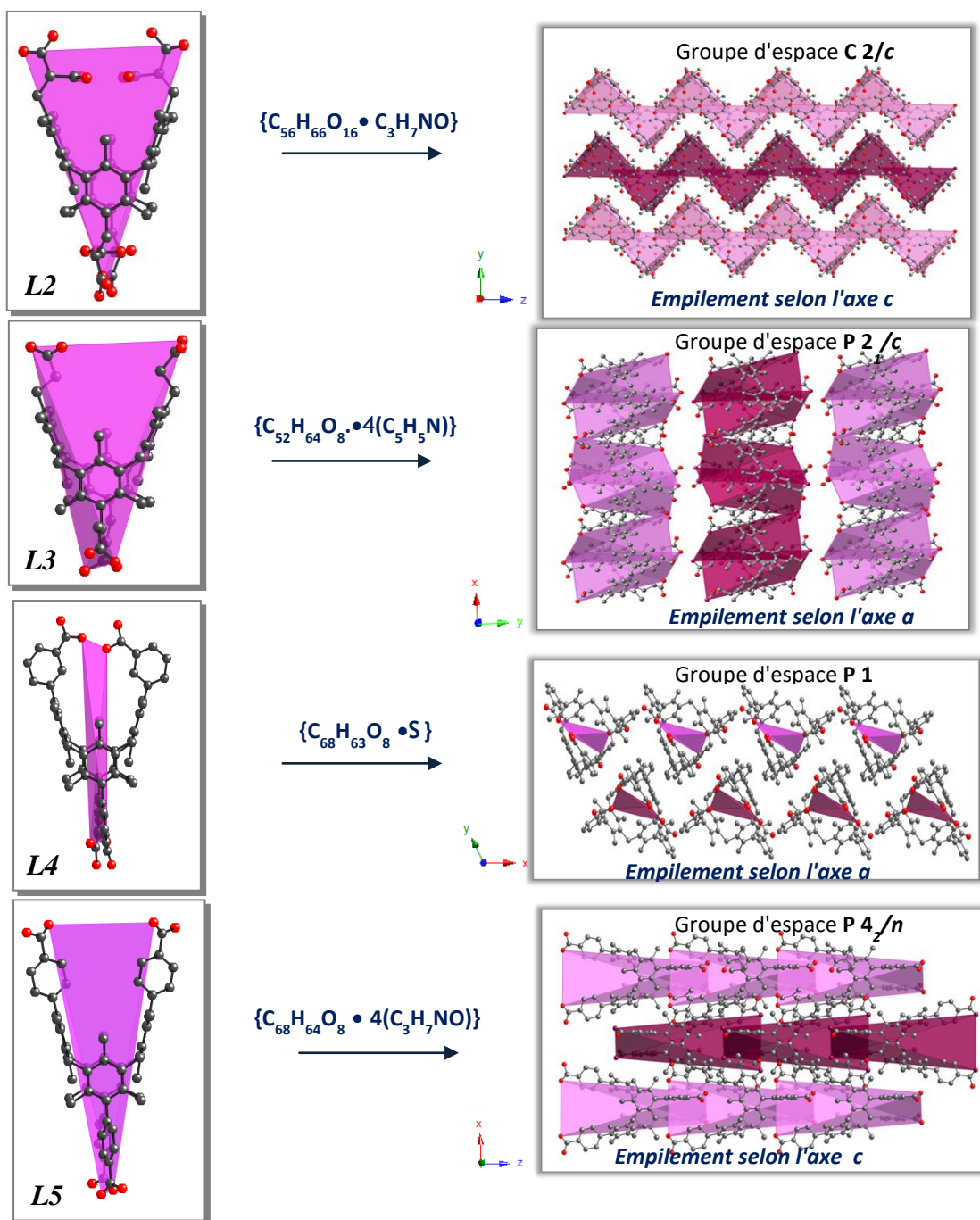


Figure 3. Représentation polyédrique des structures cristallines des ligands *L2-L5*, ainsi que leurs empilements correspondants.

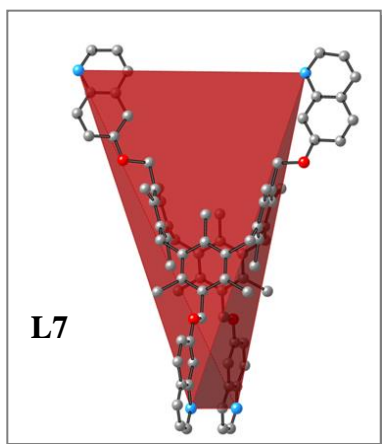
b) Synthèse de dérivés de quinolyne du [1.1.1.1] métacyclophane **L6** et **L7**.

Figure 4. Structure cristalline de **L7**

La fonction quinolyne présente un grand intérêt, car elle peut servir d'antenne pour les cations métalliques et former ainsi les composés de coordination luminescents en solution et à l'état solide.⁴⁴ Dans ce travail, les dérivés quinolyne métacyclophanes **L6-L7** ont été synthétisés par tétrasubstitution nucléophile en utilisant de la 6- ou 8-hydroxyquinoléine en tant qu'agent nucléophile et **L-Cl** en tant que précurseur. Les structures des deux composés ont également été caractérisées en solution par spectroscopie RMN ¹H et ¹³C et MALDI TOF et à l'état solide en utilisant la méthode de diffraction des rayons X pour le composé **L7** (Figure 4). Il a été démontré qu'à l'état solide, **L7** présente une structure moléculaire hautement symétrique, avec une conformation 1,3-Alternée, où les atomes coordinants de l'azote sont orientés vers l'extérieur des cavités macrocycliques et sont disponibles pour la coordination avec les cations métalliques afin de former les réseaux moléculaires étendus.

c) Synthèse du dérivé tétramercapto de [1.1.1.1]métacyclophane **L8**.

Les ligands organiques décorés avec des groupes mercapto (thiol) sont largement utilisés pour la formation de complexes avec des cations de métaux « mous » d'éléments chalcophiles et peuvent être appliqués dans la modification de surface de métaux mous. Le dérivé tétramercapto du [1.1.1.1]métacyclophane, **L8**, a été synthétisé en utilisant l'intermédiaire thioacétate qui a ensuite été réduit par l'hydrazine, selon le Schéma 4. La structure de **L8** a été étudiée et confirmée en solution par des méthodes d'analyse spectroscopiques couramment utilisées.⁴⁵

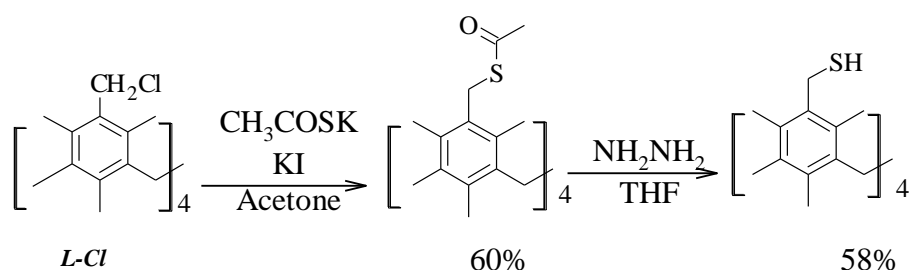


Schéma 4

d) Synthèse du dérivé cyano du [1.1.1.1] métacyclophane.

Récemment, la synthèse d'un dérivé tétrasubstitué de [1.1.1.1]métacyclophane portant le groupe mentcyano directement fixé sur les fractions aryles du squelette macrocyclique a été reportée: la combinaison avec des cations d'argent a conduit à la génération d'un polymère de coordination 1D de type tubulaire, dans la phase cristalline.^{42c} Afin d'étudier l'influence du pont méthylène flexible en tant qu'espaceur entre les groupes cyano et les groupements aryle du métacyclophane sur la capacité de liaison aux cations métalliques, un nouveau dérivé tétracyano **L9** a été synthétisé à l'aide de **L-Cl** en tant que précurseur moléculaire, selon le Schéma 2. Sa structure a également été étudiée et confirmée par les méthodes classiques d'analyse en solution.

e) Synthèse du dérivé phosphonate de [1.1.1.1] métacyclophane.

Le ligand **L10** portant des groupes phosphonate « durs » doit être adapté à la coordination des atomes « durs » tels que les lanthanides selon la théorie HSAB.³⁴

Dans le même temps, il devrait être possible de construire des réseaux liés par liaison Hydrogène, basés sur ce ligand.

Dans ce travail, le dérivé [1.1.1.1]métacyclophane portant des acides tétraphosphoniques a été synthétisé en utilisant la réaction de Michaelis-Arbuzov modifiée : l'intermédiaire **L-Cl** a été mélangé en présence de phosphite de triéthyle et d'acide de Lewis « dur » (ZnCl_2) (catalyseur de substitution nucléophile), selon le schéma 5. Puis l'hydrolyse en milieu basique a conduit au produit souhaité avec un rendement global élevé. Il a été caractérisé par les techniques classiques en solution.

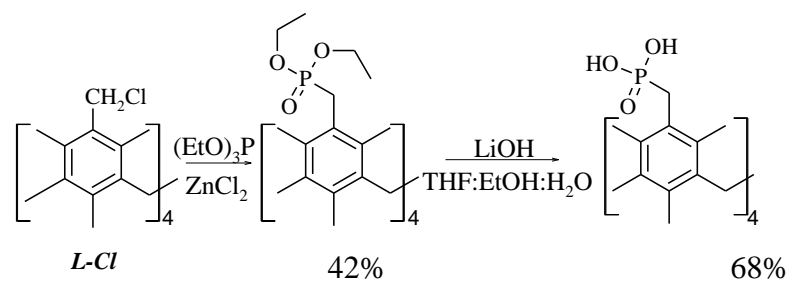
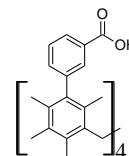


Schéma 5

III Composés de coordination à base de ligands de métacyclophane

Tous les ligands synthétisés ont été combinés avec des cations métalliques. Mais des monocristaux analysables par diffraction des RX ont été obtenus seulement pour les ligands à base de groupements carboxylates **L4** et **L5**, ainsi que pour le ligand cyano **L9**.

a) Composés de coordination avec les cations Mn: polymère de coordination **1D**
à base de **L4**



Lorsque **L4** a été combiné avec $\text{Mn}(\text{OAc})_2$ dans des conditions solvothermales (120°C , solvant Pyridine), un polymère de coordination de type hélicoïdal **1D**, de formule $[(\text{C}_{68}\text{H}_{64}\text{O}_8)_3\text{Mn}_9\text{O}_3(\text{CH}_3\text{COO})_6(\text{C}_5\text{H}_5\text{N})_{12}]$ *i.e.* $[(\text{L4})_3\text{Mn}_9\text{O}_3(\text{OAc})_6\text{py}_9 \bullet 3\text{py}]$ a été obtenu. Il cristallise dans le groupe d'espace **R 32** et présente la stoechiométrie suivante: **L4**/Mn = 1/3 (Figure 5, a). Ce composé présente une valence mixte avec les cations Mn présents aux deux états d'oxydation +II et +III.

Le cristal est composé de **L4**, deux cations Mn cristallographiquement différents, formant un cluster trinuécléaire (Mn_1 et Mn_2), des molécules de pyridine coordinées, d'un anion oxyde O^{2-} et d'un anion acétate OAc^- . Des molécules de pyridine non coordonnées sont également présentes dans le cristal. Les cations Mn_1 et Mn_2 , hexacoordinés avec une sphère de coordination de type NO_5 , présentent une géométrie octaédrique déformée avec des atomes d'azote appartenant à des molécules de pyridine situées sur les sommets d'un octaèdre, des atomes d'oxygène (O^{2-}) et O provenant de carboxylates de **L4** et OAc^- , comme le montre la figure 5; b.

Les caractéristiques des liaisons et des angles pour l'environnement octaédrique légèrement déformé des deux atomes de manganèse sont données dans les tableaux 1 et 2. Elles sont caractéristiques des espèces Mn(II)/Mn(II) dans l'environnement NO_5 , qui ne peuvent pas être distinguées avec précision. Par ailleurs, les distances entre Mn_1 et Mn_2 à l'intérieur du cluster sont de 3,508 et 3,508 Å, tandis que les distances entre deux clusters à l'intérieur du polymère sont: 16.627 and 21.528 Å ($d_{\text{Mn1-Mn1}}$), 21.038 Å ($d_{\text{Mn2-Mn2}}$). Dans le même temps, les distances entre deux groupes des chaînes voisines sont 8.273, 10.920, 12.646, 16.811 Å ($d_{\text{Mn1-Mn1}}$) et 11.125 Å ($d_{\text{Mn2-Mn2}}$).

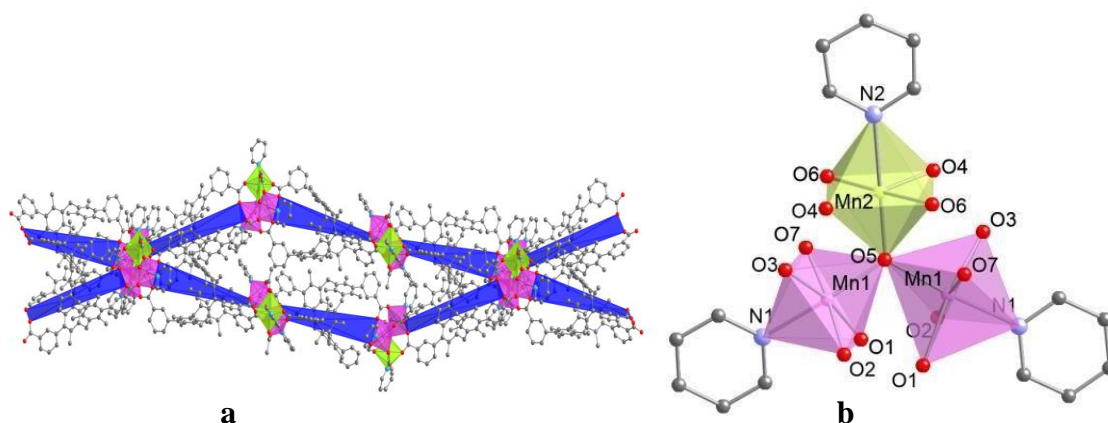


Figure 5. Une partie de la structure cristalline de $[(\text{L4})_3\text{Mn}_9\text{O}_3(\text{OAc})_6\text{py}_9 \bullet 3\text{py}]$ (a) et l'environnement des cations manganèse (b).

Tableau 1: Distances Mn-N et Mn-O (Å) dans $[(\text{L4})_3\text{Mn}_9\text{O}_3(\text{OAc})_6\text{py}_9 \bullet 3\text{py}]$

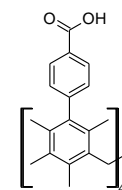
	N1	N2	O1	O2	O3	O4	O5	O6	O7
Mn1	2.159	-	2.210	1.996	2.153	-	2.012	-	1.996
Mn2	-	2.254	-	-	-	2.081	1.987	2.190	-

Tableau 2: Angles N-Mn-O et O-Mn-O (°) dans [(L4)₃Mn₉O₃(OAc)₆py₉•3py]

N1-Mn1-O3	O3-Mn1-O7	O7-Mn1-O5	O5-Mn1-O1	O1-Mn1-O2	O2-Mn1-N1	O7-Mn1-O2	O2-Mn1-O5
84.4	91.7	90.4	97.5	87.6	87.3	174.7	94.9
O2-Mn1-O3	O5-Mn1-O3	O7-Mn1-N1	O5-Mn1-N1	O7-Mn1-O1	O3-Mn1-O1	N1-Mn1-O1	
88.4	91.8	87.4	175.6	91.3	170.1	86.4	
O6-Mn2-O4	O4-Mn2-O5	O5-Mn2-O6	N2-Mn2-O6	N2-Mn2-O4	O4-Mn2-O4	O5-Mn2-O6	
88.3	91.7	90.827	89.2	88.3			
91.7	91.7		89.2	88.3	176.5	90.8	
O6-Mn2-O6	O5-Mn2-N2						
178.4	180.0						

Le noyau trinuéculaire de Mn₃O, analogue à celui trouvé dans [(L4)₃Mn₉O₃(OAc)₆py₉•3py], a déjà été rencontré dans d'autres composés de coordination.⁴⁶ Les mesures magnétiques de [(L4)₃Mn₉O₃(OAc)₆py₉•3py] sont en cours, cependant limitées par les faibles quantités de composés obtenus.

b) Composés de coordination avec les cations Mn : polymère de coordination 3D à base de L5



L5 a été combiné à Mn(NO₃)₂ dans des conditions solvothermales (120°C, DMF), un polymère de coordination 3D poreux de formule [(C₆₈H₆₄O₈)Mn₂(C₃H₇NO)₂] i.e. [(L5)Mn^{II}₂(DMF)₂] a été obtenu. Ce composé cristallise dans le groupe d'espace C2/c (figure 6, a) et présente une stœchiométrie L5/Mn²⁺ = 1/2.

Le cristal est composé de ligand L5, de deux cations Mn²⁺ cristallographiquement différents et de molécules de DMF. Dans ce cas, il n'y a aucune ambiguïté concernant l'état d'oxydation de Mn (en supposant que L5 soit totalement déprotoné), la formule complète du composé est (L5)Mn^{II}₂(DMF)₂.

La distance entre Mn₁ et Mn₂ dans le complexe dinuéculaire est égale à 3,789 Å, mais les distances entre deux clusters dans le polymère sont les suivantes: 21,876 et 21,109 Å (d_{Mn1-Mn1}), 21,876, 23,453 et 22,682 Å (d_{Mn2-Mn2}). D'autre part, la distance entre deux groupes de chaînes voisines est de 14,284 Å (à la fois pour d_{Mn1-Mn1} and d_{Mn2-Mn2}). Comme le montre le tableau 3, il existe une augmentation des angles dièdres (les deux types) et une diminution de la valeur de distance maximale entre les atomes C et O dans les groupements carboxyliques (tableau 3). D'autre part, les distances entre les atomes Mn^{II} et O des groupes carboxylate sont égales à 2,033, 2,219, 2,234, 2,270, 2,257 Å respectivement, tandis que les molécules DMF sont situées à une distance de 2,159 Å du centre de Mn^{II} (tableau 4).

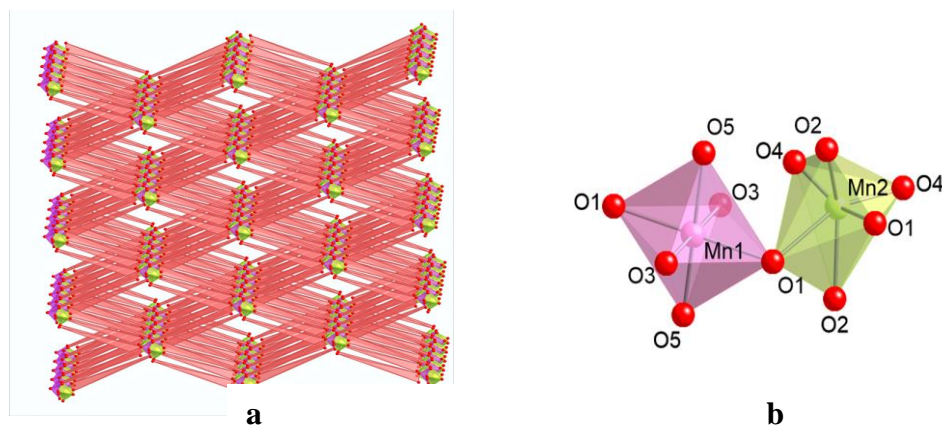


Figure 6. Une partie de la structure cristalline poreuse de $[(L5)Mn_2(DMF)_2]$ (a) et environnement des cations manganèse (b).

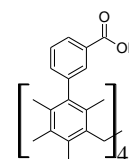
O3-Mn1-O1	O5-Mn1-O1	O3-Mn1-O5	O4-Mn1-O2	O5-Mn1-O5	O3-Mn1-O3
87.73 92.27	87.51 92.49	86.93 93.07	98.3 111.77	180	180
O4-Mn2-O4	O2-Mn2-O2	O1-Mn2-O1	O1-Mn2-O2	O1-Mn2-O4	
90.4	137.1	85.19	57.51 89.93	97.20 155.76	

Tableau 3: Angles O-Mn-O ($^\circ$) dans $(L5)Mn_2(DMF)_2$.

	O1	O2	O3	O4	O5
Mn1	2.234	-	2.219	-	2.159
Mn2	2.270	2.257	-	2.033	-

Tableau 4: Distances Mn-N et Mn-O (\AA) dans $(L5)Mn_2(DMF)_2$.

c) Composés de coordination avec les cations Co^{2+} : polymère de coordination **2D** à base de **L4**



Lorsque **L4** est combiné à $Co(OAc)_2$ dans des conditions solvothermales (120°C , DMF), un polymère de coordination 2D de formule $[(C_{68}H_{64}O_8)_4Co_{10}O_4(CH_3OH)_2(H_2O)_4(CH_3COO)_2 \cdot (C_3H_7NO)(H_2O)_7 \cdot S]$ *i. e.* $[L_4Co_{10}O_2(MeOH)_2(H_2O)_4(OAc)_2 \cdot S]$ (toutes les molécules d'eau ou de solvant n'ont pas pu être raffinées dans la structure cristalline et la commande « squeeze » a été appliquée)⁴⁷ est obtenu (Figure 7, a). Il cristallise dans le groupe d'espaces $P2_1/c$, et présente une stoechiométrie $L_4/Co^{2+} = 2/5$.

Le cristal est composé de **L4**, de cinq cations de Co^{2+} différents (Figure 7, b), de deux anions oxyde O^{2-} , d'un anion acétate OAc^- , de l'eau coordonnée et des molécules de MeOH, DMF et H_2O en tant que solvants. Les distances entre Co^{2+} au sein des clusters pentanucléaires ainsi formés sont les suivantes: 3.183 \AA ($d_{Co1-Co2}$); 5.676 \AA ($d_{Co1-Co4}$); 6.142 \AA ($d_{Co1-Co5}$); 3.149 \AA ($d_{Co1-Co3}$); 3.607 \AA ($d_{Co2-Co3}$); 3.442 \AA ($d_{Co2-Co4}$);

7.103 Å ($d_{\text{Co2-Co5}}$); 3.442 Å ($d_{\text{Co3-Co4}}$); 3.540 Å ($d_{\text{Co3-Co5}}$) et 3.239 Å ($d_{\text{Co4-Co5}}$) tandis que les distances entre les groupes proches dans une chaîne polymère sont: 24.887 Å ($d_{\text{Co1-Co1}}$); 26.004 Å ($d_{\text{Co2-Co2}}$); 21.701 Å ($d_{\text{Co3-Co3}}$); 19.463 Å ($d_{\text{Co4-Co4}}$) et 18.979 Å ($d_{\text{Co5-Co5}}$). D'autre part, les distances entre les clusters de chaînes voisines dans le cristal sont: 17.338 et 24.477 Å ($d_{\text{Co1-Co1}}$); 23.398 et 20.289 Å ($d_{\text{Co2-Co2}}$); 18.245 et 15.329 Å ($d_{\text{Co3-Co3}}$); 9.255 et 16.708 Å ($d_{\text{Co4-Co4}}$) et 13.744 et 14.119 Å ($d_{\text{Co5-Co5}}$). Les distances Co-O (Å) et angle O-Co-O (°) sont présentées ci-dessous dans les tableaux 5 et 6.

La formule précise du composé nécessite des affinements et des investigations supplémentaires, mais ce composé appartient à la famille des composés de cobalt de haute dimension, présentant des clusters métalliques de nucléarité élevée.⁴⁸ Les propriétés magnétiques de tels composés sont intéressantes.

	O1	O5	O8	O17	O18	O21	O3	O7	O6	O20	O14	O2	O19
Co 1	2.030	2.048	2.085	2.105	2.149	2.149	-	-	-	-	-	-	-
Co 2	-	-	-	1.924	-	-	1.904	1.953	1.997	-	-	-	-
Co 3	-	-	-	2.066	-	2.104	-	-	-	2.041	2.095	2.101	2.183
	O13	O20	O22	O11	O9	O23	O15	O12	O10				
Co 4	2.077	2.094	2.102	2.108	2.122	2.142							
Co 5		1.939					1.926	1.956	1.983				

Tableau 5: Distances Co-O (Å) dans $\text{L}_4\text{Co}_{10}\text{O}_2(\text{CH}_3\text{OH})(\text{H}_2\text{O})_2(\text{CH}_3\text{COOH})\bullet(\text{C}_3\text{H}_7\text{NO})(\text{H}_2\text{O})_n$.

O1-Co1-O5	O1-Co1-O8	O5-Co1-O8	O1-Co1-O17	O5-Co1-O17	O8-Co1-O17	O1-Co1-O18	O5-Co1-O18
93.6	167.9	91.3	89.1	87.5	102.2	85.0	93.2
O8-Co1-O18	O17-Co1-O18	O1-Co1-O21	O5-Co1-O21	O5-Co1-O21	O17-Co1-O21	O18-Co1-O21	
83.7	174.1	88.2	166.2	89.6	79.2	100.3	
O3-Co2-O17	O3-Co2-O7	O17-Co2-O7	O3-Co2-O6	O17-Co2-O6	O7-Co2-O6		
136.6	93.1	111.4	109.6	99.2	103.1		

O20-Co3-O17	O20-Co3-O14	O17-Co3-O14	O20-Co3-O2	O17-Co3-O2	O14-Co3-O2	O20-Co3-O21	O17-Co3-O21
173.8	90.4	88.3	86.8	95.0	174.7	104.7	81.4
O14-Co3-O21	O2-Co3-O21	O20-Co3-O19	O17-Co3-O19	O14-Co3-O19	O2-Co3-O19	O21-Co3-O19	
89.8	86.5	83.3	90.8	93.5	90.6	171.4	

O13-Co4-O20	O13-Co4-O22	O20-Co4-O22	O13-Co4-O11	O20-Co4-O11	O22-Co4-O11	O13-Co4-O9	O20-Co4-O9
84.9	90.3	100.5	175.2	97.5	85.3	91.3	84.5
O22-Co4-O9	O11-Co4-O9	O13-Co4-O23	O20-Co4-O23	O22-Co4-O23	O11-Co4-O23	O9-Co4-O23	
174.9	93.0	91.8	170.5	88.5	86.4	86.6	

O15-Co5-O20	O15-Co5-O12	O20-Co5-O12	O15-Co5-O10	O20-Co5-O10	O12-Co5-O10
133.6	99.6	108.7	104.4	102.0	106.3

Tableau 6: Angles O-Co-O (°) dans $\text{L}_4\text{Co}_{10}\text{O}_2(\text{MeOH})_2(\text{H}_2\text{O})_4(\text{OAc})_2\bullet(\text{C}_3\text{H}_7\text{NO})(\text{H}_2\text{O})_7$.

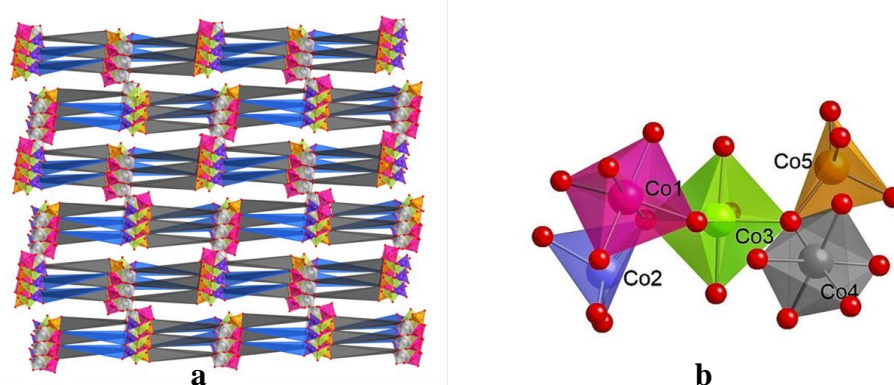
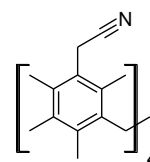


Figure 7. Une partie de la structure cristalline de $[L_4Co_{10}O_2(MeOH)_2(H_2O)_4(OAc)_2 \cdot S]$ (empilement le long de l'axe b) (a) et l'environnement de cinq atomes de cobalt indépendants du point de vue cristallographique (b).

d) Réseau de coordination et métallamacrocycle
à partir de **L9**



Le ligand **L9** a été combiné avec $AgNO_3$ et $AgBF_4$ dans des conditions douces, conduisant à des polymères de coordination isostructuraux 1D ainsi qu'à un complexe discret, présentant tous les deux le même rapport M/L = 1/1 (Figure 8). **L9**, bloqué en conformation 1,3-Alternée, combiné à des cations Ag^+ dans des conditions d'auto-assemblage, conduit soit à un réseau de coordination 1D non tubulaire (groupe d'espace **I** *a-3d*) $[LI-AgX]_\infty$ ($X=BF_4^-$, NO_3^-) ou un dimère binucléaire discret (métallamacrocycle) $[LI-AgNO_3]_2$ en fonction de la nature de l'anion utilisé (NO_3^- ou BF_4^-) et des conditions stoechiométriques utilisées.⁴⁵

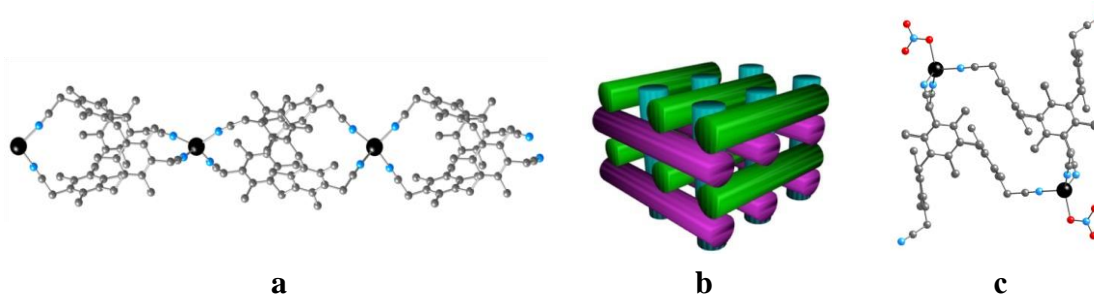


Figure 8. Chaîne 1D non tubulaire de formule $[LI-AgX]_\infty$ ($X=BF_4^-$, NO_3^-) (a) empilement cubique de $[LI-AgX]_\infty$ (b) et métallamacrocycle de formule $[LI-AgNO_3]_2$ (c).

IV Études en solution

a) Titrage UV-vis et DLS

Afin d'étudier la capacité des ligands carboxyliques **L1-L5** obtenus à former les complexes en solution, des études préliminaires ont été fournies sur le comportement de **L4** et **L5** en ce qui concerne le comportement coordinant en solution. En utilisant la technique de titrage UV-vis, il a été constaté que la stoechiométrie était conforme aux données observées à l'état solide. Dans le même temps, les études préliminaires DLS étaient également conformes aux données de titrage UV.

b) Investigations de sélectivité d'extraction des anions picrates

L'aptitude des dérivés quinoléiques de métacyclophane (**L6**) à extraire les éléments d et f de la solution aqueuse en phase organique CH₂Cl₂ a été étudiée par une méthode d'extraction des anions picrates en utilisant les sels de nitrate (triflate dans le cas de Tb (III)). Les densités optiques A_i et A₀ de la phase aqueuse avant et après extraction ont été mesurées dans la plage de longueurs d'onde de 300 à 500 nm, avec un maximum de 355,67 à 365,42 nm. Le pourcentage d'extraction (E%) a été calculé à l'aide de la formule suivante: $E\% = 100 * (A_0 - A_i) / A_0$. En conséquence, il a été démontré que le composé **L6** extrait tous les cations testés, mais la meilleure efficacité qu'il ait démontrée dans le cas des cations Cu (II) peut être expliquée par la propension accrue des cations Cu (II) à former des liaisons de coordination avec des atomes d'azote de **L6**. (tableau 7).

E%										
Gd ³⁺	Er ³⁺	Tb ³⁺	Dy ³⁺	Eu ³⁺	Pr ³⁺	Yb ³⁺	Ni ²⁺	Cu ²⁺	Co ²⁺	Mn ²⁺
85	78	78	80	82	64	86	59	92	61	62

Table 7. Efficacité d'extraction de **L6** vis-à-vis des cations d / f dans CH₂Cl₂ organique phase de la solution aqueuse à 25°C .

V Conclusion générale

Dix nouveaux ligands dérivés du macrocycle [1111]métacyclophanes ont été synthétisés avec succès: **L1-L10** différant par la nature des sites de coordination (carboxyliques, quinolye, mercapto-, cyano et phosphonate) et par le nombre de sites de liaison (4 ou 8) ainsi que par la nature de l'espaceur (aryle ou aliphatique) situé entre le groupement coordinant et la plate-forme macrocyclique.

Comme le montre l'analyse par diffraction des rayons X sur monocristaux des structures cristallines obtenues, il existe des liaisons intramoléculaires dans les trois cas suivants: liaison hydrogène carboxyle-carboxyle dans **L2**, liaison hydrogène avec la molécule de pyridine par groupement carboxyle dans **L3** et une liaison hydrogène intramoléculaire dans **L4**. À l'état solide, trois composés cristallins étendus ont été obtenus:

des structures 2D et 3D *via* la complexation de **L4** avec les cations Mn^{2+} et Co^{2+} , respectivement, et une structure 3D *via* la complexation de **L5** avec des cations Mn^{2+} présentant une stoechiométrie similaire aux complexes observée en solution par la méthode de titrage UV-visible. **L4** forme une structure impliquant des clusters métalliques, et **L5** forme une structure poreuse 3D, tandis que **L4**, combiné avec Co^{2+} , conduit à un polymère de coordination portant des unités de cobalt pentanucléaires. Il a également été démontré que la stoechiométrie M / L et la nature ou l'anion jouent un rôle important dans la création d'une structure polymérique 1D ou d'un métallamacrocycle, en utilisant des cations d'argent et un dérivé tétracyano **L9**. Lorsque l'anion non coordonnant (BF_4^-) a été utilisé, seule la formation d'un polymère de coordination 1D de type non tubulaire a été observée en utilisant différentes stoechiométries Métal/Ligand lors de la synthèse (M/L = 1/1, 2/1 ou 4/1). Mais le comportement de coordination de **L9** a été modifié en utilisant l'anion coordonnant (NO_3^-) qui permet de générer un polymère de coordination 1D isostructural au précédent lorsque la stoechiométrie M/L était égale à 2/1 et le métallomacrocycle discret lorsque M/L stoechiométrie a été augmenté jusqu'à 4/1. Ainsi, pour conclure, nous avons synthétisé 5 types de composés de coordination à base de **L4**, **L5** et **L9** et de différents cations métalliques (tableau 8).

En même temps, il a été démontré, en utilisant la méthode d'extraction des picrates, que le ligand **L6** extrait les cations Cu (II) avec la plus grande efficacité par rapport à tous les autres cations testés, en raison de la propension probablement accrue des cations Cu (II) à former des liaisons de coordination avec des atomes d'azote quinolylye.

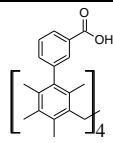
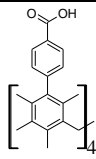
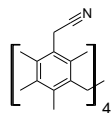
Ainsi, les principales perspectives d'avenir sont les suivantes:

a) augmenter les rendements des composés de coordination déjà obtenus, les purifier et entreprendre les études de propriétés telles que la porosité ou les propriétés magnétiques

b) études complètes du comportement en solution de **L1-L10**

c) étude de coordination de **L1-L10** étendue aux éléments d, f à l'état solide.

Tableau 8. Composés de coordination à base de **L4**, **L5** et **L9** et de différents cations métalliques

Ligands	L4 	L5 	L9 
Networks	<p>1D $(L4)_3Mn_9O_3(OAc)_6py_9 \cdot 3py$; $L4/Mn^{2+} = 1/3$</p> <p>2D $L4_4Co_{10}O_2(MeOH)_2(H_2O)_4(OAc)_2 \cdot (C_3H_7NO)(H_2O)_7$; $L4/Co^{2+}=2/5$</p>	<p>3D $(L5)Mn_2(DMF)_2$; $L5/Mn^{2+}=1/2$</p>	<p>0D $[L9_2-(AgNO_3)_2]$; $L9/Ag^+=2/2$</p> <p>1D $L9-AgBF_4$ and $L9-AgNO_3$; $L9/Ag^+=1/1$</p>

IV Références

- 1 J.-M. Lehn. Nobel Lecture, 8 December (1987).
- 2 C. Dey, T. Kundu, B. P. Biswal, A. Mallick, R. Banerjee. *Acta Crystallogr. Sect. B Struct. Sci. Cryst. Eng. Mater.*, **70**, 3-10 (2014); (b) H. Furukawa, K. E. Cordova, M. O’Keeffe, O.M. Yaghi. *Science*, **341**, 1230444 (2013).
- 3 (a) N. F. Sunday. *Arch. Org. Inorg. Chem. Sci.*, **1**, 1-13 (2018); (b) S. Mann, *J. Chem. Soc. Dalt. Trans.*, 3953-3962 (1997); (c) S. Mann. *J. Chem. Soc. Dalt. Trans.*, 1-9 (1993).
- 4 M. J. Hardie. *Structure and Bonding*, **111**, 139-174 (2004).
- 5 S. Grabowski. *Crystals*, **6**, 1-5 (2016).
- 6 J. H. Jordan, B. C. Gibb. *Chem. Soc. Rev.*, **44**, 547-585 (2015).
- 7 (a) Y. Liu, H. Liu. *Met. Fram.*, 85-104 (2016); (b) S. Lin, J. K. Bediako, C. W. Cho, M. H. Song, Y. hao, J. A. Kim, J. W. Choi, Y. S. Yun. *Chem. Eng. J.*, **345**, 337-344 (2018).
- 8 (a) L. Zhu, X-Q. Liu, H-L. Jiang, Sun L-B. *Chem. Rev.*, **117**, 8129-8176 (2017); (b) X. He, F. Yin, H. Wang, B. Chen, G. Li. *Chinese J. Catal.*, **39**, 207-227 (2018); (c) Z. Liang, C. Qu, D. Xia, R. Zou, Q. Xu. *Angew. Chem. Int. Ed.*, **57**, 9604-9633 (2018); (d) H. Yang, X. Wang. *Adv. Mater.*, 1800743, (2018).
- 9 Y. Cui, J. Zhang, H. He, G. Qian. *Chem. Soc. Rev.*, **47**, 5740-5785 (2018).
- 10 (a) D. MasPOCH, D. Ruiz-Molina, J. Veciana. *J. Mater. Chem.*, **14**, 2713-2723 (2004); (b) P. Dechambenoit, J. R. Long, *Chem. Soc. Rev.* **40**, 3249-3265 (2011). (c) G. M. Espallargas, E. Coronado *Chem. Soc. Rev.*, **47**, 533-557 (2018).
- 11 (a) P. Xiao, Y. Xu. *J. Mater. Chem. A*, 1-21 (2018); (b) Y. Li, Y. Xu, W. Yang, W. Shen, H. Xue, H. Pang. *Small*, **14**, 1-24 (2018); (c) H. Zhang, J. Nai, L. Yu, X. W. Lou. *Joule*, **1**, 77-107 (2017); (d) C. C. Hou, Q. Xu. *Adv Energy Mater.*, 1801307-1801307 (2018); (e) H. Tang, M. Zheng, Q. Hu, Y. Chi, B. Xu, S. Zhang, H. Xue, H. Pang. *J. Mater. Chem. A*, **6**, 13999-14024 (2018); (f) I. A. Indra, T. Song, U. Paik. *Adv. Mater.*, 1705146 (2018).
- 12 (a) X. Sun, S. Dong, E. Wang. *J. Am. Chem. Soc.*, **127**, 13102-13103 (2005); (b) M. Oh, C. A. Mirkin. *Nature*, **438**, 651-654 (2005); (c) A. M. Spokoyny, D. Kim, A. Sumrein, C. A. Mirkin. *Chem. Soc. Rev.*, **38**, 1218-1227 (2009).
- 13 (a) I. Higler, P. Timmerman, W. Verboom, D. N. Reinhoud. *Eur. J. Org. Chem.*, 2689-2702 (1998); (b) A. V. Mossine, P. Thavornnyutikarna, J. L. Atwood *CrystEngComm*, **15**, 1673-1675 (2013); (c) K. Kobayashi, M. Yamanaka. *Chem. Soc. Rev.*, **44**, 449-466 (2015); (d) K. Helttunen, M. Nissinen *CrystEngComm*, **18**, 4944-4951 (2016).
- 14 A. D. Hamilton. *Compr. Heterocycl. Chem.*, **7**, (2009).
- 15 (a) R. Makiura, S. Motoyama, Y. Umemura, H. Yamanaka, O. Sakata, H. Kitagawa *Nat. Mater.*, **9**, 565-71 (2010); (b) Q. Zha, X. Rui, T. Wei, Y. Xie *CrystEngComm*, **16**, 7371-7384 (2014); (c) W.Y. Gao, M. Chrzanowski, S. R. Ma *Chem Soc Rev.*, **43**, 5841-5866 (2014).
- 16 (a) M. M. Nitalikar, D. M. Sakarkar, P. V. Jain *J. Curr. Pharm Res.* **10**, 1-6 (2012); (b); H.Xu, S.Rodríguez- Hermida, J.Pérez-Carvajal, J. Juanhuix, I. Imaz, D. .A MasPOCH *Cryst. Growth Des.*, **16**, 5598-5602 (2016).
- 17 (a) M. S. Collins, M. E. Carnes, B. P. Nell, L. N. Zakharov, D. W. Johnson. *Nat. Commun.*, **7**, 1-7 (2016). (b) Z. Liu, S. K. M. Nalluri, J. Fraser Stoddart. *Chem. Soc. Rev.*, **46**, 2459-2478 (2017).
- 18 B. Esser, A. Bandyopadhyay, F. Rominger, R. Gleiter. *Chem. - A Eur. J.*, **15**, 3368-3379 (2009).

- 19 *Calixarenes: a Versatile Class of Macrocyclic Compounds*; J. Vicens, V. Böhmer, Eds.; Kluwer Academic Publishers, Dordrecht, Netherlands, (1991).
- 20 S. Pappalardo, F. Bottino, G. Ronsisvalle. *Phosphorus Sulfur Relat. Elem.*, **19**, 327-333 (1984).
- 21 (a) M. Wierzbicki, H. Jędrzejewska, A. Szumna. *Ref. Modul. Chem. Mol. Sci. Chem. Eng.*, 1-23 (2014); (b) G. E. Arnott. *Chem. - A Eur. J.*, **24**, 1744-1754 (2018); (c) A. Sirit, M. Yilmaz. *Turkish J. Chem.*, **33**, 159-200 (2009); (d) S. Y. Li, Y. W. Xu, J. M. Liu, C. Y. Su. *Int. J. Mol. Sci.*, **12**, 429-455 (2011); (e) M. Durmaz, E. Halay, S. Bozkurt. *Beilstein J. Org. Chem.*, **14**, 1389-1412 (2018).
- 22 (a) J. L. Atwood, L. J. Barbour, A. Jerga *Science* **296** 2367-2369S (2002); (b) P. K. Thallapally, L. Dobrzańska, T. R. Gingrich, T. B. Wirsig, L. J. Barbour, J. L. Atwood *Angew. Chem. Int. Ed.* **45** 6506- 6509 (2006); (c) J. Dalgarno, P. K. Thallapally, L. J. Barbour, J. L. Atwood, *Chem. Soc. Rev.*, **36**, 236- 245 (2007); (d) O. I. Koifman, N. Z. Mamardashvili, O. V Surov. *Russ. Chem. Bull.*, **66**, 241-253 (2017).
- 23 (a) Z. Asfari, J. Weiss, S. Pappalardo, J. Vicens, V. A. Doria. *Pure & Appl. Chem.*, **65**, 585-590 (1993); (b) A. Casnati, F. Giunta, F. Sansone, R. Ungaro, M. Montalti, L. Prodi, N. Zaccheroni. *Supramol. Chem.*, **13**, 419-434 (2001); (c) T. Gu, C. Bourgogne, J.-F. Nierengarten. *Tetrahedron Lett.*, **42**, 7249-7252 (2001); (d) R. De Zorzi, N. Guidolin, L. Randaccio, R. Purrello, S. Geremia. *J. Am. Chem. Soc.* **131**, 2487-2489 (2009); (e) J. Biigler, N. A. J. M. Sommerdijk, A. J. W. G. Visser, A. Van Hoek, R. J. M. Nolte, J. F. J. Engbersen, D. N. Reinhoudt. *J. Am. Chem. Soc.*, **121**, 28-33 (1999).
- 24 (a) P. Murphy, S. J. Dalgarno, M. J. Paterson. *J. Phys. Chem. A*, **120**, 824-839 (2016); (b) C. D. Gutsche, M. Iqbal, K. S. Nam, K. See, I. Alam. *Pure Appl. Chem.*, **60**, 483-488 (1988).
- 25 A. Ovsyannikov, S. Solovieva, I. Antipin, S. Ferlay *Coord Chem Rev.* **352**, 151-186 (2017).
- 26 S. P. Bew, A. D. Burrows, T. Düren, M. F. Mahon, P. Z. Moghadam, V. M. Sebestyen, S. Thurston. *Chemical Communications*, **48**, 4824-4826 (2012).
- 27 P. P. Cholewa, C. M. Beavers, S. J. Teat, S. J. Dalgarno. *Cryst. Growth Des.*, **13**, 5165-5168 (2013).
- 28 E. K. Lee, Y. Heo, J. Park, K. Min. *Cryst. Growth Des.*, **15**, 3556-3560 (2015).
- 29 (a) S. Kennedy, S. J. Dalgarno, *Chem. Commun.* 5275-5277 (2009); (b) S. Kennedy, G. Karotsis, C. M. Beavers, S. J. Teat, E. K. Brechin, S. J. Dalgarno. *Angew. Chem. Int. Ed.*, **49**, 4205 (2010); (c) M. Liu, W. Liao *CrystEngComm*, **14**, 5727-5729 (2012) (d) Z. Zhang, A. Drapailo, Y. Matvieiev, L. Wojtas, M. J. Zaworotko *Chem. Commun.*, **49**, 8353-8355 (2013).
- 30 (a) J. L. Atwood, L. J. Barbour, A. Jerga *Science* **296** 2367-2369S (2002); (b) P. K. Thallapally, L. Dobrzańska, T. R. Gingrich, T. B. Wirsig, L. J. Barbour, J. L. Atwood *Angew. Chem. Int. Ed.* **45** 6506- 6509 (2006); (c) J. Dalgarno, P. K. Thallapally, L. J. Barbour, J. L. Atwood, *Chem. Soc. Rev.*, **36**, 236- 245 (2007); (d) O. I. Koifman, N. Z. Mamardashvili, O. V Surov. *Russ. Chem. Bull.*, **66**, 241-253 (2017); (e) (a) S. P. Bew, A. D. Burrows, T. Düren, M. F. Mahon, P. Z. Moghadam, V. M. Sebestyen, S. Thurston. *Chem. Commun.*, **48**, 4824-4826 (2012); (f) S. Pasquale, S. Sattin, E.C. Escudero-Adán, M. Martínez- Belmonte, J. De Mendoza. *Nat Commun.*, **3**, 785 (2012).
- 31 (a) G. Mislin, E. Graf, M. W. Hosseini, A. De Cian, N. Kyritsakas, J. Fischer. *Chem Commun.*, 2545-2546 (1998); (b) M. N. Kozlova, S. Ferlay, S. E. Solovieva, I. S. Antipin, A. I. Konovalov, N. Kyritsakas, M. W. Hosseini. *Dalton*, **44**, 5126-5131 (2007).
- 32 E. Elisabeth, L. J. Barbour, G. W. Orr, K. T. Holman, J. L. Atwood. *Supramol. Chem.*, **12**, 317-320 (2000).
- 33 (a) O. I. Kalchenko, A. V. Solovyov, S. A. Cherenok, N. F. Starodub, V. I. Kalchenko. *J. Incl. Phenom. Macrocycl. Chem.*, **46**, 19-25 (2003); (b) O. Kalchenko, A. Marcinowicz, J. Poznanski, S. Cherenok, A. Solovyov, W. Zielenkiewicz, V. Kalchenko. *J. Phys. Org. Chem.*, **18**, 578-585 (2005); (c) A. I. Vovk, V. I. Kalchenko, S. A. Cherenok, V. P. Kukhar, O. V. Muzychka, M. O. Lozynsky. *Org. Biomol. Chem.*, **2**, 3162-3166 (2004); (d) S. Cherenok, A. Vovk, I. Muravyova, A. Shivanyuk, V. Kukhar, J. Lipkowski, V. Kalchenko. *Org. Lett.*, **8**, 549-552 (2006); (e) M. Bayrakci, Ş. Ertul, M. Yilmaz. *J. Incl. Phenom. Macrocycl.*

Chem., **74**, 293-303 (2012).

34 R. G. Pearson. *J. Chem. Educ.*, **45**, 581 (1968); (b) R.G. Pearson. *J. Chem. Educ.*, **45**, 643 (1968).

35 X. Delaigue, J. M. B. Harrowfield, M. W. Hosseini, A. De Cian, J. Fischer, N. Kyritsakas *J. Chem. Soc., Chem. Commun.*, 1579-1580 (1994).

36 (a) J. L. Ballard, W. B. Kay, E. L. Kropa. *Journal of Paint Technology*, **38**, 251-262 (1966); (b) F. Bottino, G. Montaudo, P. Maravigna *Ann. Chim.*, **57**, 972-978, (1967); (c) T.-T. Wu, J. R. Speas *J. Org. Chem.*, **52**, 2330- 2332(1987); (d) B. Gawdzik, W. Iwanek, A. Hoser, K. Wozniak *Supramol. Chem.*, **20**, 273-277 (2008).

37 J. Ehrhart, J-M. Planeix, N. Kyritsakas-Gruber, M. W. Hosseini, *Dalton Trans.*, **14**, 2552-2557 (2009).

38 A. S. Ovsyannikov, S. Ferlay, E. F. Chernova, S. E. Solovieva, I. S. Antipin, M. W. Hosseini. *Macroheterocycles*, **10**, 410-420 (2017).

39 C. Klein, E. Graf, M. W. Hosseini, A. De Cian, N. Kyritsakas, *Eur. J. Org. Chem.*, **5**, 802-809 (2002).

40 C. Klein, E. Graf, M. W. Hosseini A. De Cian. *Tetrahedron Lett*, **41**, 9043-9047(2000).

41 X. Delaigue, M. W. Hosseini, *Tetrahedron Lett.*, **34**, 8111-8112 (1993).

42 a) J. Ehrhart, J-M. Planeix, N. Kyritsakas-Gruber, M. W. Hosseini, *Dalton Trans.*, **14**, 2552-2557 (2009); b) J. Ehrhart, J. M. Planeix, N. Kyritsakas-Gruber, M. W. Hosseini. *Dalt. Trans.*, **39**, 2137-2146 (2010); c) C. Klein, E. Graf, M. W. Hosseini, A. De Cian, J. Fischer. *Chem. Commun.*, 239-240 (2000); d) C. Klein, E. Graf, M. W. Hosseini, A. De Cian. *New J. Chem.*, **25**, 207-209 (2001); e) C. Klein, E. Graf, M. W. Hosseini, A. De Cian, N. Kyritsakas. *Eur. J. Inorg. Chem.*, 1299-1302 (2003); f) C. Klein, E. Graf, M. W. Hosseini, N. Kyritsakas-Gruber *Transactions ACA*, **39**, 103-109 (2004); g) J. Ehrhart, J-M. Planeix, N. Kyritsakas-Gruber, M. W. Hosseini. *Dalton Trans.*, 6309-6314 (2009).

43 E. F. Chernova, A. S. Ovsyannikov, S. Ferlay, S. E. Solovieva, I. S. Antipin, A. I. Konovalov, N. Kyritsakas, M. W. Hosseini. *Tetrahedron Lett.*, **59**, 1377-1381 (2018).

44 V. A. Montes, R. Pohl, J. Shinar, P. Anzenbacher. *Chem.- A Eur. J.*, **12**, 4523-4535 (2006).

45 E. Chernova, A. Ovsyannikov, S. Ferlay, S. E. Solovieva, I. S. Antipin, A. I. Konovalov, N. Kyritsakas, M. W. Hosseini, *Mendeleev Comm.*, **27**, 260-262 (2017).

46 a) A. Kornowicz, S. Komorski, Z. Wróbel, I. Justyniak, N. Nedelko, A. Ślawska-Waniewska, J. Lewiński. *Dalton Trans.*, **43**(8), 3048-3051 (2014); b) C. J. Milios, T. C. Stamatatos, P. Kyritsis, A. Terzis, C. P. Raptopoulou, R. Vicente, A. Escuer, S. P. Perlepes. *Eur. J. Inorg. Chem.*, 2885-2901 (2004).

47 A. Spek. *J. Appl. Cryst.* **36**, 7-13 (2003)

48 (a) G.E. Kostakis, S.P. Perlepes, V.A. Blatov, D.M. Proserpio, A.K. Powell. *Coord. Chem. Rev.*, **256**, 1246–1278 (2012); (b) S. Zhang, X. Liu, B. Liu, Z. Xia, W. Wang, Q. Yan, H. Ke, Q. Wei, G. Xie, S. Chen, S. Gao. *Science China Chemistry*. **58** (6), 1032-1038 (2015); (c) T. C. Stamatatos, A.K. Boudalis, K. V. Pringouri, C. P. Raptopoulou, A. Terzis, J. Wolowska, E. J. L. McInnes, S.P. Perlepes. *Eur. J. Inorg. Chem.*, 5098-5104 (2007).

Acknowledgements

I want to sincerely thank the jury members for their agreement to judge my thesis work: Pr. Jean-Bernard Regnouf de Vains, Dr. Brigitte Bibal and Dr. David Sémeril.

I would like to express special gratitude to Professor Mir Wais Hosseini that he hosts me to his laboratory to work on an interesting project in a team of remarkable researchers. And also I am grateful to him for the belief in me and inspiration, support and kindness towards me.

I also want to thank Professor Sylvie Ferlay for her enormous help in this research work and writing the thesis as well as the patience and guidance, constant assistance in administrative matters, invaluable help in the adaptation in France and for human spiritual support.

Many thanks to Aziz Jouaiti for recommendations in conducting the organic synthesis, for helping to perform dangerous reactions and for safety when working with a gas burner ☺.

Also I would like to thank Audrey Fluck for the help in everything that is connected with work in the laboratory: for estimable suggestions, safety, as well as help in setting up any instruments and searching for any substances for the synthesis.

I express my particular gratitude to Nathalie Gruber for her great contribution to my work due to the X-ray structural analysis and also I am grateful for her friendly attitude.

Many thanks to Valérie Rey for help in preparing the documents and informing about important events.

I would like to thank all the other permanent members of the laboratory: Stéphane Baudron, Véronique Bulach, Aurélie Guenet as well as the PhD students: Elsa Tufenkjian, Berangere Godde, Romain Corso, Cyril Adolf, Maxime Florent, Donata Asnaghi, Ivan Meshkov and all the other PhD and Master students who took part in the research work of our laboratory, for their help in any questions and situations and kind feedback.

I am grateful to my young colleagues from a neighboring laboratory: Anton Nicolaev, Filipa Seica, Natalia Gritsik for endless kindness, supporting attitude in relation to my research work and life in France and for their friendship.

I want to thank my Russian supervisors: Professor Igor Antipin and Svetlana Solovieva for support, guidance, important recommendations and attractive ideas for scientific work, benevolent attitude and inspiration. Without them, I would never have known about this laboratory and would not have had a chance to do research work in Strasbourg and get financial support.

I want to express my great gratitude to Alexander Ovsyannikov for support in all undertakings and development along the way of this research work, as well as recommendations and guidance in everything, including any details concerning scientific work and chemistry as well as for his enormous contribution to my adaptation abroad.

I also want to thank from the bottom of my heart the wonderful and beloved team of our Russian laboratory, especially Elena Popova for her humor, assistance in syntheses, valuable advice and fruitful talks, Farida Galieva and Gulia Allahverdili for their endless support and optimism.

I would like to express special gratitude to Zalia Ahmetzyanova for her extraordinary human responsiveness and sincerity, willingness and desire to help in any case, and also for her invaluable contribution to the work with UV-vis titration.

Many thanks to Sofia Kleshnina for her help in everything. And also I thank her for her kindness and humanity.

Also I would like to express gratitude for the members of the Kazan Federal University Laboratory: Vladimir Burilov, Diana Mironova and Elsa Sultanova for clarification and access to various research instruments and devices.

Special thanks to the French Government for the Vernadsky scholarship.

Finally, I am grateful to my lovely family for being with me along all of this pathway.

TABLE OF CONTENTS

CHAPTER I:

I SUPRAMOLECULAR CHEMISTRY BASIC CONCEPTS OF AS A KEY TO UNDERSTAND MOLECULAR TECTONICS AND CRYSTAL ENGINEERING.....	31
II THE CRYSTAL ENGINEERING APPROACH.....	33
II 1. Supramolecular interactions for crystal engineering.....	35
II 2. Metal-organic compounds and coordination polymers.....	38
III METACYCLOPHANE TYPE MACROCYCLES	40
<i>III.1.1. Generalities about calixarene.....</i>	41
<i>III 1.2. Examples of coordination networks with calix[4]arene</i>	43
III 2. [1111]Metacyclophanes as a representatives of metacyclophane family.....	50
III 3. [1111]Metacyclophanes: macrocyclic ligands for the formation of coordination networks	52
<i>III 3.1. Ligand design</i>	52
<i>III 3.2. Synthesis of the ligands</i>	55
<i>III 3.3. Structural studies of the ligands</i>	55
<i>III 3.4. Synthesis of coordination compounds</i>	57
III 4. Coordination polymers based on [1111]metacyclophanes	58
<i>III 4.1. The use of disubstituted ligands LC2, LP-d2, Lim2, and LP-z2</i>	58
<i>III 4.2. The use of tetrasubstituted ligands LC4, LP-d4, Lim4, LP-z4 and LP-dz</i>	61
IV SCIENTIFIC PROJECT	64
IV 1. Functional groups for the formation of new tetrasubstituted [1111]metacyclophane based ligands.....	65
IV 2. Expected coordination polymers	66
V CONCLUSION.....	67

CHAPTER II:

I 1. Synthesis of the carboxylic derivatives L1-L5	73
I 2. Behaviour in solution.....	76
I 3. Structural studies in the solid state.....	77
I 3. 1. General trends.....	77
I 3. 2. Carboxylic derivatives with aliphatic spacer	79
I 3. 2. 1. Ligand L2.....	79
I 3. 3. Carboxylic derivatives with aromatic spacer.....	83
I 3. 3. 1. Ligand L4.....	83
I 3. 3. 2. Ligand L5.....	85
I 4. Conclusion.....	87
II QUINOLYL DERIVATIVES OF [1111]METACYCLOPHANE	88
II 1. Synthesis of Ligands L6 and L7	88
II 2. Behaviour in solution.....	88
II 3. Structural studies in the solid state for L7	89
III MERCAPTO- DERIVATIVE OF [1111]METACYCLOPHANE	91
III 1. Synthesis of ligand L8	92
III 2. Behaviour in solution.....	92
IV CYANO- DERIVATIVE OF [1111]METACYCLOPHANE	93
IV 1. Synthesis of Ligand L9.....	93
IV 2. Behaviour in solution.....	94
V 1. Synthesis of ligand 10.....	95
V 2. Behaviour in solution.....	96
VI CONCLUSION.....	97

CHAPTER III:

I INTRODUCTION	81
II. COORDINATION NETWORKS BASED ON CARBOXYLIC DERIVATIVES OF [1111]METACYCLOPHANE.....	104
II 1. Coordination compounds with Mn cations	107
II 1.1. 1D coordination polymer based on L4.....	107

II 1.2. 3D coordination polymer based on L5.....	108
II 1.3 Conclusion	111
II 2. Coordination compound with Co cations.....	112
II 2.1. 3D coordination network based on L4	112
II 2.2. Conclusion	117
III COORDINATION NETWORKS BASED ON CYANOMETHYL DERIVATIVE OF [1111] METACYCLOPHANE.....	117
III 1. 1D coordination polymer	118
III 2. Coordination with Ag ⁺ of L5: formation of Metallamacrobicycle	120
III 3. Conclusion	123
IV COORDINATING ABILITIES OF L4 AND L5 IN SOLUTION DETERMINED BY UV-TITRATION METHODS AND DLS	125
IV 1. UV-titration	125
IV 1.1 L4 + Mn(OAc) ₂	126
IV 1.2 L4 + Co(OAc) ₂	128
IV 1.3 L5 + Mn(NO ₃) ₂	129
IV 1.4 Conclusion	131
V DYNAMIC LIGHT SCATTERING (DLS).....	131
V 1. Measurements	131
V 2. Conclusion.....	133
VI PICRATE EXTRACTION SELECTIVITY OF L6	133
VII CONCLUSION.....	135

CHAPTER IV:

GENERAL CONCLUSION AND PERSPECTIVES.....	137
---	------------

REFERENCES.....	143
------------------------	------------

ANNEXES AND EXPERIMENTAL PART	153
--	------------

General information	155
Intermediates used for synthesis	157
Synthesis of targeted ligands	158
Crystallisation methods of synthesized ligands and networks	163
Crystal data for synthesized ligands	165
Crystal data for coordination polymers based on the synthesized ligands.....	175
I DYNAMIC LIGHT SCATTERING (DLS).....	197
II UV-VIS TITRATION METHOD FOR STOICHIOMETRY DETERMINATION	198
III PICRATE EXTRACTION FOR DETERMINATION OF COMPLEXING ABILITY.....	200

Chapter I: Introduction

Our scientific project focuses on the formation of molecular networks based on new molecular tectons derived from the macrocyclic [1111] metacyclophane platform combined with d- and f-metallic cations.

This type of molecular networks may lead to porous crystals with possible applications in liquid and gas storage, separation and catalysis.¹ The formation of networks may be based on establishment of hydrogen² or coordination bonds.³ This approach may be useful in the context of global warming related in part to emission of CO₂ and SO₂ into the atmosphere.⁴ Furthermore, molecular networks may also be used as luminescent sensors,⁵ for example, for different substrates.

The aim of the project developed in the context of this thesis is the design of new ligands and their combination with metallic cations for the formation of coordination networks. The project is based on principles developed *supramolecular chemistry*⁶ and *molecular tectonics*.⁷

I Supramolecular Chemistry basic concepts of as a key to understand Molecular Tectonics and Crystal Engineering

Molecular self-assembly and self-organization is the basis of life because all components of living organisms such as DNA, proteins, enzymes are subject to self-assembly and self-organization.

Due to fundamental work performed by Nobel laureates C. Pedersen, D. Cram and J.-M. Lehn, “supramolecular chemistry” became a domain of interest. This approach opens the way to numerous possibilities for designing unknown assemblies by mastering intermolecular interactions which are essential for molecular recognition and self-assembly and self-organization. However, owing to the complexity of biology, so far it is impossible to build abiotic supramolecular systems mimicking living organisms.⁸

A relevant example of self-organization is the formation of the DNA double helix. In the late 60s, artificial molecules able to recognize other chemical moieties, and over the last two decades, molecular assemblies able to self-organize were designed. So, between *ca* 70's and 90's, "*Supramolecular Chemistry*", a multidisciplinary field⁹ including organic and inorganic chemistry, solid state chemistry as well as biochemistry and chemistry of materials was developed (Figure 1).

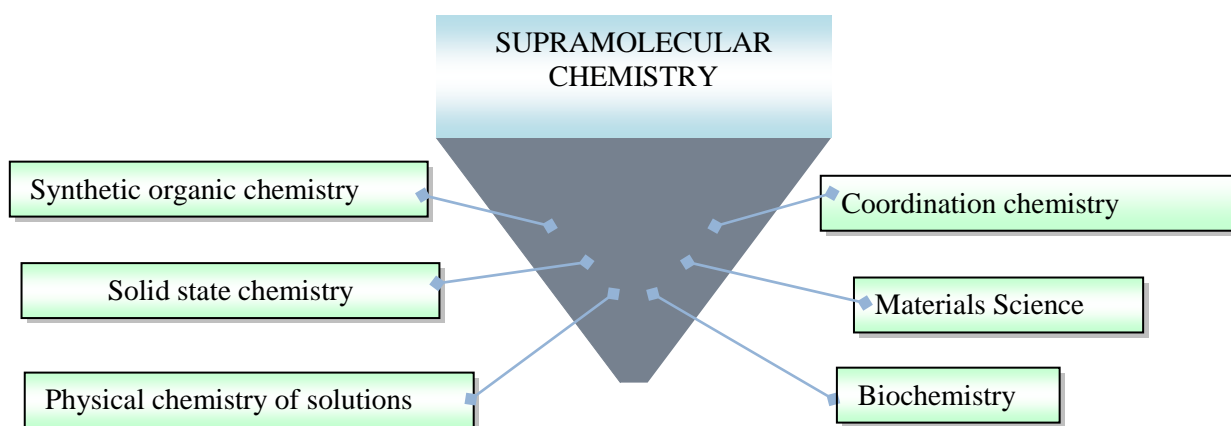


Figure 1. Schematic representation of the interconnections of fields related to supramolecular chemistry

In other words, supramolecular chemistry has developed a wide field of knowledge, including several directions and is used for the generation of new assemblies (Figure 2). Pr. J-M Lehn defined supramolecular chemistry as the “chemistry of intermolecular bonds”, studying the association of two or more chemical moieties. Supramolecular chemistry studies, among many aspects, the role of the environment in chemical reactions for example, the synthesis of assemblies of molecules, and intermolecular interactions, together with the creation of devices based on molecular components.¹⁰

The formation of supramolecular structures, not an easy task for synthetic chemists, requires several events such as:

- Self-organization
- Molecular recognition
- Complementarity of interactions and geometric compatibility
- Principle of "key-lock"
- High selectivity etc...

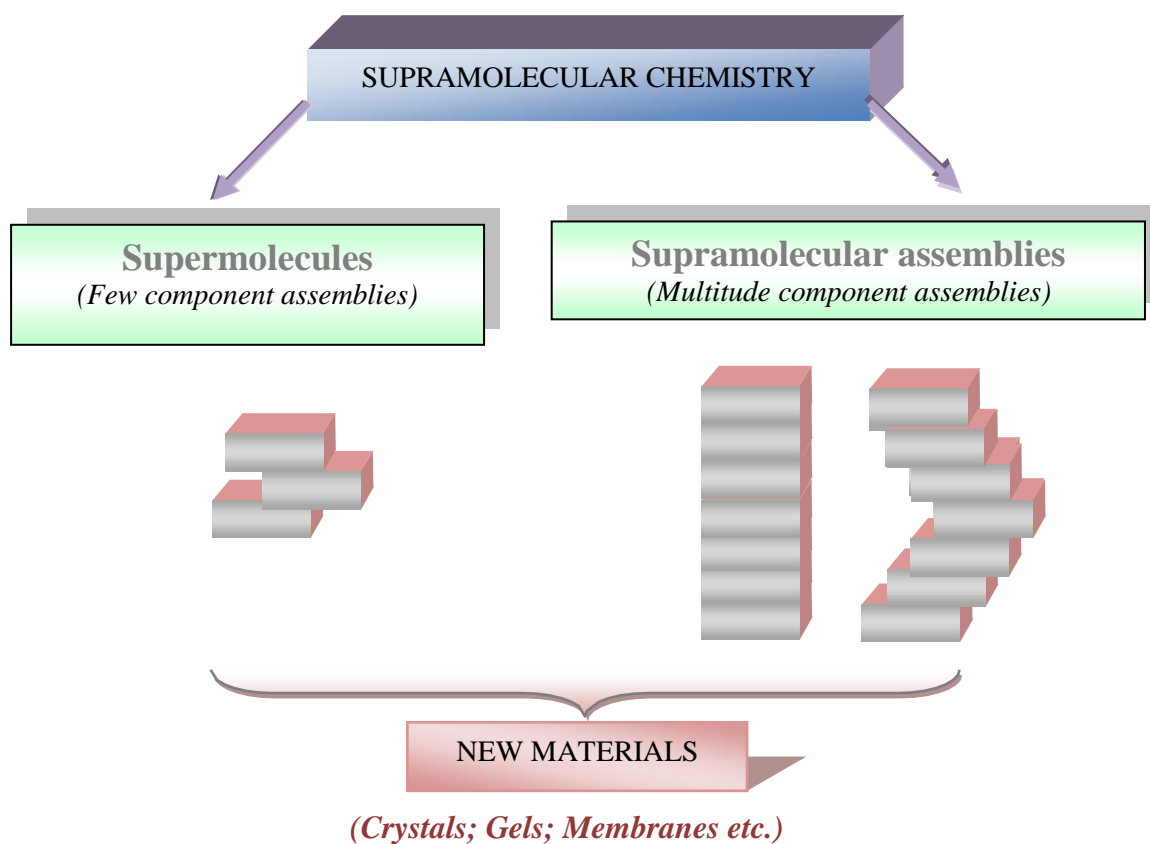


Figure 2. Schematic representation of the influence of supramolecular chemistry for the preparation of various new materials *via* self-assembly processes.

This area beyond the boundaries of classical chemistry is dedicated to the study of the structures and properties of supramolecular assemblies. The main principle of supramolecular chemistry relies on almost exclusively non-covalent interactions: hydrogen bonding, electrostatic interactions, hydrophobic forces, etc. which will be discussed below (§ II 1. of this chapter).

Dealing with our project, we intend to describe the field of “*Crystal Engineering*”, as a subdomain of supramolecular chemistry.

II The Crystal engineering approach

Molecular crystalline solid matter focuses on molecular components (such as atoms, molecules or ions) organized as periodic highly ordered architectures resulting from specific interactions between components composing the crystal. There are various scientific disciplines dealing with the study of crystalline structures. For example, crystallography is dedicated to crystals, their structure, origin and properties, while crystal chemistry studies the relationship between the chemical composition of a substance and its physical and chemical properties. In our project, we are interested in another area of research on crystalline materials, namely, “*crystal engineering*”.

The engineering of molecular crystals, the organized part of the solid-state matter, in which metal centres are linked by organic ligands containing coordinating groups, is a promising branch of supramolecular chemistry. The aims and goals of *crystal engineering*, which can also be called “crystal synthesis”, are the design of crystalline structures by using molecules as building blocks or tectons. This domain may also be defined as the art of designing and synthesizing functional solid-state structures which may contribute to the development of molecular materials displaying specific properties.¹¹

While *Supramolecular Chemistry* controls the building of highly ordered supramolecular assemblies with programmed structures and properties both in the solid and in the liquid state, *Crystal Engineering* focused on the self-assembly in the solid-state and particularly on ordered crystalline phase. Crystal engineering has grown and developed over the past 50 years as a natural result of the interactions between crystallography and chemistry.¹² Crystal engineering deals with the understanding and mastering of intermolecular interactions in the context of the crystal packing and their use to build new solids with desired physico-chemical properties,¹³ enhancing the *structure-properties relationships*. The subject of crystal engineering goes beyond the traditional divisions of organic, inorganic, and physical chemistry.¹⁴

In order to reach a high diversity of chemical structures in the field of coordination polymers through a crystal engineering approach, the key parameters are, among many features: a judicious design of the organic ligand, the nature of the metal, the nature of the solvent and counterions.¹⁵ Such control allows to reach a high diversity of architectures presenting, in principle, different applications. Through this approach, the chemistry of MOFs (*i.e.* metal–organic frameworks consisting of metal ions or clusters coordinated to organic ligands) has

produced a large number of molecular assemblies presenting porosity¹⁶, adsorption properties¹⁷, catalysis,¹⁸ luminescence,¹⁹ magnetism,²⁰ energy applications²¹ etc...

In the case of molecular chemistry, crystal engineering also results from processes associated with the earliest stages of association, the nucleation and finally the growth processes leading to the formation of single-crystals (crystallization process). Crystals, ordered matter may be analysed by X-Ray diffraction on single crystals. Crystal structures cannot be easily predicted from the knowledge of individual components.²² The interplay between kinetics and thermodynamics during the nucleation process and the difficulty to predict the structure of a crystal²³ represent a serious difficulty in modelling the structure of crystals. Spectroscopy²⁴ and calculation method²⁵ may provide partial answers to these questions. Simplification is required, ensured by the definition of representative kinetic units, called *supramolecular synthons*.²⁶

A reliable synthetic strategy for obtaining complex supramolecular crystalline architectures is to control the molecular recognition events (from the electrostatic and geometric point of view).²⁷ This leads to molecular networks presenting various dimensionalities, *i.e.* one-dimensional chains, (1D) two-dimensional networks planes (2D) or three-dimensional frameworks (3D), as shown in Figure 3. This will be used for the description of coordination networks obtained in this thesis (Chapter III).

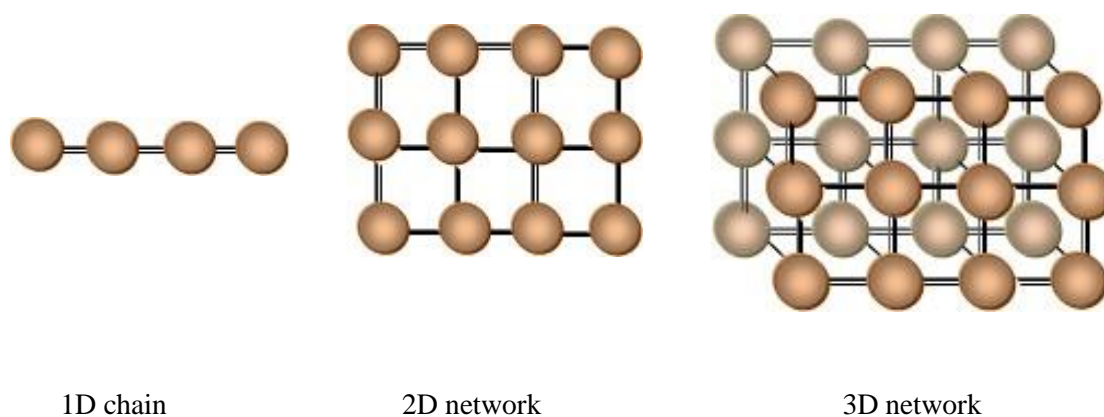


Figure 3. Schematic representation of 1-D, 2-D, and 3-D molecular networks formed upon molecular recognition processes based on predictable recognition patterns between the molecular components.

All of the above crystal structures are based on the use of non-covalent interactions which play an essential role in all molecular recognition processes and crystal engineering. They are described below.

II 1. Supramolecular interactions for crystal engineering

In the present work, we are focusing on the nature of the interactions between the molecular components, in particular, the formation molecular networks based on either hydrogen bonds or coordination bonds.

Contrary to hydrogen bonded networks, coordination networks or coordination polymers are formed mainly through coordination interactions and sometimes other concomitant weak non-covalent bonds, as shown in figure 4, among many available: Ion-Ion and ion-dipole interactions, hydrogen bond, dipole-dipole interactions, van der Waals interactions. There are also hydrophobic effects, metal bonds etc...

Each bond has its own energy being an average value of the gas-phase bond dissociation energies, according to IUPAC conventions. It is known that the energy of non-covalent interactions, as shown in Figure 4, is 1-2 orders of magnitude lower than the energy of the covalent bonds, while the coordination bonds together with electrostatic interactions ($50\text{--}350\text{ kJ/mol}^{-1}$) in its turn are stronger than hydrogen bonds ($4\text{--}120\text{ kJ/mol}^{-1}$), but at the same time, both types of bonding are stronger than the rest of the weak interactions. Intermolecular weak interactions and their subsequent use and influence during the formation of solid crystalline structures are of high importance in the arrangement of molecules in the solid state.

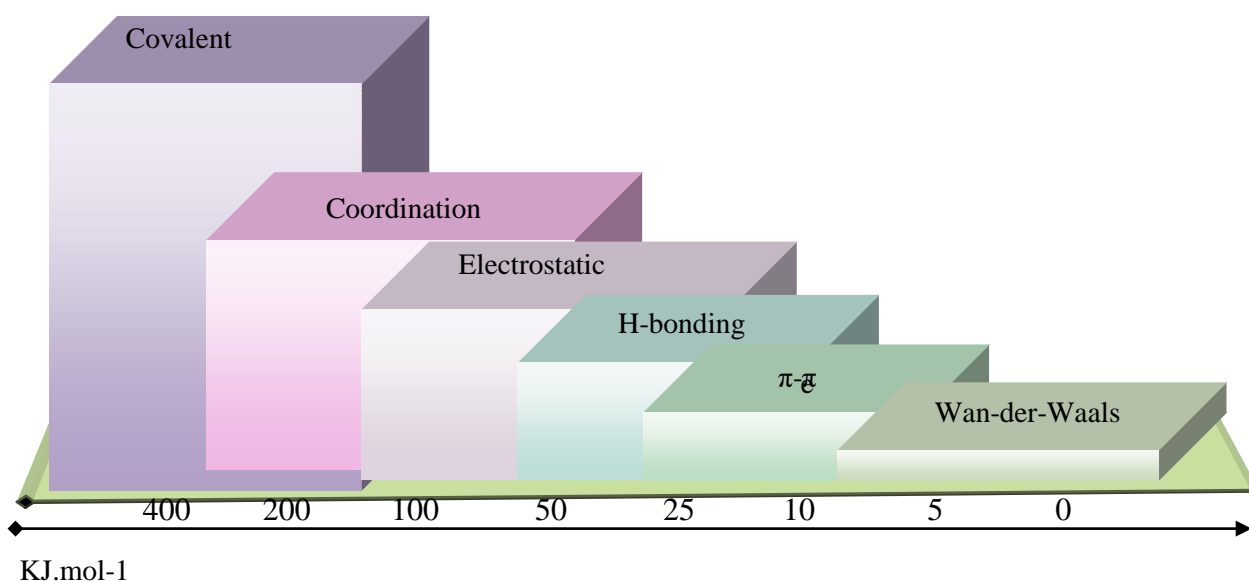


Figure 4. Schematic representation of typical non-covalent intermolecular interactions and their corresponding bonding energies.

Manipulating weak interactions (supramolecular interactions) can be used to control the

recognition pattern in solid-state crystalline structures. They can be considered as cooperative for the formation of metal-organic compounds and coordination polymers.²⁸

These supramolecular interactions are crucial for the formation of supramolecular assemblies in solution and in the solid-state. They will be detailed below and their relative energies are represented in figure 4. Coordination bonds will be discussed in §II 2. of this chapter.

Hydrogen bonds are often taking part in the formation of supramolecular systems²⁹ and play a particularly important role in the preparation of predefined crystalline structures, despite the fact that they are weaker than electrostatic bonds.³⁰ This can be explained by the fact that intramolecular hydrogen bonds are easily formed by proton transfer during the formation of the crystals. For its effectiveness, it is necessary that the interacting functional groups are properly oriented. Usually, hydrogen bond has an average equilibrium length of 2.8 Å and an energy of 5 kcal / mol. The distance between hydrogen bonded atoms (2.5-3.0 Å) is less than the distance characteristic for van der Waals interaction, but greater than the length of the covalent bonds. An example of chemical group involved in this work is carboxylic acid, engaged in the formation of 6 members ring through proton transfer frequently observed in the solid-state, as shown on Figure 5a. This is a reliable recognition mode between carboxylic acids.³¹ But, for this group, sometimes chains type architectures may be observed as shown on Figure 5b.

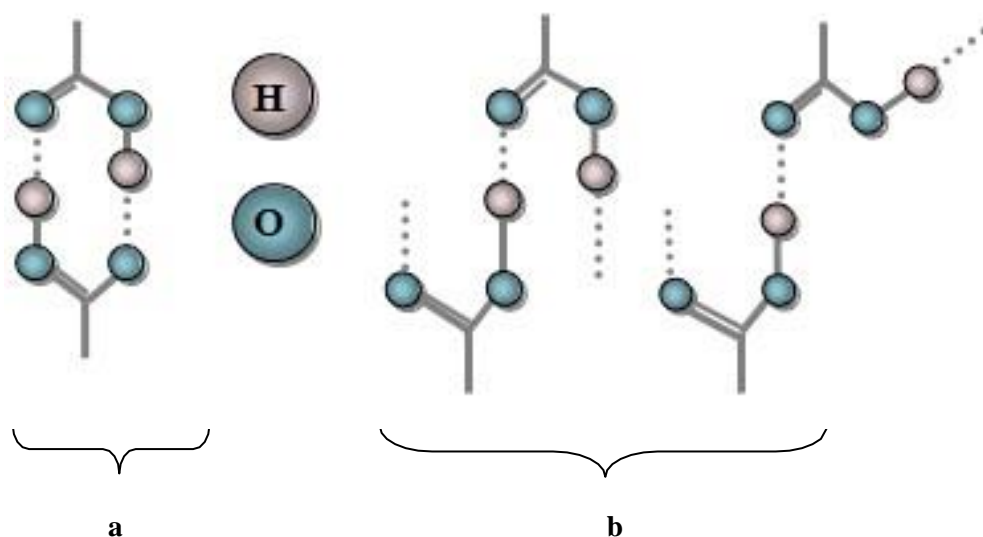


Figure 5. The representation of possible types of hydrogen-interactions between carboxylic/ate-groups: dimers (formation of a 6-members ring (a) or chain-type of interaction (b)).

The strength of H-bonds may be further enhanced by adding an electrostatic charge–charge component (charge-assisted Hydrogen bonding CAHB).³²

In a number of cases, the so-called **hydrophobic interaction** plays an important role in the formation of supramolecular systems.³³ It is related to the hydration structure around hydrophobic molecules. At the same time, the mechanism and nature of the hydrophobic interaction is still not fully understood.³⁴

π - π stacking is another type of typical non-covalent interactions observed in supramolecular systems, involving aromatic molecules and conjugated double bonds.

Electrostatic interaction makes a significant contribution to the formation of metal-ligand complexes. It becomes stronger in a more hydrophobic environment with a smaller dielectric constant. Dipole-dipole and dipole-ion interactions play important roles in neutral environment instead of electrostatic interactions.

The attractive forces acting between any pair of electrically neutral atoms or molecules are called the **van der Waals forces**, which can be observed in all types of the molecules.⁵³ Numerous van der Waals interactions provide a strong contribution to the processes of molecular recognition, despite the fact that when isolated, they are insignificant. van der Waals interactions is a short-range interaction with the energy equal to nearby 0.2 kcal.³⁵

These are the main examples, but other interactions may also be considered. Concerning our project, as already mentioned, we will focus below on the formation of coordination polymers.

II 2. Metal-organic compounds and coordination polymers.

Significant progresses in the study of metal-organic compounds are associated with the development of supramolecular coordination chemistry and crystal engineering, which were discussed above (§ I and II).

Infinite coordination polymers³⁶ exist due to the relatively weak and reversible coordination bond which allows self-repairing processes. These architectures are controlled by the geometry of binding sites, their number and their orientation in both organic ligand,

presenting coordinating sites, and the metal cation (or complex). Crystalline synthetic strategies are similar to classical chemical experiments, with some slight differences: the first step focuses on the molecular design of organic building blocks or tectons by classical molecular synthesis and in a second step, the synthesized building blocks are organised in the solid state, as shown in Figure 6, in order to obtain the crystalline materials with the targeted characteristics. The construction event takes place by self-assembly processes.³⁷ This process will be presented in Chapter III.

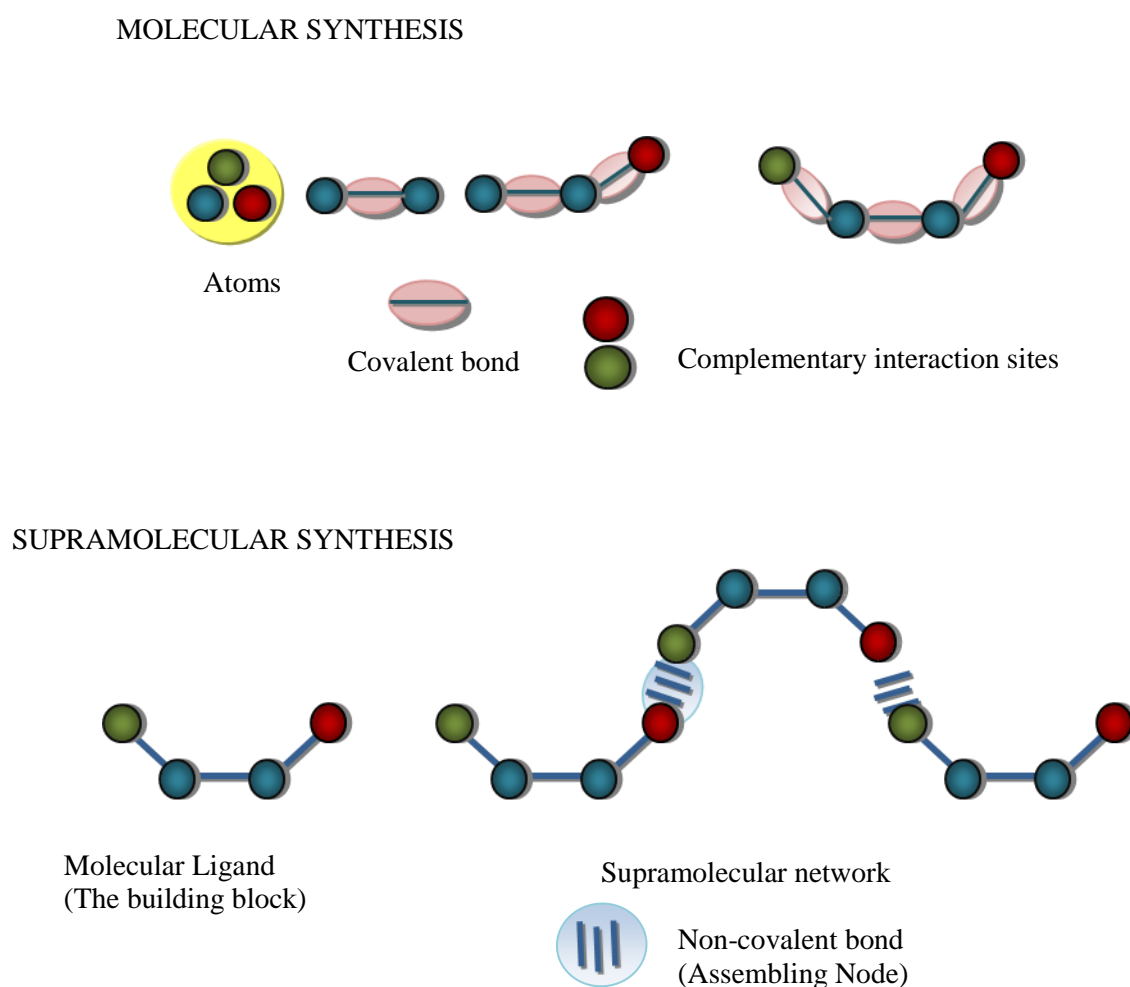


Figure 6. Schematic representation of two steps of molecular-crystal synthesis for the formation of coordination polymers based on two components.

For the formation of coordination polymers, beside the use of simple organic ligands bearing coordinating groups, macrocyclic compounds are of interest: families of potential macrocyclic ligands for the formation of coordination polymers are resorcinarenes,³⁸ crown-ethers and cryptands,³⁹ porphyrines,⁴⁰ cyclodextrins,⁴¹ cyclophanes⁴² and cyclacenes⁴³ etc.

In this work, we intend to use a rarely explored family of macrocyclic ligands:

metacyclophanes. Metacyclophanes (including calixarenes, that will be considered in §III 1. of this chapter) have attracted considerable attention in recent decades, due to the diversity of their structures and properties, which allows the formation of a large number of coordination networks and MOFs.

In the coming chapter, we will focus on the use of metacyclophanes for the formation of coordination polymers.

III Metacyclophane type macrocycles

Metacyclophane describes a family of macrocyclic compounds for which an aliphatic chain connects different aryl moieties. Typically, such chemical structures are called [n] metacyclophanes, where n is the number of carbon atoms in the aliphatic chain. An interesting fact is that the shorter is the bridged aliphatic chain, the stronger is the ring deformation, and consequently leading to a decrease of stability. For example, instead of a flat conformation, the benzene ring is forced to exist in a twisted boat conformation for the [6]meta- (a) and [6]paracyclophanes, as shown on Figure 7.



Figure 7. Representation of conformations of [6]meta- (a) and [6]paracyclophanes (b).

The number of carbon atoms in the connecting bridges affects the geometry and the chemistry of these macrocyclic compounds. For example, compounds possessing long aliphatic bridges ($> 3\text{C}$, for example), leads to structures analogue of simple open chain.⁴⁴ The [2,2]metacyclophane⁴⁵ (in solution Figure 8, a and in the solid-state Figure 8, b) is one of the representatives of this family.

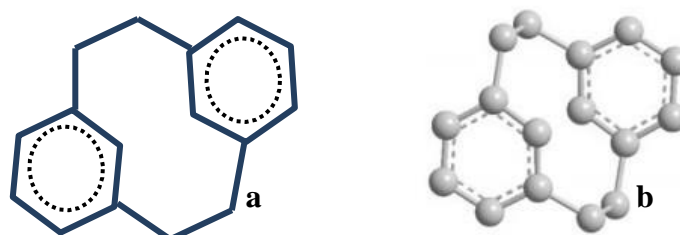


Figure 8. [2,2]metacyclophane structure in solution (a) and in the solid state (b).

Related to our project, we will focus now on new compounds bearing four benzene rings and methylene bridges between them: calix[4]arenes.

III 1. Classical calix[4]arenes as analogues of the metacyclophanes together with corresponding coordination polymers

III.1.1. Generalities about calixarene

Another well-known macrocycles entities belonging to metacyclophane family is composed of Calixarenes,⁴⁶ obtained by condensation of phenol with aldehyde in the presence of base. The chemistry of these compounds has been intensively developed over the last 40 years. We will also focus on the family of symmetrical Calix[4]arenes, although other phenolic units have been also employed. Their availability (many calixarenes can be obtained by one-step synthesis), the presence of active reaction centres allowing the modification of their structure and their ability to form host-guest inclusion complexes with both charged and nonpolar molecules, have contributed to their tremendous development.⁴⁷

The term "calixarene" was introduced by C.D. Gutsche to characterize the shape of these cyclic tetramers (a "cup", "calix" in Greek meaning "bowl", "goblet").⁴⁸ Improvement of the "receptor ability" of calixarenes is achieved due to the functionalization of phenolic groups, aromatic rings and bridging fragments of the initial macrocycles with suitable organic reagents; therefore, they are widely used as a molecular platform for creating spatially preorganized three-dimensional receptors capable of molecular recognition of complex chemical objects. Due to rotation around the C-C bonds, Calix[4]arenes can adopt four different conformations such as *cone*, *1,2-alternate*, *1,3-alternate* and *partial cone* as shown in Figure 9. The *cone* conformation is the most stable due to the presence of stabilizing hydrogen bonds.

Before mentioning the complexation properties of calixarenes, it should be noted that many reports related to the use of calix[4]arene in supramolecular chemistry and crystal engineering describing: the chirality,⁴⁹ porosity,⁵⁰ complexes with various macromolecules from other macrocyclic families such as crown ethers,⁵¹ fullerenes,⁵² porphyrines,⁵³ cyclodextrins⁵⁴ etc. Also there were reported cluster formation⁵⁵ and the possibilities of chelation⁵⁶ have been published. At the same time, there are also information on metallacalix[4]arenes,⁵⁷ with potential ionophoric properties.⁵⁸ The conformational features of

calix[4]arene derivatives has been documented.⁵⁹ In particular, its *1,3*-Alternate conformation. The latter is of particular interest to our project, since our target ligands based on [1111] metacyclophane backbone predominantly adopt the *1,3*-alternate conformation over a wide range of temperatures (60°C to 150°C).⁶⁰

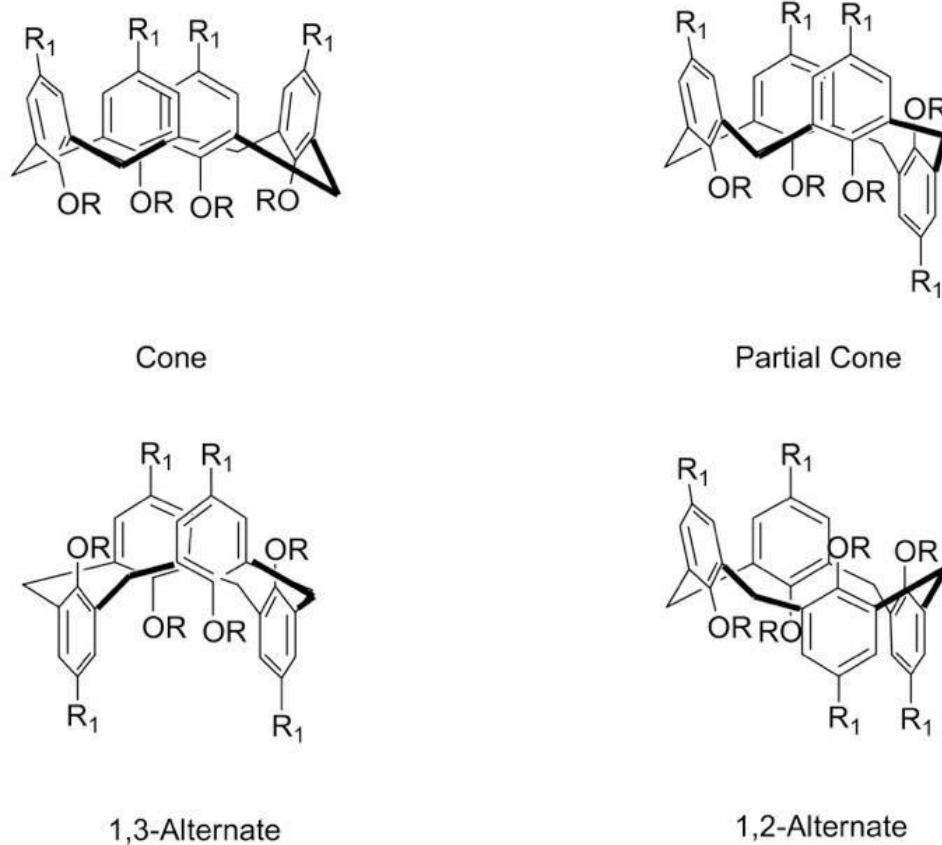


Figure 9. Representation of four possible conformations of *para*-*tert*-But-calix[4]arene.

A variety of coordination compounds based on calix[4]arene derivatives has been investigated. Some interesting examples of coordination compounds⁶¹ and coordination polymers⁶² based on calix[4]arene derivatives bearing *cyano*, *carboxylato*, *mercapto* and *phosphonato* coordinating groups is briefly described below.

This survey inspiring for the design of the new ligands based [1111]metacyclophane, for the generation of extended coordination polymers and supramolecular networks (see Chapter II).

III 1.2. Examples of coordination networks with calix[4]arene

Example of coordination compounds based on calix[4]arene derivative bearing *carboxylato*-, *cyano*-, *mercapto*- and *phosphonato*- coordinating group are presented below. The description will begin with the use of carboxylic/ate groups (*LX*, *LY* and *LZ*), then cyano (*LN*), phosphonato (*LP*) and thiol (*LS*) coordinating groups.

Burrows *et al.* reported the upper rim-functionalised calix[4]arene dicarboxylic acid which has been used for MOFs preparation displaying channels.⁶³ The calix unit adopts a *cone* conformation. It means that the aforementioned compound may be employed as a molecular component offering a cavity. The network formation by the dicarboxylic calix[4]arene derivative bearing propylene chains at the lower rim (*LX*) in the presence of copper (II) cations in DMF, $[\text{Cu}_2(\text{LX})_2(\text{DMF})_2]$. The crystal does not exhibit channels. Its combination with Cadmium cation leads to the formation of a 3D network $[\text{Cd}_2(\text{LX})_2(\text{DMF})_2]$ as shown in Figure 10.

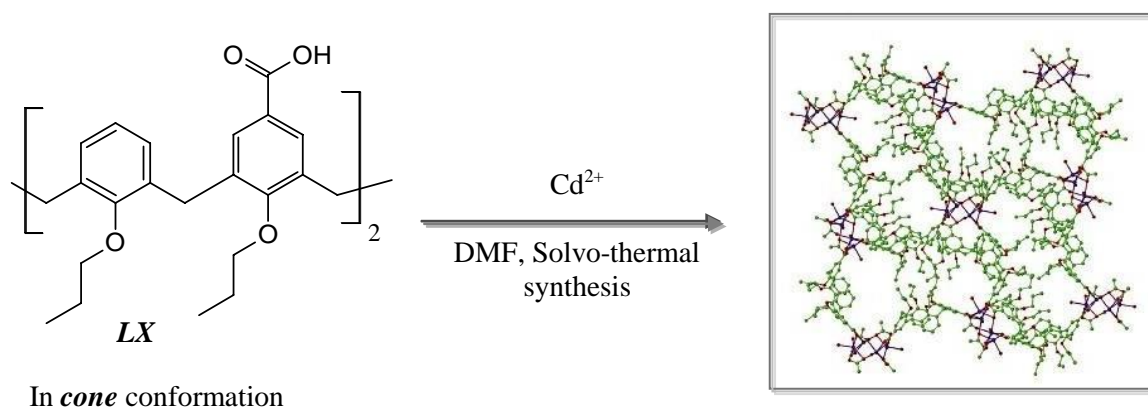


Figure 10. A portion of the porous networks composed of calix[4]arene dicarboxylic derivative (*LX*) in *cone* conformation and Cd^{2+} cation in DMF, presenting the following formula $[\text{M}_2(\text{LX})_2(\text{DMF})_2]$ ($\text{M} = \text{Cd}$).⁶³

Using this ligand, other crystal structures were reported for combinations of **LX** with Zn^{2+} or Co^{2+} leading to two coordination networks of formula $[\text{Co}_5(\text{LX})_4(\text{OH})_2(\text{H}_2\text{O})_4] \cdot 8\text{DMF}$ and $[\text{Zn}_2(\text{LX})_2(\text{DMF})_2]$.⁵⁸

Dalgarno *et al.* reported coordination compounds for four disubstituted *p*-Carboxylatocalix[4]arenes⁶⁴ (**LY**) in *cone* conformation for which two types are represented on scheme 1. **LY** forms a 1D or a 3D coordination polymer (Figure 11(a)) as well as capsules (Figure 11(b)) *via* combination with the cadmium cation (II) and 1,10-phenanthroline (Phen) as the co-ligand in DMF solution under solvo-thermal conditions.

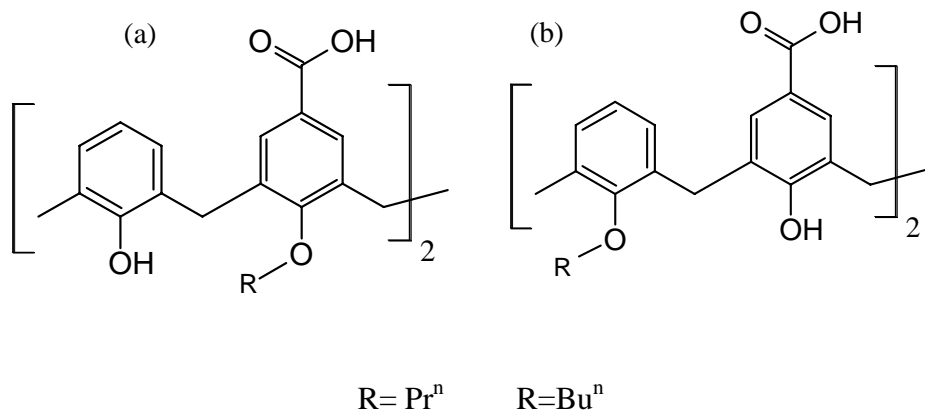


Figure 11. Type I (a) and II (b) of **LY** compounds.⁶⁴

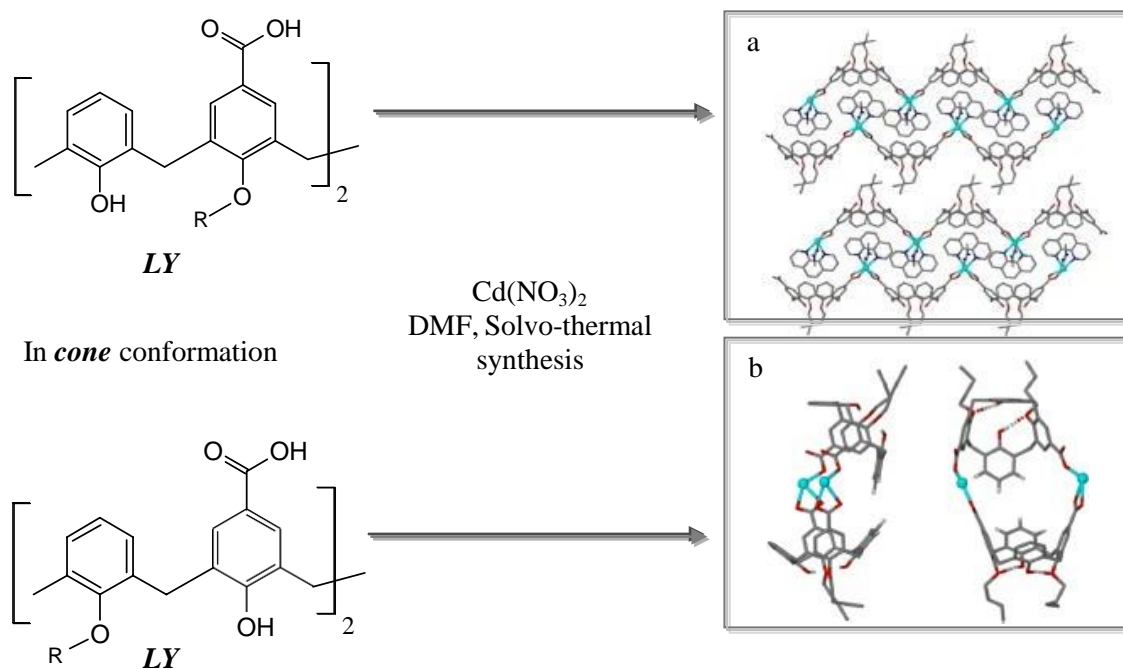


Figure 12. Some portion of X-ray structures of 1D coordination polymer of formula $[\text{Cd}(\text{LY})(\text{Phen})(\text{H}_2\text{O})_{0.5}(\text{DMF})_{0.5}](\text{H}_2\text{O})_{0.5}(\text{DMF})_{0.5}$ (a) and capsule (b) formed upon combination of **LY** two types with cadmium(II) nitrate and Phen as ancillary ligand in DMF.⁶⁴

Moreover, a related 3D coordination network of formula $[\text{Cd}_2(\text{LY})_2(\text{DMF})_2](\text{DMF})_3$ was also reported⁶⁴ which accounts for the fact that the introduction of small alkyl groups around the ligand framework controlling the metal directed assembly.

All the work on coordination networks presented above is based on the use of disubstituted calix[4]arene with coordinating carboxylic ligands located at the upper rim and in *cone* conformation. Dealing with our project, we have investigated tetrasubstituted [1111]metacyclophanes in *1,3*-alternate analogues of tetrasubstituted calix[4]arene.

Park *et al.* reported a lower-rim carboxylic-functionalized calix[4]arene **LZ**, in *1,3*-alternate conformation, without *tert*-butyl groups, and its capacity to form 3D coordination polymers when combined with $\text{Pb}(\text{NO}_3)_2$ in DMF under solvothermal conditions $[\text{Pb}_2(\text{LZ})](\text{DMF})_2$ (Figure 13, (a)).⁶⁵ This compound exhibits a single-crystal to single-crystal transformation upon removing the solvent molecules (Figure 13 (b)).

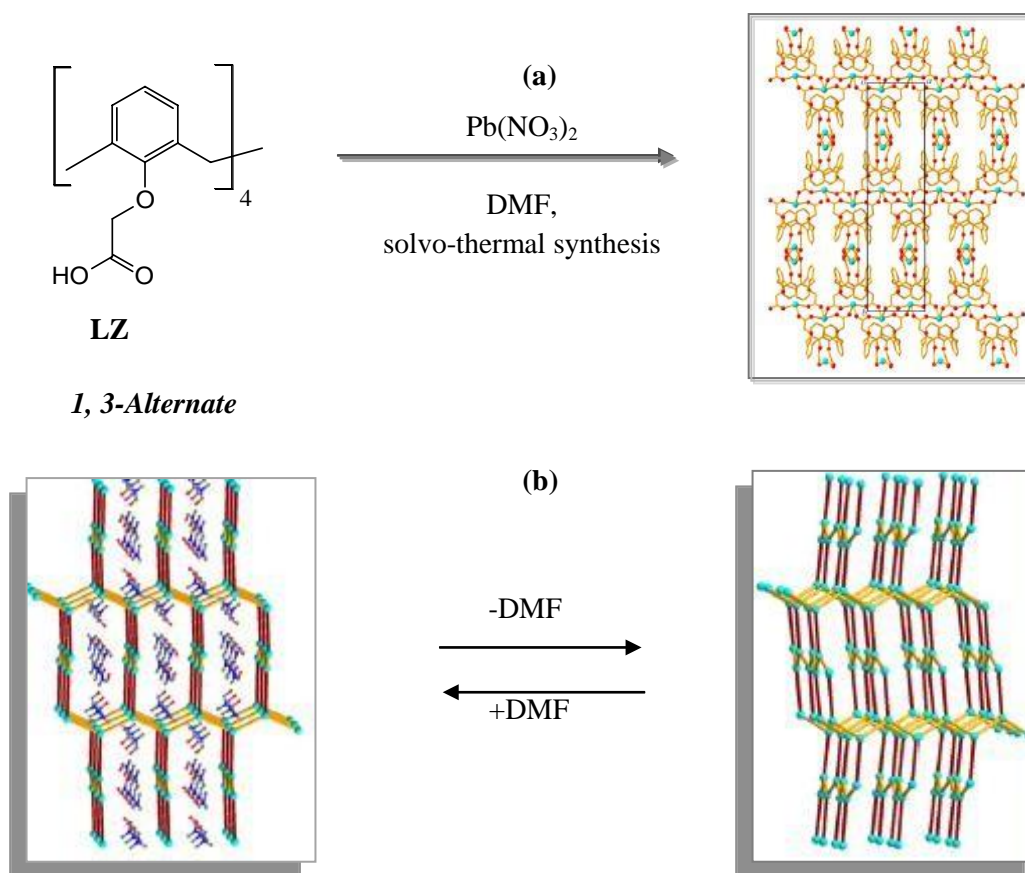


Figure 13. X-Ray crystal structure of a 3D porous coordination network $[\text{Pb}_2(\text{LZ})](\text{DMF})_2$ (a) and crystal structure transformation after removal of the DMF solvent molecules (b).⁶⁵

In the literature, there are other examples of coordination polymers based on carboxylato derivatives of calix[4]arene.⁶⁶ While ligands in *cone* conformation (**LX** or **LY**) provide 1D coordination networks with selected metals (and in some conditions 3D), **LZ** adopting the *1,3-alternate* conformation forms a 3D coordination network when combined with Pb^{2+} . In Chapter III, we will present the abilities of [1111]metacyclophane derivatives to form high dimensional coordination polymers.

The porous properties of such assemblies, especially by carboxylato derivatives of thiacalix[4]arene with transition metal ions and also ancillary ligands, have been reported, revealing low surface area but a good selectivity.^{50,67}

The coordination abilities of calix[4]arene bearing coordinating cyano groups has also been reported.⁶⁸ This groups presents a special affinity towards silver cations. For example Atwood *et al.* reported a tetracyanocalix[4]arene derivative decorated with benzyl ester at the lower rim, adopting a *cone* conformation. The latter ligand forms a linear 1D chain in the

presence of AgPF_6 in acetonitrile with a ligand:metal stoichiometry of 1:1.⁶⁹

Another example has been provided by Hosseini *et al.*, that showed that tetracyanocalix[4]arene *LN* decorated with methyl-ethyl ester moieties at the lower rim forms a linear 1D non-tubular chains of formula $(\text{LN})\text{AgAsF}_6 \cdot 2\text{H}_2\text{O} \cdot \text{CH}_3\text{CH}_2\text{OH}$ where the tetracyanocalix[4]arenes are located in a head-to-tail fashion, as shown in figure 14.^{68a}

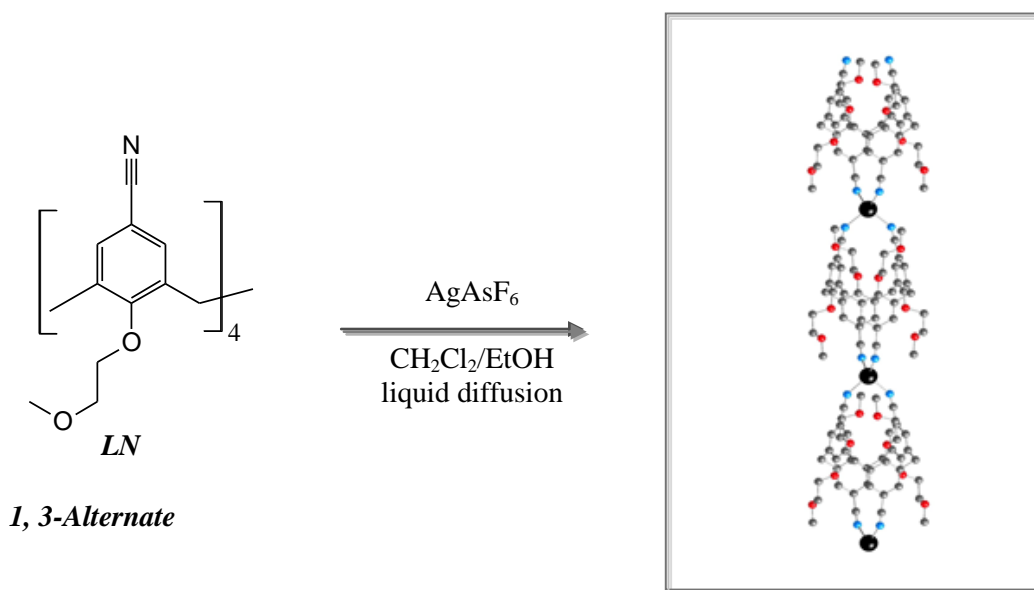


Figure 14. X-ray structure of two parallel linear $(\text{LN})\text{AgAsF}_6 \cdot 2\text{H}_2\text{O} \cdot \text{CH}_3\text{CH}_2\text{OH}$ coordination networks obtained by the combination *LN* of with AgAsF_6 .^{68a}

Concerning phosphonated calixarene, several examples of coordination networks based on calix[4]arene have been reported.⁷⁰

Raston *et al* reported the complexation of *p*-phosphonated calix[4]arene in *cone* conformation *LP* with sodium ions, presenting the following formula $[\text{LP} \cdot \text{DMF} \cdot 5\text{Na}^+ \cdot n\text{H}_2\text{O}]$.⁷¹ Bilayers are formed and columnar arrays with Na^+ clustering above the calixarene cavity (complex 2) together with the bridging water molecules, “gluing” DMF molecules, as shown in figure 15. Using other synthetic conditions and imidazolium moieties (MZ, 1-ethyl-3-methylimidazoliums), a layered compound of formula $[\text{LP} \cdot 2\text{MZ} \cdot \text{CO}_3^{2-} \cdot \text{OH}^- \cdot 9\text{Na}^+ \cdot m\text{H}_2\text{O}]$ (Figure 15(b)) was obtained.

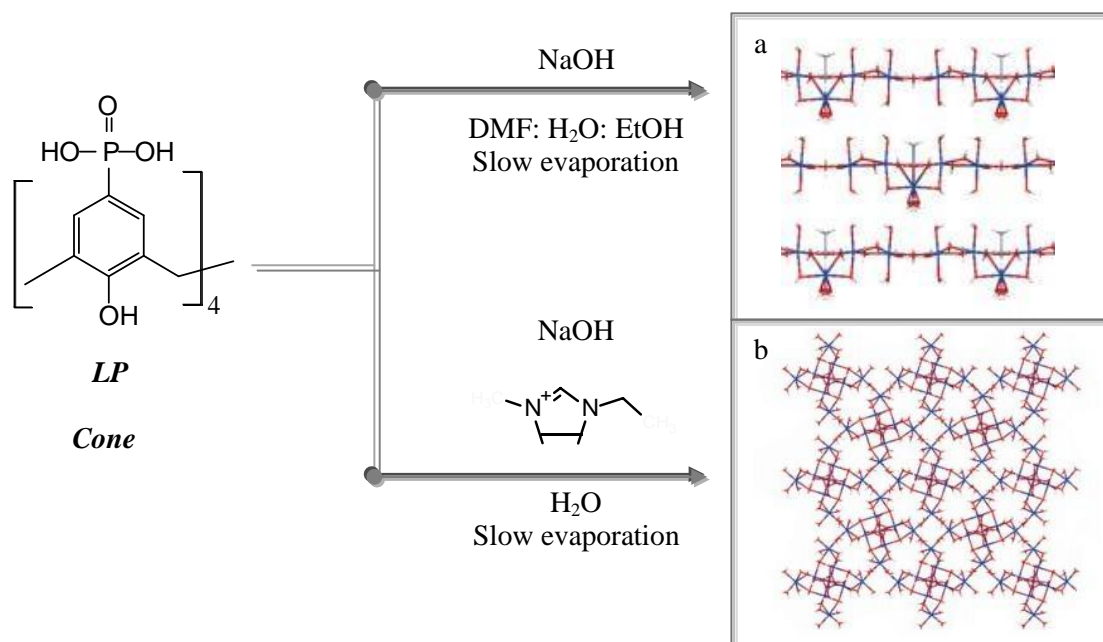


Figure 15. Extended layered networks obtained with **LP** and sodium cations.⁷¹

All the described phosphonate derivatives of calix[4]arene platform adopt the *cone* conformation, while in our project, as previously mentioned, it is planned to create phosphonato-metacyclophanes in the *1,3*-alternate conformation in order to obtain coordination networks with higher dimensionality. Furthermore, the phosphonate group, according to HSAB theory,⁷² should be well adapted for the binding of lanthanide cations: we plan to investigate the complexing abilities of [1111]metacyclophanes tetrasubstituted with phosphonato coordination centres to bind lanthanide cations.

Another investigated coordinating group appended to calix[4]arene for the formation of coordination networks is, as already mentioned, the thiol group. Hosseini *et al.* published the formation of a binuclear complex **LS**-Hg₂ of *p*-tert-butyl-tetramercaptocalix[4]arene **LS** in *1,3*-alternate conformation with mercury cation as shown in figure 16.⁷³

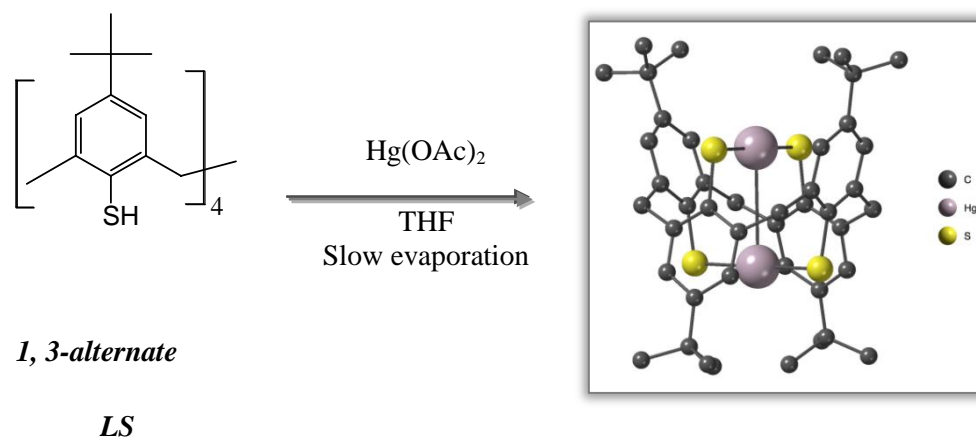


Figure 16. Molecular structure of the binuclear complex $LS\text{-Hg}_2$.⁷³

LS possess two types of interaction sites due to its *1,3*-alternate conformation: “soft” and strong SH-coordination sites and “soft” but weak aromatic rings which also participate in the binding processes.

Concerning our project, we designed a new ligand based on the [1111]metacyclophane platform bearing mercapto groups (thiol) using the methylene spacers. In a previous reported example the mercapto groups are attached directly to calix[4]arene platform. It is interesting to evaluate how the change of the macrocyclic platform from calixarene to metacyclophane as well as the increase in the distance between the mercapto group and the aryl rings may affect the binding process.

All these data, based on calix[4]arene analogues, motivated us to investigate the coordination abilities of tetrasubstituted [1111]metacyclophane derivatives displaying a stable *1,3*-alternate conformation. Thus, 10 new ligands have been designed and synthesised. They are presented in chapter II.

In the next section we will present the [1111]metacyclophane backbone and derivatives mainly synthesized by Hosseini group.

III 2. [1111]Metacyclophanes as a representatives of metacyclophane family.

Macrocyclic [1111] metacyclophane derivatives have been mainly studied over the last 30 years. While the type of aliphatic bridge and aromatic moiety have a considerable effect on the reactivity of the [n,n]cyclophanes,⁷⁴ for [1111]metacyclophane, **LH**, the presence of methyl groups located in *ortho* positions on the phenyl rings imposes, for steric reasons, considerable structure restriction. Indeed, the macrocycle, presented in figure 17, adopts only one stable *1,3-alternate* conformation under a wide range of temperatures in solution, and in the solid state.⁶⁰

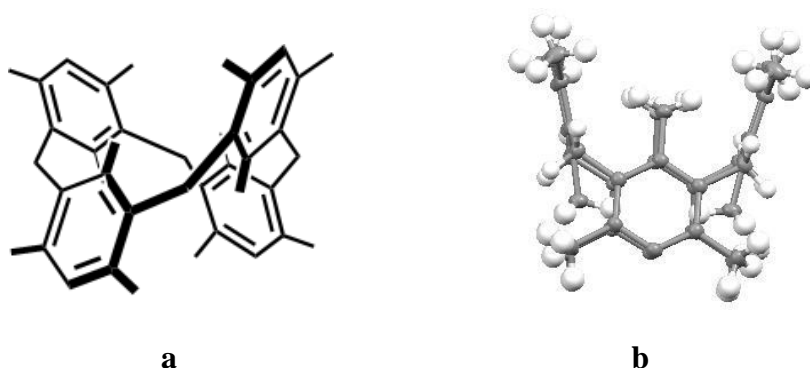
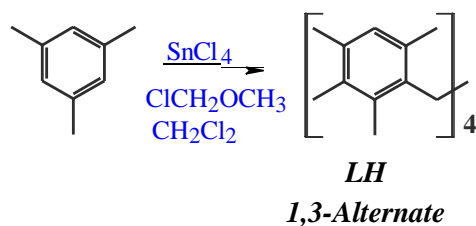


Figure 17. The structure of [1111] metacyclophane **LH** backbone composed of four benzene rings and methylene bridges between them (a) and its structure in the crystalline state (b).⁶⁰

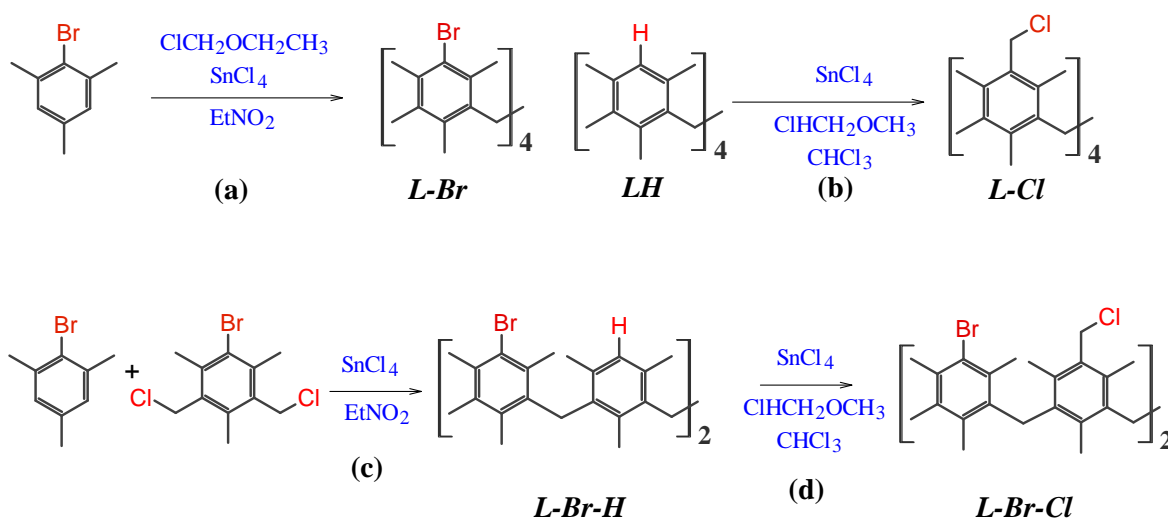
[1111]Metacyclophane **LH** was synthesized several decades ago by a condensation reaction for which four mesitylene fragments were linked by methylene bridges.⁷⁵ For such compound, the introduction of methyl substituents disturbs the rotational process of the macrocyclic ligands and blocks its conformation. Classical unsubstituted [1111] metacyclophane (general notation herein **LH**) can also be obtained by condensation of mesitylene and chloromethyl methyl ether in the presence of tin chloride in methylene chloride (scheme 2).⁷⁶



Scheme 2. The synthesis⁷⁶ of [1111] metacyclophane backbone **LH** composed of four benzene rings and methylene bridges between them.

¹H-NMR (CDCl₃) spectrum of [1111] metacyclophane is characterized by: a singlet for the *ortho* and *para* methyl substituents (2.34 ppm and 1.19 ppm respectively) and also a singlet for protons of the aromatic rings and methylene bridges (6.80 ppm and 3.89 ppm respectively). The *1,3-Alternate* conformation can be immediately deduced by ¹H-NMR data.

For the formation of [1111]metacyclophane derivatives substituted with coordinating groups, two important [1111]metacyclophane derivatives as precursors were described: tetrabrominated (general notation herein **L-Br**) and tetra chloromethylated (general notation herein **L-Cl**) compounds. The chemical structures and the synthesis of tetrasubstituted **L-Cl**^{60,77} and **L-Br**^{76,77} and are shown below on Scheme 3. One can also mention the precursors for the synthesis of di-substituted derivatives di-brominated (herein **L-Br-H**) and the dichloromethylene dibromo (herein **L-Br-Cl**) derivatives.⁷⁸



Scheme 3. The synthesis of tetrabromo **L-Br** (a) and tetrachloromethylen **L-Cl** (b) derivatives of [1111] metacyclophane precursors.^{76,77,78}

III 3. [1111]Metacyclophanes: macrocyclic ligands for the formation of coordination networks

III 3.1. Ligand design

It is well established, that the complexation propensity of calixarenes depends on numerous factors such as the size of the cavity and of the guest, surface charge density, structural rigidity of host and guest, spatial arrangement of the donor atoms, molecular symmetry, and the nature of substituents. By analogy, it is reasonable to assume that the same factors holds for [1111] metacyclophanes derivatives.

Thereby, before we have initiated the design and synthesis of new [1111]metacyclophane based derivatives, we did a survey of the literature. The majority of published dealing with [1111]metacyclophanes were published by the group of Hosseini. This group has reported several examples of [1111]metacyclophanes bearing (N,O) donor coordination sites and their combinations with metal cations leading to the formation of coordination polymers.

Before taking into account the coordination abilities of [1111]metacyclophanes, we have to mention the “non-coordinating” chemical modifications of the macrocyclic backbone such as tetrasubstitution with appending chiral and diethylphosphonate groups,⁷⁹ formation of doubly crowned metacyclophane and Schiff base,⁸⁰ modification by a nitroxide,⁸¹ tetrasubstitution for some organic anions recognition,⁸² combination with the classical calix[4]arenes.⁸³

Recently, in a review article, Ferlay and Hosseini reported that, in the last 20 years, the [1111]metacyclophane platform has been chemically modified⁸⁴ in order to obtain macrocyclic coordinating ligands that may be combined with various d- and f- metal cations for the formation of new coordination polymers and supramolecular networks in the solid-stat. The reported tectons based on tetrasubstituted [1111]metacyclophane bearing carboxylato⁷⁷, nitro,⁷⁷ thiomethyl⁷⁷, aldehyde⁷⁷, amino⁷⁷, diphenylphosphoryl⁷⁷, diphenylphosphanyl⁷⁷, bipyridyl⁸⁵ and quinolinyl⁸⁵, thiol,⁸⁶ appended groups. With these compounds, no coordination networks have been reported.

Other N-donor coordinating groups have been used for di- and tetra-substituted ligands based on [1111]metacyclophane^{76,78,87,88,89,90,91} together with the formation of coordination

polymers or coordination complexes in some cases. These will be detailed below. Each of these types (di and tetrasubstituted) of ligands displays its own peculiarities concerning the synthesis and the formation of coordinating compounds.

Concerning the *di*-substituted [1111] metacyclophanes, four different ligands decorated with nitrogen donor binding centres were designed: cyano (*LC2*), pyridyl (*LP-d2*), imidazolyl (*Lim2*), and pyrazolyl (*LP-z2*). The coordinating groups are located on the same side of the macrocyclic ring. For these ligands, when starting with *L-Br-Cl* precursors, the other side of the macrocyclic ring decorated with bromine atoms (*Lim2* and *LP-z2*); The ligands, together with their brief synthetic pathways are depicted in Figure 18.


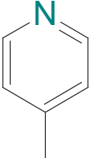
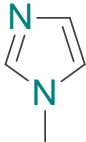
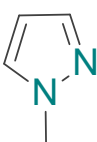
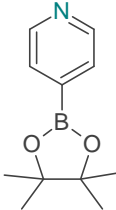
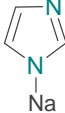
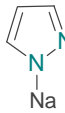
Coordination groups (<i>di</i> -substitution)			
Cyano-	Pyridyl-	Imidazolyl-	Pyrazolyl-
<i>LC2</i> 	<i>LP-d2</i> 	<i>Lim2</i> 	<i>LP-z2</i> 
General synthetic pathway			
<i>L-Br-H</i> CuCN DMF ↓ <i>LC2</i>	<i>L-Br-H</i> Pd(PPh ₃) ₄ Cs ₂ CO ₃ DMF/ Toluene ↓ <i>LP-d2</i> 	<i>L-Br-Cl</i> NaI DMF ↓ <i>Lim2</i> 	<i>L-Br-Cl</i> NaI DMF ↓ <i>LP-z2</i> 

Figure 18. Schematic representation of coordination sites of di-substituted ligands based on [1111]metacyclophane together with the general synthetic pathways.⁸⁴

Concerning the *tetra*-substituted ligands, five different ligands decorated with nitrogen donor binding centres were designed: (cyano (*LC4*), pyridyl (*LP-d4*), imidazolyl (*Lim4*), and pyrazolyl (*LP-z4*). Furthermore, ligands decorated by two different binding sites located on the same platform (*LP-dz*) have been also described.⁸⁴


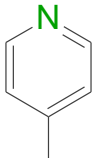
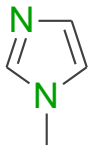
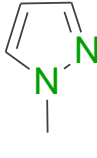
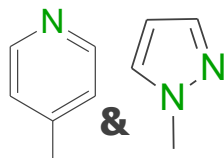

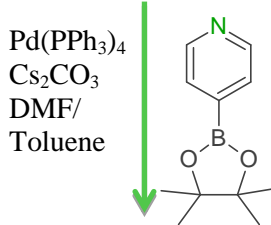
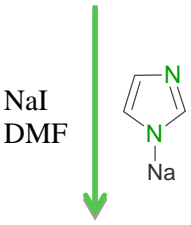
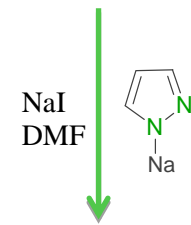
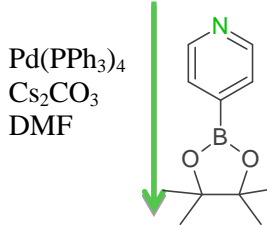
Coordination groups (<i>tetra</i> -substitution)				
Cyano-	Pyridyl-	Imidazolyl-	Pyrazolyl-	Dipyridyl- and Dipyrazolyl-
				
LC4	LP-d4	Lim4	LP-z4	LP-dz
General synthetic pathway				
<i>L-Br</i>	<i>L-Br</i>	<i>L-Cl</i>	<i>L-Cl</i>	<i>LP-z2</i>
				
LC4	LP-d4	Lim4	LP-z4	LP-dz

Figure 19. Schematic representation of coordination sites of tetra-substituted ligands based on [1111]metacyclophane together with their general synthetic pathways.⁸⁴

It is worth noting that all these 9 macrocyclic entities based on [1111]metacyclophane have been reported by Hosseini *et al.*⁸⁴ Their complexation property and the formation of networks are discussed below. Before that, their synthesis, schematically represented in figures 19-20 are presented and commented.

III 3.2. Synthesis of the ligands

Various synthetic strategies have been used to obtain *LC2*, *LP-d2*, *Lim2*, *LP-z2*, *LC4*, *LP-d4*, *Lim4*, *LP-z4* and *LP-dz*. As mentioned earlier, condensation reactions were performed with chloromethyl methyl ether in the presence of tin chloride to obtain the precursors *L-Br*, *LH*, *L-Cl*, *L-Br-H* and *L-Br-Cl* (see Scheme 3). The reaction requires at least 12 hours (see the experimental part) and proceed with rather high yield (> 60 %).

Once the precursors prepared, either a nucleophilic substitution reactions was performed which proceeded with a high yields (>70%), or Suzuki cross-coupling reactions involving a boronic ester derivative which afforded *LP-d2*, *LP-d4* and *LP-dz* (see figures 18-19) with the less but acceptable yields (30-40%). For the other ligands, condensation reactions were performed either using *L-Br* or *L-Cl* in the presence of either CuCN or NaI as catalysts (see figures 18-19). These reactions proceeded with 54% and 81% yields respectively.

III 3.3. Structural studies of the ligands

In principle, the symmetrical tetrasubstituted ligands in *1,3*-alternate conformation *LC4*, *LP-d4*, *Lim4* and *LP-z4* display six different isomers in the solid-state. These species differ by the orientation of the substituents with respect to each other.⁷⁶ For example, the secondary nitrogen atoms in the imidazole groups can be oriented towards the cavity (*i*) or outwardly (*o*). These isomers are *rotamers* and six of them are depicted in Figure 20. One may assume that in solution, the differentiation of the different rotamers is not possible at room-temperature due to low rotational barriers.

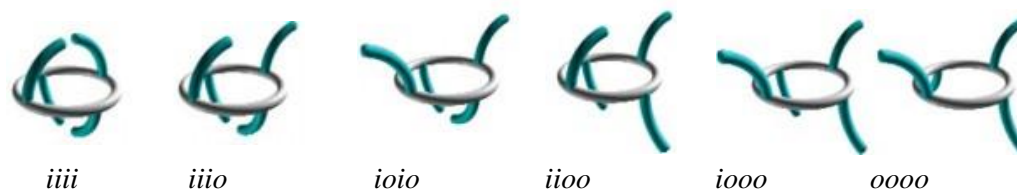


Figure 20. A set of six possible rotamers for the tetrasubstituted ligands *LC4*, *LP-d4*, *Lim4* and *LP-z4*.⁷³

It is worth noting that among the six rotamers, the *iiii* isomer could lead to the formation of *exo*- complexes.

Good quality single crystals of all ligands *LC2*, *LP-d2*, *Lim2*, *LP-z2*, *LC4*, *LP-d4*, *Lim4*, *LP-z4* and *LP-dz*, were obtained and their structure in the crystalline phase investigated by X-ray diffraction on single crystals.⁸⁵ Their crystal structures are presented below in Figure 21.

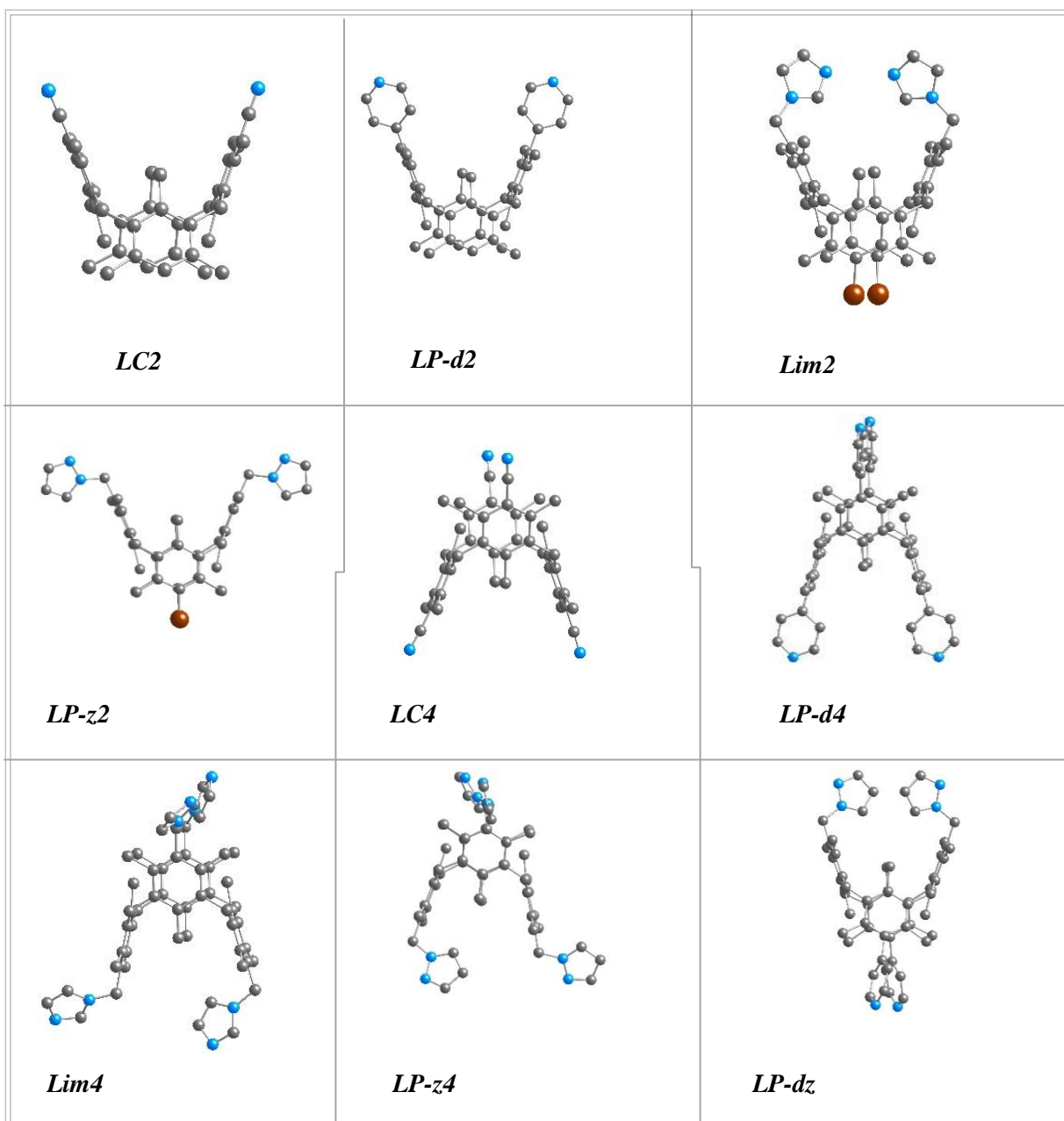


Figure 21. Crystal structure of the nine ligands *LC2*, *LP-d2*, *Lim2*, *LP-z2*, *LC4*, *LP-d4*, *Lim4*, *LP-z4* and *LP-dz* based on the [111]metacyclophane platform bearing N-donor coordinating sites.⁷⁶⁻⁹¹

III 3.4. Synthesis of coordination compounds

The coordination abilities in the solid-state of *LC2*, *LP-d2*, *Lim2*, *LP-z2*, *LC4*, *LP-d4*, *Lim4*, *LP-z4* and *LP-dz* were studied by combining these ligands with various transition metal cations such as Co^{2+} , Zn^{2+} , Cu^{2+} , Hg^{2+} and Ag^+ .

Various methods can be used to generate coordination polymers, such as solvo-thermal synthesis, liquid or vapor diffusion and slow evaporation, as described in the experimental part.

Thus, many different extended and periodic architectures, schematically represented as polyhedra and shown in Figure 22, were obtained.

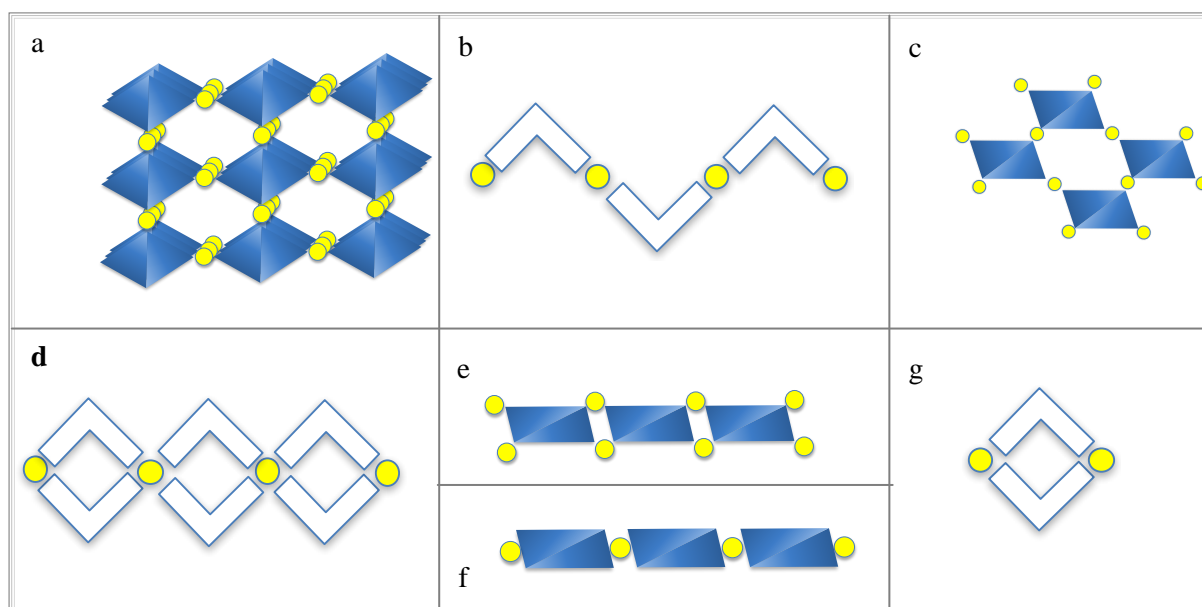


Figure 22: Schematic polyhedral representation of dimensionality and type of coordination networks obtained upon combinations of above-mentioned ligands with MX_2 or salts ($\text{M} = \text{Cu}$, Co , Zn , Hg and $\text{X} = \text{Cl}$, Br or I) or MX silver salts. Blue shapes are representing the tecton and yellow circles represent the metal centre.

Mono-dimensional crystalline structures (Figure 22; b, d, e and f), as well as bi- (Figure 22; c) and tri-dimensional (Figure 22, a) coordination polymers based on the [1111]metacyclophane platform adopting a stable *1,3*-alternate conformation bearing nitrogen donor sites have been obtained and structurally analysed. Moreover, discrete complexes

(binuclear metallamacrocycles) were also obtained. They will be detailed in the following section (§ III 4. of this chapter).

III 4. Coordination polymers based on [1111]metacyclophanes.

As already mentioned, the type of interactions between the macrocyclic ligands and the metal cation depends on several factors. In our case, we have to distinguish two cases: the di and tetrasubstituted ligands.

The di-substituted pendent monodentate N-donor sites may act as a bidentate ligand. Depending on the metal/ligand stoichiometry, the position of interaction sites, different types of complexes may be obtained.

The tetra-substituted monodentate N-donor ligands may act as tetradentate ligand. Again, depending on the metal/ligand stoichiometry, the position of interaction sites, different types of complexes may be obtained

This will be illustrated and discussed through examples of coordination polymers obtained with [1111]metacyclophane derivatives.⁸⁴

III 4.1. The use of disubstituted ligands *LC2*, *LP-d2*, *Lim2*, and *LP-z2*

The bidentate ligand *LP-d2*, adopting a hooped shape (V-shape) leads to coordination polymers of various dimensionalities in the presence of metal cations.

When combined with Hg^{2+} cation, a zig-zag type chain (Figure 22, b) of general formula [*LP-d2* (HgCl_2)]· $\text{C}_2\text{H}_2\text{Cl}_4$ is formed in the crystalline phase as shown in Figure 23.⁹⁰ For this architecture, the stoichiometry is M:L = 1:1. The network results from the association of two V-shaped components: *LP-d2* and the HgCl_2 .

The 1D chain is formed because HgCl_2 node, adopting a tetrahedral coordination geometry, offers only two free coordination sites and it is surrounded by only two different *LP-d2* ligands. By using other metals centres, other geometry may be formed.

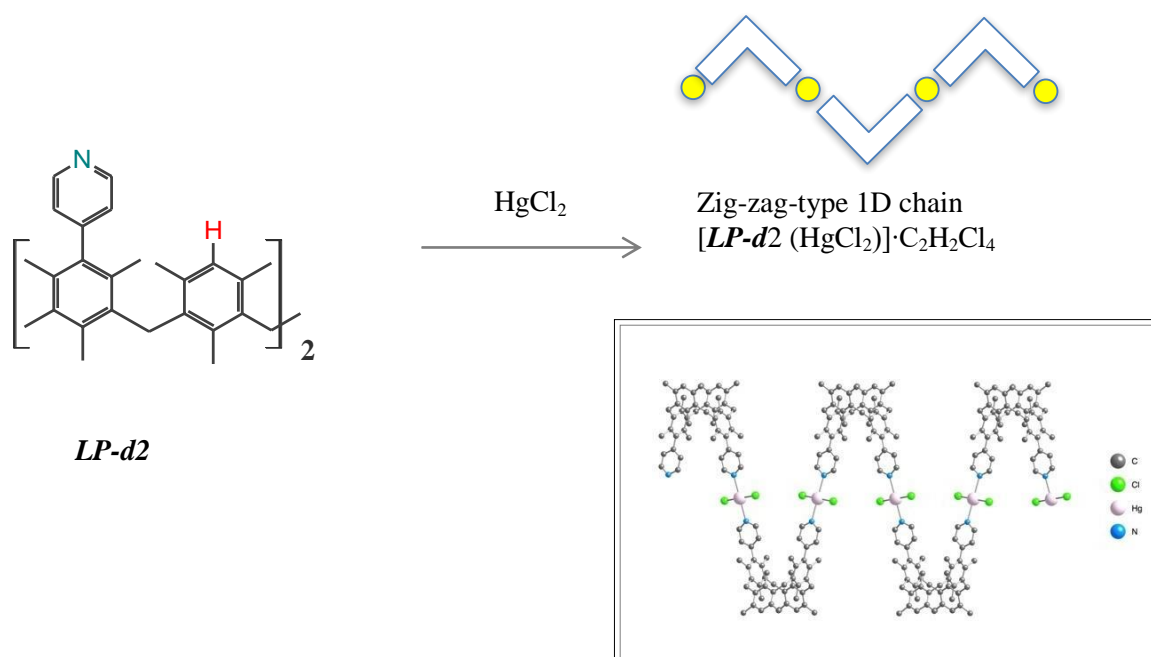


Figure 23. Schematic representation and X-Ray structure of the 1D chain generated upon combination of the V-shaped bidentate ligand **LP-d2** with Hg^{2+} cation, leading to $[\text{LP-d2}(\text{HgCl}_2)]\cdot\text{C}_2\text{H}_2\text{Cl}_4$.⁹⁰

As an example, when **LP-d2** is associated with Zn^{2+} cation, a bimetallic metallamacrocycle $[\text{LP-d2}(\text{ZnX}_2)]_2\text{S}$ ($\text{X} = \text{Cl, Br or I}$ and $\text{S} = \text{C}_6\text{H}_5\text{Cl, C}_6\text{H}_4\text{Cl}_2$ or $\text{C}_2\text{H}_5\text{OH}$ depending on the nature of X) is formed (Figure 22, g).⁸⁹ Again, the stoichiometry is $\text{M:L} = 1:1$. The schematic representation of the metallamacrobicycle is presented in Figure 24 together with the portion of X-ray structure.

In this case, although the same stoichiometry is observed, the size of ZnX_2 when compared to HgCl_2 probably imposes the 2+2 recognition, leading to discrete binuclear species.

The 1D chain and metallamacrocycles were obtained in the presence of HgCl_2 or ZnX_2 , both adopting a tetrahedral coordination geometry and offering only two free coordination sites. Using a metal cation such as Ag^+ , for example, other types of architectures may be expected.

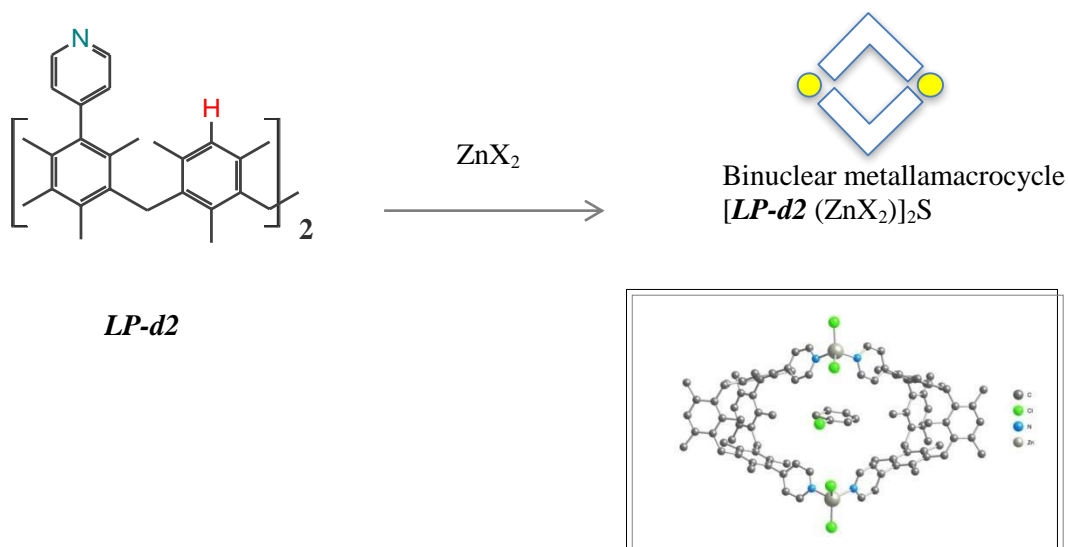


Figure 24. Schematic representation and X-Ray structure of the binuclear metallamacrocycle (**[LP-d2 (ZnX₂)]·C₂H₂Cl₄**) formed upon combination of the bidentate ligand **LP-d2** with the zinc cations (Zn²⁺) with Cl, Br or I as counter-anions.⁸⁹

Upon combination of **LC2** with AgSbF₆, a 1D coordination polymer of formula **[(LC2)₂(AgSbF₆)]·3H₂O·C₂H₅OH** was observed.⁹⁰ In this case, the stoichiometry is M:L = 1:1 (Figure 22, d). The structure may be described as interconnected discrete complexes with an antiparallel arrangement in the crystal. For this network, the geometry around silver cation is tetrahedral and each Ag⁺ is surrounded by four different macrocyclic ligands. A schematic representation of the 1D chain is presented in Figure 25 together with a portion of the X-ray structure.

It is important to note, that the same recognition pattern was also observed for the combination of **LP-z2** with CoX₂ (X = Cl and Br), leading to 1D coordination polymers of formula **[LP-z2 (CoX₂)]**.⁷⁸

Thus, the disubstituted ligands **LP-d2**, **LP-z2** and **LC-2**, displaying a V-shape, when combined with different metal cations form either a discrete complex or a 1D zig-zag chain. The observed coordination pattern depends on the nature of the metal (shape, number of free coordination sites, size, electronic density etc).

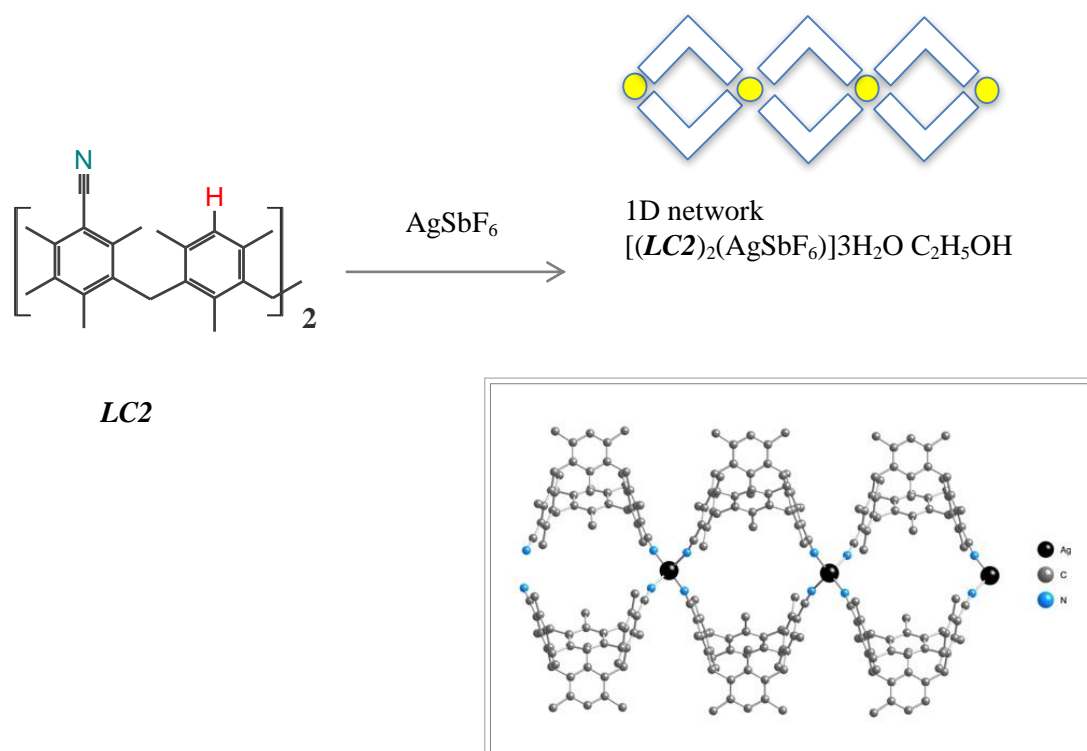


Figure 25. Schematic representation and X-Ray structure of the 1D network formed upon combination of **LC-2** with the silver cation (Ag^+), leading to $[(LC2)_2(AgSbF_6)]3H_2O C_2H_5OH$.⁹⁰

III 4.2. The use of tetrasubstituted ligands **LC4**, **LP-d4**, **Lim4**, **LP-z4** and **LP-dz**

The formation of macrocycles (Figure 22, e) of formula $[Lim4(MX_2)_2]S$ ($M = Co, Cu, Zn$ and Hg ; $X = Cl$ or Br), was achieved by combination of **Lim4** with MX_2 is not presented.⁹⁰

A 1D tubular linear chain $[LP-z4(CuBr_2)_2]$ (Figure 22, e) was obtained by combining tetrasubstituted derivative of [1111]metacyclophane **LP-z4** decorated by four pyrazolyl binding sites with copper cation (Cu^{2+}).⁹¹ The observed stoichiometry is $M:L = 2:1$. The schematic representation of the 1D compound is presented in Figure 26 together with a portion of X-ray structure.

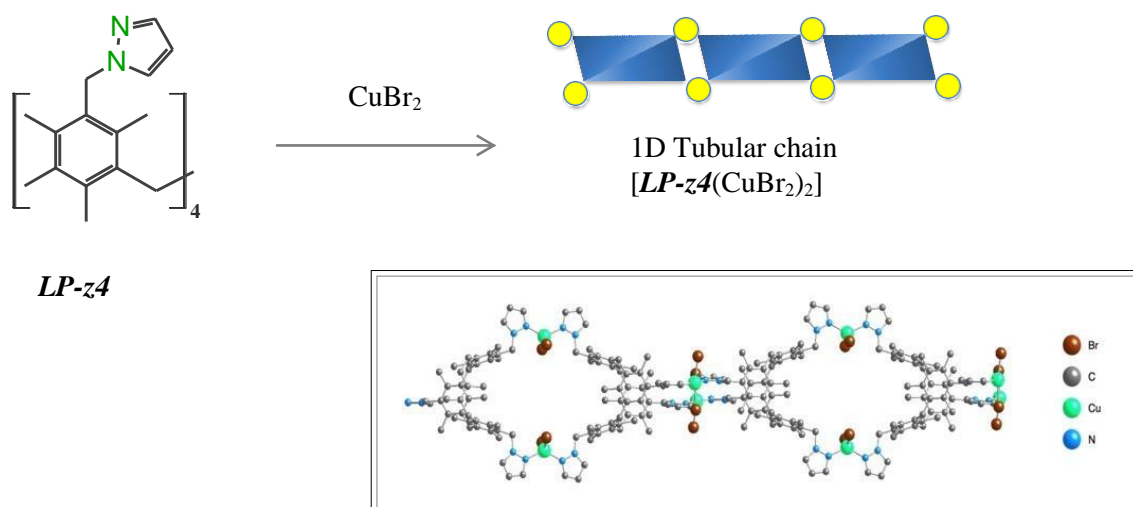


Figure 26. Schematic representation and X-Ray of the 1D tubular chain of formula [**LP-z4**(CuBr₂)₂], obtained upon combination of the ligand **LP-z4** with the copper cation (Cu²⁺).⁹¹

Such a structure is obtained by assembling the rectangle-shape tetradentate macrocyclic tecton with the V-shaped CuBr₂ complex acting as a bent connector. This recognition pattern also leads to a tubular 1D network [**LC4**(AgPF₆)₂] \cdot 2MeOH \cdot 1.5CH₂Cl₂ composed of the macrocyclic ligand and silver cation when **LC4** was combined with AgPF₆.⁸⁷ This type of architecture has been also observed with other macrocyclic ligands.⁹²

Within the framework of this project, in addition to the tubular structure, a non-tubular 1D molecular chain (figure 22, f) was also obtained using the tetracyanomethyl [1111]metacyclophane derivative.⁹³ The architecture will not be discussed here, but in chapter **III**. This non-tubular 1D network resulting from the recognition of rectangle-shape tetradentate macrocyclic ligand with tetrahedral metal cations has also been encountered in several coordination polymers involving macrocyclic ligands.⁹⁴

In addition to 1D structures and discrete complexes, the substituted metacyclophane platform also forms 2D coordination polymers.

A grid-like 2D structure (as shown in Figure 22, c), was obtained by combining the tetrapyrazolyl derivative of [1111]metacyclophane **LP-z4** with MX_2 ($\text{M} = \text{Co}^{2+}$ or Zn^{2+} , and $\text{X} = \text{Cl}^-$ or Br^-).⁹¹ The stoichiometry is $\text{M}:\text{L} = 2:1$. The schematic representation of the 2D network is presented in Figure 27 together with a portion of the X-ray structure.

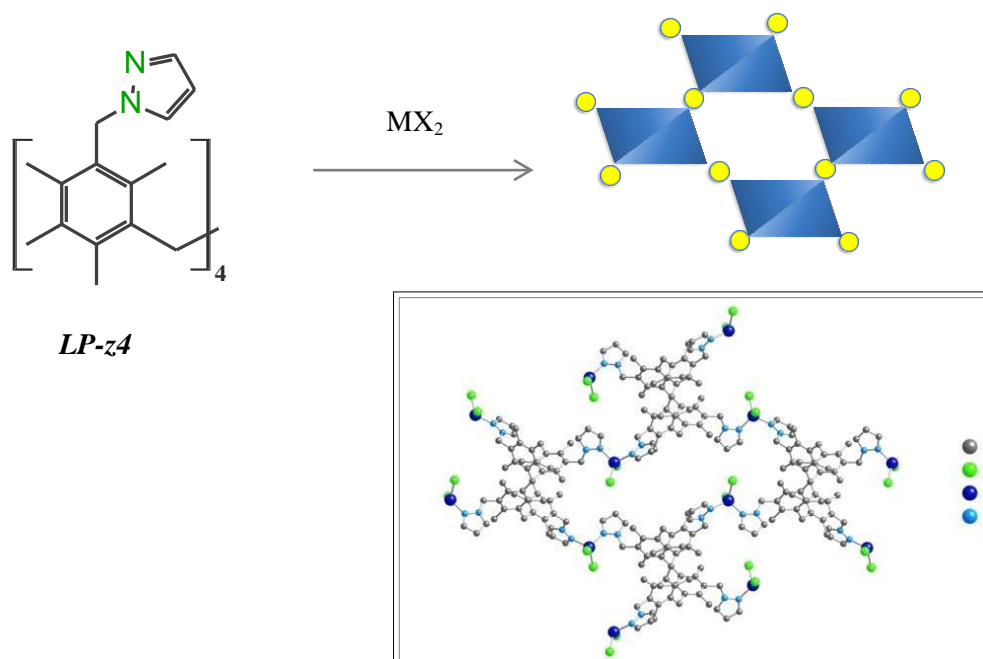


Figure 27. Schematic representation of the 2D grid type architecture formed upon combination of **LP-z4** with Co^{2+} , Zn^{2+} [**LP-z4**(MX_2)₂], ($\text{M} = \text{Co}$ or Zn and $\text{X} = \text{Cl}$ or Br). Here $\text{M} = \text{Co}$ and $\text{X} = \text{Cl}$.⁹¹

It is important to note, that an analogous recognition pattern, not represented here, was also observed for the combination of the unsymmetrical **LP-dz** with ZnCl_2 leading to a 2D coordination polymer of formula [**LP-dz** (ZnCl_2)₂]₄·2(CH_3OH)·2(H_2O).⁷⁸

For all the reported coordination networks mentioned above, no porosity nor particular physical properties have been observed.

One of the most attractive structure in terms of porosity is the pseudo diamond 3D molecular network (figure 22, a), obtained by combination of the pyridyl tetrasubstituted derivative of [1111]metacyclophane **LP-d4** with AgPF_4 [**LP-d4**(AgPF_6)₂]·2 $\text{C}_6\text{H}_4\text{Cl}_2$ ·10 H_2O . In this case, the stoichiometry is $\text{M}:\text{L} = 2:1$.⁸⁸ The schematic representation of the 3D compound

is presented in Figure 28 together with a portion of the X-ray structure.

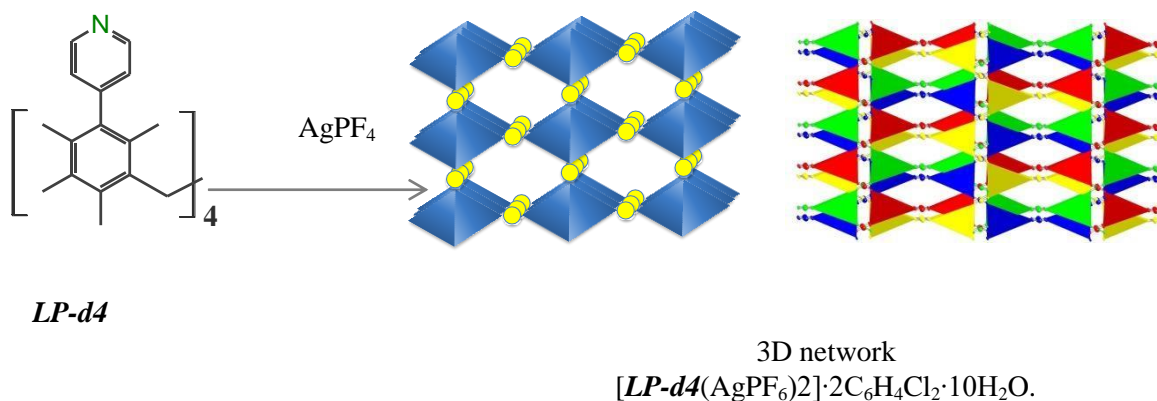


Figure 28. Schematic representation of the diamandoid-like 3D network formed upon combination of *LP-d4* with silver cation $AgPF_4$ $[LP-d4(AgPF_6)_2] \cdot 2C_6H_4Cl_2 \cdot 10H_2O$.⁸⁷

From these investigations, we can notice that a variety of connection modes can take place when the tetrasubstituted ligands *LC4*, *LP-d4*, *Lim4*, *LP-z4* and *LP-dz*: are combined with metallic cations meaning that it is virtually impossible to predict the final structures.

IV Scientific Project

Through this project, we attempt to investigate the coordination propensity of [1111]metacyclophane derivatives bearing interaction sites to form polymeric architectures. From the data presented in § III 4. of this chapter, we believe that the use of new macrocyclic tectons based on the [1111]metacyclophane backbone may of interest for the generation of molecular networks. Like their calix[4]arene analogues, they can lead to crystalline materials, owing to the rigid nature of the macrocyclic platform locked in 1,3 A conformation.

Since many monodentate N-donor groups have been grafted on the [1111]metacyclophane backbone and its calix[4]arene analogues (§ III 1.2. of this chapter), we shall focus on *phosphonato*, *mercapto*, *quinolyl*, *cyano*- and *carboxylate* coordinating groups, the latter plays an important role in the formation of MOFs, for example. The choice of these coordinating groups is justified below.

These new tetra functionalized [1111]metacyclophanes, may lead to the formation of extended architectures with targeted properties such a storage (of gas or liquids), separation, sensing etc.

IV 1. Functional groups for the formation of new tetrasubstituted [1111]metacyclophane based ligands

The complexing ability of **carboxylic/ate** derivatives grafted on the calix[4]arene platform were discussed above. We have extended our investigations by designing and preparing new [1111]metacyclophane derivatives bearing carboxylic groups.

Calixarene based derivatives bearing carboxylato coordinating groups have been shown to form coordination polymers with interesting adsorption properties.^{63-65,95} Moreover, this type of interaction site can also lead to association through H-bonds (see § II 1. of this chapter, figure 5). The new derivatives may lead to H-bond based molecular networks which may be of interest.

The choice of **hydroxy-quinoline** as a coordinating group is justified by the presence of a conjugated π -system. 8-hydroxyquinoline, represented in figure 29, has an amphoteric character, since the presence of a hydroxyl group bound to an aryl ring causes its acidic character, while the presence of nitrogen atom leads to basic properties.

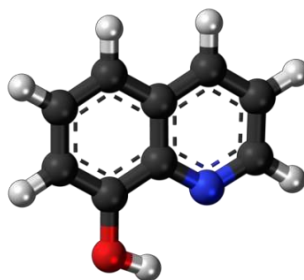


Figure 29: Solid state structure of 8-hydroxyquinoline.

Concerning its complexing ability, it acts as an monoanionic bidentate ligand (O and N binding sites). As a consequence, this group binds a large number of cations through coordination processes involving both N and O donor atoms.⁹⁶ Moreover, it was reported that 8-hydroxyquinoline and its derivatives are widely used as chelating reagents in analytical chemistry, radiochemistry, metal ion extraction and fluorometric devices.⁹⁶ Variations in the substituents on the quinoline rings affect its luminescence properties.⁹⁷

Hydroxy-quinoline groups grafted on calixarene backbone has already been reported,⁹⁸

along with their coordination abilities in solution towards lanthanide ions, together with their photophysical properties.⁹⁹ Hosseini *et al.* reported the synthesis of a bisquinoline tetrasubstituted [1111]metacyclophane, which is a N,N bidentate ligand, but no [1111]metacyclophane equipped with Hydroxyquinoline have been reported to date.

The **mercapto (thiol)** functional group is well known for its propensity to bind transition metal cations leading to the formation of thiolato complexes.¹⁰⁰ It should be noted that, according to HSAB principle,⁷² sulfur is a relatively soft (polarizable) atom suitable to bind soft ions such as mercury or cadmium cations. As already mentioned, calix[4]arene derivatives bearing mercapto groups have been reported.⁷³ Hosseini *et al.* reported the synthesis of a thiol tetrasubstituted [1111]metacyclophane.⁸⁶ For this compound, the SH groups are directly attached to the aryl moieties. We designed a new ligand for which the SH group is connected to the cyclophane backbone using a methylene spacer.

Cyano-group contains a N-donor atom has been widely used as coordinating site in particular for the binding of silver cation. As in the previous case, Hosseini *et al.* reported the synthesis of a cyano tetrasubstituted [1111]metacyclophane for which the CN groups are directly attached to aryl ring.⁸⁷ In order to complete the investigation carried out calix[4] arene and thiacalix[4] arene derivatives,⁶⁸ we have investigated the influence of the nature of the spacer on the coordination abilities of [1111]metacyclophane derivatives bearing CN groups.

Concerning the **phosphonate**- coordination sites, as already mentioned, this coordinating group should be well adapted for binding of lanthanide cations. It is worth noting that the tetrasubstituted [1111]metacyclophane derivatives bearing phosphonato moieties have not been previously reported.

IV 2. Expected coordination polymers

After choosing the suitable coordinating groups on the organic ligand, the synthesised ligands were combined with metal cations (d or f, or combinations of both) in order to obtain coordination polymers or coordination complexes. As already mentioned, the prediction of recognition pattern between different metals and macrocyclic ligands appears rather difficult.

For this type of approach, structural characterization is of prim importance. When crystalline materials are obtained, their structure is determined by X-Ray diffraction on single crystals.

V Conclusion

Based on literature survey focused on the formation of coordination compounds by macrocyclic ligands, new ligands based on the [1111] metacyclophane adopting the stable 1,3-alternate conformation have been designed. The rigid ligands differ by:

- The nature of the coordinating sites
- The length and nature of the spacer between the coordinating sites and the macrocyclic backbone.
- Number (four or eight) and position (*para*, *meta*) of coordinating sites.

The addition of aryl rings as spacers increases the stiffness of the structures, which may be useful for creating porous crystals.

In the coming chapters, the following details will be described:

- Chapter II will describe in details the synthesis and characterization of the 10 new tectons. Some of them will be studied in the solid state, using X-ray diffraction on single crystals.
- Chapter III will describe in details the formation of solid-state structures formed upon combining ligands and transition metal cations. A preliminary study of the complexation in solution will also be described.
- Finally, some perspectives are presented.

Chapter II:
Tetrasubstituted ligands based on
[111]metacyclophane

It was already mentioned in Chapter I, § III 3., that macrocyclic compounds based on the [1111]metacyclophane backbone⁸⁴ are of particular interest due to their stable 1,3-alternate conformation under a wide range of temperatures. This is one of the requirements for the design and building of infinitely extended coordination polymers or Hydrogen bonded networks. These architectures may offer specific properties which may be exploited in catalysis, gas and liquid storage and design of luminescent materials and/or sensitive sensors.^{20a,101} Through the control of their coordination propensity like the nature, the number and location of the coordinating sites, it should be possible, in principle, to adjust and master the properties of the targeted crystalline materials.

Having in mind these issues, the [1111]metacyclophane molecular scaffold, as discussed in Chapter I, is a promising backbone for the design of new ligands offering various types of coordinating centres. Furthermore, one may also vary the nature of spacers between the coordinating sites and the macrocyclic platform. As shown in Figure 30, a series of **10** new ligands or tectons, **L1-L10**, based on [1111]metacyclophane and bearing *carboxylato*, *quinolyl*, *mercapto*, *cyano* and *phosphonato* coordinating groups, has been designed. **Figure 30:** Ten new ligands **L1-L10** based on [1111]metacyclophane.

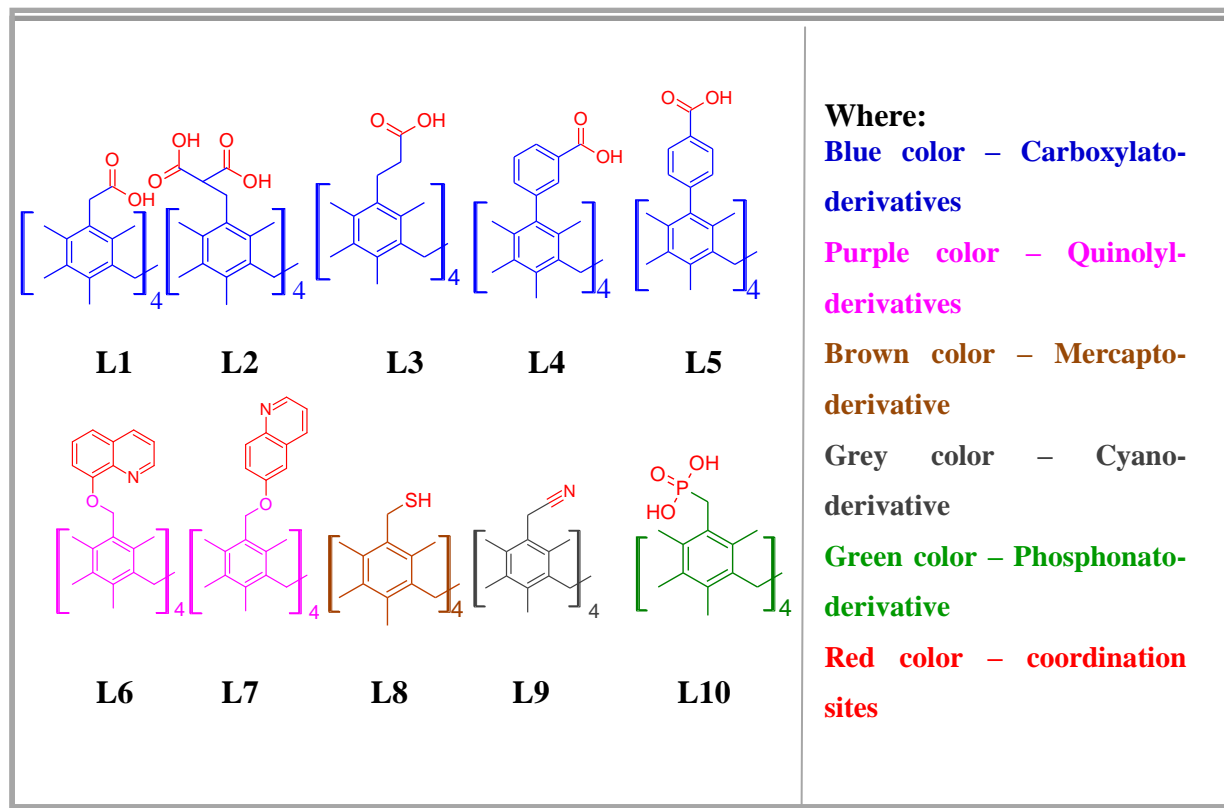
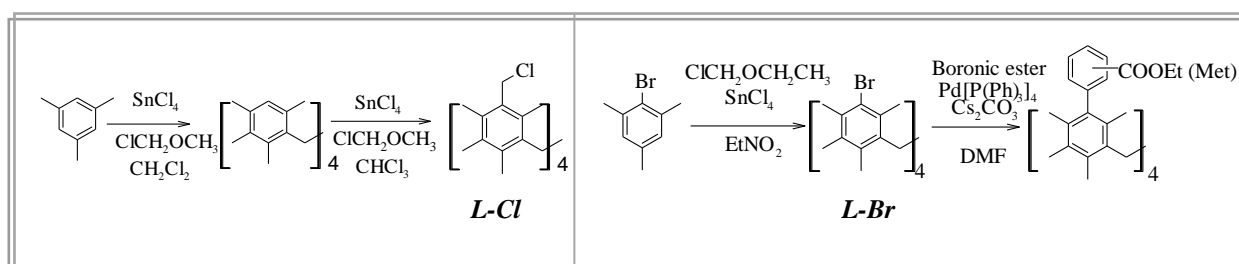


Figure 30: Ten new ligands **L1-L10** based on [1111]metacyclophane.

By designing ligands with a rigid aryl spacer (**L4** or **L5**) or flexible polymethylene chains (**L1-L3** and **L6-L10**) between the macrocyclic backbone and binding sites, we intend to investigate the propensity of these macrocyclic species to form extended periodic supramolecular structures with high dimensionality in the crystalline phase, in the presence of metallic cations. The presence of *four* coordinating groups on the [1111]metacyclophane platform should, in principle, lead to the formation of 1D, 2D and 3D structures, as discussed in chapter I, while the use of the ligand with *eight* coordinating groups (**L2**) could lead to the formation of metallic clusters, when combined with various d- and f metallic cations.

In the following, the synthesis of ligands will be discussed, together with their solution behaviour, using mainly NMR spectroscopy. In all cases, the *1,3-Alternate* conformation was confirmed in solution. When possible, *i.e.* generation of single crystals, the description of solid-state structures will be presented and compared to reported ones for related compounds. All ten ligands were obtained from the following starting materials: tetrasubstituted chloromethylmetacyclophane (**L-Cl**) as precursor for the ligands with an aliphatic spacer⁷⁷ and tetrasubstituted bromometacyclophane (**L-Br**) as precursor for the ligands with an aromatic spacer.^{76,77} They were synthesized according to scheme 3, presented below.



Scheme 3: Synthetic pathway for obtaining the **L-Cl** and **L-Br** precursors for the synthesis of **L1-L10** bearing aliphatic (a, b) and aromatic (c, d) spacers.

I CARBOXYLIC DERIVATIVES OF [1111]METACYCLOPHANE

Carboxylato derivatives are rather interesting compounds owing to their propensity to form intra- and inter-molecular hydrogen bonds, thus leading to the formation of H-bonded molecular networks in the crystalline state. Furthermore, when deprotonated (carboxylate), they can efficiently bind metal cations and, thus, leading to the formation of discrete metal complexes and/or coordination polymers in the crystalline state. In this work, four types of

structural parameters influencing the coordination abilities of [1111]metacyclophane based carboxylic derivatives were studied in solution, as well as in the solid state:

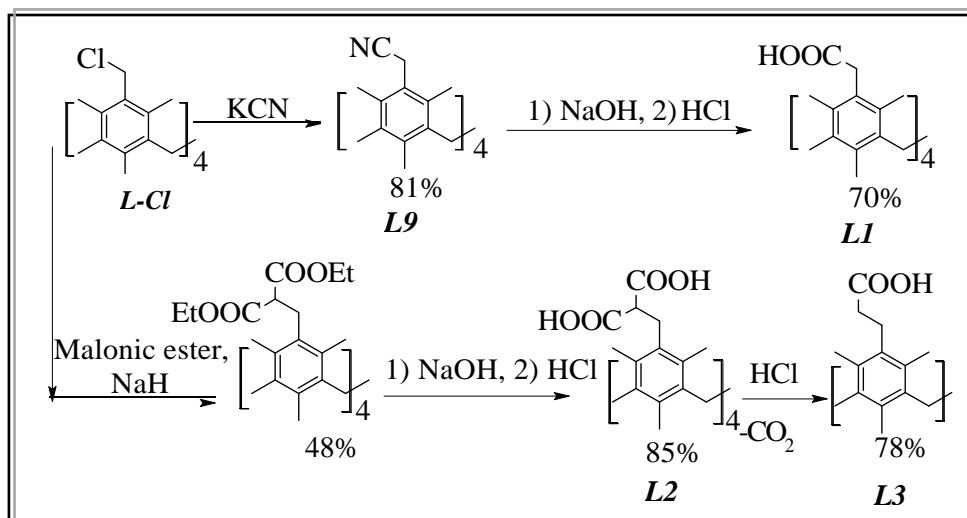
1. The nature of the spacer between the coordinating group and the macrocyclic platform: aryl group (rigid **L4** and **L5**) and aliphatic chains (flexible, **L1-L3**);
2. The length of aliphatic spacer (**L1-L3**);
3. The position of carboxylic coordinating group on the rigid spacer (in *para*- or *meta*-position on the aryl moiety) (**L4** and **L5**);
4. The number of carboxylic groups (four or eight) decorating the spacer (**L2**).

Thus, **five** new ligands containing carboxylic/ate coordinating groups, **L1-L5**, have been successfully designed and synthesized. The syntheses were achieved through sequential chemical modifications of the [1111]metacyclophane backbone, using the already mentioned tetrachloromethyl- or tetrabromo- derivatives *L-Cl* and *L-Br* as starting materials.

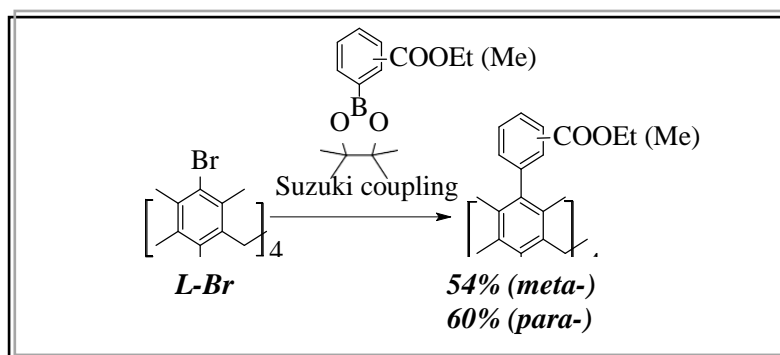
I 1. Synthesis of the carboxylic derivatives L1-L5

The aliphatic carboxylic derivatives **L1-L3** have been synthesized by an ester functionalization of the tetrasubstituted *chloromethylmetacyclophane L-Cl* using a classical nucleophilic substitution, followed by an hydrolysis of the ester derivative leading to **L2** and decarboxylation of the malonic acid derivative leading to **L3**, as shown in scheme 2. Whereas the hydrolysis of aliphatic esters was carried out under rather mild conditions (60-70 °C), **L1** was synthesized from the cyanomethyl-derivative **L9** which was then hydrolysed in DMSO at high temperature (120 °C) leading to higher yields (70%) (Scheme 4) (see Experimental part for the details).

For the synthesis of **L4-L5**, the used synthetic pathway was based on the synthesis of the corresponding ester derivatives,¹⁰² followed by the hydrolysis under basic conditions,¹⁰³ as shown in Scheme 5.



Scheme 4. Synthetic pathway for the synthesis of the tetrasubstituted aryl carboxylic derivatives of [1111]metacyclophane (**L1-L3**).



Scheme 5. General synthetic pathway for the synthesis of carboxylic ligands (**L4** and **L5**).

The key step for the synthesis of the targeted ligands bearing aryl spacers **L4-L5** was the Suzuki coupling reaction with aryl-halide catalyzed by Pd (0) complexes¹⁰⁴ as shown in Figure 31. Tetrasubstituted *bromometacyclophane* **L-Br** was chosen as a precursor because of its high reactivity compared to the one of *chlorometacyclophane* **L-Cl** ($R-I > R-Br \gg R-Cl$) and less reactivity compared to the one of the iododerivative.¹⁰⁵ However, when we tried to synthesize the tetrasubstituted *iodometacyclophane*, only very low yields (<10%) were obtained whereas the tetrasubstituted *bromometacyclophane* **L-Br** can be easily synthesized in one step, using bromomesitylene as starting compound with a high yield > 60%.⁷⁷

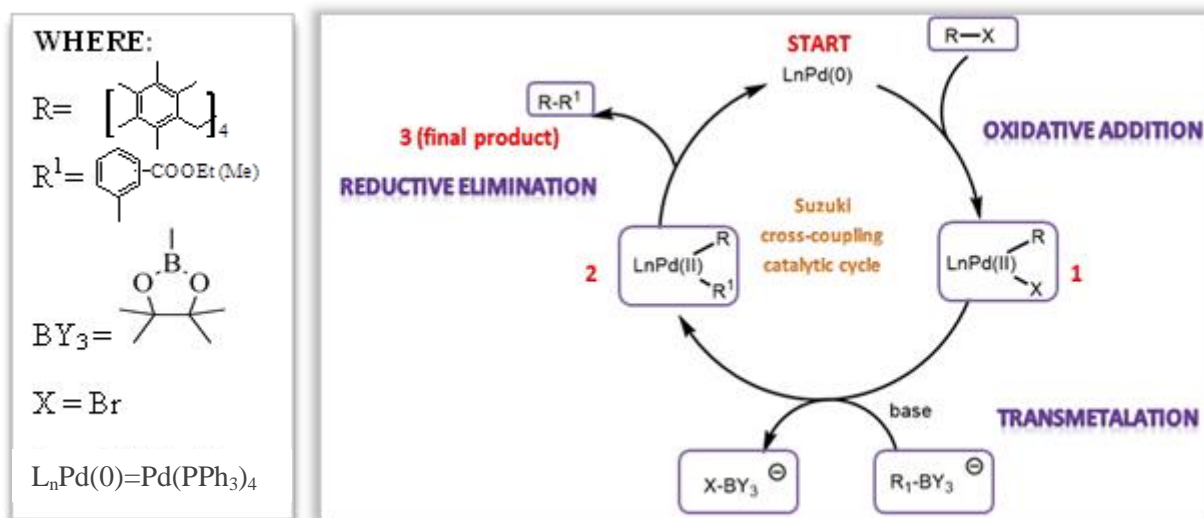
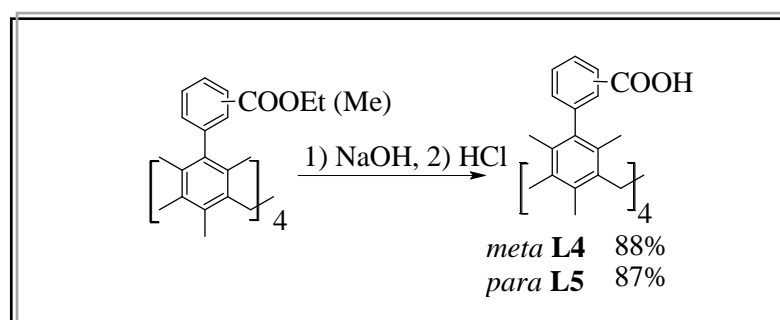


Figure 31. Schematic representation of the mechanism of Suzuki coupling reaction for the formation of tetrabromoderivative of [1111]metacyclophane.

The last step was the hydrolysis of the ester derivative (see scheme 6). For **L4** and **L5**, the optimal mixture of solvents and ratio have been chosen in order to increase the solubility of the reactants. The most suitable solvent mixture was found to be THF: H₂O: EtOH = 2: 1: 2. For the choice of the base, NaOH or LiOH was used. The desired products **L4** and **L5** were separated in high yields (88% and 87%) by simple filtration of the precipitate after adding diluted HCl (see experimental part for the details).



Scheme 6. Synthetic pathway for the synthesis of tetrasubstituted carboxylic derivatives of [1111]metacyclophane with rigid spacer (**L1-L3**), through the hydrolysis of the ester precursors.

The new carboxylic compounds **L1-L5** were characterized in solution by ¹H- and ¹³C-NMR spectroscopy, MS, as well as in the solid state by IR, EA and X-ray diffraction on single crystals, when single crystals were obtained.

I 2. Behaviour in solution

The NMR data for all compounds **L1-L5** are in accordance with the *1,3*-alternate conformation (see experimental part).

As already mentioned, in marked contrast with calix[4]arene, the [1111] metacyclophane backbone and consequently its derivatives adopt the *1,3*-alternate conformation under a wide range of temperatures, owing to the absence of rotation around the methylene bridges due to repulsion between methyl groups in the *ortho*- positions (*cf.* Chapter I § III 2). At the same time, the presence of methyl groups destroys the planarity and thus conjugation of both aryl moieties connected through one C_{Ar}-C_{Ar} bond preventing thus the spontaneous rotation of aryl substituents around this bond (for **L4** and **L5**). This peculiar feature of the metacyclophane containing aryl based substituents should have a specific signature in NMR spectroscopy. For example, the ¹H-NMR spectra (DMSO-d₆) of **L4** and **L5** (DMSO-d₆) exhibit a splitting of protons in the aryl region caused by the absence of the symmetry. For **L4** and **L5**, this leads to the observation of sets of peaks belonging to non-equivalent protons at 7.15-7.63 ppm, as shown in Figure 3. Moreover, the presence of intramolecular H-bond between opposite carboxylic units in the case of **L4** (as shown in the solid-state studies Chapter II, § I 3.3.1.) may decrease the rotation rate around C_{Ar}-C_{Ar} bonds and further complicate the observed spectrum. Concerning the carboxylic derivatives bearing an aliphatic spacer (**L1-L3**), such a clear evidence of prevention of rotation around the C_{Ar}-C_{Ar} bonds is not observed. Thus, we can clearly distinguish the proton signals belonging to each group of aliphatic substituents and determine their multiplicity (Figures 32 and 33).

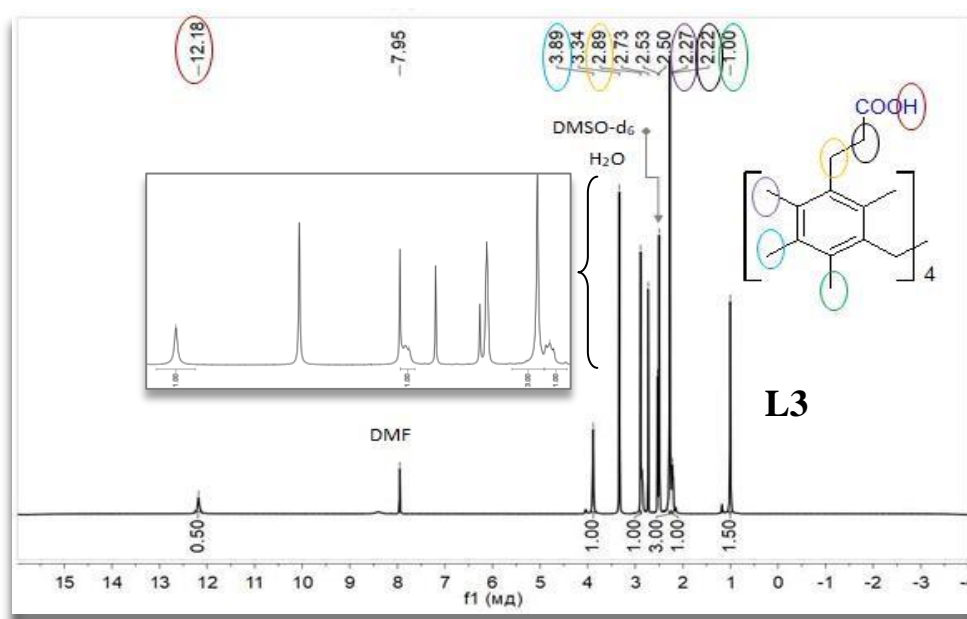


Figure 32: ¹H-NMR spectra of the metacyclophane based aliphatic spacer ligand **L3**.

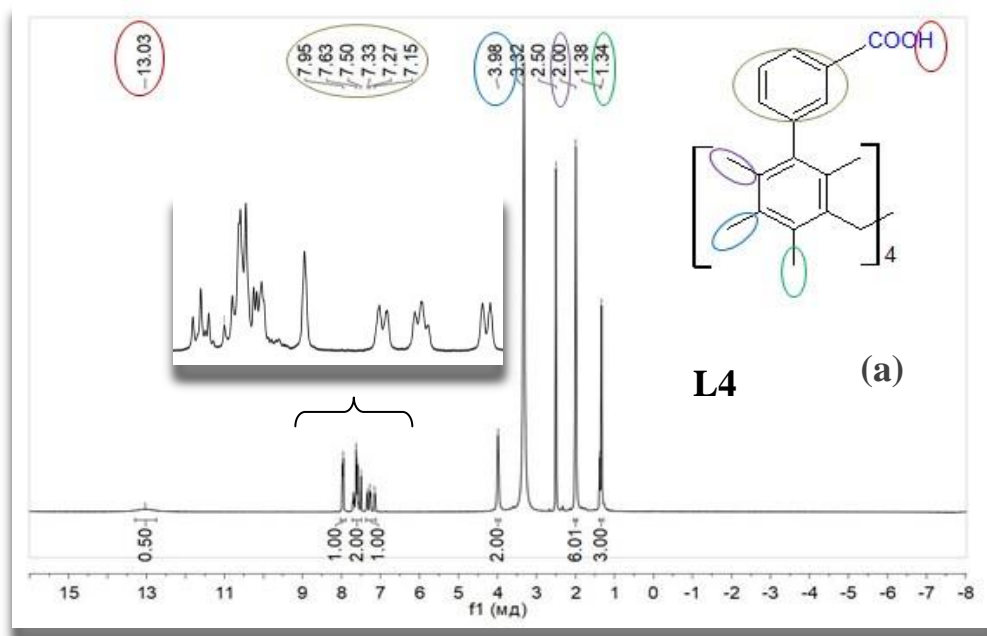


Figure 33: ^1H -NMR spectra of the metacyclophane based aromatic spacer ligand **L4**.

Colour correspondence for each peak:

- - H belong to carboxylic- groups.
- - H belong to methylene bridges.
- - H belong to methyl- groups in *ortho*- positions of the aromatic rings.
- - H belong to methyl groups in *para*- position of the aromatic rings.
- - H belong to aliphatic spacers (1st CH_2 - group).
- - H belong to aliphatic spacers (2nd CH_2 -group)
- - H belong to aromatic spacers.

I 3. Structural studies in the solid state

I 3. 1. General trends

The solid state structures of carboxylic derivatives based on [1111]metacyclophane core have been studied by X-ray diffraction on single crystals. We have obtained single crystals by using different crystallization methods: liquid diffusion (for **L4**), vapour diffusion (**L2**), slow evaporation (**L5**) and vapour diffusion while heating at the beginning of the process (**L3**) (see Experimental part). Unfortunately, no single crystal of **L1** suitable for X-ray analysis could be obtained.

Table 1 presents some of the bond characteristics for **L2**, **L3**, **L5**¹⁰³ and **L4**.

It was also found that the $\text{C}_{\text{Ar}}\text{-CH}_2$ -bridge bond distances ($\approx 1.52 \text{ \AA}$) are similar to the

ones found in the calix[4]arene backbone ($\approx 1.51 \text{ \AA}$).¹⁰⁶

L2, **L3**, **L4** and **L5** were found to adopt an *1,3*-alternate conformation in the solid state, with the carboxylic groups located, in an alternate fashion, above and below the metacyclophane core. At the same time, owing to the absence of intermolecular H-bonding between consecutive macrocycles, no hydrogen bonded network is formed for the studied ligands.

For **L4-L5**, a description of the arrangement and the orientation of the oxygen atoms of the carboxylic coordination sites may be achieved by projecting a polyhedron formed by four O atoms on the vertices and six edges *a*, *a'*, *b*, *b'*, *c*, *c'* (Figure 33).

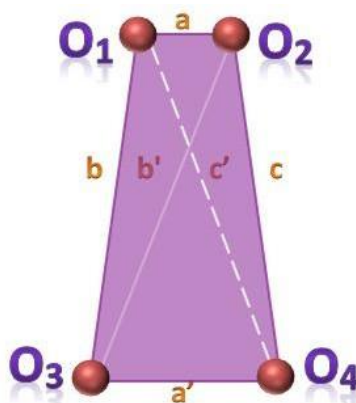


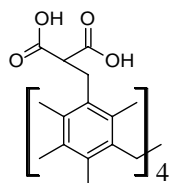
Figure 33. Geometric descriptors for the polyhedron formed by the O atoms of the *carboxyl*-units in **L2-L5** (analogy with **L7**, where *N* atoms replace *O* atoms).

Table 1: Some angles and CO-distances for the **L2-L5** carboxylic ligands.

Parameters	L2	L3	L4	L5
dCO (Å)	1.149		1.082	
	1.179		1.186	
	1.205		1.194	
	1.230	1.173	1.236	
	1.249	1.203	1.250	1.167
	1.275	1.295	1.267	1.301
	1.279	1.301	1.363	
	1.319		1.389	
Dihedral angle between opposite mesitylene moieties (°)	43.2	43.8	36.21	28.4
Dihedral angle between aryl spacers and mesitylene moieties (°)	-	-	89.51 89.68	71.23

I 3. 2. Carboxylic derivatives with aliphatic spacer

I 3. 2. 1. Ligand L2



4,11,18,25-tetra((malonate)-methylene)-3,5,7,10,12,14,17, 19,21,24,26,28-dodecamethyl-[1.1.1.1]metacyclophane.

L2, with the formula $\{C_{59}H_{73}O_{17}N\}$, crystallises in the monoclinic $C2/c$ space group. The dihedral angle of **L2** is greater than the one in the above-mentioned ligands (**L5**): 43.18° , as shown in Figure 34.

C-O distances for the eight carboxylic moieties were analysed, it was found that for the four fork-type hydrogen bonding carboxylic groups, with two donor-acceptor pairs, participate in H-bonding. The length of the C-O bonds varies from 1.230-1.275 Å (Figure 35, a-b) for one carboxyl group and 1.242-1.250 Å (Figure 35, c-d) for the other (see table 1), this indicates the formation of hydrogen bond between a and b, c and d groups.

There are also four carboxylic moieties which do not participate to the formation of intramolecular hydrogen bonds, there are two short double C=O bonds (1.149 and 1.179 Å) and two long distances single C-OH (1.279 and 1.319 Å), thus the length corresponds to the multiplicities of the bonds. All details are given on Figure 35.

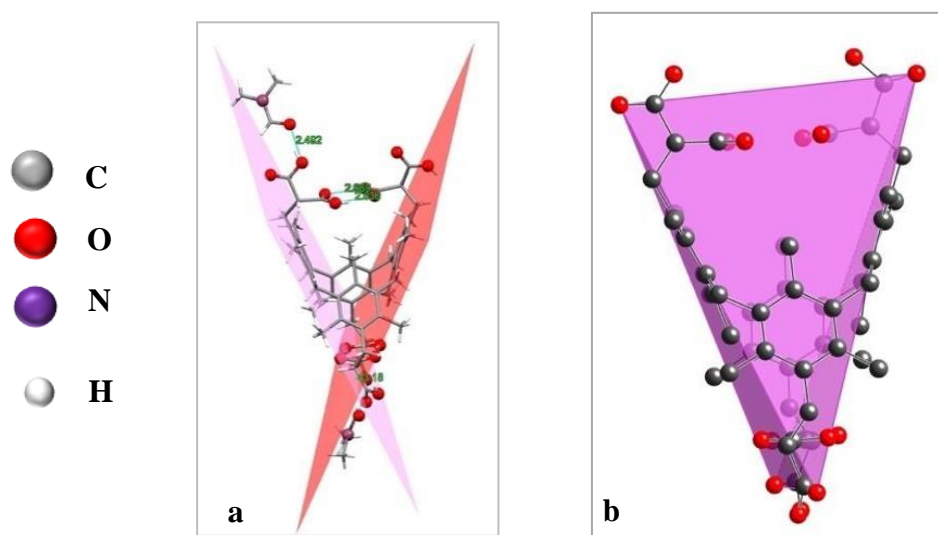


Figure 34: a) The crystalline structure of **L2** and b) the corresponding tetrahedron formed by the O atoms of the carboxylic groups.

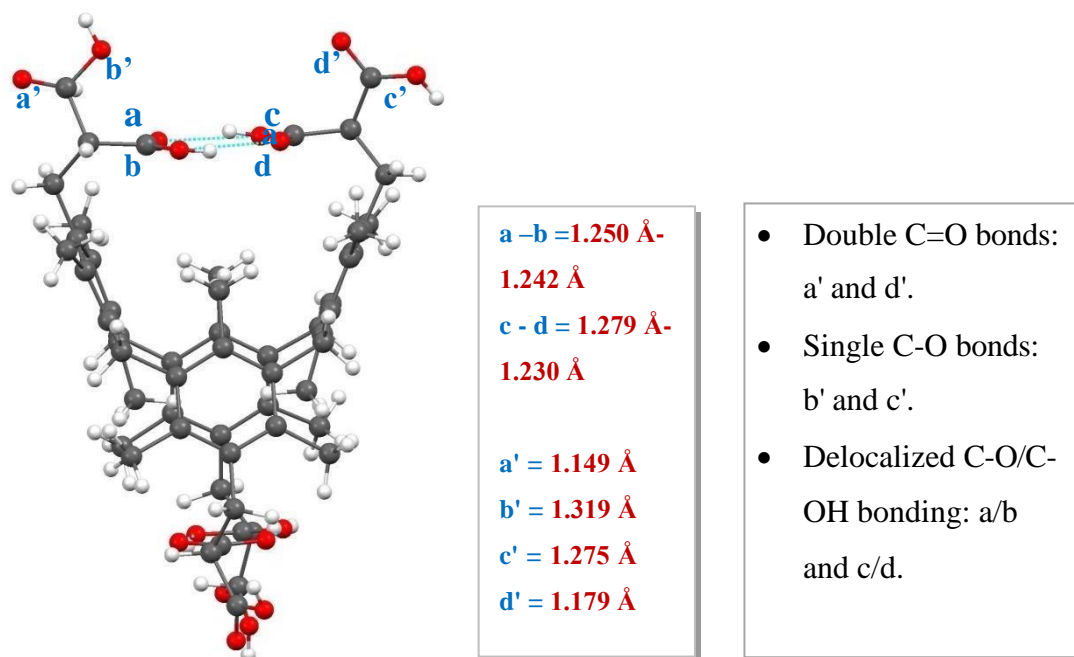


Figure 35: Distances between the O and C atoms of the carboxylic units in L2.

Along the *a* axis, antiparallel layers are formed, as shown in Figure 7 a, and also along the *c* axis (see Figure 36 b). Along the *b* axis, the layers are stacked in a parallel fashion, as shown in Figure 36 c.

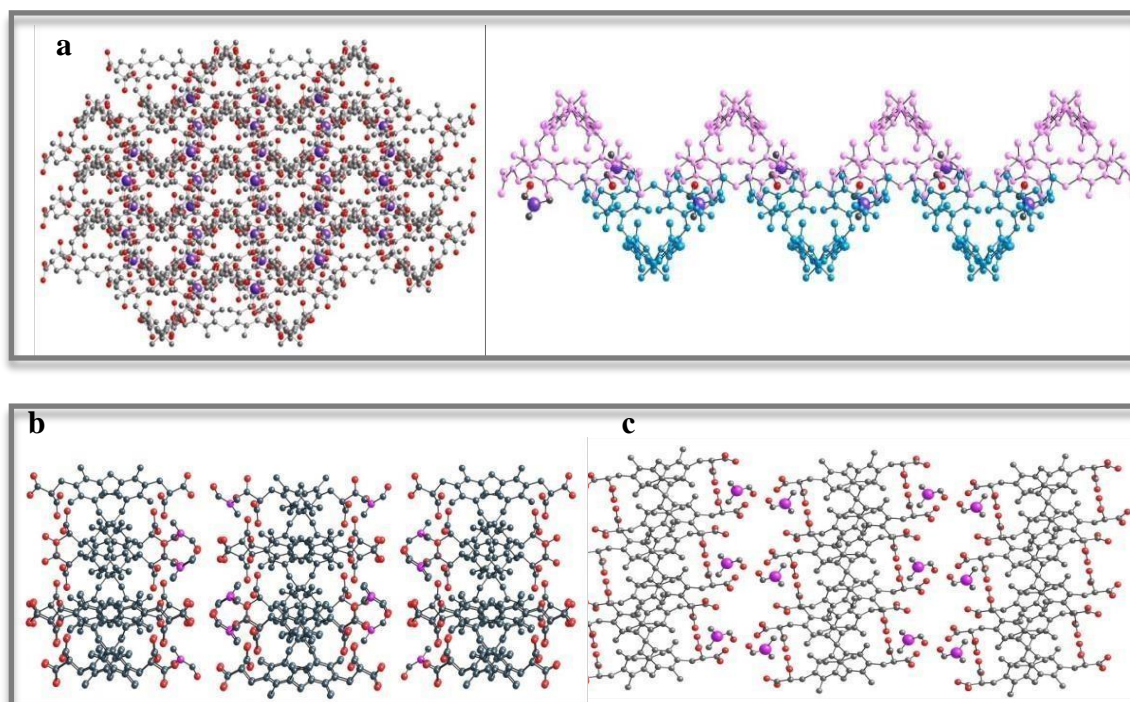
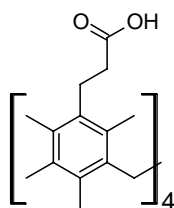


Figure 36: Portion of the packing of L2 along *a* (a), *c* (b) and *b* axes (c).

I 3. 2. 2. Ligand L3



4,11,18,25-tetra((malonate)-methylene)-3,5,7,10,12,14,17, 19,21,24,26,28-dodecamethyl-[1.1.1.1]metacyclophane.

L3 forms a solvate with a pyridine molecule, crystallizing in the monoclinic $P2_1/c$ space group and displaying the following formula: $\{C_{52}H_{64}O_8 \cdot 4(C_5H_5N)\}$. The formation of an intramolecular bond between O atoms of the carboxylic is not energetically favoured (d_{O-O} about 7\AA , as shown in figure 37 a). Oxygen atoms of the carboxylic ligands are involved in hydrogen bonds with pyridine molecules, with d_{N-O} distances in the 2.623 to 2.684\AA range. For **L3**, the dihedral angle was found to be equal to 43.80° , as shown in figure 37 b.

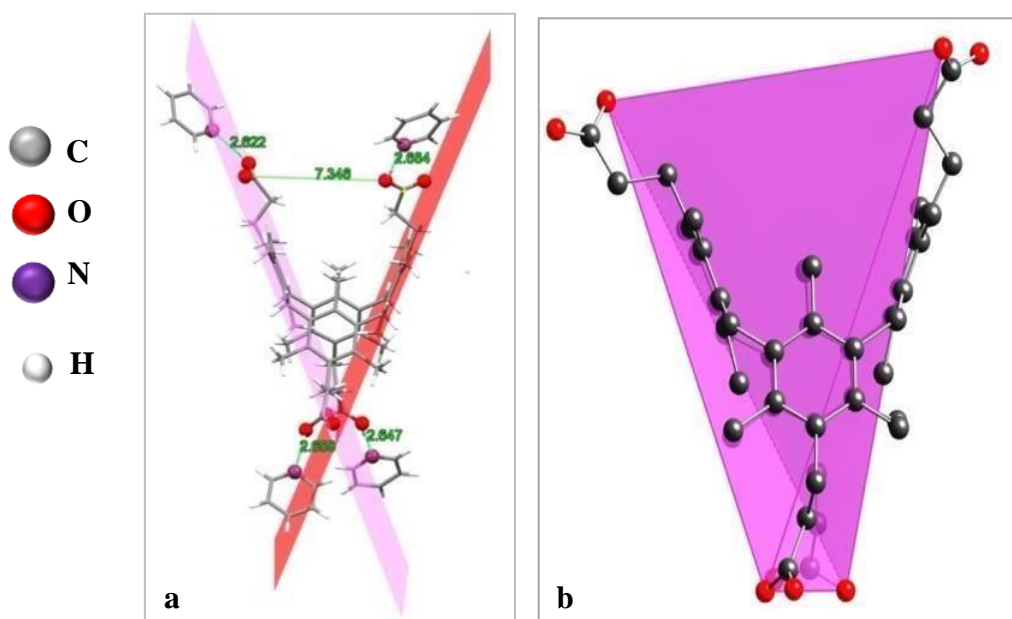


Figure 37: The crystalline structure of **L3** (a) and corresponding tetrahedron formed by the O atoms of the carboxylic groups (b).

There were found four C-OH bonds inside the four carboxylic groups (with the C-OH length of 1.295 Å (b) and 1.301 Å (c)). The length of the four C=O bonds are 1.203 Å (a) and 1.173 Å (d) respectively (Figure 38, table 1). The C-OH, as H donor groups, are interacting with the H-acceptor N-atoms of the four pyridine molecules with O-N distances of 2.623 and 2.684 Å.

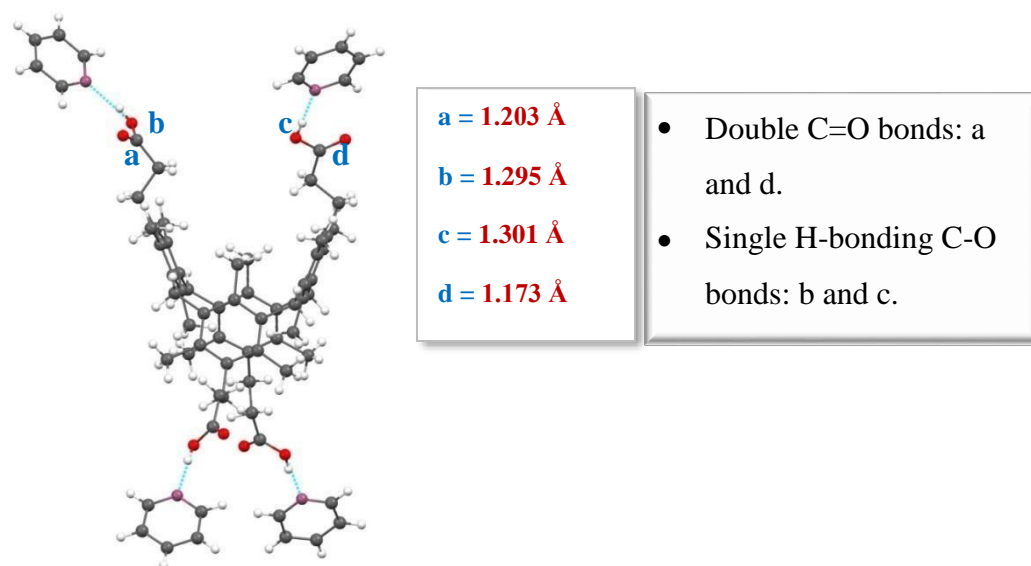


Figure 38: Distances between the O and C atoms in carboxylic units in L3.

Concerning the packing of the molecules in the crystal, pseudo 1D chains are formed, as depicted in figure 39 a. In the crystal, there is a parallel arrangement of chains together with planes, as depicted in Figure 39 b and c.

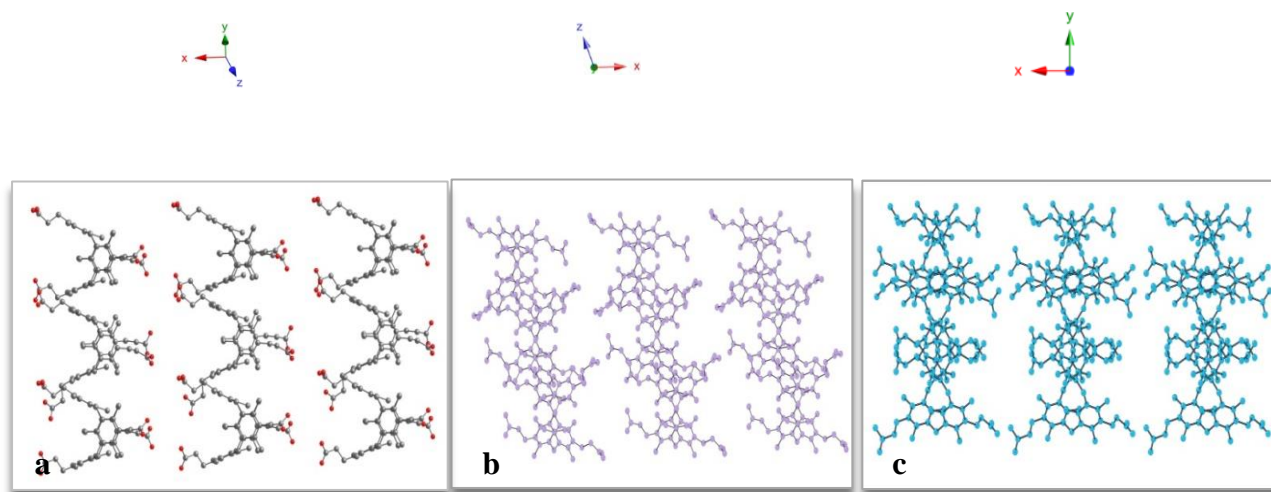
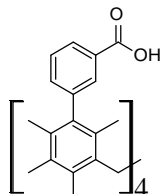


Figure 39: Packing of L3 along all three axes *a*, *b* and *c* presenting parallel chains (a) and layers (b and c).

I 3. 3. Carboxylic derivatives with aromatic spacer

I 3. 3. 1. Ligand L4



4,11,18,25-tetra (3-(carboxyl)phenyl)-3,5,7,10,12,14,17,19, 21,24,26,28 -
dodecamethyl-[1.1.1.1]Metacyclophane.

The molecular structure of **L4** is rather symmetrical in the crystalline phase (it crystallises in the trigonal crystal system with a $R\bar{3}2$ space group) with the chemical formula $\{C_{68}H_{64}O_8\}$ (no molecule of solvent is found in the crystal, and the squeeze command was preliminarily applied).¹⁰⁷ Among the many potential rotamers (isomers which can be interconverted by rotation of the part of the molecule around a particular bond) possible, only one rotamer is stabilized by the formation of intramolecular H-bonds between two opposite *meta*-carboxylic groups ($d_{O-O} = 2.163 \text{ \AA}$ and 2.292 \AA), as shown in figure 40 a and table 1. The polyhedron formed by O atoms of the carboxylic moieties (we considered one of the two O atoms) is rather elongated, leading to a deformed tetrahedron (figure 40 b). Molecules of **L4** in the crystal, are packed along the *a* axis to form supramolecular chains (a and b) anti-parallelly oriented (Figure 41).

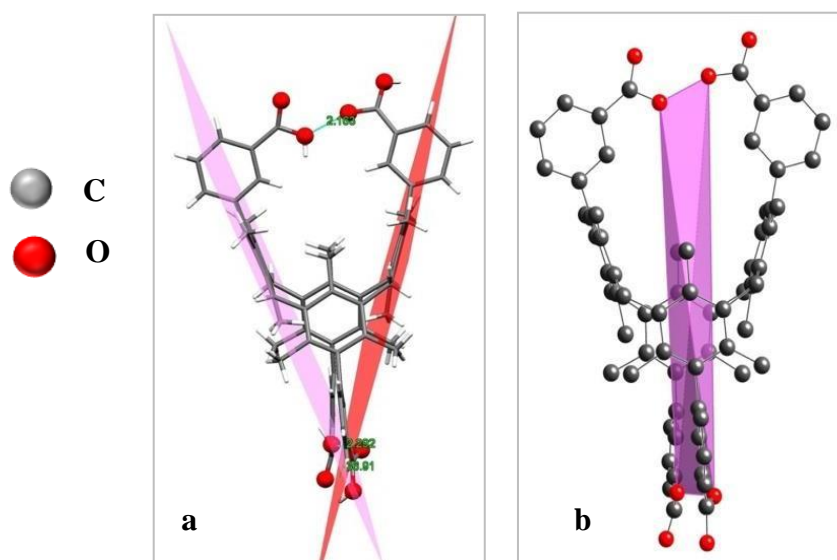


Figure 40. Representation of the crystal structure of **L4**: a) the formed rotamer, b) the tetrahedron formed by the O atoms of the four carboxylic groups.

Concerning the C-O distances for the carboxylic moieties, for two of the four C-O groups, there is one short (C=O) and one long distance (C-OH), as usually observed for the protonated species (the same observation is typical for two other carboxylic groups located on the opposite side of the macrocyclic skeleton, the data are provided above, see Table 1). For the other two, the C-O distances are very similar, which corresponds to a delocalisation in the C-O bonds. The long C-OH distance bears H donor, and is involved in a hydrogen bonds with the C=O bond (Figure 42).

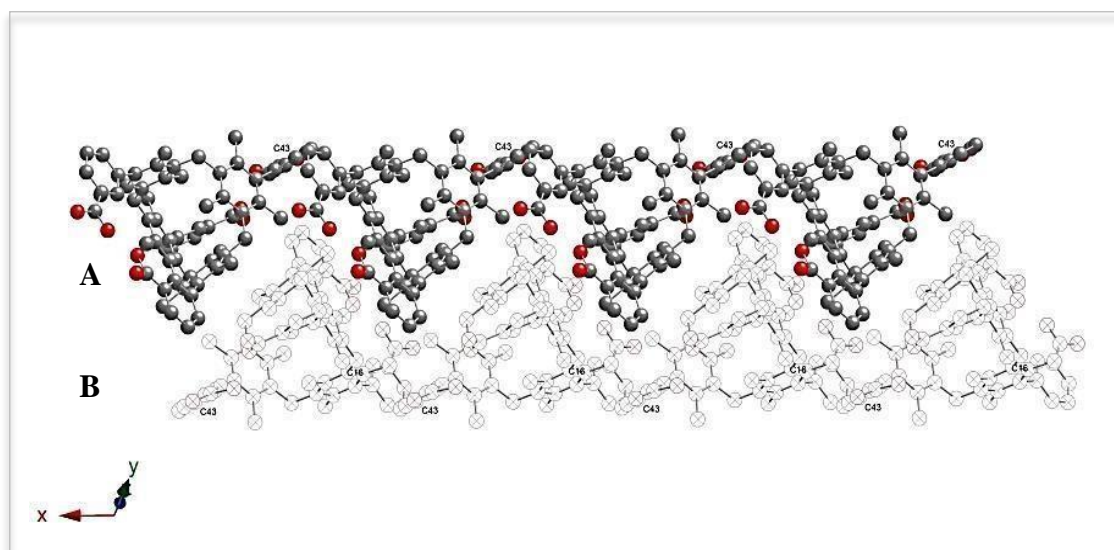


Figure 41: The anti-parallelly oriented supramolecular chains A and B within the unit cell for **L4**, running along the *a* axis.

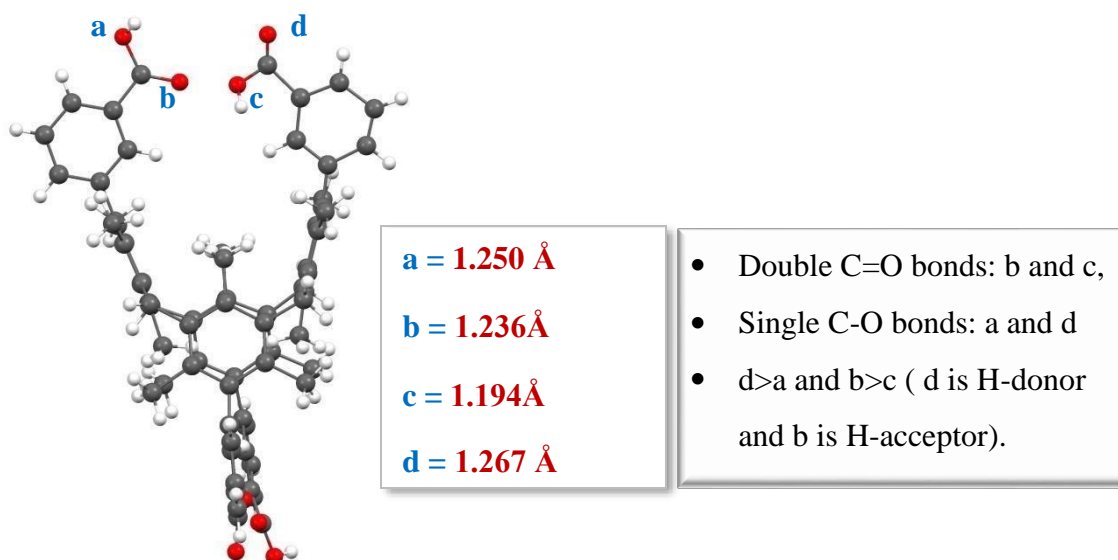
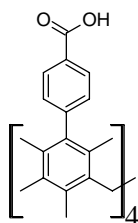


Figure 42: Distances between the O and C atoms in carboxylic units (a and b), showing the value of each bond in hydrogen bonds for **L4**.

I 3. 3. 2. Ligand L5



4,11,18,25-tetra(4-(carboxyl)phenyl)-3,5,7,10,12,14,17,19,21,
24,26,28-dodecamethyl-[1.1.1]Metacyclophane.

Compound **L5** forms a solvate, where the **L5** molecule is H-bonded with DMF molecules in the lattice (with $d_{O\cdots O}$ distance of 2.605 Å), giving rise to a crystal presenting the following formula $\{C_{68}H_{64}O_8, 4(C_3H_7NO)\}$ (Figure 43). Unlike the previous case, there are no intramolecular H-bonds between the carboxylic groups within **L5**. The absence of intramolecular hydrogen bond can be explained by the energetically unfavourable arrangement of the oppositely disposed carboxylic groups with respect to each other, in contrast with what was observed in **L4** (9.09 Å instead of 2.183 Å).

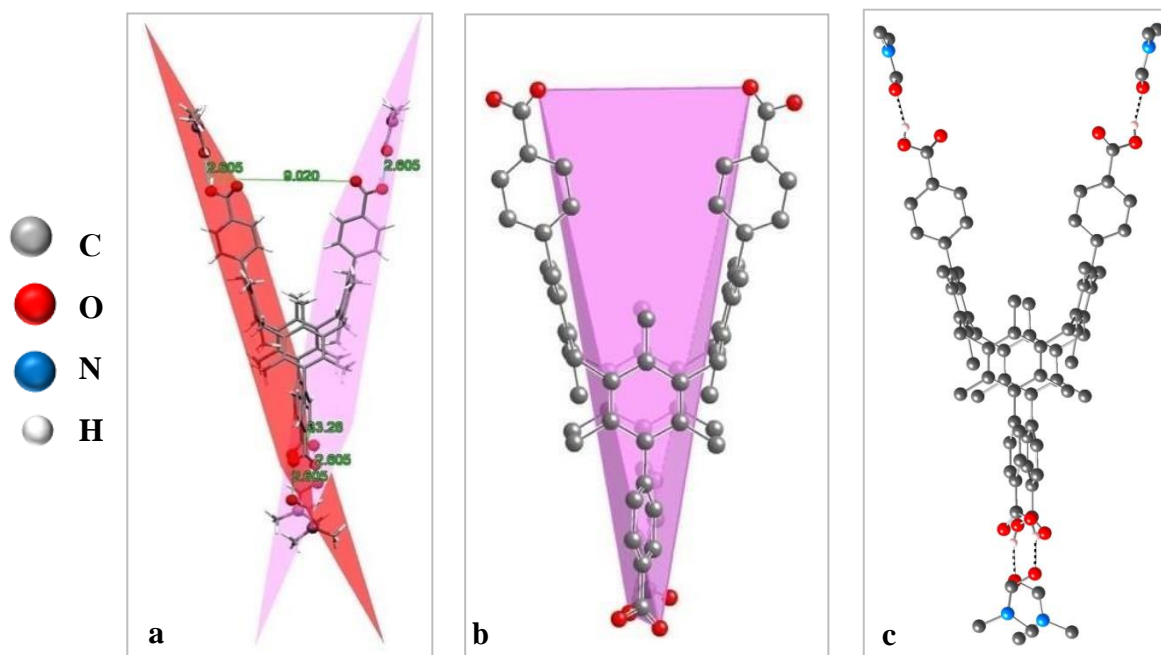


Figure 43: Representation of the crystal structure of **L5** (a), the tetrahedron formed by the O atoms of the carboxylic groups (b) and solvate with DMF molecules (c).

For its carboxylic moieties, **L5** presents a long and a short bond length (1.301 Å for single C-OH bonds and 1.167 for double C=O bond). The dihedral angle between the opposite mesitylene units of this compound is equal to 28.4° as shown in table 1.

As already mentioned, **L5** crystallizes together with a DMF molecule and forms layers (“ α ” and “ β ”) in the crystal along the c crystallographic plane, displaying an antiparallel arrangement along b axis (Figure 44). These 2D layers are stacked in the crystal along c axis without any specific interactions.

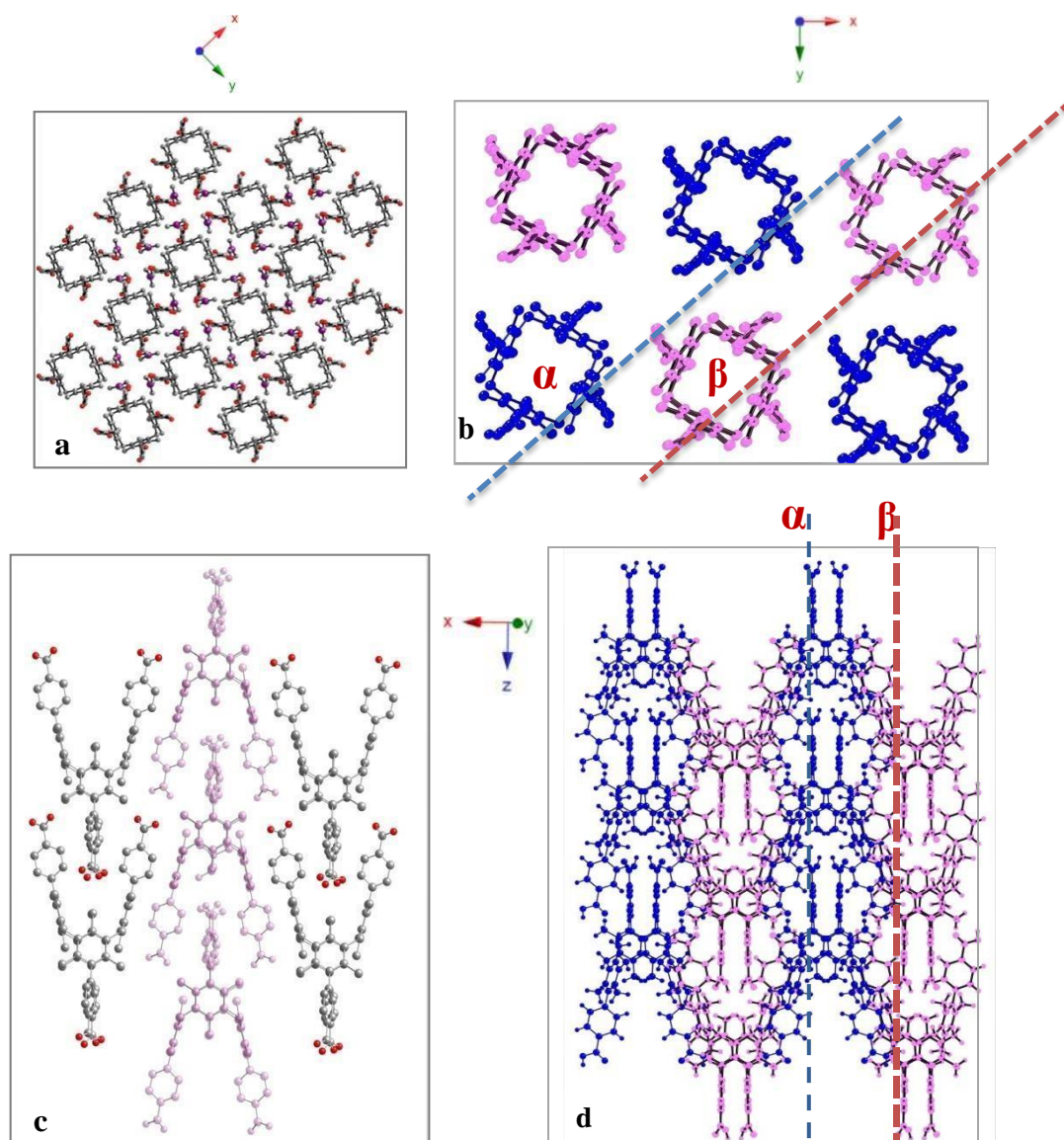


Figure 44: Packing of **L5**: a) within the unit cell along the c axis with DMF molecules, b) and d). Simplified packing along c axis showing “ α ” and “ β ” layers; C) antiparallel packing of the chains in the xOz plane (H-atoms and DMF molecules are hidden for clarity).

I 4. Conclusion

Five new carboxylic [1111]metacyclophane based derivatives, blocked in the stable *1,3*-alternate conformation due to the presence of methyl substituents in *ortho*-positions on the aromatic rings, were designed, synthesized and characterized. Three of synthesized ligands (**L1-L3**) possess aliphatic methylene spacer and two (**L4** and **L5**) contain aromatic spacer between the coordinating site and the macrocyclic metacyclophane platform.

Studies in solution using $^1\text{H-NMR}$ spectroscopy evidenced that all obtained carboxylic derivatives correspond to the desired tetrasubstituted compounds in the desired conformation. At the same time, for some of the ligands, their structures were studied in solid state by X-ray diffraction on single crystal, which showed that there are intramolecular bonds by three carboxyl compounds: **L2** possesses the fork-type hydrogen bonding motif involving both carboxylic groups located on the same side of the macrocyclic skeleton. At the same time, in **L3**, hydrogen bonds were found with the four solvent molecules per ligand, *i.e.*, one pyridine molecule for one carboxylic group. However, neither binding to the pyridines of the molecule **L3** nor the presence of the intramolecular hydrogen bonding in **L2** influenced the amplitude of the dihedral angle between the opposite mesitylene fragments in the aliphatic-spacer ligands, and thus the dihedral angles of **L3** and **L2** are nearly equal (43.8 for **L3** and 43.2 for **L2**, respectively).

The ligands with an aromatic spacer (**L4** and **L5**), display significant differences concerning dihedral angles, depending on the presence of hydrogen bond in the molecule. An intramolecular hydrogen bond was found in **L4** due to favourable arrangement of carboxylic groups with respect to each other, while in **L5**, where the carboxylic groups are located far away from each other, no intramolecular interactions were found. This influences the dihedral angle between the opposite mesitylene fragments and between the mesitylene fragments and aromatic spacers. In both cases, in **L4**, much larger dihedral angles were found than in **L5**.

It is interesting to investigate and compare in the future the interaction of these ligands with the metal cations, this will be discussed in chapter III.

II QUINOLYL DERIVATIVES OF [1111]METACYCLOPHANE

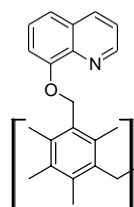
Quinolyl derivatives are of particular interest for coordination with metal cations, due to the presence of two aromatic rings separated from the main aryl core by a flexible spacer. Such rich in electrons systems may present an antenna effect, and these compounds may be of interest for luminescent molecular materials, as already discussed in chapter I § IV 1.^{72, 108-110}

In this study, two types of quinolyl derivatives with the 6- and 8- positions of the donor nitrogen atom leading to **L6** and **L7** respectively, have been synthesized. Unfortunately, no single crystal of the ligand **L6** could be obtained.

II 1. Synthesis of Ligands L6 and L7

4,11,18,25-Tetra-6-quinolinomethyl-3,5,7,10,12,14,17,19,21,24,26,28-dodecamethyl[1.1.1.1]metacyclophane.

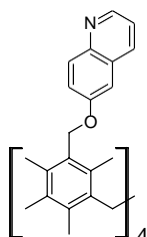
L6



and

4,11,18,25-Tetra-8-quinolinomethyl-3,5,7,10,12,14,17,19,21,24,26,28-dodecamethyl[1.1.1.1]metacyclophane.

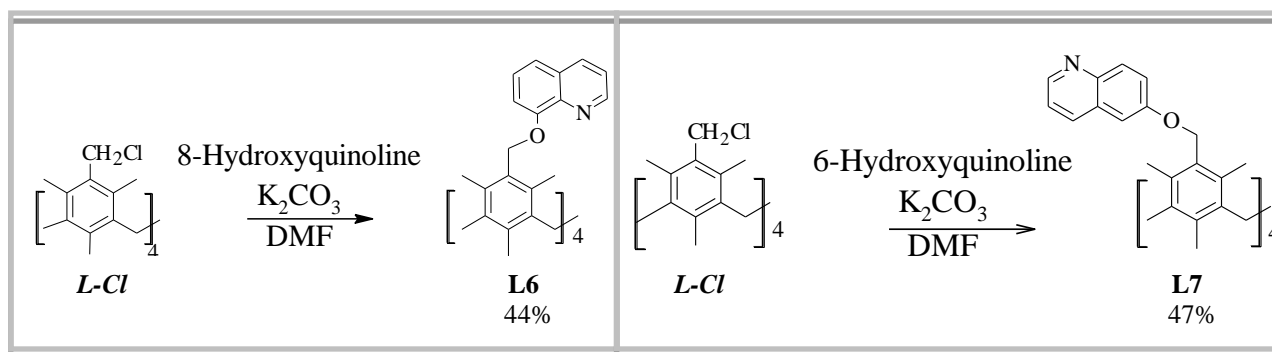
L7



The quinolyl derivatives **L6** and **L7** were obtained through a nucleophilic tetrasubstitution reaction of a *chloromethylmetacyclophane L-Cl* where the nucleophilic agents

were 6-hydroxyquinoline or 8-hydroxyquinoline respectively, as shown in scheme 7, in presence of K_2CO_3 , in refluxing DMF (see experimental part).

For this reaction, we tested two types of solvents: THF and DMF. DMF is the most efficient (48h, yields 44% for **L6** and 47% for **L7**). The optimal temperature was found to be 100 °C with DMF, for both compounds.



Scheme 7: Synthetic pathways for obtaining compounds **L6** and **L7**.

II 2. Behaviour in solution

The 1H -NMR ($CDCl_3$) of **L6** and **L7** spectra (see experimental section) exhibit doublets and multiplets for the quinolyl-fragment (8,81-7,32 ppm for **L6** and 8.92-7.18 ppm for **L8**), and singlet for methylene spacer (5.24 ppm for **L6** and 5.39 ppm for **L7**), singlet peaks for methylene bridges between mesitylene rings (4.13 ppm for **L6** and 4.01 ppm for **L7**) and protons of the *ortho*- and *para*- methyl groups respectively (2.48 ppm and 1.25 ppm for **L6**; 2.46 ppm and 1.24 ppm for **L7**).

It can be concluded that both the integration and multiplicity of peaks correspond to the structure of the desired tetrasubstituted product in the symmetric 1,3-alternate conformation, as expected.

II 3. Structural studies in the solid state for L7

4,11,18,25-Tetra-6-quinolinomethyl-3,5,7,10,12,14,17,19,21,24,26,28-dodecamethyl[1.1.1.1]metacyclophane.

It was possible to obtain single crystals of **L7** suitable for X-Ray diffraction using the liquid-diffusion technique (see Experimental part). Unfortunately, and as already mentioned, no single crystals could be obtained for **L6**.

L7 is crystallized in the symmetrical $I4_1cd$ (tetragonal) space group presenting the following formula $\{C_{80}H_{76}N_4O_4 \cdot 6(H_2O)\}$.

Its dihedral angle differs from the dihedral angles of all the previously listed molecules by its much smaller value of 29.18° . At the same time, the distance between the two opposing coordinating sites is quite large and is equal to 12.676 \AA (see figure 45).

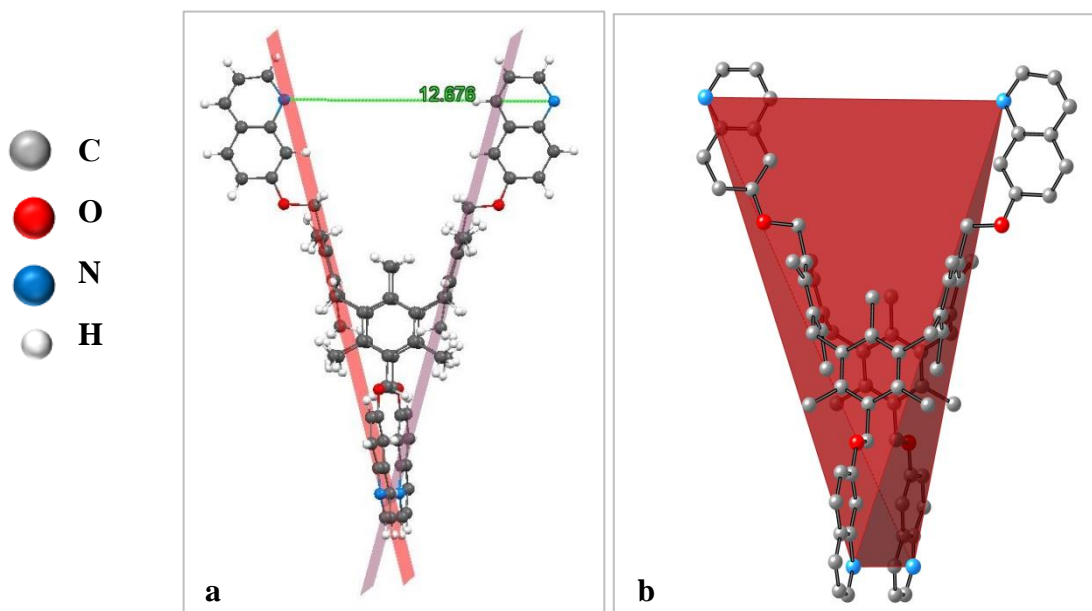


Figure 45: The crystalline structure of **L7** (a) and corresponding tetrahedron formed by the *N* atoms of the quinolyl groups (b).

Concerning the packing of the molecules in the crystal, two types of perpendicular chains arise, one is parallel to the *a* axis, and the other to the *b* axis, as shown in figures 46 a, b and c.

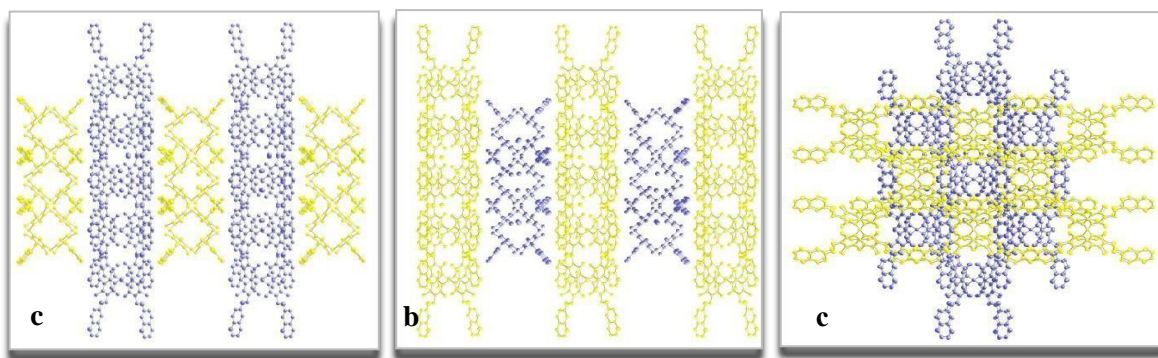
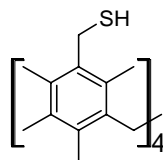


Figure 46: Representation of some portions of the crystal packing of L7 along *a* (a), *b* (b) and *c* (c) axis.

III MERCAPTO- DERIVATIVE OF [1111]METACYCLOPHANE

Ligand L8



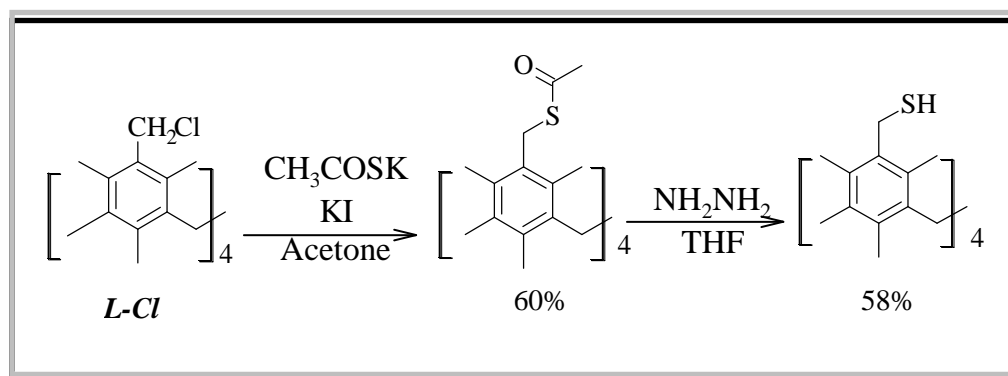
4,11,18,25-Tetramercaptomethyl-3,5,7,10,12,14,17,19,21,24,26,28-dodecamethyl
[1.1.1.1]metacyclophane.

Ligand **L8**, containing soft sulphur atoms, was designed to bind soft metal cations (for example, mercury, lead and silver cations) following hard and soft acid and bases (HSAB) rules.⁷²

The structural description in the solid state of **L8** was not possible since no single crystal could be obtained, though many attempts were performed.

III 1. Synthesis of ligand L8

L8 was obtained after applying a two-steps synthetic pathway, as shown in scheme 8. The precursor chloromethylmetacyclophane *L-Cl* was transformed in the tetrasubstituted thioacetate derivative by a nucleophilic substitution using potassium thioacetate as nucleophilic agent and potassium iodide (catalyst). (see experimental section) It is interesting to note that a small amount of water present in the solvents (acetone, THF or DMF) was found to promote the conversion of this reaction. The thioacetate intermediate was obtained in high yield (60%). The second step is based on a reduction reaction. Various reductants, such as Lithium Aluminium Hydride, hydrazine hydrate and hydrazine have been tested, following well described procedures.¹¹¹



Scheme 8: Synthetic pathway for **L8**.

Since reducing agents such as LiAlH_4 and N_2H_4 hydrate led to low yields, finally Hydrazine was used (76%).

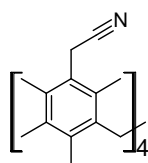
III 2. Behaviour in solution

The $^1\text{H-NMR}$ (CDCl_3) spectra of **L8** is presented in the experimental part. We were not able to observe proton peaks for SH-group owing to exchange processes, however, a doublet instead of a singlet for the aliphatic spacer (at 3.80-3.82 ppm) indicates the presence of sulphur atoms, in the presence of which the splitting of singlet peaks from neighbouring hydrogen atoms is characteristic. There is a singlet for the *ortho*- and *para*-methyl groups (2.43 ppm and 1.09 ppm respectively) and the singlet for methylene bridges (4.01 ppm).

It can be concluded that the integration and multiplicity of the peaks correspond to the structure of the desired tetrasubstituted compound in *1,3*-alternate conformation.

IV CYANO- DERIVATIVE OF [1111]METACYCLOPHANE

Ligand L9

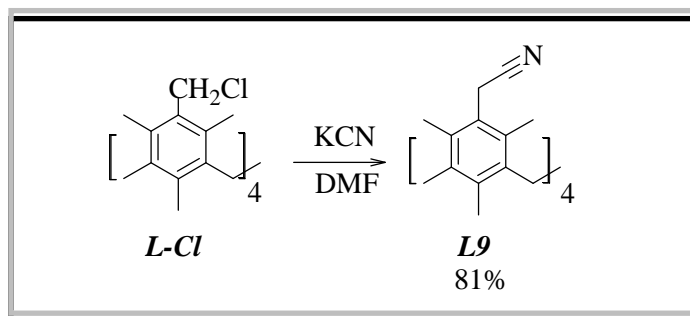


4,11,18,25-Tetracyanomethyl-3,5,7,10,12,14,17,19,21,24,26,28-dodecamethyl[1.1.1.1]metacyclophane.

IV 1. Synthesis of Ligand L9

Since single crystals for **L9** could not be obtained, although after many attempts, its structure in the solid state cannot be discussed.

Tetrasubstituted cyanomethyl derivative of metacyclophane **L9** was synthesized from chloromethylmetacyclophane *L-Cl* as precursor, potassium cyanide as nucleophilic agent and dry DMF, as shown in scheme 9, leading to **L9** in high yield (81%).⁹³ Using other agent such as CuCN leads to lower yields, in contrast to the cyano derivative with the cyano group directly attached to the metacyclophane backbone which was synthesized *via* addition CuCN to *L-Br* in dry DMF (30 mL) with the further pouring of FeCl₃ in 10% aqueous HCl.⁸⁷ Apparently, despite the use of a toxic compound, the **L9** synthesis method proved, in our case, to be a simple procedure, that doesn't require the addition of catalysts.



Scheme 9: Synthetic pathway for the obtention of **L9**.

IV 2. Behaviour in solution

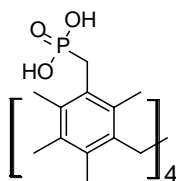
^1H -NMR (CDCl_3) spectrum of **L9** is presented in the experimental part and is specific for the metacyclophane backbone: well defined singlets for *ortho*- and *para*- methyl substituents (2.43 ppm and 1.07 ppm respectively) and a singlet for protons from methylene spacers and methylene bridges (3.73 ppm and 4.02 ppm respectively).

The data of ^1H -NMR spectra indicates a successful synthesis of the tetrasubstituted compound in the symmetrical *1,3*-alternate conformation.

V PHOSPHONATO DERIVATIVE OF [1111]METACYCLOPHANE

4,11,18,25-Tetrakisphosphonatomethyl-3,5,7,10,12,14,17,19,21,24,26,28-dodecamethyl[1.1.1.1]metacyclophane

L10



Although the synthesis of the phosphonate derivative of metacyclophane is complex and requires a multi-step strategy, it was nevertheless interesting to explore its behaviour due to the coordination properties of the phosphonate group with respect to the lanthanide cations¹¹²⁻

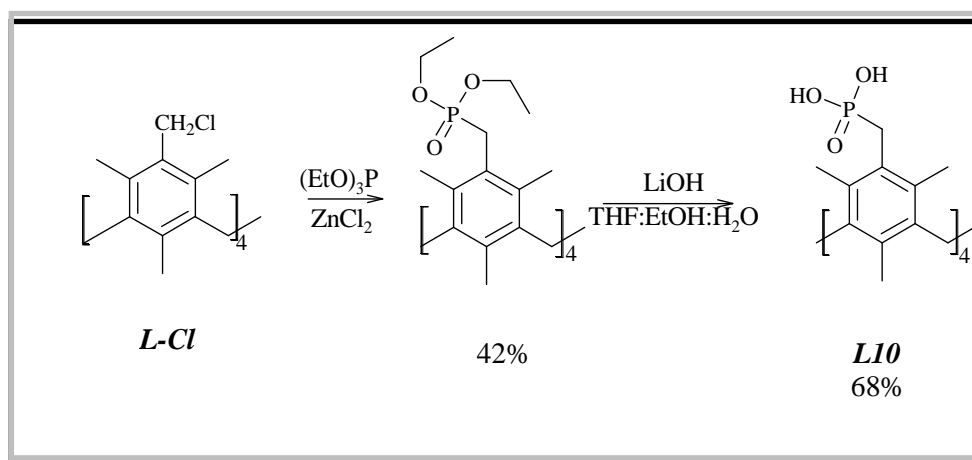
¹¹⁴ since the phosphonate group offers hard donor group.¹¹⁵

Again, since single crystal of **L10** could not be obtained, its structural features can not be discussed.

V 1. Synthesis of ligand 10

For the synthesis of **L10**, **L-Cl** was transformed by the Arbuzov reaction¹¹⁶⁻¹¹⁸ into the phosphonate derivative containing two ethoxy groups through an alkylation of triethyl phosphite with metacyclophane-methylchloride to form diethylphosphonates on the [1.1.1.1]metacyclophane platform. Then, this intermediate was converted into dihydroxylphosphonate by hydrolysis reaction (Scheme 10).

The mechanism of this multi-step reaction is rather complicated, it is detailed below. First, triethyl phosphite alkylation by chloromethylmetacyclophane *via* a S_N2 mechanism, leads to triethoxyphosphonium salt. Then, a nucleophilic attack of the chloride anion on the electrophilic carbon atom of the ethoxy group, with the elimination of ethyl chloride, leads to the formation of diethylphosphonate group on the metacyclophane platform (Arbuzov rearrangement) as shown in Figure 47.



Scheme 10: Synthetic pathway for obtaining **L10**.

Usually, this reaction takes place at rather high temperatures ($> 100\text{ }^{\circ}\text{C}$) which leads to the decrease of the yield in the desired product. This issue was solved by addition of zinc chloride as Lewis acid catalyst to increase the yield.¹¹⁶ The optimal temperature was found to be $70\text{ }^{\circ}\text{C}$. Zinc chloride is able to form a polarized complex with alkyl halides, thereby it is also able to increase the electrophilicity of the carbon atom and increase the affinity of the phosphorus atom for the carbon atom during the reaction of the nucleophilic attack of phosphorus.

The final hydrolysis reaction was carried out under analogous conditions as for the preparation of carboxyl derivatives (see Experimental part), and LiOH was particularly well adapted for this reaction while in case with carboxylic derivatives no difference between LiOH or NaOH was observed.

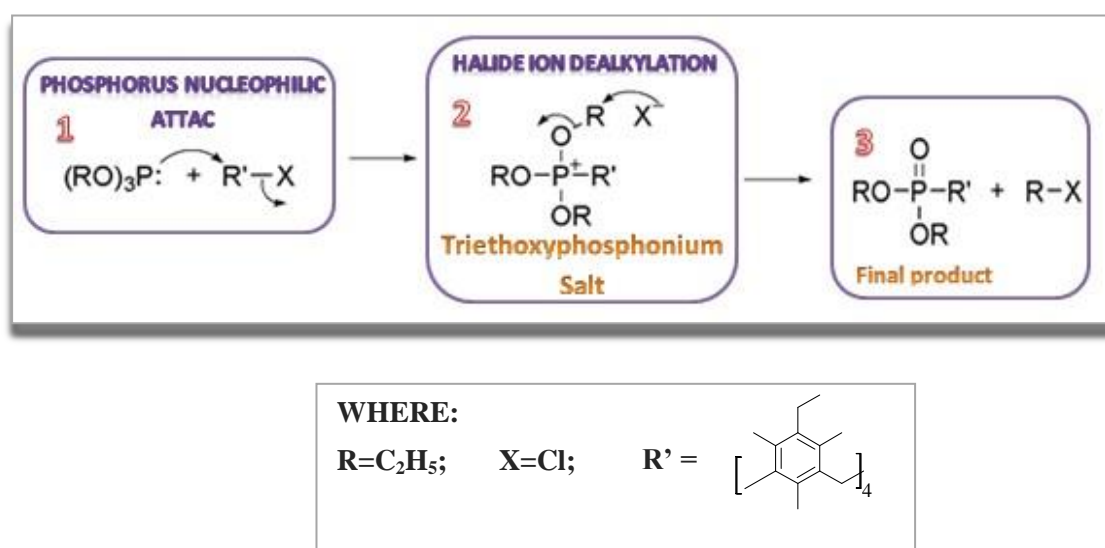


Figure 47: Schematic representation of the Arbuzov reaction mechanism used for the obtention of **L10**.

V 2. Behaviour in solution

$^1\text{H-NMR}$ (DMSO-d_6) spectrum of **L10** is presented in the experimental part and consist of singlet of *ortho*- and *para*- methyl substituents (2.26 ppm and 1.08 ppm respectively) and singlet for protons from the methylene bridges (3.89 ppm) typical to metacyclophane platform. A doublet appears (3.19 ppm) for protons of methylene group located near the phosphorus atom.

As in previous cases, it can be concluded that both the integration and multiplicity of

the peaks correspond to the structure of the desired tetrasubstituted compound exhibiting the symmetric *1,3*-alternate conformation, as expected.

VI CONCLUSION

The present results confirm that in addition to the new carboxyl derivatives of [1111]metacyclophane, which are interesting for the building of extended porous structures, a series of new molecular ligands has also been synthesized. The ligands with quinoline-coordinating sites containing donor nitrogen atoms (at the 6- or 8- positions) and oxygen are attractive and interesting for their luminescent properties and the formation of luminescent molecular materials.¹⁰⁷⁻¹⁰⁹

The mercapto derivative was obtained in connection with the “softness” of the sulfur atom according to the HSAB rules⁷² for binding “soft” or in the other words easily polarizable metal cations (such as Cu^+ , Hg^{2+} , Cd^{2+} etc.), while in the contrary, the phosphonate derivative should behave as a typical “hard” donor group.^{112, 115} This ligand is also interesting for the binding of lanthanides. Furthermore, this type of compounds is also interesting for catalytic and materials science applications.^{119, 120}

It was also interesting to prepare the cyanomethylene derivative to compare its complexing ability to the cyano derivative that was obtained in previous studies.⁸⁷

A comparison of the complexation with silver of these two ligands will be discussed in chapter III.

Chapter III

Coordination propensity of [111]metacyclophane derivatives

I Introduction

Structure-properties relationships are determining for the formation of new functional molecular networks. Tunable properties of extended hybrid metal-organic networks may be reachable by the rational design of organic ligands while playing with the nature and the geometry of the binding sites and by choosing the adapted metallic cations. One of the most effective methods to obtain 3D molecular networks, which are the most interesting for application (magnetic, electronic and porous properties, for example, see chapter I §), is the use of rigid ligands, where the binding sites are divergently oriented with regards to the molecular scaffold. For this purpose, the use of either octahedral or tetrahedral building blocks is of

¹²¹ interest. Along this line, the skeleton involving the macrocyclic platform [1.1.1.1]metacyclophane is particularly attractive because it offers the possibility of designing ligands with tetrahedral orientation of the binding sites due to the rigidity *1,3-Alternate* conformation adopted by the macrocyclic platform. The latter conformation results from the repulsion of the methyl groups located in *ortho*-positions, as shown by examples of coordination networks combining the [1.1.1.1]metacyclophane derivatives and metal cations discussed in Chapter I. Furthermore, the relative simplicity of the tetra-functionalization of the [1.1.1.1]metacyclophane platform opens the way to the design of new tetradentate ligands with a variety of coordinating binding sites for building new H-bonded or coordination networks.

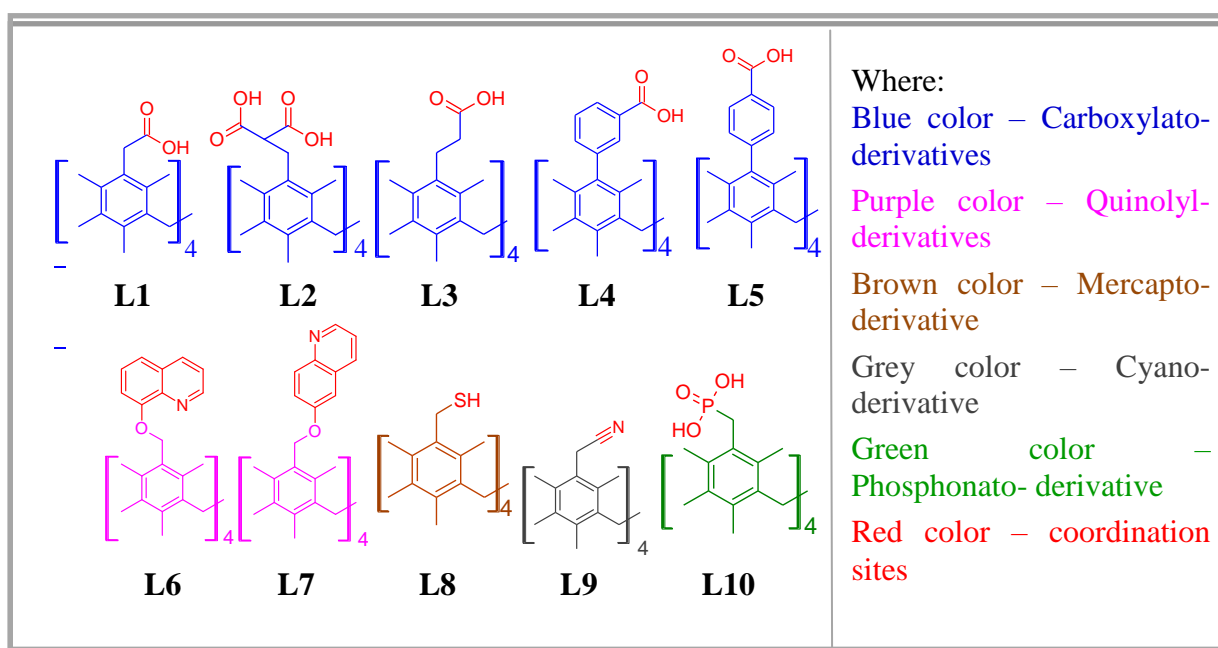


Figure 48: The 10 new targeted ligands.

The synthesis of ligands **L1-L10** (Figure 48) have been already described in chapter II, together with their structure in the solid state, for some of them.

As shown in chapter I, **L1-L5** are carboxylic based ligands, whereas **L6, L7** and **L9** are N-donor tetrasubstituted ligands.

The ability of **L1-L10** to form molecular coordination compounds upon interaction with d and f metal cations was investigated both in the *solid-state* and in *solution*.

The *solid-state* studies were mainly carried out by single crystal X-Ray diffraction. For the formation of such assemblies, common crystallization techniques were used, such as slow evaporation, vapor and liquid diffusion, as well as the solvothermal synthesis (see experimental section). The synthesis of all reported single crystals is described in the experimental section, together with crystallographic tables. Unfortunately, for the majority of compounds, due to the low quantity of crystals or microcrystalline powder, only EA could be performed and no other characterization such as IR for example could be carried out. For the same reason, XRPD was performed only for few compounds (see *Annexes*).

All attempts to obtain single crystals of complexes or extended coordination networks upon the combination of quinolyl (**L6** & **L7**), mercapto (**L8**) and phosphonato (**L10**) derivatives with d and f metal cations failed. In these cases, only formation of polycrystalline materials was observed. In spite of many attempts to obtain suitable single crystals by combination of metal cations with carboxylic derivatives bearing aliphatic spacers between the carboxylic groups and the macrocyclic platform (**L1-L3**) using different crystallization conditions (variation of concentrations and temperature) and techniques (liquid or gas diffusion, evaporation or solvothermal synthesis) were unsuccessful. When using both d- and f-metal cations, new high dimensional coordination networks may be formed along with discrete complexes.

Unfortunately, with various metal cations such as Cu^{2+} , Zn^{2+} , Ni^{2+} , Co^{2+} and Ag^+ only colored or non-colored gel-like materials were obtained (the picture of some of them is presented in figure 49). This phenomenon can result from the enhanced flexibility of ligands.

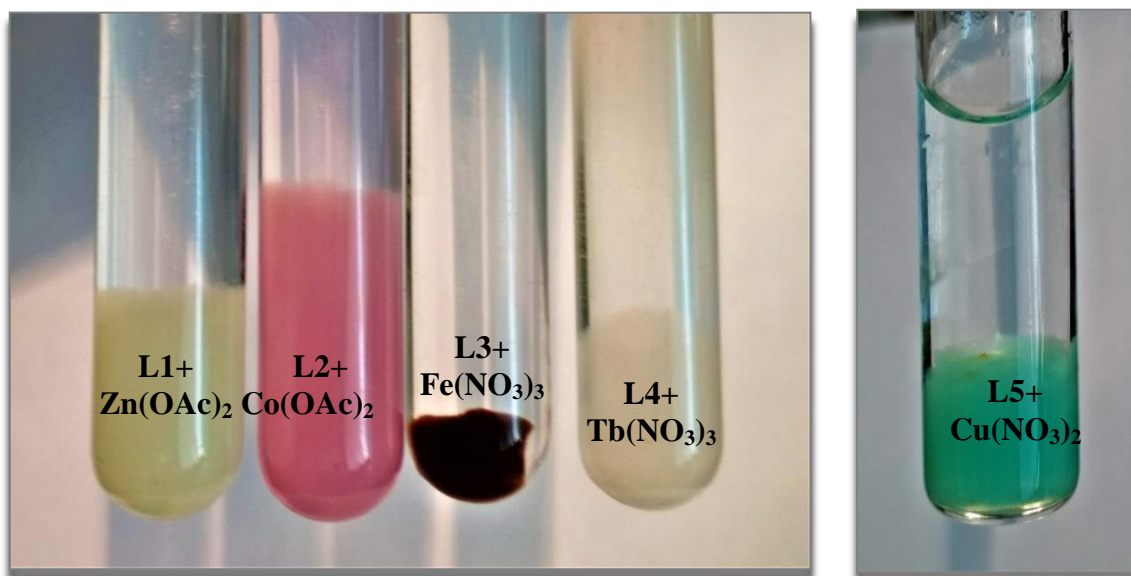


Figure 49. Picture of some gel-like compounds based on [1111]metacyclophane derivatives (**L1-L5**) when combined with $\text{Zn}(\text{NO}_3)_2$, $\text{Co}(\text{OAc})_2$, $\text{Fe}(\text{NO}_3)_3$, $\text{Tb}(\text{NO}_3)_3$ and $\text{Cu}(\text{NO}_3)_2$ salts.

Coordination compounds have been obtained in the crystalline state for the N donor ligand **L9** tetracyanomethyl [1.1.1.1]metacyclophane derivative and Ag^+ cation. In this case, as shown, the stoichiometry plays a crucial role as well as the nature of the anion (NO_3^- or BF_4^-) on the formation of 1D coordination network or a discrete binuclear metallomacrocycle.⁹³

On the other hand, using Mn (II) cation combined with tetra carboxylic derivatives (**L4** and **L5**) bearing aryl spacers, the formation of 1D and 3D coordination polymers is observed.

Chapter §III focuses on description and discussion of the different factors playing a significant role in the formation of coordination networks and their influence on the observed coordination patterns and resulting dimensionalities of the coordination polymer. Among the discussed factors, one can mention: i) the nature of the spacer between the coordinating groups and the macrocyclic platform (aliphatic or aromatic) *i.e.* the rigidity or relative flexibility of the ligand, ii) the localization of the coordinating sites (*ortho*- or *para*- position of the aromatic spacer), iii) the nature of coordinating site *i.e.* the nature of donor atoms and iv) the nature of the metal cation and its counter-anion.

For the studies in **solution**, the UV titration experiments have been performed, together with DLS measurements and, for one family, the picrate extraction. The titrations have been performed for the combination of ligands and metals that led to the formation of coordination polymers in the solid-state.

II. Coordination networks based on carboxylic derivatives of [1111]metacyclophane

Carboxylate bearing ligands, offering an ionic character for binding metal cations, are well known for the formation of MOFs, generally combined with divalent metal cations, under solvothermal conditions, in DMF as the solvent.¹²²

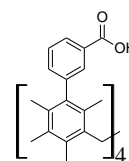
Concerning macrocyclic compounds, only one tetrasubstituted carboxylic acid derivative of [1.1.1.1]metacyclophane bearing four carboxylic groups directly attached to the macrocyclic backbone has been reported.⁷⁷ But, to the best of our knowledge, carboxylic derivatives of [1111]metacyclophane have never been used for the generation of coordination polymers, despite the fact that these are very attractive ligands for the construction of polymers due to the rigidity of the macrocyclic platform and the tetrahedral geometry for the location of the coordinating centers. This should allow the formation of stable structures, which is a requirement for their potential application.

In order to crystallize the carboxylic derivatives of [1111]metacyclophane **L1-L5** appended with aliphatic and aromatic spacers, many attempts have been developed, using various crystallization conditions. Unfortunately and as already mentioned, single crystals suitable for X-ray diffraction analysis were obtained only for carboxylic derivatives with aromatic spacers: **L4** and **L5**. Thus, two different 1D and 2D coordination polymers based on **L4** and manganese (II) or cobalt (II) cations, and one 3D coordination polymer involving **L5** manganese (II) cations were obtained.

II 1. Coordination compounds with Mn cations

Manganese(II) cation was chosen due to their ability to form magnetic active materials like Single Molecular Magnets.¹²³⁻¹²⁵ Manganese salts were combined with **L4** and **L5**, with the aim of obtaining new magnetic materials.

II 1.1. 1D coordination polymer based on **L4**



The combination of $\text{Mn}^{\text{II}}(\text{OAc})_2$ with **L4** (see experimental section) leads to the formation of a 1-D manganese (trigonal space group: R32 (chiral space group) see Annex,

crystallographic part) coordination polymer with the formula $(C_{68}H_{64}O_8)_3Mn_9O_3(CH_3COO)_6(C_5H_5N)_{12}$ *i.e.* $(L4)_3Mn_9O_3(OAc)_6py_9 \bullet 3py$ presenting the following stoichiometry: $L4/Mn^{2+} = 1/3$.

The crystal is composed of **L4**, two crystallographically different Mn cations with the formation of a Mn trinuclear cluster, molecules of coordinated pyridine, an oxide anion O^{2-} and OAc^- anions. Uncoordinated pyridine molecules are also located within the crystal. Both Mn1 and Mn2 cations, hexacoordinated with a NO_5 set of heteroatoms, are presenting a distorted octahedral geometry with N atoms belonging to pyridine molecules in the vertices of a triangle, oxide O^{2-} atoms and oxygen atoms from carboxylate of **L4** and OAc^- anions, as shown in figure 1a. More detailed characteristics of angles and bonds are given below in the tables 2 and 3.

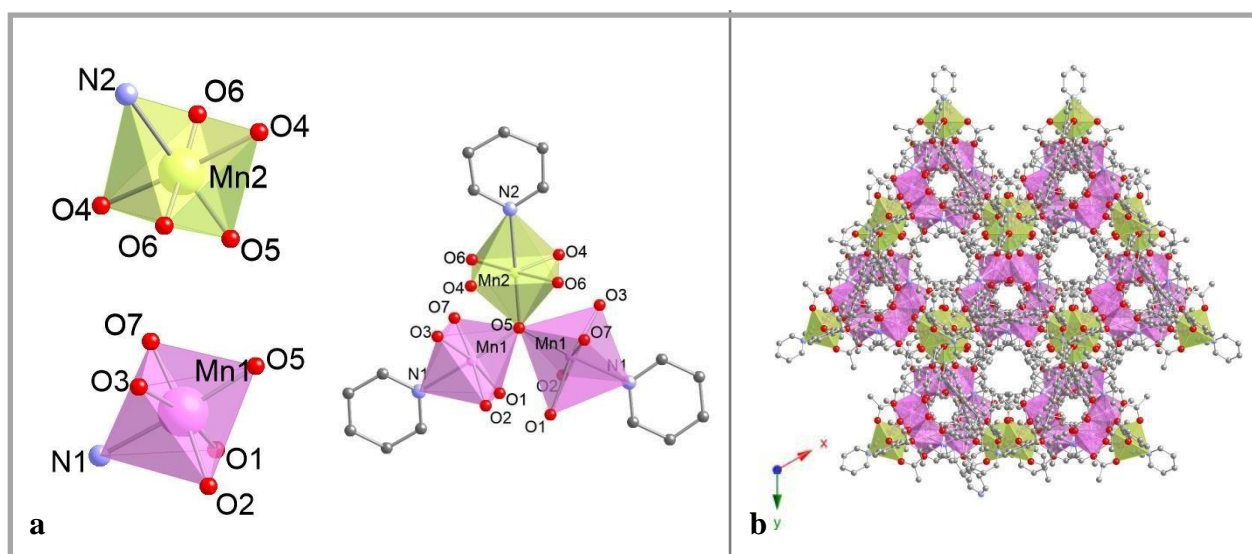


Figure 50: (a) Mn environment and some portion of $(L4)_3Mn_9O_3(OAc)_6py_9 \bullet 3py$ (b) crystal structure along c axis evidencing the pores formed in the structure.

Concerning the charge balance, one has to analyze first the protonation state of ligand **L4**. As shown in table 4, the C-O distances are in accordance with full deprotonation of ligand **L4**. This is also the case for OAc^- anions, and probably for the central oxygen atom, that can be assumed to be O^{2-} anion. In this case, the presence of a mixed valence state for 3 Mn with 1 Mn^{II} / 2 Mn^{III} ratio should be observed, as usually reported for manganese clusters. The proposed formula is $\{(L4)_3Mn_9O_3(OAc)_6py_9 \bullet 3py\}$. This has to be confirmed by magnetic measurements and also XPS measurements, for example by magnetic measurements and also XPS measurements, for example.

The bonds and angles characteristics for the slightly deformed octahedral environment of both manganese atoms are given in tables 2 and 3. They are characteristics of Mn^{II} / Mn^{III} species in O₅N environment, which cannot be precisely distinguished. On the other hand, the distances between Mn1 and Mn2 inside the cluster are 3.508 and 3.508 Å while the distances between two clusters inside the polymer are: 16.627 and 21.528 Å ($d_{\text{Mn1-Mn1}}$), 21.038 Å ($d_{\text{Mn2-Mn2}}$). At the same time, the distances between two clusters of the neighboring chains (such as in Figure 51) are 8.273, 10.920, 12.646, 16.811 Å ($d_{\text{Mn1-Mn1}}$) and 11.125 Å ($d_{\text{Mn2-Mn2}}$).

Table 2: Mn-N and Mn-O distances (Å) in (L4)₃Mn₉O₃(OAc)₆py₉•3py

	N1	N2	O1	O2	O3	O4	O5	O6	O7
Mn1	2.159	-	2.210	1.996	2.153	-	2.012	-	1.996
Mn2	-	2.254	-	-	-	2.081	1.987	2.190	-

Table 3: N-Mn-O and O-Mn-O angles (°) in (L4)₃Mn₉O₃(OAc)₆py₉•3py

N1-Mn1-O3	O3-Mn1-O7	O7-Mn1-O5	O5-Mn1-O1	O1-Mn1-O2	O2-Mn1-N1	O7-Mn1-O2	O2-Mn1-O5
84.4	91.7	90.4	97.5	87.6	87.3	174.7	94.9
O2-Mn1-O3	O5-Mn1-O3	O7-Mn1-N1	O5-Mn1-N1	O7-Mn1-O1	O3-Mn1-O1	N1-Mn1-O1	
88.4	91.8	87.4	175.6	91.3	170.1	86.4	
O6-Mn2-O4	O4-Mn2-O5	O5-Mn2-O6	N2-Mn2-O6	N2-Mn2-O4	O4-Mn2-O4	O5-Mn2-O6	
88.3	91.7		89.2	88.3			
91.7	91.7	90.827	89.2	88.3	176.5	90.8	
O6-Mn2-O6	O5-Mn2-N2						
178.4	180.0						

In the crystal, the coordination pattern leads to formation of a spiral-like structure where each trinuclear cluster is bonded to two adjacent macrocyclic molecules acting as bis-bidentate ligands, as shown in figure 51 b. The chains are packed in antiparallel fashion forming the layers along the [110] crystallographic plane, as shown in figure 2b. The crystal structure is completed by the stacking of these layers in antiparallel orientation (see figure 51 c and d) leading to pores formation along the *c* axis with a diameter of *ca* 3.00 Å.

The R32 chiral space arises from the fact that the 1D coordination polymer forms a

helix in the crystal lattice, as shown in scheme 11 and figure 51 b, and that in the crystal, only one type of helix (P or M) is present.



Scheme 11. Schematic representation of the helix formed in the crystal by the 1D $(\mathbf{L4})_3\text{Mn}_9\text{O}_3(\text{OAc})_6\text{py}_9$ coordination polymers

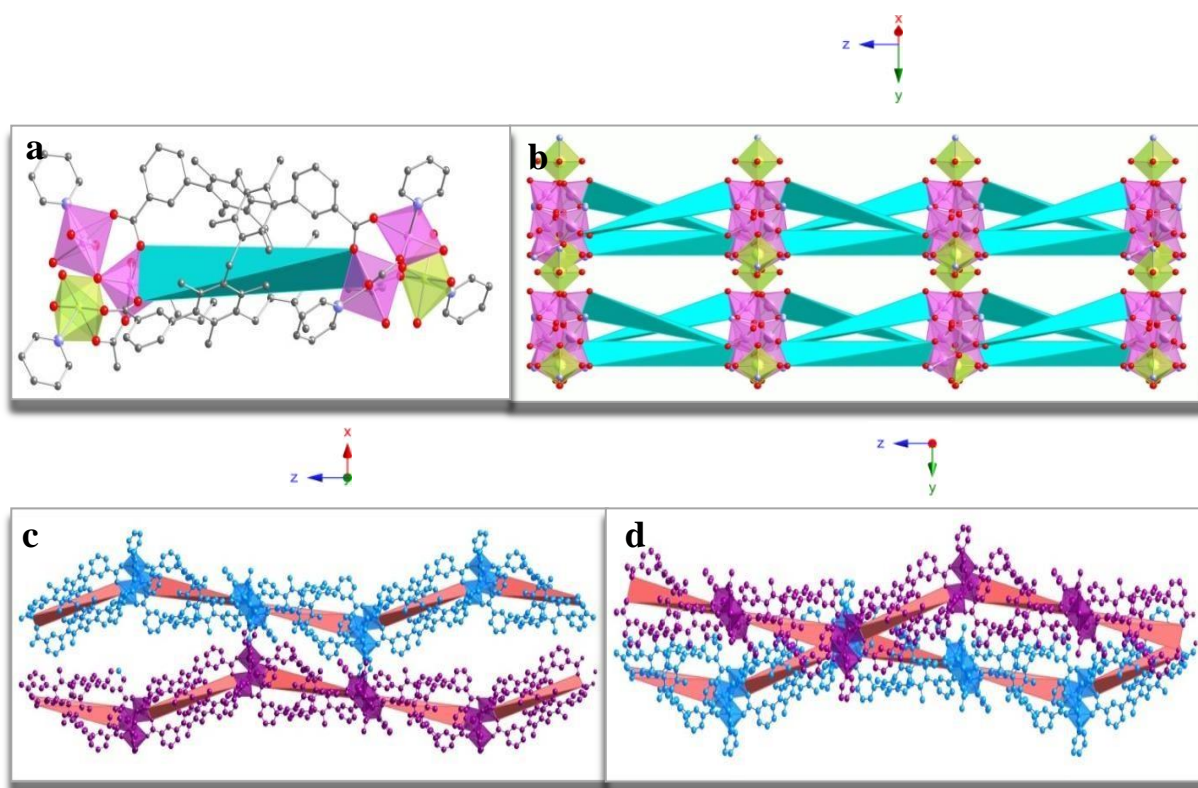


Figure 51: Representation of $(\mathbf{L4})_3\text{Mn}_9\text{O}_3(\text{OAc})_6\text{py}_9 \cdot 3\text{py}$ (a, b) portion of the corresponding 1D network and (c, d) chains inside the layers along a (c) and b (d). H atoms are omitted for clarity.

Since $\mathbf{L4}$ was crystallized with metallic cations, it seems interesting to compare the bonds and angles for $\mathbf{L4}$ (protonated) in the crystalline phase (see Chapter II) with the one of

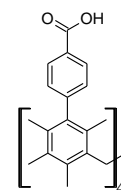
L4 (deprotonated) in $(\mathbf{L4})_3\text{Mn}_9\text{O}_3(\text{OAc})_6\text{py}_9 \bullet 3\text{py}$. Thus, it was found that the dihedral angle between mesitylene rings of **L4** (36.91°) slightly decreased to 34.88° , as shown in table 4. C-O distances display a significant decrease as well as the dihedral angles between aryl spacers and mesitylen groups, as represented in table 1. Whereas in the free ligand crystal practically the highly symmetrical structure presenting a perpendicular orientation of mesitylene moieties respecting the aryl spacers is observed, in $(\mathbf{L4})_3\text{Mn}_9\text{O}_3(\text{OAc})_6\text{py}_9 \bullet 3\text{py}$, the cluster formation imposes the distortion of ligand symmetry.

Parameters	L4	$(\mathbf{L4})_3\text{Mn}_9\text{O}_3(\text{OAc})_6\text{py}_9 \bullet 3\text{py}$
d_{CO} (Å)	1.186	1.233
	1.250	1.237
	1.267	1.253
	1.389	1.283
Dihedral angle between opposite mesitylene moieties ($^\circ$)	36.21	34.88
Dihedral angle between mesitylene moieties and aryl spacers ($^\circ$)	89.51	70.87
	89.68	64.73

Table 4: Comparison of distances in **L4**, for **L4** and $(\mathbf{L4})_3\text{Mn}_9\text{O}_3(\text{OAc})_6\text{py}_9 \bullet 3\text{py}$

The trinuclear Mn_3O core, analogue to the one found in $(\mathbf{L4})_3\text{Mn}_9\text{O}_3(\text{OAc})_6\text{py}_9 \bullet 3\text{py}$ has already been encountered in other coordination compounds.¹²⁶ The magnetic measurements of $(\mathbf{L4})_3\text{Mn}_9\text{O}_3(\text{OAc})_6\text{py}_9 \bullet 3\text{py}$ are under progress, limited by the low quantities of obtained compounds.

II 1.2. 3D coordination polymer based on **L5**



The combination, under solvothermal conditions, of **L5** and $\text{Mn}^{\text{II}}(\text{NO}_3)_2$ in DMF (see experimental section) successfully led to the formation of a 3D coordination polymer crystallizing in the monoclinic $C2/c$ space group and presenting the following formula $\{(\text{C}_{68}\text{H}_{64}\text{O}_8)\text{Mn}_2 (\text{C}_3\text{H}_7\text{NO})_2\}$ *i.e.* $[(\mathbf{L5})\text{Mn}_2(\text{DMF})_2]$ (see Annex, crystallographic part)

presenting the following stoichiometry: $\mathbf{L5}/\text{Mn}^{2+} = 1/2$.

XRPD diagram is presented in *Annexes*. From the experimental data, we can conclude that the observed microcrystalline powder contains the phase observed in the single-crystals. But the quality of the diagram is poor.

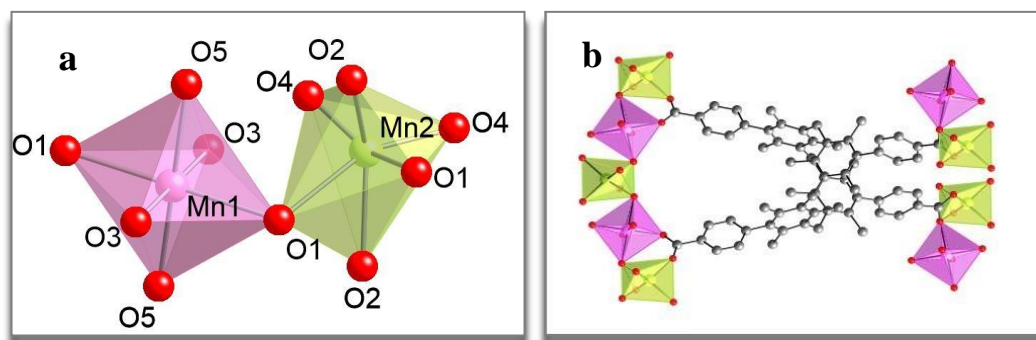


Figure 52: Mn^{2+} environment (a) and localization (b) in the crystal structure of $(\mathbf{L5})\text{Mn}_2(\text{DMF})_2$.

The crystal is composed of ligand **L5**, two crystallographically different Mn^{2+} cations and DMF molecules (Figure 52). In this case, there is no ambiguity concerning the oxidation state of Mn, assuming that **L5** is fully deprotonated (see the C-O distances in table 7), the oxidation state of Mn is +2 and the complete formula $(\mathbf{L5})\text{Mn}^{\text{II}}_2(\text{DMF})_2$

The distance between Mn1 and Mn2 within the dinuclear cluster is equal to 3.789 Å, at the same time, the distances between two clusters within the polymer are: 21.876 and 21.109 Å ($d_{\text{Mn1-Mn1}}$), 21.876, 23.453 and 22.682 Å ($d_{\text{Mn2-Mn2}}$). On the other hand, the distance between two clusters of the neighboring chains (such as in Figure 53) is 14.284 Å (both for $d_{\text{Mn1-Mn1}}$ and $d_{\text{Mn2-Mn2}}$).

	O1	O2	O3	O4	O5
Mn1	2.234	-	2.219	-	2.159
Mn2	2.270	2.257	-	2.033	-

Table 5: Mn-N and Mn-O distances (Å) in $(\mathbf{L5})\text{Mn}_2(\text{DMF})_2$.

O3-Mn1-O1	O5-Mn1-O1	O3-Mn1-O5	O4-Mn1-O2	O5-Mn1-O5	O3-Mn1-O3
87.73 92.27	87.51 92.49	86.93 93.07	98.3 111.77	180	180
O4-Mn2-O4	O2-Mn2-O2	O1-Mn2-O1	O1-Mn2-O2	O1-Mn2-O4	
90.4	137.1	85.19	57.51 89.93	97.20 155.76	

Table 6: O-Mn-O angles (°) in (L5)Mn₂(DMF)₂.

Parameters	L5	(L5)Mn ₂ (DMF) ₂
d _{CO} (Å)	1.240	1.215
	1.301	1.245
		1.256
		1.288
Dihedral angle between opposite mesitylene moieties (°)	28.4	31.17
Dihedral angle between mesitylene moieties and aryl spacers (°)	71.23	74.45

Table 7: Comparison of distances in L5 and (L5)Mn₂(DMF)₂

Within the crystal lattice, the Mn²⁺ cations form chains along the *c* axis supported by tetradeprotonated L5 ligands orientated side by side in an alternate fashion along the *a* axis acting as molecular pillars (Figures 53 a, b, d and e). Such coordination pattern produces the formation of square-like pores with size approximately equals to 12x5 Å² (Figure 53 c).

As in the previous case, it seems interesting to compare the bonds and angles for L5 (protonated) in the crystalline phase (see Chapter II) with the one of L5 (deprotonated) in (L5)Mn₂(DMF)₂.

As shown in table 6, there is an increase in the dihedral angles (both types) and decrease of maximal distance value between C and O atoms in carboxylic groups (Table 6). On the other hand, the distances between Mn²⁺ and O atoms of carboxylate groups are equal to 2.033, 2.219, 2.234, 2.270, 2.257 Å respectively, while DMF moieties are located at the distance of 2.159 Å from Mn²⁺ center.

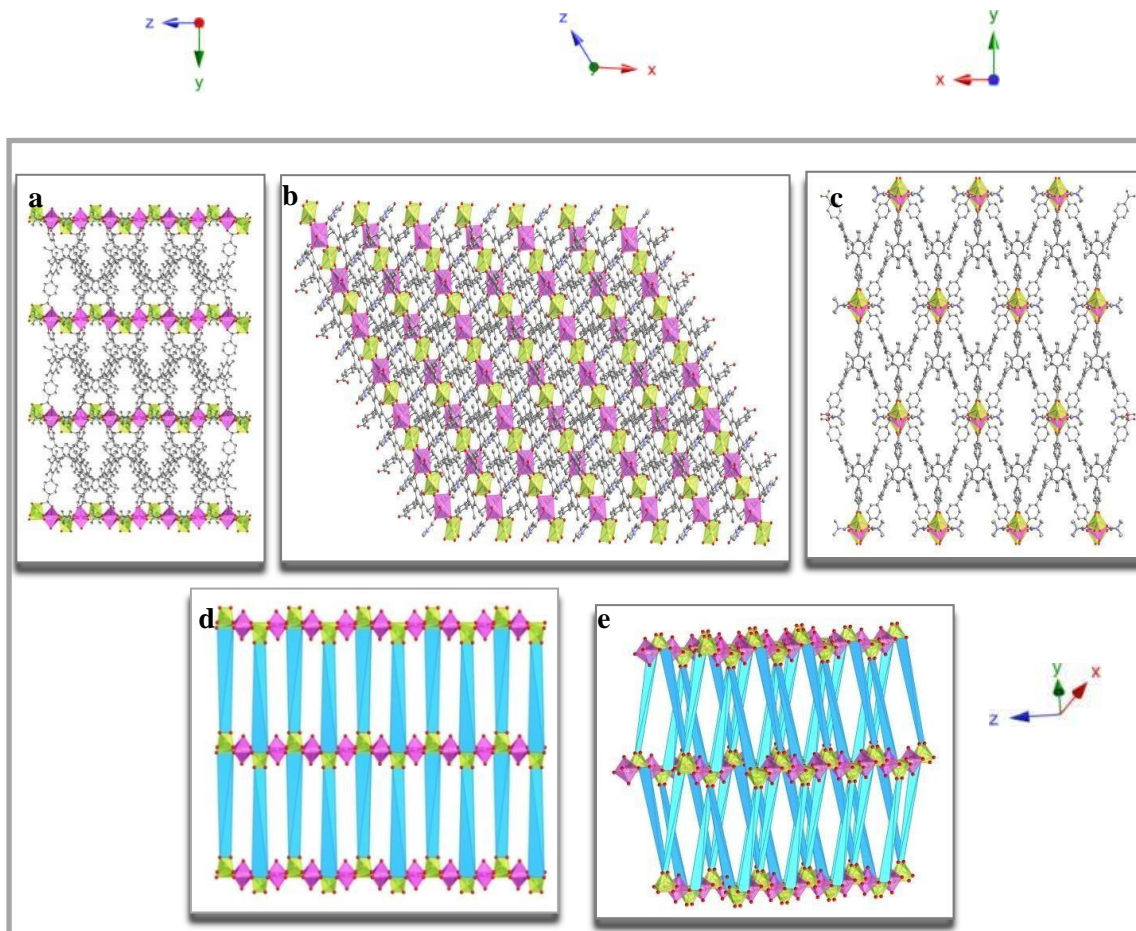


Figure 53: Some portions of $(\mathbf{L5})\text{Mn}_2(\text{DMF})_2$ networks along a , b and c axes, together with their corresponding polyhedral representation.

II 1.3 Conclusion

Under solvothermal conditions, two extended crystalline Mn^{2+} 1D and 3D structures based on ligand **L4** (in pyridine, $(\mathbf{L4})_3\text{Mn}^{\text{II}}_3\text{Mn}^{\text{III}}_6\text{O}_3(\text{OAc})_6\text{py}_9 \bullet 3\text{py}$) and **L5** (in DMF, $(\mathbf{L5})\text{Mn}^{\text{II}}_2(\text{DMF})_2$), displaying coordinating carboxylate moieties were obtained and structurally characterized.

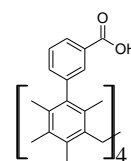
In both coordination polymers, ligands were found to be totally deprotonated, and the most significant changes in **L4** structure was the decrease of the dihedral angle between mesitylene moieties and aryl spacers while for **L5**, there was only low shifts for characteristic values such as dihedral angles and bond distances. The ability of ligand **L4** to form cluster-like structures was also discovered, together with a partial oxidation of the Mn cations into Mn^{III} , while **L5** formed a 3D porous structure, presenting Mn cations in the oxidation state +2.

The formation of trinuclear compounds with mixed valence manganese is of interest from the magnetic point of view, $(\mathbf{L4})_3\text{Mn}^{\text{II}}\text{Mn}^{\text{III}}\text{O}(\text{OAc})\text{py}\cdot 3\text{py}$ may present SMM properties. This should be confirmed by magnetic measurements.

II 2. Coordination compound with Co cations

As already known, the cobalt cation is distinguished by its flexibility and diversity in its coordination sphere, unlike manganese, which requires an octahedral coordination sphere. Moreover, cobalt offers two stable oxidation states (2 and 3), while manganese exhibits oxidation states 2, 3 and 4. At the same time, both cobalt and manganese cations find applications in redox switching systems and offers physical property like magnetism.

II 2.1. 2D coordination network based on $\mathbf{L4}$



The combination of $\mathbf{L4}$ with $\text{Co}(\text{OAc})_2$ in DMF under solvo-thermal conditions (see experimental section) afforded crystalline materials. The X-ray diffraction on single crystal revealed the formation of a 2D structure crystallizing in the monoclinic $P2_1/c$ space group with the $2/5 \mathbf{L4}/\text{Co}^{2+}$ stoichiometry (formula $\{(\text{C}_{68}\text{H}_{64}\text{O}_8)_4\text{Co}_{10}\text{O}_4(\text{CH}_3\text{OH})_2(\text{H}_2\text{O})_4(\text{CH}_3\text{COO})_2 \cdot (\text{C}_3\text{H}_7\text{NO})(\text{H}_2\text{O})_7 \cdot \text{S}\}$ *i.e.* $\{\mathbf{L4}_4\text{Co}_{10}\text{O}_2(\text{MeOH})_2(\text{H}_2\text{O})_4(\text{OAc})_2 \cdot \text{S}\}$: not all water or solvent molecules could be refined in the crystalline structure, and squeeze command¹⁰⁷ was applied). The crystal is composed of $\mathbf{L4}$, five different Co cations (Figure 54), two oxide anions, one acetate anion, coordinated water and MeOH, DMF and H_2O molecules as solvents. The data were recorded at the synchrotron and the refinement was only partial and preliminarily as shown in the experimental section. As shown in table 4, in $\mathbf{L4}$, the C-O distances are coherent with a partial deprotonation of $\mathbf{L4}$, that could lead to an oxidation state of cobalt of +II, leading to the formula $\mathbf{L4}_4\text{Co}^{\text{II}}_{10}\text{O}_2(\text{MeOH})_2(\text{H}_2\text{O})_4(\text{OAc})_2 \cdot (\text{C}_3\text{H}_7\text{NO})(\text{H}_2\text{O})_7$. But this has to be confirmed first by a new refinement of the structure with a crystal of higher quality and by magnetic and XPS measurements.

The three crystallographically independent Co cations are hexacoordinated with a O_6 coordination sphere and present a distorted octahedral geometry, while two crystallographically independent Co cations are tetracoordinated with a O_4 coordination sphere

as shown in figures 5a and c. In the pentanuclear system, the oxygen atoms are belonging to: i) the deprotonated carboxylate species, ii) two water molecules, iii) a methanol molecule and iv) acetic acid. For precise values of bond distances and angles of the deformed coordination spheres of the 5 crystallographically independent Co atoms, see the tables 8 and 9.

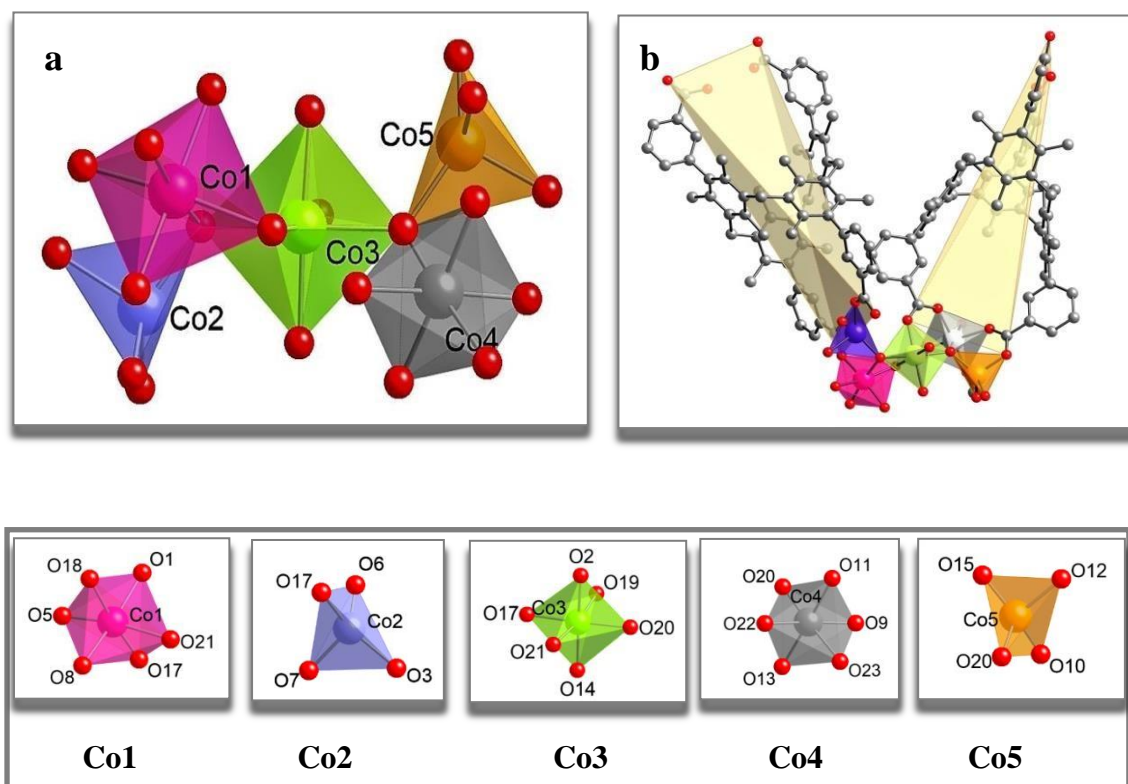


Figure 54: Co^{2+} environment (a) and localization of **L4** (b) in the crystal structure of $\text{L}_4\text{Co}_{10}\text{O}_2(\text{MeOH})_2(\text{H}_2\text{O})_4(\text{OAc})_2 \cdot (\text{C}_3\text{H}_7\text{NO})(\text{H}_2\text{O})_7$

At the same time, the distances between Co^{2+} within the cluster are: 3.183 Å ($d_{\text{Co1-Co2}}$); 5.676 Å ($d_{\text{Co1-Co4}}$); 6.142 Å ($d_{\text{Co1-Co5}}$); 3.149 Å ($d_{\text{Co1-Co3}}$); 3.607 Å ($d_{\text{Co2-Co3}}$); 3.442 Å ($d_{\text{Co2-Co4}}$); 7.103 Å ($d_{\text{Co2-Co5}}$); 3.442 Å ($d_{\text{Co3-Co4}}$); 3.540 Å ($d_{\text{Co3-Co5}}$) and 3.239 Å ($d_{\text{Co4-Co5}}$) while the distances between the proximate clusters within one polymeric chain are: 24.887 Å ($d_{\text{Co1-Co1}}$); 26.004 Å ($d_{\text{Co2-Co2}}$); 21.701 Å ($d_{\text{Co3-Co3}}$); 19.463 Å ($d_{\text{Co4-Co4}}$) and 18.979 Å ($d_{\text{Co5-Co5}}$). On the other hand, the distances between the clusters of neighboring chains (like in figure 9 (a)) in the crystal are: 17.338 and 24.477 Å ($d_{\text{Co1-Co1}}$); 23.398 and 20.289 Å ($d_{\text{Co2-Co2}}$); 18.245 and 15.329 Å ($d_{\text{Co3-Co3}}$); 9.255 and 16.708 Å ($d_{\text{Co4-Co4}}$) and 13.744 and 14.119 Å ($d_{\text{Co5-Co5}}$). The 2D networks form antiparallel arrays along the *b* axis as shown in figures 55 a, b and c.

	O1	O5	O8	O17	O18	O21	O3	O7	O6	O20	O14	O2	O19
Co 1	2.030	2.048	2.085	2.105	2.149	2.149	-	-	-	-	-	-	-
Co 2	-	-	-	1.924	-	-	1.904	1.953	1.997	-	-	-	-
Co 3	-	-	-	2.066	-	2.104	-	-	-	2.041	2.095	2.101	2.183
	O13	O20	O22	O11	O9	O23	O15	O12	O10				
Co 4	2.077	2.094	2.102	2.108	2.122	2.142							
Co 5		1.939					1.926	1.956	1.983				

Table 8: Co-O distances (Å) in $L4_4Co_{10}O_2(CH_3OH)(H_2O)_2(CH_3COOH)\bullet(C_3H_7NO)(H_2O)_n$.

O1-Co1-O5	O1-Co1-O8	O5-Co1-O8	O1-Co1-O17	O5-Co1-O17	O8-Co1-O17	O1-Co1-O18	O5-Co1-O18
93.6	167.9	91.3	89.1	87.5	102.2	85.0	93.2
O8-Co1-O18	O17-Co1-O18	O1-Co1-O21	O5-Co1-O21	O5-Co1-O21	O17-Co1-O21	O18-Co1-O21	
83.7	174.1	88.2	166.2	89.6	79.2	100.3	

O3-Co2-O17	O3-Co2-O7	O17-Co2-O7	O3-Co2-O6	O17-Co2-O6	O7-Co2-O6
136.6	93.1	111.4	109.6	99.2	103.1

O20-Co3-O17	O20-Co3-O14	O17-Co3-O14	O20-Co3-O2	O17-Co3-O2	O14-Co3-O2	O20-Co3-O21	O17-Co3-O21
173.8	90.4	88.3	86.8	95.0	174.7	104.7	81.4
O14-Co3-O21	O2-Co3-O21	O20-Co3-O19	O17-Co3-O19	O14-Co3-O19	O2-Co3-O19	O21-Co3-O19	
89.8	86.5	83.3	90.8	93.5	90.6	171.4	

O13-Co4-O20	O13-Co4-O22	O20-Co4-O22	O13-Co4-O11	O20-Co4-O11	O22-Co4-O11	O13-Co4-O9	O20-Co4-O9
84.9	90.3	100.5	175.2	97.5	85.3	91.3	84.5
O22-Co4-O9	O11-Co4-O9	O13-Co4-O23	O20-Co4-O23	O22-Co4-O23	O11-Co4-O23	O9-Co4-O23	
174.9	93.0	91.8	170.5	88.5	86.4	86.6	

O15-Co5-O20	O15-Co5-O12	O20-Co5-O12	O15-Co5-O10	O20-Co5-O10	O12-Co5-O10
133.6	99.6	108.7	104.4	102.0	106.3

Table 9: O-Co-O angles (°) in $L4_4Co_{10}O_2(MeOH)_2(H_2O)_4(OAc)_2\bullet(C_3H_7NO)(H_2O)_7$.

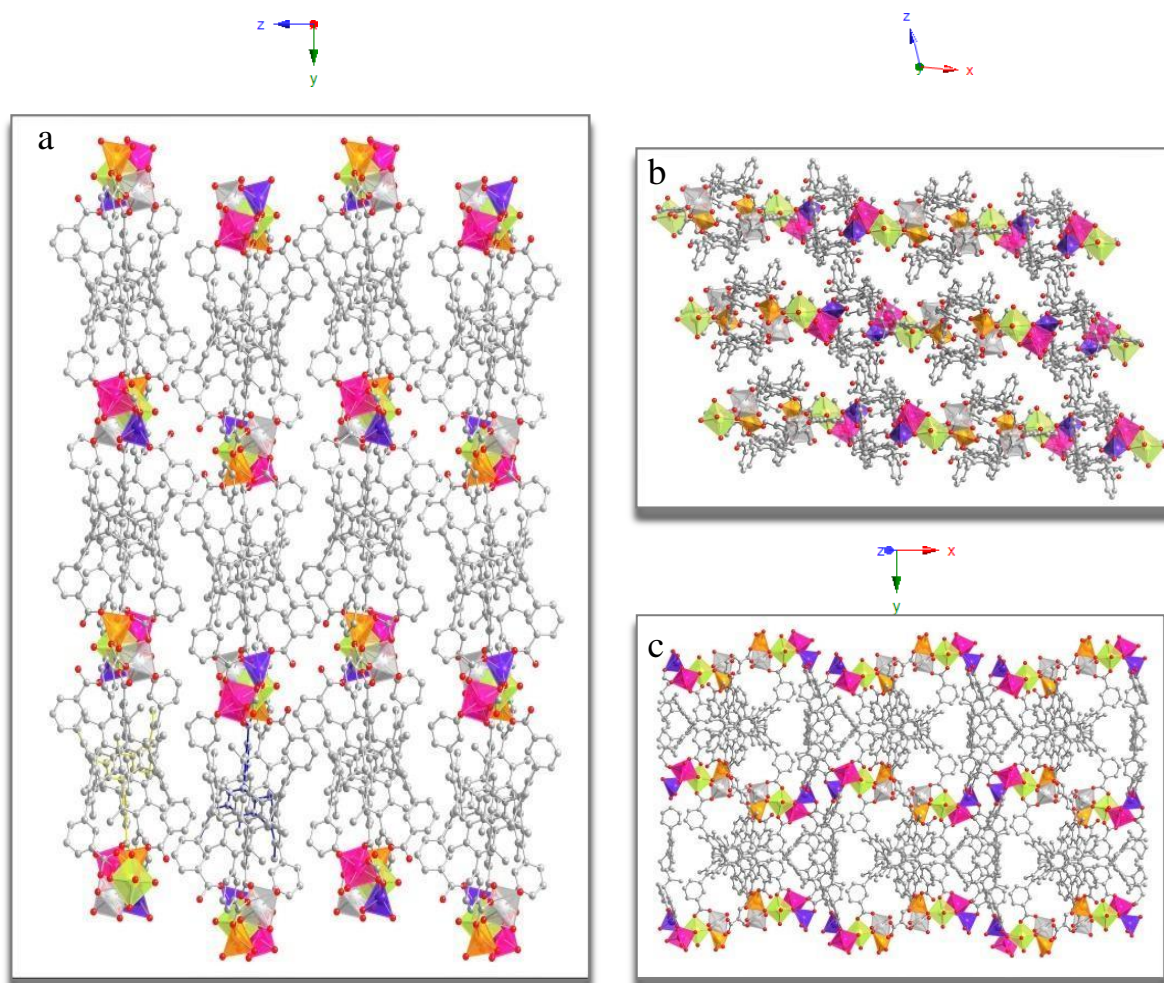


Figure 55: $\text{L4}_4\text{Co}_{10}\text{O}_2(\text{MeOH})_2(\text{H}_2\text{O})_4(\text{OAc})_2 \cdot (\text{C}_3\text{H}_7\text{NO})(\text{H}_2\text{O})_7$ networks along a (a), b (b) and c (c) axes.

In comparison with the crystalline structure of **L4** (protonated), in $\text{L4}_4\text{Co}_{10}\text{O}_2(\text{MeOH})_2(\text{H}_2\text{O})_4(\text{OAc})_2 \cdot (\text{C}_3\text{H}_7\text{NO})(\text{H}_2\text{O})_7$ (**L4** partially deprotonated), we observe an increase of the dihedral angles between opposite mesitylene moieties and at the same time, a decrease of dihedral angles between mesitylene moieties and aryl spacers (see table 10). Thus, the structure in the coordination compound is “less distorted” in comparison with the one of the free ligand.

As already mentioned, the C-O-distances of **L4** in $\text{L4}_4\text{Co}_{10}\text{O}_2(\text{MeOH})_2(\text{H}_2\text{O})_4(\text{OAc})_2 \cdot (\text{C}_3\text{H}_7\text{NO})(\text{H}_2\text{O})_7$ are not fully compatible with a total deprotonation of the carboxylic moieties within the coordination network (see table 10). From

the obtained data, we could determine that among the two crystallographically independent **L4** molecules, one is fully deprotonated and the other has 3 deprotonated and 1 protonated carboxylic moieties. As a consequence, the formal charge dedicated to **L4** is (-14).

Parameters	L4	L4 ₄ Co ₁₀ O ₄ (MeOH) ₂ (H ₂ O) ₄ (OAc) ₂ • (C ₃ H ₇ NO)(H ₂ O) ₇ • S
d CO (Å)	1.186 1.250 1.267 1.389	1.261 1.283 1.245 1.281 1.235 1.242 1.272
Dihedral angle between opposite mesitylene moieties (°)	36.21	41.21
Dihedral angle between mesitylene moieties and aryl spacers (°)	89.51 89.68	78.99 73.16

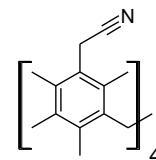
Table 10: Comparison of distances in **L4**, for **L4** and **4**₄Co₁₀O₂(MeOH)₂(H₂O)₄(OAc)₂ • (C₃H₇NO)(H₂O)₇.

II 2.2. Conclusion

The combination, under solvothermal conditions, of L4, presenting coordinating carboxylic moieties, with $\text{Co}(\text{OAc})_2$ leads to a coordination complex bearing pentanuclear cobalt units (five instead of three) with preservation of the chelate type binding. The precise formula of the compound requires further refinement and investigations, but this compound belongs to the family of high-dimensional Cobalt compounds presenting high nuclearity clusters.¹²⁷ The magnetic properties of such compounds are of interest due high spin orbit coupling of the cobalt cations.

This type of compound may be promising for further studies because of its potential redox and magnetic properties.

III Coordination networks based on cyanomethyl derivative of [1111] metacyclophane L9



The cyano coordinating group belongs to the weak N-donor coordinating groups, nevertheless it is widely used for the formation of coordination networks in the crystalline phase in the presence of monovalent metal cations, in particular Ag(I), Au(I) or Cu(I) cations. Moreover, the generation of 1-3D coordination polymers has been successfully demonstrated when tetrasubstituted calixarene and metacyclophane based ligands decorated with cyano coordinating sites were combined with silver ions. For example, a 1D non tubular coordination polymers based on *p-tert*butylthiacalix[4]arene and *p-H*-thiacalix[4]arene with appended cyano group using flexible propylene spacer have been obtained in the crystalline phase in the presence of AgPF_6 .^{68b,128} It was shown that, the use an excess of silver cation and coordinating anions such as nitrate anion and a tetracyanobenzyl thiacalix[4]arene derivative, leads to the formation of clusters organized inside the coordination polymer.¹²⁹ On the another hand, the most interesting example concerning the formation of 1D coordination polymer using metacyclophane platform was reported for a cyano metacyclophane derivative for which the nitrile fragment is directly attached to the mesitylene backbone. The combination of the latter

with silver cation leads to formation of a 1D tubular structure (see also figure 60 a).⁸⁷ The previously reported examples prompted us, as shown in Chapter I §XX, to investigate other positioning of the cyano coordinating groups on the [1.1.1.1]metacyclophane platform. Through this work, we intend to investigate the influence of the spacers between cyano coordinating groups and the macrocycle on the formation of coordination polymers. We were interested in how the addition of one methylene spacer between the coordinating center and the meta-cyclophane skeleton could affect the self-assembly process. For this reason, we designed ligand **L9** of the cyanomethylene metacyclophane type.

When combined with silver cations, we obtained two types of coordination compounds presented below. Unfortunately, combinations with Cu(I) or Au(I) cations didn't lead to the formation of single crystals.

The results presented below evidenced a behavior depending on the stoichiometry between **L9** with AgBF₄ or AgNO₃.

III 1. 1D coordination polymer

Using a **L9** : M = 1 : 2 stoichiometry, the combination of **L9** with AgBF₄ or AgNO₃ under liquid diffusion conditions (CHCl₃/MeOH) and in the darkness, (see experimental section) afforded two 1D *isostructural* coordination polymers.⁹³ They both crystallize in the high symmetrical cubic *Ia3d* space group and present a **L9** /Ag⁺ = 1/1 stoichiometry in the solid state, with the formula **L9**-AgBF₄ and **L9**-AgNO₃. Both compounds are *isostructural* (isomorphous and isometric).

XRPD diagrams of the microcrystalline powder of **L9**-AgNO₃ and **L9**-AgBF₄ presented in *Annexes*. The quality of the experimental diagrams are rather good, and there is a good match between the observed peaks and the one derived from the simulation of the structure obtained by single crystal diffraction.

The single crystal is composed of ligand **L9**, Ag⁺ cation and free uncoordinated NO₃⁻ (or BF₄⁻) anions. Ag⁺ cations is in a tetracoordinated environment adopting a distorted tetrahedral coordination geometry and surrounded by 4 N atoms of 4 cyano-groups belonging to 4 different **L9** ligands, as shown in figures 56 a and b. No solvent molecules are present in the crystal.

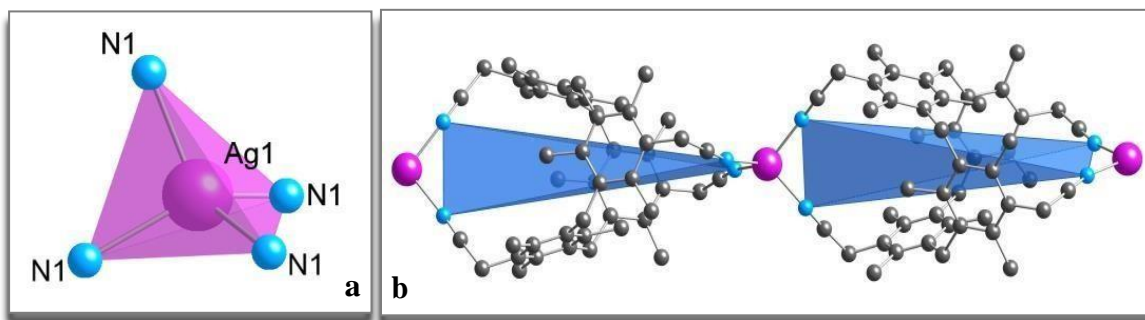


Figure 56: Ag^+ environment (a) and localization (b) in the crystal structure of **L9-AgBF₄** and **L9-AgNO₃**.

Bond distances and angles characteristics for tetrahedral deformed environment of Ag^+ are presented in table 11. The distance between two neighboring Ag^+ cations within one polymeric chain is equal to 14.635 Å while the distance between two silver cations of two neighboring chains in the crystal (see Figure 57) is equal to 16.362 Å.

Parameter	L9-AgBF₄	L9-AgNO₃
d Ag-N (Å)	2.257	2.265
d C≡N (Å)	1.190	1.169
N-Ag-N (°)	96.9	98.2
	102.9 131.1	100.3 132.7
Dihedral angle between opposite mesitylene moieties (°)	30.95	31.79

Table 11: Bond distances and angles for isostructural 1D networks **L9-AgBF₄** and **L9-AgNO₃**.

The packing of this 1D networks is cubic: three identical 1D networks are aligned along the *a*, *b* and *c* axes (Figure 57 a and b). Moreover, the packing of **L9-AgBF₄** and **L9-AgNO₃** is similar to the packing of the quinolyl derivative **L7** (see chapter II, § II 3), and can be described as a “bundle of firewood in a woodpile” where layers are stacked on top of each other in the perpendicular directions.

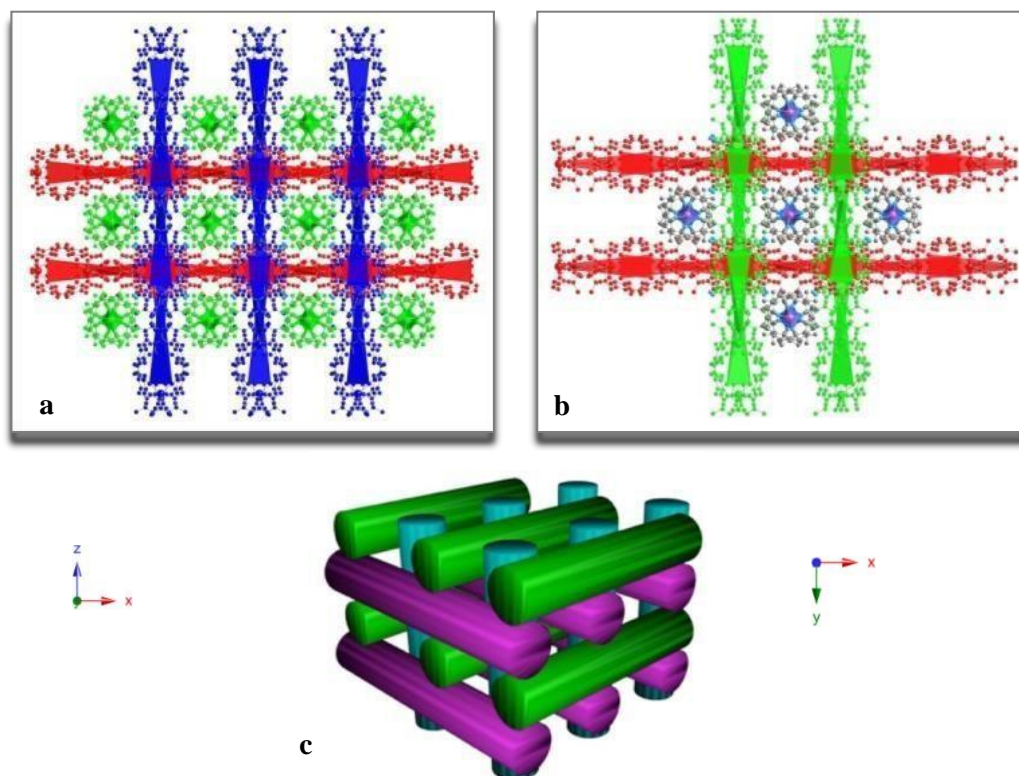


Figure 57: Portion of **L9**-AgBF₄ and **L9**-AgNO₃ networks along *a* (a) and *c* (b) axes and schematic representation of “bundle of firewood in a woodpile” (cubic packing of the 1D networks).

III 2. Coordination with Ag⁺ of **L9**: formation of Metallamacrobicycle

Another compound was obtained while using silver nitrate (I) and **L9** with an experimental stoichiometry $\text{L9}/\text{Ag}^+ = 1/4$. In this case, X-Ray diffraction analysis of the single crystals revealed the formation of a metallic macrobicycle *via* self-assembly processes (see experimental section) of formula $[\text{L9}_2-(\text{AgNO}_3)_2]$.

XRPD diagram of the microcrystalline powder of $[\text{L9}_2-(\text{AgNO}_3)_2]$ is presented in *Annexes*. From the experimental data, we can conclude that the observed microcrystalline powder contains the phase observed in the single-crystals. But the quality of the diagram is poor.

The bicycle is built from two molecules of **L9**, two Ag^+ cations and two coordinating NO_3^- anions (Figures 58 a and b). This compound was formed because the coordination sphere of the metal cation is filled with three nitrogen atoms from cyano groups of two different **L9** ligands, one oxygen atom of the coordinating nitrate anions. Ag^+ adopts tetrahedral geometry.

All bonds and angles for the coordination sphere of Ag in $[\text{L9}_2-(\text{AgNO}_3)_2]$ are given in Table 12. In the crystal, the distance between two silver atoms within the metallamacrobicycle is 13.843 Å. On the other hand, the distance between two neighboring silver cations within a chain (like yellow or blue chains in Figure 59) is 12.702 Å while the distance between the silver atoms of two neighboring chains (for example the distance between silver atom from yellow chain and silver atom from blue chain on Figure 59) is 15.559 Å.

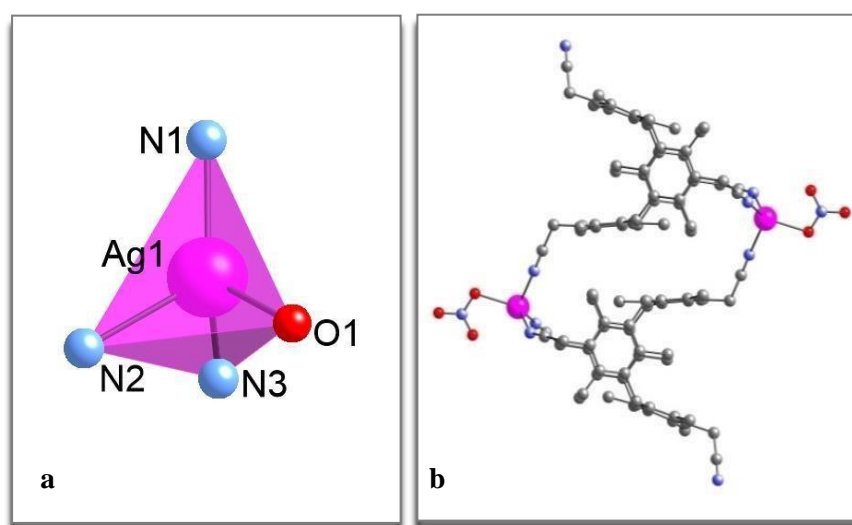


Figure 58: Representation of the silver coordination sphere (a), in the metallamacrobicycle $[\text{L9}_2-(\text{AgNO}_3)_2]$. (b) and its packing along the *b* axis (c).

	d Ag-N1	d Ag-N2	d Ag-N3	d Ag-O1	
	2.238	2.272	2.382	2.371	
N1-Ag-N2	N1-Ag-N3	N1-Ag-O1	N2-Ag-O1	N2-Ag-N3	N3-Ag-O1
122.308	110.238	123.890	95.778	87.447	111.073

Table 12: Angle values (°) (a) and bond distances (Å) (b) for $[\text{L9}_2-(\text{AgNO}_3)_2]$.

The molecules form parallel layers along *a* axis, as shown in figures 59 a and b.

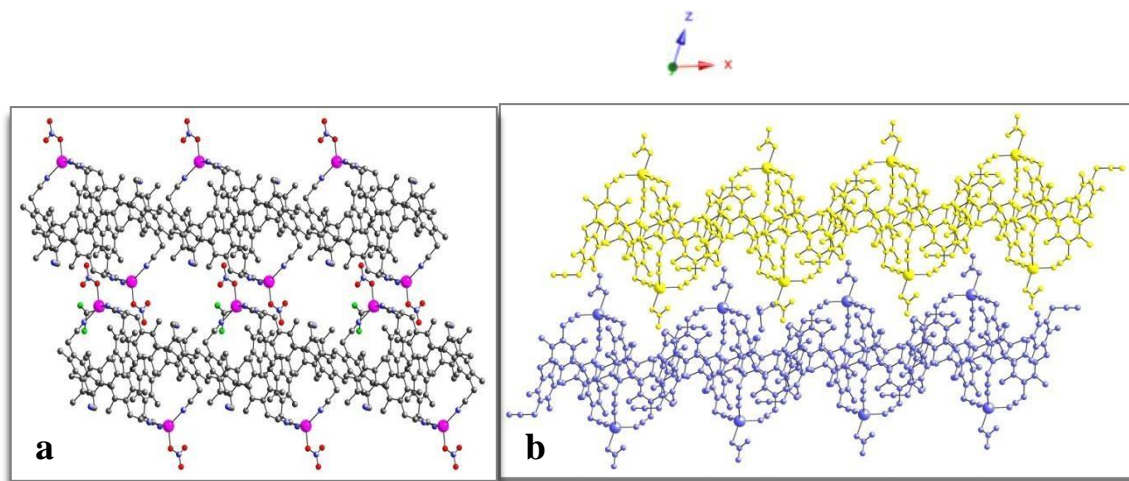


Figure 59: Packing of the metallamacrobicyclic $[\mathbf{L9}]_2-(\text{AgNO}_3)_2$ along the *b* axis (c).

The structural investigation (see table 13) showed that within the metallamacrocyclic the smallest $\text{C}\equiv\text{N}$ bond length of 1.134 Å (in comparison with 1.190 and 1.169 in 1D $\mathbf{L9}$ - AgBF_4 and $\mathbf{L9}$ - AgNO_3 polymers is observed (see table 11). At the same time, because of the presence of NO_3^- anions in the coordination sphere of silver cation, new values of bond lengths and angles are obtained, as indicated in the Table 13. An interesting fact is that there is a significant decrease of the value of dihedral angle between opposite mesitylene moieties (22.98 Å). These values cannot be compared to the one of uncoordinated $\mathbf{L9}$, since single crystals of the ligand could not be obtained, and thus, the structure has not been determined.

Parameter	$(\mathbf{L9})_2-(\text{AgNO}_3)_2$
d $\text{C}\equiv\text{N}$ (Å)	1.134
Dihedral angle between opposite mesitylene moieties (°)	22.98

Table 13: Bond distances and angles for the metallamacrobicyclic $[(\mathbf{L9})_2-(\text{AgNO}_3)_2]$.

III 3. Conclusion

The combination of **L9** with two different silver salts (AgBF_4 or AgNO_3) with an experimental stoichiometry $\text{L9}/\text{Ag}^+ = 1/2$, leads to the formation of two *isostructural* 1D coordination polymers **L9**- AgBF_4 and **L9**- AgNO_3 . Structural features of the crystalline materials as well as the packing of 1D networks were analyzed. A metallamacrocycle of formula $[\text{L9}_2-(\text{AgNO}_3)_2]$ was also observed when using a different stoichiometry during the self-assembly processes.

One may note that the stoichiometry used during the crystallization, plays a decisive role in the generation of 1D polymers and the metallamacrocycle. At the same time, the replacement of one anion by another (BF_4^- to NO_3^-) did not lead to significant changes, and two *isostructural* 1D coordination polymers were obtained.

Also, it was shown that by enhancing the distance between cyano group and metacyclophane skeleton by a methylene spacer, it is possible to address the self-assembly process leading to non-tubular type of 1D networks such as **L9**- AgBF_4 and **L9**- AgNO_3 (Figure 60, a) while absence of the spacer leads to tubular type architecture (Figure 60, b).⁸⁷

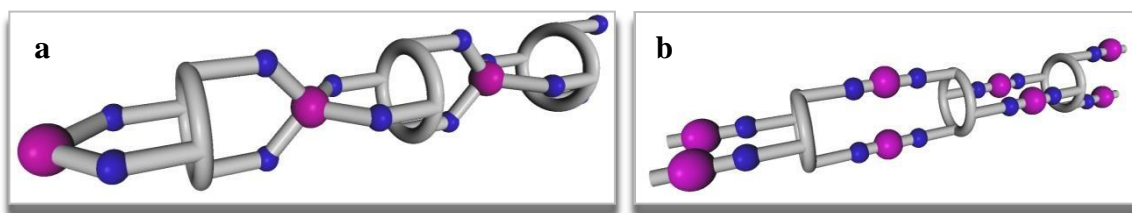


Figure 60. Two possible types of 1D supramolecular chains formed *via* self-assembly conditions: non-tubular (a) and tubular (b) architectures.

Thus, the addition of a flexible methylene spacer leads to the formation of a 1D non-tubular architecture with $M / L = 1/1$ stoichiometry, whereas the ligand described in previous studies for which the cyano group is directly attached to the metacyclophane platform,⁸⁷ forms a 1D tubular coordination polymer with stoichiometry $M / L = 2/1$. Moreover, due to the very tight packing of networks in the crystal, no solvent molecules were present in **L9**- AgBF_4 (or **L9**- AgNO_3). Interestingly, in the case of the ligand with no spacer between cyano groups and the metacyclophane backbone, methanol and chloroform solvent molecules were found in the crystal.⁸⁷

Besides these structural studies in the crystalline state, solution studies were also

performed. For controlling the formation of coordination polymers, titration of a solution containing the ligand, with a solution containing the metal cation were performed. The process was monitored by UV spectroscopy. The use of the Yoe-Jones method,¹³⁰ based on the variation of the absorbance with the M/L ratio, allows to determine the stoichiometry of the complexes in solution. This has been performed for the couple (M, **LX**) for which a coordination polymer has been obtained in the solid-state: (Mn, **L4**), (Mn, **L5**) and (Co, **L4**). This has not been measured for the silver derivatives, due to lack of time. Complementary to this study, DLS measurements, enabling the estimation of the size of the particles for the polymeric structures in solution, have been also carried out.

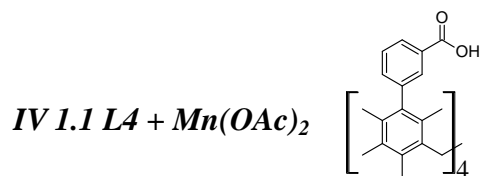
In addition, determination of extractant capacity of metal cations has been performed, using the well-known picrate extraction, especially for **L6** and d and f metal cations.

III Coordinating abilities of L4 and L5 in solution determined by UV-titration methods and DLS

IV 1. UV-titration

Optical spectroscopy based on the interaction of electromagnetic radiation with matter leads, in solution, to various energy transitions that can be experimentally measured by absorption, emission spectroscopies, reflection and scattering of the electromagnetic radiation. Photo adsorption spectroscopy exploiting the relatively weak photon energy which is generally related to the excitation of electrons located on the high HOMO transferred to the LUMO, leads to light adsorption, is one of the most widely used methods to investigate chemical compounds and their associations. By careful analysis of adsorption spectra of coordination compounds, information on the stoichiometry, the strength of bonding (stability constant) and type of binding site involved in coordination may be obtained using different models.

In this work, in order to investigate the binding behavior of prepared ligands in solution towards transition metal cations, UV-Vis spectroscopy was used to carry out titration experiments, *i.e.* titration of a solution containing the ligand by a solution containing a metallic salt. Owing to small quantities of ligands, only preliminary results showing the formation of coordination compounds between **L4** and **L5** and $\text{Mn}(\text{AcO})_2$, $\text{Mn}(\text{NO}_3)_2$ and $\text{Co}(\text{NO}_3)_2$, was demonstrated. Through these experiments, only the stoichiometry of the observed complexes in solution has been determined. However, their stability constants were not calculated



The measurements of UV/Vis spectra of DMSO solutions containing **L4** and Mn(OAc)₂ with different Mn/**L4** ratios were recorded at room temperature (Figure 61) in the $\lambda = 260\text{-}800$ nm range (see experimental part).

DMSO was chosen as the solvent because of the best dissolving ability due to the ligands in the range of selected concentrations.

For this mixture, a maximum of absorption at $\lambda = 257$ nm was observed (see figure 61). The corresponding titration graph ($A = f(\text{Mn}/\mathbf{L4})$ at $\lambda = 257$ nm for $A =$ absorbance and Mn/**L4** is the metal to ligand ratio) has been generated, as shown in figure 62.

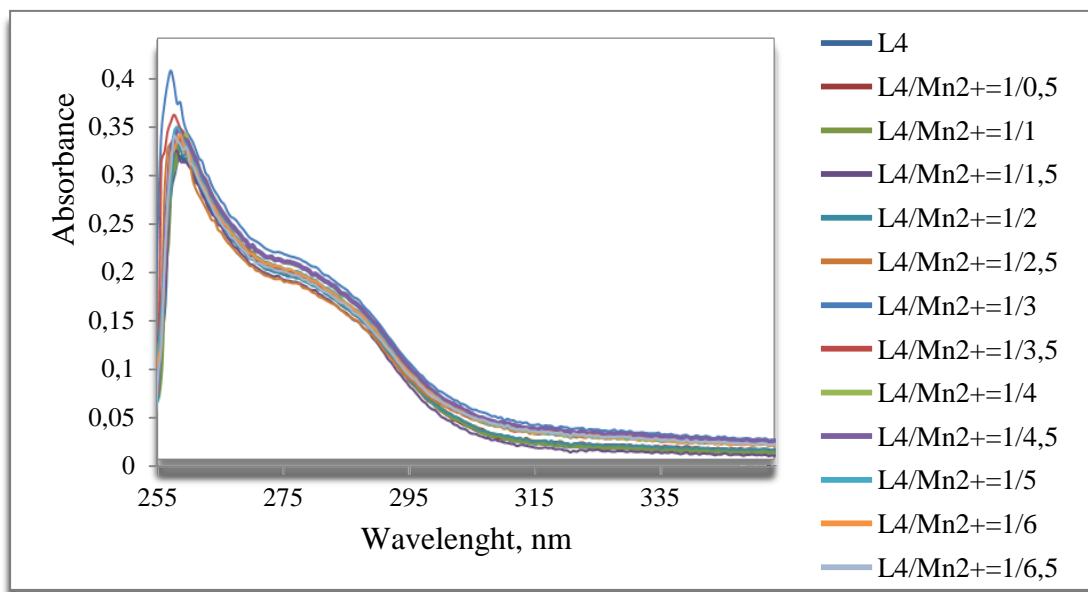


Figure 61: UV-Vis spectra of **L4** titration ($C = \text{const} = 0,04$ mM) with Mn(OAc)₂ in DMSO, at Room-Temperature.

As shown from the titration curve presented in figure 62, the maximum of absorbance was observed for a Mn/**L4** ratio equal to 3/1. This is in accordance with the stoichiometry obtained by the X-ray analysis for the solid-state compound (**L4**)₃Mn₉O₃(OAc)₆py₉•3py (§III 1.1).

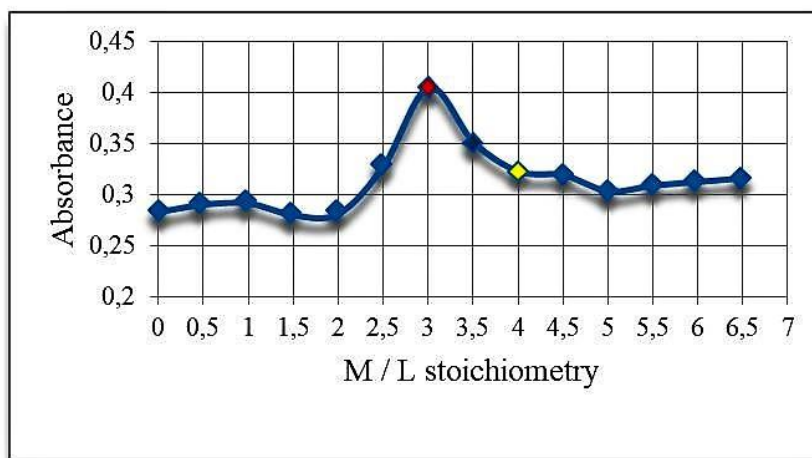
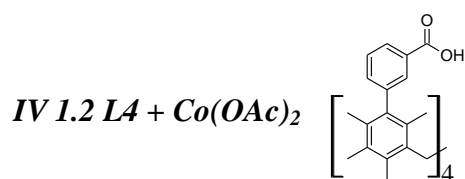


Figure 62: Titration curve $A = f(\text{Mn/L4})$ at $\lambda = 257 \text{ nm}$ for $A = \text{absorbance}$ and Mn/L4 is the metal to ligand ratio. Red point means complex formation and yellow means the alteration of complexation in solution.

The alteration of the complex in solution, probably followed by the formation of a complex presenting another stoichiometry is determined when the $A = f(\text{Mn/L4})$ curve presents value analogous to the ones found before the formation of the complex where $\text{Mn/L4} = 4/1$ (figure 62). Then, the increase of concentration of metal cation doesn't affect the absorbance value that probably corresponds to the saturation of coordinating sites (carboxylic groups) of **L4**.

From these data, one can conclude that the formation of a complex presenting the following $\text{Mn/L4} = 3/1$ stoichiometry is formed, followed by the formation of another complex of stoichiometry $\text{Mn/L4} = 4/1$.



As in the previous case, the measurements of UV/Vis spectra of DMSO solutions containing **L4** and Co(OAc)_2 with different Co/L4 ratios were recorded at room temperature (Figure 63) in the $\lambda = 260\text{-}800 \text{ nm}$ range (see experimental part). For this mixture, a maximum of absorption was found to be at $\lambda = 258 \text{ nm}$, as shown in figure 63. The corresponding titration graph ($A = f(\text{Co/L4})$ at $\lambda = 258 \text{ nm}$ for $A = \text{absorbance}$ and Co/L4 is the metal to ligand ratio) has been generated, as shown in figure 64.

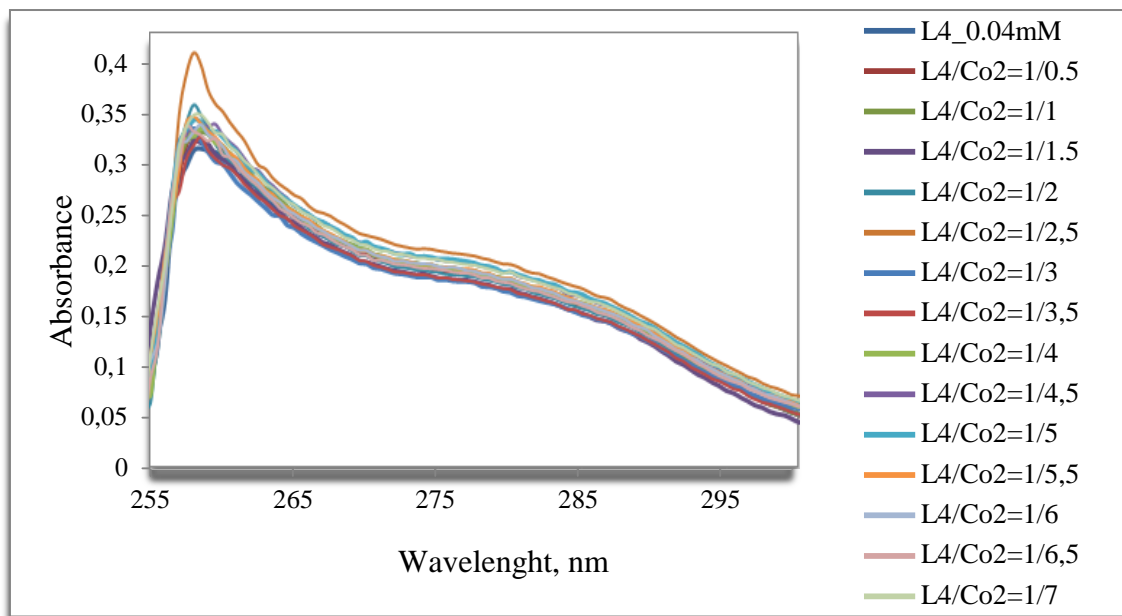


Figure 63: UV-Vis spectra of **L4** titration ($C = \text{const} = 0,04 \text{ mM}$) with $\text{Co}(\text{OAc})_2$ in DMSO, at Room-Temperature.

As shown from the titration curve presented in figure 64, the maximum of absorbance was observed for a $\text{Co}/\text{L4}$ ratio equal to $2,5/1$. This is in accordance with the stoichiometry obtained from the X-ray analysis in the solid-state for $\text{L4}_4\text{Co}_{10}\text{O}_2(\text{MeOH})_2(\text{H}_2\text{O})_4(\text{OAc})_2 \cdot (\text{C}_3\text{H}_7\text{NO})(\text{H}_2\text{O})_7$ (§III 1.2).

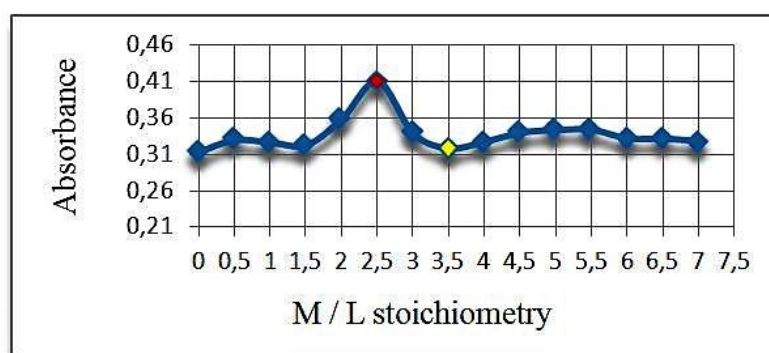
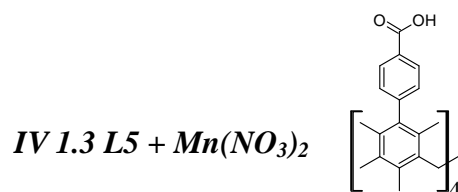


Figure 64: Titration curve $A = f(\text{Co}/\text{L4})$ at $\lambda = 258 \text{ nm}$ for $A = \text{absorbance}$ and $\text{Co}/\text{L4}$ is the metal to ligand ratio. Red point means complex formation and yellow means the alteration of complexation in a solution.

The alteration of the complex in solution, probably followed by the formation of a complex presenting another stoichiometry, is determined at $\text{Co}/\text{L4} = 3,5/1$ (figure 64). Then the

increase of concentration of metal cation doesn't affect the absorbance value that probably corresponds to the saturation of coordinating sites (carboxylic groups) of **L4**.

From these data, one can conclude that the formation of a complex presenting the following $\text{Co/L4} = 2,5/1$ stoichiometry is formed, followed by the formation of another complex of stoichiometry $\text{Co/L4} = 3,5/1$.



The measurements of UV/Vis spectra of DMSO solutions containing **L5** and $\text{Mn}(\text{NO}_3)_2$ with different Mn/L5 ratios were recorded at room temperature (Figure 65) in the $\lambda = 260\text{-}800$ nm range (see experimental part). For this mixture, the maximum of absorption was found to be at $\lambda = 258$ nm, as shown in figure 65. The corresponding titration graph ($A = f(\text{Mn/L5})$ at $\lambda = 257$ nm for $A =$ absorbance and Mn/L4 is the metal to ligand ratio) has been generated, as shown in figure 66.

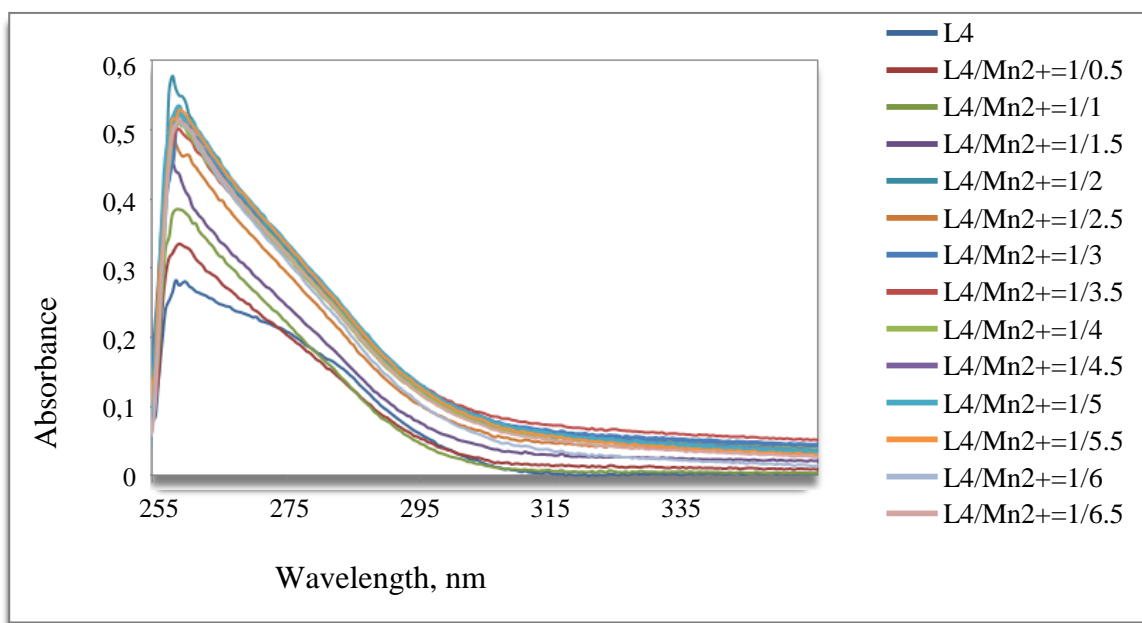


Figure 65: UV-vis spectra of **L4** titration ($C = \text{const} = 0,04$ mM) with $\text{Mn}(\text{NO}_3)_2$ in DMSO, at Room Temperature.

As shown from the titration curve presented in figure 66, the maximum of absorbance was observed for a Mn/L5 ratio equal to 2/1. It is in accordance with the stoichiometry observed by X-ray analysis in the solid-state for $(\text{L5})\text{Mn}_2(\text{DMF})_2$ (§IV 1.3).

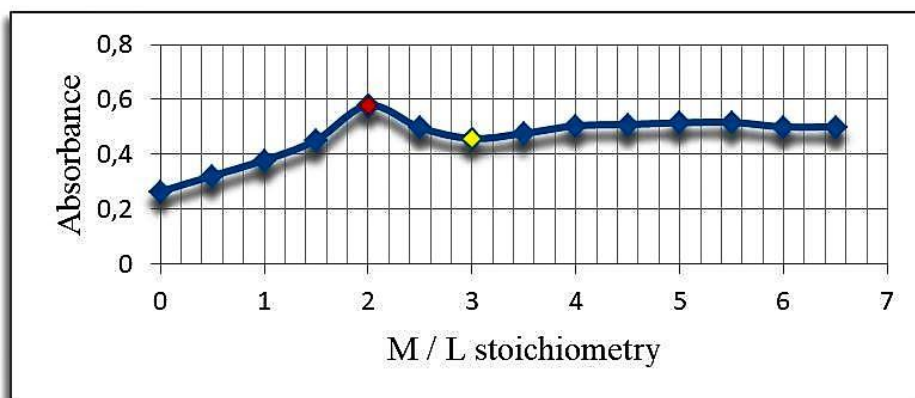


Figure 66: Titration curve $A = f(\text{Mn}/\text{L5})$ at $\lambda = 257 \text{ nm}$ for $A = \text{absorbance}$ and $\text{Mn}/\text{L5}$ is the metal to ligand ratio. Red point means complex formation and yellow means the alteration of complexation in a solution.

From these data, one can conclude that the formation of a complex presenting the following $\text{Mn}/\text{L5} = 2/1$ stoichiometry is formed in solution. Unlike the previous cases, the data present a multitude of inflection points which indicates either the lack of precision of this method for determining the stoichiometry of complex compounds for ligands prepared or due to constantly changing stoichiometry in solution. We cannot conclude about the stoichiometry of complexes found in solution with $\text{Mn}/\text{L5} > 2/1$.

IV 1.4 Conclusion

For three of the UV-titrations, the behavior of the ligand in solution is in accordance with the M/LX stoichiometry found in the solid-state for **L4** and **L5** combined with Mn^{2+} and for **L4** combined with Co^{2+} . The other cases M/LX were not analyzed, due to the difficulty of analyzing the data without a model derived from the solid state.

Parallel to these studies, DLS measurements were performed in order to determine the size of the particles of the complexes in DMSO solution.

IV Dynamic Light Scattering (DLS)

V 1. Measurements

As already mentioned in the *Annexes* § I .1, the Dynamic Light Scattering (DLS) method uses the phenomenon of light scattering allowing to determine the size of nano- and sub-micronic dispersed particles. It allows to access the diffusion coefficient of dispersed particles in a liquid phase. The method is non-destructive, without introducing perturbation into the medium under investigation and is characterized by high speed of operation and accuracy.

In order to evaluate the ability of each ligand to form polymeric assemblies, several series of solutions were investigated: solutions of pure ligands (**L1-L10**) in DMSO, solutions of d- and f-metal cations in DMSO, ligand + metallic cation mixture also in DMSO. Unfortunately, despite numerous attempts, the reproducibility of the results was not convincing for many combinations.

In accordance with the previous results obtained in the solid-state and by UV-titrations mentioned above, only the DLS measurements of [1111] metacyclophane **L4** and **L5** combined with Mn^{2+} and **L4** combined with Co^{2+} in solution are presented in figure 67 below (see experimental part). The data are related with average size of the nanoparticles and also the *polydispersity indexes* (PDI).

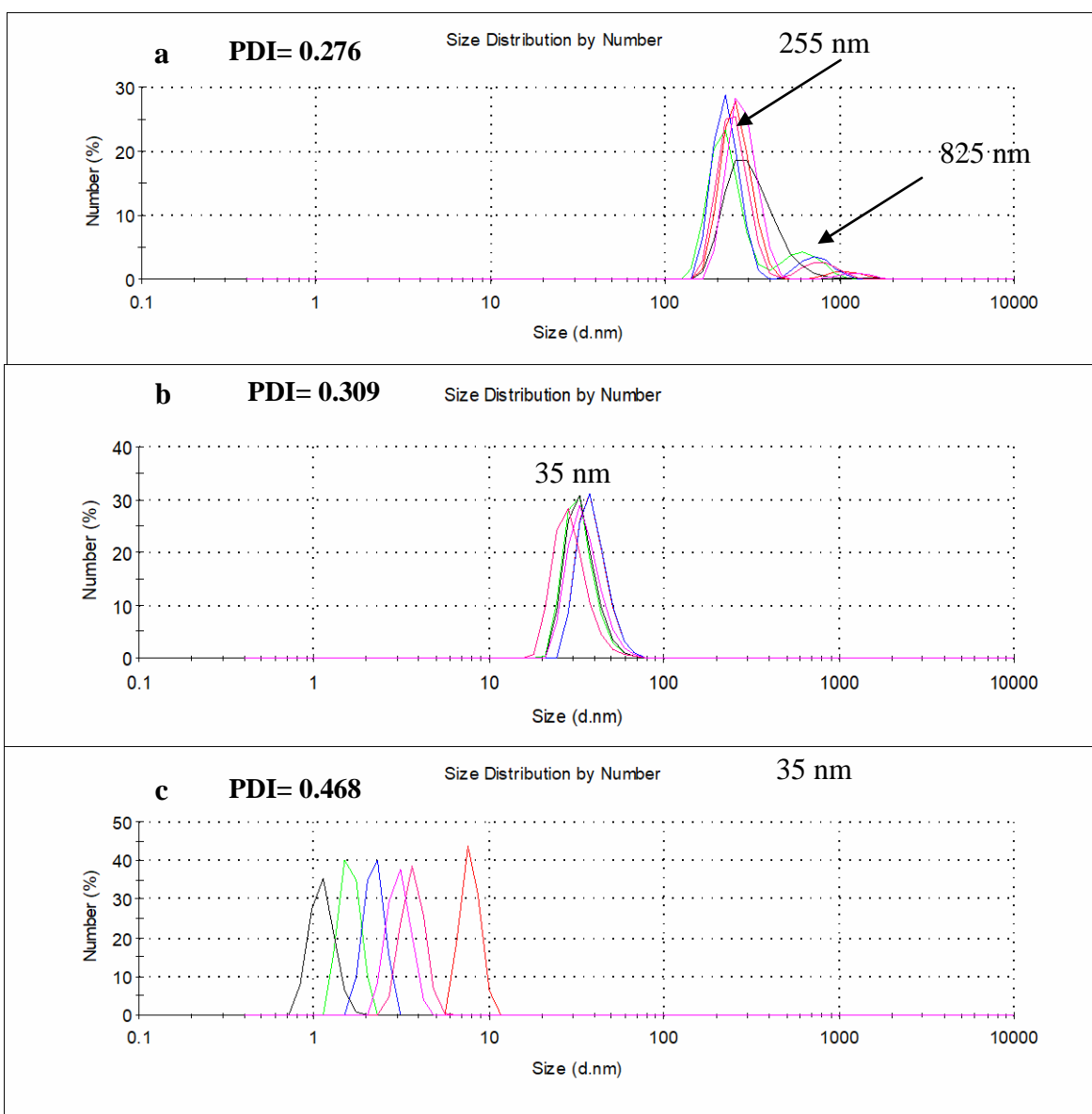


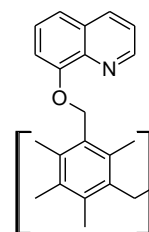
Figure 67: Data obtained in DMSO solutions, at RT, by DLS method for **L5** ($C = 0.04$ mM) combined with 2 eq of $Mn(OAc)_2$ (a), **L4** ($C = 0.04$ mM) with 3 eq of $Mn(NO_3)_2$ (b) and **L4** ($C = 0.04$ mM) with 2.5 eq of $Co(OAc)_2$ (c): size of the nanoparticles and values of polydispersity indexes (PDI).

V 2. Conclusion

The obtained DLS data revealed a capacity of formation of large particles for **L5** combined with $\text{Mn}(\text{OAc})_2$ (255 nm and PDI of 0,276) and also for **L4** with $\text{Mn}(\text{NO}_3)_2$ (35 nm and PDI of 0,309) while the complexation of **L4** with the cobalt cations leads to the formation of a polydispersed system (monomers in solution) with higher PDI value (0,468). This is in accordance with the UV titration data. But further conclusions cannot be derived from these data, since the exact content of the formed nanoparticles were not precisely determined.

These data should be confirmed by other techniques, such as EXAFS for example, in order to determine the exact coordination sphere around the metal cation in each case.

V Picrate extraction selectivity of L6



The extraction behavior of the [1111] metacyclophane derivatives of metal cation (d and f) has also been undertaken. This is an indication for the binding behavior of the organic ligands, and perhaps applications in decontamination, for example.

For this, due to lack of time, we concentrated only on the quinolyl derivatives of metacyclophane (**L6**) to extract the d and f elements from aqueous solution into CH_2Cl_2 organic phase, using the picrate extraction method and by using the corresponding nitrate salts and triflate salt in case of source of Tb (III) cation. The picrate method is based on the use of UV measurements and variation of the absorption observed generally in the 355 - 365 nm range for **L6** (see experimental section).

The optical densities A_i and A_0 of the aqueous phase before and after extraction were measured in the 300-500 nm wavelength range with a maximum at 355-365 nm. The extraction percentage (E%) was calculated using the formula $E\% = 100 * (A_0 - A_i) / A_0$ (see Annex). The chosen metallic salts were $\text{Gd}(\text{NO}_3)_3$, $\text{Er}(\text{NO}_3)_3$, $\text{Tb}(\text{OTf})_3$, $\text{Dy}(\text{NO}_3)_3$, $\text{Eu}(\text{NO}_3)_3$, $\text{Pr}(\text{NO}_3)_3$, $\text{Yb}(\text{NO}_3)_3$, $\text{Ni}(\text{NO}_3)_2$, $\text{Cu}(\text{NO}_3)_2$, $\text{Co}(\text{NO}_3)_2$ and $\text{Mn}(\text{NO}_3)_2$.

The results are presented in table 14.

It was shown that compound **L6** extracts all tested cations but the best efficiency was observed for Cu (II) cation that can be explained by the enhanced propensity of Cu (II) cation

to form coordination bonds with quinolyl nitrogen atoms (table 14). These data have to be confirmed with further measurements, and extended to other ligands.

E%										
Gd³⁺	Er³⁺	Tb³⁺	Dy³⁺	Eu³⁺	Pr³⁺	Yb³⁺	Ni²⁺	Cu²⁺	Co²⁺	Mn²⁺
85	78	78	80	82	64	86	59	92	61	62

Table 14. Extraction efficiency of **L6** towards Gd(NO₃)₃, Er(NO₃)₃, Tb(OTf)₃, Dy(NO₃)₃, Eu(NO₃)₃, Pr(NO₃)₃, Yb(NO₃)₃, Ni(NO₃)₂, Cu(NO₃)₂, Co(NO₃)₂ and Mn(NO₃)₂ in CH₂Cl₂ organic phase from the aqueous solution at 25° C.

VI Conclusion

The coordination abilities of the [1.1.1.1]metacyclophane derivatives **L1-L10** were investigated both in the solid-state and in solution.

Concerning the **solid-state** studies, for the moment, five types of supramolecular networks *via* self-assembly processes based on **L4**, **L5** and **L9** in the presence of Mn^{2+} , Co^{2+} , Ag^+ cations as connecting nodes have been observed. This leads to 0D, 1D and 3D coordination networks respectively (see Table 14). It was shown that [1.1.1.1]metacyclophane carboxylate derivatives (**L4** and **L5**) are well adapted for the formation of coordination networks with Mn^{2+} and Co^{2+} , leading to the formation of clusters, one of them presenting a mixed valence character ($(\text{L4})_3\text{Mn}^{\text{II}}\text{Mn}^{\text{III}}\text{O}(\text{OAc})_3\text{py}_3$). This peculiar behavior has to be investigated further, for the formation of new SMM, for example.

On the other hand, for the combination of silver cation and **L9**, two types of supramolecular architectures were obtained: one 0D (metallamacrobicycle) as well as two *isostructural* 1D coordination polymers; the key role of the stoichiometry was identified.

Unfortunately, despite numerous attempts and various methods, it was not possible to obtain crystals.

In Parallel, the studies of complexation in **solution**, including the determination of stoichiometry by UV titration, confirmed the data obtained by X-ray diffraction analysis for **L4** and **L5** combined with $\text{Mn}(\text{AcO})_2$, $\text{Mn}(\text{NO}_3)_2$ and $\text{Co}(\text{NO}_3)_2$. Meanwhile, the DLS method showed the ability of **L4** and **L5** ligand to form polymeric compounds in solution *via* interactions with manganese cation.

For the quinoline derivative **L9**, picrate extraction was performed and the highest efficiency was obtained for Cu^{2+} and Yb^{3+} cations. On the basis of these data, further methods of obtaining crystals based on quinoline derivatives will be developed, since the presence of condensed rings rich in π -electrons is of interest for the development of materials with potential photo-luminescent properties.

Chapter IV

General conclusion and perspectives

As it was mentioned earlier (Chapter I, § III 2), the macrocyclic family of [1111]metacyclophane favourably differs from their relative calix[4]arenes by such an attractive property that is the rigidity of the macrocyclic skeleton, adopting the stable 1,3-alternate conformation (under a large temperature range) due to the presence of the methyl groups in ortho-positions. At the same time, not only the structure of [1111]metacyclophane is especially attracted but also the comparative simplicity of its synthesis and further platform functionalization. Through exploring the coordination ability of metacyclophane derivatives and taking in account the aforementioned advantages comparing to the calix[4]arene platform, we designed and synthesised new series of ligands able to form extended molecular networks in the solid state. This allows to improve basic knowledge in the field of supramolecular, coordination chemistry and crystal engineering.

The general aim of this study was to better understand the coordination ability of [1111]metacyclophane derivatives bearing different binding sites in order to form the porous crystalline materials.

Hereby, 10 ligands were successfully synthesized: **L1-L10** differing by the nature of coordination sites (*carboxylic*, *quinolyl-*, *mercapto-*, *cyano* and *phosphonato-*) and the number of binding sites (4 or 8) as well as the nature of the spacer (aryl- or aliphatic) located between the functional group and the macrocyclic platform.

As it was already mentioned in the Chapter III, § IV 1, each of the above functional groups were chosen due to the already investigated coordination abilities of such binding centres that were described in the literature devoted to calix[4]arenes, for example.

After successful synthesis of precursors and then the targeted ligands, investigation and the confirmation of the structures of tetrasubstituted compounds by various physical methods such as $^1\text{H-NMR}$ or $^{13}\text{C-NMR}$ spectroscopy, MALDI-mass spectrometry, X-ray diffraction analysis and microanalysis were performed. As it can be seen from analysis of the obtained crystal structures, there is intramolecular bonding in the three carboxyl compounds: the carboxyl-carboxyl hydrogen bonds in **L2**, a hydrogen bond with the one pyridine molecule per one carboxyl group in **L3** and an intramolecular hydrogen bond in **L4**. Despite numerous attempts, in all other cases, it was not possible to obtain single crystals, which were suitable for X-ray structural analysis, for the other ligands.

The next stage after the successful confirmation of the desired ligand structures was the exploration of their ability to form the complexes with the different d- (Ag^+ , Ni^{2+} , Co^{2+} ,

Cu²⁺, Mn²⁺, Zn²⁺ etc.) and f- (Er³⁺, Eu³⁺, Yb³⁺, Dy³⁺ etc.) metallic cations. Moreover, it should be noted that studies of complexation of the obtained ligands were performed both in solution (using picrate extraction, DLS and UV-titration methods Chapter III, § IV - VI) as well as in the solid state by the X-ray diffraction method.

Complexation in solution was the base of a predictive-descriptive approach for preparation for crystallization, in order to study the compound in the solid-state and for comparing the coordinating ability of ligands in solution and crystalline phase. Correspondingly, it was established by UV-titration data and X-ray analysis that the coordination ability behaviour of some ligand in solution is in accordance with the **M/LX** stoichiometry found in the solid-state for **L4** and **L5** combined with Mn²⁺ and for **L4** combined with Co²⁺. Preliminarily DLS studies were in accordance with the UV titration data, however, as it was mentioned earlier, these DLS results should be confirmed by some other analysis methods, like EXAFS for example, in order to determine the exact coordination sphere around the metallic cations.

It was also demonstrated, using the picrate extraction method, that ligand **L6** extracts Cu (II) cations with the highest efficiency in comparison with all other tested cations, due to the probable enhanced propensity of Cu (II) cations to form coordination bonds with quinolylic nitrogen atoms.

The UV-titration investigations provided an important opportunity to predict the most characteristic M/L stoichiometry in the complexation of used ligands with the different metallic cations. Indeed, in the solid-state, three extended crystalline compounds were obtained: 1D, 2D structures via complexing **L4** with Mn²⁺ and Co²⁺ cations respectively and 3D structure via complexing **L5** with Mn²⁺ cations presenting stoichiometry similar to complexes found in solution. It is important to note that **L4** forms cluster-like chelated-type structures, and **L5** forms 3D porous structure, while **L4** interconnecting with Co²⁺ leads to a coordination complex bearing pentanuclear cobalt units with the chelate type of binding.

At the same time, it was shown that the M/L stoichiometry and the nature or anion plays a significant role in the creation of 1D polymeric structure or metallamacrocycle, using silver cations and tetracyano derivative **L9**. When the non-coordinating anion (BF₄⁻) was used only the formation of 1D coordination polymer of non-tubular type was observed using the different range of metal excess (M/L=1/1, 2/1 or 4/1). But the coordination behaviour of **L9** has been changed while using the coordinating anion (NO₃⁻) which affords the generation of 1D coordination polymer isostructural to the previous one when the M/L stoichiometry was equal

to 2/1, and discrete metallomacrocycle when the M/L stoichiometry was increased up to 4/1.

Thus, to conclude, there were synthesized 5 types of coordination compounds based on **L4**, **L5** and **L9** and different metallic cations, that are schematically represented below in table 15.

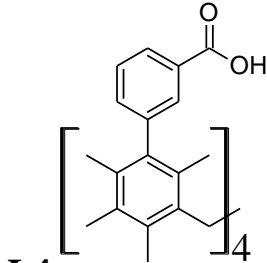
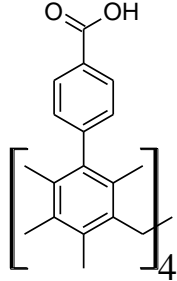
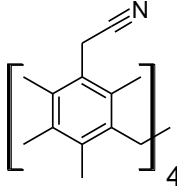
Ligands	 <p>L4</p>	 <p>L5</p>	 <p>L9</p>
Networks	<p>1D (L4)₃Mn₉O₃(OAc)₆py₉ •3py; L4/Mn²⁺ = 1/3</p> <p>2D L₄Co₁₀O₂(MeOH)₂ (H₂O)₄(OAc)₂ • (C₃H₇NO)(H₂O)₇; L4/Co²⁺ = 2/5</p>	<p>3D (L5)Mn₂(DMF)₂; L5/Mn²⁺ = 1/2</p>	<p>0D [L₉₂-(AgNO₃)₂]; L₉/Ag⁺ = 2/2</p> <p>1D L₉-AgBF₄ and L₉-AgNO₃; L₉ /Ag⁺ = 1/1</p>

Table 15: The five types of coordination networks, together with the stoichiometry, obtained by combination of **L4**, **L5** and **L9** with metals.

Perspectives

Concerning this study, there are several important issues. For example, related to *supramolecular chemistry* and *molecular tectonics*, there is an increasing interest over the transition metal clusters which are the attractive systems with the partly filled *d-electronic* shells, possessing complicated energy landscape that depends on both structural and total spin of cluster system.¹³¹ Self-recognition processes can lead to the association of magnetic subunits connected by bridging organic ligands, which provide magnetic (spin) communication within a single molecular entity.¹³¹ Such new metallic clusters are fascinating systems because of the novel physical properties, which is the subject of the field “molecular magnetism”.¹³² Through

this study, we want to promote the macrocyclic ligands to bring new object in that very active field.

The design and synthesis of magnetic grids or supramolecular compounds based on metallic clusters interconnected with the organic ligands, is the challenging task for the organic chemist and is difficult. Despite this, during this project there were synthesized cluster-like chelated-type structures together with a partial oxidation of the Mn cations into Mn^{III} (based on **L4**), as well as 3D porous structure, presenting Mn cations in the oxidation state +2 (based on **L5**). In addition, the electrochemical oxidation of Mn atoms within the molecular network may also lead to creation of new magnetically active materials with the switchable magnetic properties. But this highly depends on the stability in solution and in the solid-state of such entities, and this has to be further studied.

Thus, the further task of this study is to clarify several aspects of magnetic properties of obtained compounds by magnetic measurements while the exploration of the magnetism in supramolecular metal clusters and synthesis of such new compounds are of great practical importance for huge number of applications in data storage or spin transport.¹³³

A considerable amount of literature has been published on coordination crystalline compounds, while some work is devoted to supramolecular gels based on carboxylic derivatives with their potential application. This is interesting since, in this scientific project, we obtained some gels and gel-like compounds (see Chapter III, § I). Possessing the weak character of the bonding inside the supramolecular gels, they have stimuli-responsive abilities¹³⁴ and can be used in chemo-sensors,¹³⁵ pollutant capture and removal, drug delivery and other applications.¹³⁶ Along this line, it is fascinating to be concentrated in the near future on further physical investigations of performed gel-compounds together with their viscoelastic properties.

REFERENCES

- (a) B. Van De Voorde, B. Bueken, J. Denayer, D. De Vos. *Chem. Soc. Rev.*, **43**, 5766-5788 (2014); (b) X. Zhao, Y. Wang, D. S. Li, X. Bu, P. Feng. *Adv. Mater.*, **1-34**, 1705189, (2018); (c) C. H. Hendon, A. J. Rieth, M. D. Korzyński, M. Dincă. *ACS Cent. Sci.*, **3**, 554-563 (2017); (d) A. A. Olajire. *Renew. Sustain. Energy Rev.*, **92**, 570-607 (2018); (e) K. Yusuf, A. Aqeel, Z. Allothman. *J. Chromatogr. A*, **1348**, 1-16 (2014); (f) H. Li, K. Wang, Y. Sun, C. T. Lollar, J. Li, H-C. Zhou. *Materials Today* **21**, 108-121 (2018).
- Y. F. Han, Y. X. Yuan, H. B. Wang. *Molecules*, **22**, 1-29 (2017).
- C. Mottillo, T. Friščić. *Molecules*, **22**, 1-27 (2017).
- C. Chen, Y.-R. Lee, W.-S. Ahn. *J. Nanosci. Nanotechnol.*, **16**, 4291-4301 (2016).
- Q. Zhang, C.-F. Wang, Y.-K. Lv. *Analyst*, 1-7 (2018).
- A. Nangia. *Curr. Trends Sci. - Platin. Jubil. Spec.*, **122**, 35-51 (2009).
- (a) J. D. Wuest, *Chem. Commun.*, 5830, (2005); (b) M. W. Hosseini, *Chem. Commun.*, 5825, (2005).
- J.-M. Lehn. *Nobel Lecture*, 8 December (1987).
- D. Braga, F. Grepioni. *Coord. Chem. Rev.*, **183**, 19-41 (1999).
- M.W. Hosseini. *CrystEngComm.*, **6**, 318-322 (2004).
- C. Dey, T. Kundu, B. P. Biswal, A. Mallick, R. Banerjee. *Acta Crystallogr. Sect. B Struct. Sci. Cryst. Eng. Mater.*, **70**, 3-10 (2014); (b) H. Furukawa, K. E. Cordova, M. O’Keeffe, O.M. Yaghi. *Science*, 341, 1230444 (2013).
- C. Janiak. *Dalt Trans.*, **14**, 2781-2804 (2003).
- (a) N. F. Sunday. *Arch. Org. Inorg. Chem. Sci.*, **1**, 1-13 (2018); (b) S. Mann, *J. Chem. Soc. Dalt. Trans.*, 3953- 3962 (1997); (c) S. Mann. *J. Chem. Soc. Dalt. Trans.*, 1-9 (1993).
- M. W. Hosseini, A. De Cian. *Chem. Commun.*, 727-733 (1998).
- M. J. Zaworotko. *Chem. Commun.*, 1-9 (2001).
- (a) B. Chen, S. Xiang, G. Qian. *Acc. Chem. Res.*, **43**, 1115-1124 (2010); (b) D. Liu, D. Zou, H. Zhu, J. Zhang. *Small*, **1801454**, 1-40 (2018); (c) R.-B. Lin, S. Xiang, B. Li, Y. Cui, W. Zhou, G. Qian, B. Chen. *Isr. J. Chem.*, **6102**, 1-14 (2018); (d) X. F. Wang, X. Z. Song, K. M. Sun, L. Cheng, W. Ma. *Polyhedron*, **152**, 155-163 (2018).
- (a) Y. Liu, H. Liu. *Met. Fram.*, 85-104 (2016); (b) S. Lin, J. K. Bediako, C. W. Cho, M. H. Song, Y. Zhao, J. A. Kim, J. W. Choi, Y. S. Yun. *Chem. Eng. J.*, **345**, 337-344 (2018).
- (a) L. Zhu, X-Q. Liu, H-L. Jiang, Sun L-B. *Chem. Rev.*, **117**, 8129-8176 (2017); (b) X. He, F. Yin, H. Wang, B. Chen, G. Li. *Chinese J. Catal.*, **39**, 207-227 (2018); (c) Z. Liang, C. Qu, D. Xia, R. Zou, Q. Xu. *Angew. Chem. Int. Ed.*, **57**, 9604-9633 (2018); (d) H. Yang, X. Wang. *Adv. Mater.*, 1800743, (2018).
- Y. Cui, J. Zhang, H. He, G. Qian. *Chem. Soc. Rev.*, **47**, 5740-5785 (2018).
- (a) D. Maspoch, D. Ruiz-Molina, J. Veciana. *J. Mater. Chem.*, **14**, 2713-2723 (2004); (b) P. Dechambenoit, J. R. Long, *Chem. Soc. Rev.* **40**, 3249-3265 (2011). (c) G. M Espallargas, E. Coronado. *Chem. Soc. Rev.*, **47**, 533-557 (2018).
- (a) P. Xiao, Y. Xu. *J. Mater. Chem. A*, 1-21 (2018); (b) Y. Li, Y. Xu, W. Yang, W. Shen, H. Xue, H. Pang. *Small*, **14**, 1-24 (2018); (c) H. Zhang, J. Nai, L. Yu, X. W. Lou. *Joule*, **1**, 77-107 (2017); (d) C. C. Hou, Q. Xu. *Adv Energy Mater.*, 1801307-1801307 (2018); (e) H. Tang, M. Zheng, Q. Hu, Y. Chi, B. Xu, S. Zhang, H. Xue, H. Pang. *J. Mater. Chem. A*, **6**, 13999-14024 (2018); (f) I. A. Indra, T. Song, U. Paik. *Adv. Mater.*, 1705146 (2018).

22. D. L. Caulder, K. N. Raymond. *Acc. Chem. Res.*, **32**, 975-982 (1999).
23. (a) A. Gavezzotti *Acc. Chem. Res.*, **27**, 309-314, (1994); (b) Dunitz J.D. *Chem. Commun.*, 545-548, (2003).
24. J. Brus, J. Czernek, L. Kobera, M. Urbanova, S. Abbrent, M. Husak. *Cryst. Growth Des.*, **16**, 7102-7111 (2016).
25. (a) S. L. Price. *Chem. Soc. Rev.*, **43**, 2098-2111 (2014); (b) K. Szalewicz. *Acc Chem Res.*, **47**, 3266-3274 (2014).
26. (a) G. R. Desiraju. *Stimul. Concepts Chem.*, 293-306 (2005); (b) A. Mukherjee. *Cryst. Growth Des.*, **15**, 3076- 3085 (2015).
27. J. Lee, J. H. Kwak, W. Choe. *Nat. Commun.* **8**, 1-8 (2017).
28. K. T. Mahmudov, M. N. Kopylovich, M. F. C. Guedes da Silva, A. J. L. Pombeiro. *Coord. Chem. Rev.*, **345**, 54- 72 (2017).
29. M. J. Hardie. *Structure and Bonding*, **111**, 139-174 (2004).
30. S. Grabowski. *Crystals*, **6**, 1-5 (2016).
31. T. Steiner *Angew. Chem. Int. Ed.*, **41**, 48-76 (2002).
32. M. D. Ward, *Chem. Commun.*, 5838-5842, (2005).
33. J. H. Jordan, B. C. Gibb. *Chem. Soc. Rev.*, **44**, 547-585 (2015)
34. (a) J. Berne, J. D. Weeks, R. Zhou. *Annu. Rev. Phys. Chem.*, **60**, 85-103 (2009); (b) E. E. Meyer, K. J. Rosenberg, J. Israelachvili. *Proc. Natl. Acad. Sci. U. S. A.*, **103**, 15739-15746 (2006).
35. H. Margenau. *Rev. Mod. Phys.*, **11**, 1-35 (1939).
36. (a) X. Sun, S. Dong, E. Wang. *J. Am. Chem. Soc.*, **127**, 13102-13103 (2005); (b) M. Oh, C. A. Mirkin. *Nature*, **438**, 651-654 (2005); (c) A. M. Spokoynny, D. Kim, A. Sumrein, C. A. Mirkin. *Chem. Soc. Rev.*, **38**, 1218-1227 (2009).
37. G. M. Whitesides, J. P.; Mathias, T. Seto, *Science*, **254**, 1312-1319 (1991).
38. (a) I. Higler, P. Timmerman, W. Verboom, D. N. Reinhoud. *Eur. J. Org. Chem.*, 2689-2702 (1998); (b) A. V. Mossine, P. Thavornnyutikarna, J. L. Atwood *CrystEngComm*, **15**, 1673-1675 (2013); (c) K. Kobayashi, M. Yamanaka. *Chem. Soc. Rev.*, **44**, 449-466 (2015); (d) K. Helttunen, M. Nissinen *CrystEngComm*, **18**, 4944-4951 (2016).
39. A. D. Hamilton. *Compr. Heterocycl. Chem.*, **7**, (2009).
40. (a) R. Makiura, S. Motoyama, Y. Umemura, H. Yamanaka, O. Sakata, H. Kitagawa *Nat. Mater.*, **9**, 565-71 (2010); (b) Q. Zha, X. Rui, T. Wei, Y. Xie *CrystEngComm*, **16**, 7371-7384 (2014); (c) W.Y. Gao, M. Chrzanowski, S. R. Ma *Chem Soc Rev.*, **43**, 5841-5866 (2014).
41. (a) M. M. Nitalikar, D. M. Sakarkar, P. V. Jain *J. Curr. Pharm Res.* **10**, 1-6 (2012); (b); H.Xu, S.Rodríguez- Hermida, J.Pérez-Carvajal, J. Juanhuix, I. Imaz, D. .A MasPOCH *Cryst. Growth Des.*, **16**, 5598-5602 (2016).
42. (a) M. S. Collins, M. E. Carnes, B. P. Nell, L. N. Zakharov, D. W. Johnson. *Nat. Commun.*, **7**, 1-7 (2016). (b) Z. Liu, S. K. M. Nalluri, J. Fraser Stoddart. *Chem. Soc. Rev.*, **46**, 2459-2478 (2017).
43. B. Esser, A. Bandyopadhyay, F. Rominger, R. Gleiter. *Chem. - A Eur. J.*, **15**, 3368-3379 (2009).
44. V. Y. Shuvalov, I. V. Eltsov, N. A. Tumanov, E. V. Boldyreva, A. A. Nefedov, G. P. Sagitullina. *European J. Org. Chem.*, **2017**, 5410-5416 (2017).
45. F. Vögtle, P. Neumann. *Angew. Chemie Int. Ed.*, **11**, 73-83 (1972).
46. *Calixarenes: a Versatile Class of Macrocyclic Compounds*; J. Vicens, V. Böhmer, Eds.; Kluwer

- Academic Publishers, Dordercht, Netherlands, (1991).
47. R. Ungaro, A. Arduini, A. Casnati, A. Pochini, F. Ugozzoli. *Pure Appl. Chem.*, **68**, 1213-1218 (1996).
 48. *Calixarenes* By C. David Gutsche, Royal Society of Chemistry, Cambridge, (1989).
 49. (a) M. Wierzbicki, H. Jędrzejewska, A. Szumna. *Ref. Modul. Chem. Mol. Sci. Chem. Eng.*, 1-23 (2014); (b) G. E. Arnott. *Chem. - A Eur. J.*, **24**, 1744-1754 (2018); (c) A. Sirit, M. Yilmaz. *Turkish J. Chem.*, **33**, 159-200 (2009); (d) S. Y. Li, Y. W. Xu, J. M. Liu, C. Y. Su. *Int. J. Mol. Sci.*, **12**, 429-455 (2011); (e) M. Durmaz, E. Halay, S. Bozkurt. *Beilstein J. Org. Chem.*, **14**, 1389-1412 (2018).
 50. (a) J. L. Atwood, L. J. Barbour, A. Jerga. *Science* **296** 2367-2369S (2002); (b) P. K. Thallapally, L. Dobrzańska, T. R. Gingrich, T. B. Wirsig, L. J. Barbour, J. L. Atwood. *Angew. Chem. Int. Ed.* **45** 6506-6509 (2006); (c) J. Dalgarno, P. K. Thallapally, L. J. Barbour, J. L. Atwood, *Chem. Soc. Rev.*, **36**, 236-245 (2007); (d) O. I. Koifman, N. Z. Mamardashvili, O. V. Surov. *Russ. Chem. Bull.*, **66**, 241-253 (2017).
 51. (a) Z. Asfari, J. Weiss, S. Pappalardo, J. Vicens, V. A. Doria. *Pure & Appl. Chem.*, **65**, 585-590 (1993); (b) A. Casnati, F. Giunta, F. Sansone, R. Ungaro, M. Montalti, L. Prodi, N. Zaccheroni. *Supramol. Chem.*, **13**, 419-434 (2001).
 52. T. Gu, C. Bourgoigne, J.-F. Nierengarten. *Tetrahedron Lett.*, **42**, 7249-7252 (2001).
 53. R. De Zorzi, N. Guidolin, L. Randaccio, R. Purrello, S. Geremia. *J. Am. Chem. Soc.* **131**, 2487-2489 (2009).
 54. J. Biigler, N. A. J. M. Sommerdijk, A. J. W. G. Visser, A. Van Hoek, R. J. M. Nolte, J. F. J. Engbersen, D. N. Reinhoudt. *J. Am. Chem. Soc.*, **121**, 28-33 (1999).
 55. (a) D. M. Roundhill Calixarenes. *Comprehensive Coordination Chemistry II*:485-491 (2003); (b) A. Bilyk, J. W. Dunlop, R. O. Fuller, A. K. Hall, J. M. Harrowfield, M. W. Hosseini, G. A. Koutsantonis, I. W. Murray, B. W. Skelton, R. L. Stamps, A. H. White. *Eur. J. Inorg. Chem.*, 2106-2126 (2010); (c) G. Karotsis, S. Kennedy, S. J. Teat, C. M. Beavers, D. A. Fowler, J. J. Morales, M. Evangelisti, S. J. Dalgarno, E. K. Brechin. *J. Am. Chem. Soc.*, **132**, 12983-12990 (2010).
 56. (a) P. Murphy, S. J. Dalgarno, M. J. Paterson. *J. Phys. Chem. A*, **120**, 824-839 (2016); (b) C. D. Gutsche, M. Iqbal, K. S. Nam, K. See, I. Alam. *Pure Appl. Chem.*, **60**, 483-488 (1988).
 57. J. Kulesza, B. S. Barros, S. Alves. *Coord. Chem. Rev.*, **257**, 2192-2212 (2013).
 58. C. Wieser-Jeunesse, D. Matt, M. R. Yaftian, M. Burgard, J. Harrowfield, *C.R.A.S.* 479-502 (1998).
 59. (a) L. Baklouti, J. Harrowfield, B. Pulpoka, J. Vicens. *Mini-Reviews in Organic Chemistry*, **3**, 355-384 (2006); (b) B. Pulpoka, V. Ruangpornvisuti, J. Vicens, H. Takemura. *Cyclophane Chemistry for the 21st Century*, Research Signpost, Kerala, India, chapter 3. (2002).
 60. S. Pappalardo, F. Bottino, G. Ronsisvalle. *Phosphorus Sulfur Relat. Elem.*, **19**, 327-333 (1984).
 61. (a) T. Kajiwara, N. Iki, M. Yamashita. *Coord. Chem. Rev.*, **251**, 1734-1746 (2007); (b) G. Karotsis, S. J. Teat, W. Wernsdorfer, S. Piligkos, S. J. Dalgarno, E. K. Brechin. *Angew. Chem. Int. Ed.*, **48**, 8285-8 (2009); (c) B. S. Creaven, D. F. Donlon, J. McGinley. *Coord. Chem. Rev.*, **253**, 893-962 (2009); (d) Y. Bi, S. Du, W. *Coord. Chem. Rev.*, **276**, 61-72 (2014).
 62. A. Ovsyannikov, S. Solovieva, I. Antipin, S. Ferlay. *Coord. Chem. Rev.* **352**, 151-186 (2017).
 63. S. P. Bew, A. D. Burrows, T. Düren, M. F. Mahon, P. Z. Moghadam, V. M. Sebestyen, S. Thurston. *Chemical Communications*, **48**, 4824-4826 (2012).
 64. P. P. Cholewa, C. M. Beavers, S. J. Teat, S. J. Dalgarno. *Cryst. Growth Des.*, **13**, 5165-5168 (2013).

65. E. K. Lee, Y. Heo, J. Park, K. Min. *Cryst. Growth Des.*, **15**, 3556-3560 (2015).
66. (a) S. Kennedy, S. J. Dalgarno, *Chem. Commun.* 5275-5277 (2009); (b) S. Kennedy, G. Karotsis, C. M. Beavers, S. J. Teat, E. K. Brechin, S. J. Dalgarno. *Angew. Chem. Int. Ed.*, **49**, 4205 (2010); (c) M. Liu, W. Liao *CrystEngComm*, **14**, 5727-5729 (2012) (d) Z. Zhang, A. Drapailo, Y. Matvieiev, L. Wojtas, M. J. Zaworotko *Chem. Commun.*, **49**, 8353-8355 (2013).
67. (a) S. P. Bew, A. D. Burrows, T. Düren, M. F. Mahon, P. Z. Moghadam, V. M. Sebestyen, S. Thurston. *Chem. Commun.*, **48**, 4824-4826 (2012); (b) S. Pasquale, S. Sattin, E.C. Escudero-Adán, M. Martínez-Belmonte, J. De Mendoza. *Nat Commun.*, **3**, 785 doi: 10.1038/ncomms1793 (2012).
68. (a) G. Mislin, E. Graf, M. W. Hosseini, A. De Cian, N. Kyritsakas, J. Fischer. *Chem Comm.*, 2545-2546 (1998); (b) M. N. Kozlova, S. Ferlay, S. E. Solovieva, I. S. Antipin, A. I. Konovalov, N. Kyritsakas, M. W. Hosseini. *Dalton*, **44**, 5126-5131 (2007).
69. E. Elisabeth, L. J. Barbour, G. W. Orr, K. T. Holman, J. L. Atwood. *Supramol. Chem.*, **12**, 317-320 (2000).
70. (a) O. I. Kalchenko, A. V. Solovyov, S. A. Cherenok, N. F. Starodub, V. I. Kalchenko. *J. Incl. Phenom. Macrocycl. Chem.*, **46**, 19-25 (2003); (b) O. Kalchenko, A. Marcinowicz, J. Poznanski, S. Cherenok, A. Solovyov, W. Zielenkiewicz, V. Kalchenko. *J. Phys. Org. Chem.*, **18**, 578-585 (2005); (c) A. I. Vovk, V. I. Kalchenko, S. A. Cherenok, V. P. Kukhar, O. V. Muzychka, M. O. Lozynsky. *Org. Biomol. Chem.*, **2**, 3162- 3166 (2004); (d) S. Cherenok, A. Vovk, I. Muravyova, A. Shivanyuk, V. Kukhar, J. Lipkowski, V. Kalchenko. *Org. Lett.*, **8**, 549-552 (2006); (e) M. Bayrakci, Ş. Ertul, M. Yilmaz. *J. Incl. Phenom. Macrocycl. Chem.*, **74**, 293-303 (2012).
71. I. Ling, I. K. Swaminathan, C. S. Bond, A. N. Sobolev, Y. Alias, C. L. Raston. *CrystEngComm*, **14**, 8541-8546 (2012).
72. R. G. Pearson. *J. Chem. Educ.*, **45**, 581 (1968); (b) R.G. Pearson. *J. Chem. Educ.*, **45**, 643 (1968).
73. X. Delaigue, J. M. B. Harrowfield, M. W. Hosseini, A. De Cian, J. Fischer, N. Kyritsakas *J. Chem. Soc., Chem. Commun.*, 1579-1580 (1994).
74. S. Kotha, M. E. Shirbhate, G. T. Waghule. *Beilstein J. Org. Chem.*, **11**, 1274-1331 (2015).
75. (a) J. L. Ballard, W. B. Kay, E. L. Kropa. *Journal of Paint Technology*, **38**, 251-262 (1966); (b) F. Bottino, G. Montaudo, P. Maravigna *Ann. Chim.*, **57**, 972-978, (1967); (c) T.-T. Wu, J. R. Speas *J. Org. Chem.*, **52**, 2330- 2332 (1987); (d) B. Gawdzik, W. Iwanek, A. Hoser, K. Wozniak *Supramol. Chem.*, **20**, 273-277 (2008).
76. J. Ehrhart, J-M. Planeix, N. Kyritsakas-Gruber, M. W. Hosseini, *Dalton Trans.*, **14**, 2552-2557 (2009).
77. C. Klein, E. Graf, M. W. Hosseini, A. De Cian, N. Kyritsakas, *Eur. J. Org. Chem.*, **5**, 802-809 (2002).
78. J. Ehrhart, J. M. Planeix, N. Kyritsakas-Gruber, M. W. Hosseini. *Dalt. Trans.*, **39**, 2137-2146 (2010).
79. G. A. Consiglio, P. Finocchiaro, S. Failla, A. Albert, D. Moot, *Phosphorus Sulfur Silicon Relat. Elem.*, **149**, 29- 38 (1999).
80. S. Wenger, Z. Asfari and J. Vicens. *J. Incl. Phenom. Mol. Recognit. Chem*, **20**, 151-156 (1995).
81. T. Sawai, K. Sato, T. Ise, D. Shiomi, K. Toyota, Y. Morita, T. Takui. *Angew. Chem. Int. Ed.*, **47**, 3988-3990 (2008).
82. M. Staffilani, G. Bonvicini, J. W. Steed, T. K. Holman, J. L. Atwood,^[1] M. R. J. Elsegood. *Organometallics* **17**, 1732-1740 (1998).

83. O. Mogck, P. Parzuehowski, M. Nissinen, V. Biihmer, G. Rokicki, K. Rissanen. *Tetrahedron*, **54**, 10053-10068 (1998).
84. A. S. Ovsyannikov, S. Ferlay, E. F. Chernova, S. E. Solovieva, I. S. Antipin, M. W. Hosseini. *Macroheterocycles*, **10**, 410-420 (2017).
85. C. Klein, E. Graf, M. W. Hosseini A. De Cian. *Tetrahedron Lett*, **41**, 9043-9047(2000).
86. X. Delaigue and M. W. Hosseini, *Tetrahedron Lett.*, **34**, 8111-8112 (1993).
87. C. Klein, E. Graf, M. W. Hosseini, A. De Cian, J. Fischer. *Chem. Commun.*, 239-240 (2000).
88. C. Klein, E. Graf, M. W. Hosseini, A. De Cian. *New J. Chem.*, **25**, 207-209 (2001).
89. C. Klein, E. Graf, M. W. Hosseini, A. De Cian, N. Kyritsakas. *Eur. J. Inorg. Chem.*, 1299-1302 (2003).
90. C. Klein, E. Graf, M. W. Hosseini, N. Kyritsakas-Gruber. *Transactions ACA*, **39**, 103-109 (2004).
91. J. Ehrhart, J-M. Planeix, N. Kyritsakas-Gruber, M. W. Hosseini. *Dalton Trans.*, 6309-6314 (2009).
92. (a) G. Laugel, E. Graf, M. W. Hosseini, J-M. Planeix, N. Kyritsakas. *New J. Chem.*, **30**, 1340-1346 (2006); (b) A. Ovsyannikov, S. Ferlay, S. E. Solovieva, I. S. Antipin, A. I. Konovalov, N. Kyritsakas, M. W. Hosseini. *Dalton Trans.*, **43**, 158-165 (2014).
93. E. F. Chernova, A. S. Ovsyannikov, S. Ferlay, S. E. Solovieva, I. S. Antipin, A. I. Konovalov, N. Kyritsakas, M. W. Hosseini. *Mendeleev Commun.*, **27**, 260-262 (2017).
94. (a) G. Laugel, E. Graf, M. W. Hosseini, J-M. Planeix, N. Kyritsakas. *New J. Chem.*, **30**, 1340-1346 (2006); (b) A. Ovsyannikov, S. Ferlay, S. E. Solovieva, I. S. Antipin, A. I. Konovalov, N. Kyritsakas, M. W. Hosseini. *Dalton Trans.*, **43**, 158-165 (2014). (c) A. Ovsyannikov, M. H. Noamane, R. Abidi., S. Ferlay, S. E. Solovieva, I. S. Antipin, A. I. Konovalov, N. Kyritsakas, M. W. Hosseini. *CrystEngComm*, **18**, 691-703 (2016).
95. S. P. Bew, A. D. Burrows, T. Düren, M. F. Mahon, P. Z. Moghadam, V. M. Sebestyen, S. Thurston. *Chem. Commun.*, **48**, 4824-4826 (2012).
96. K. K. Zborowski, M. Solá, J. Poater, L. M. Proniewicz. *Cent. Eur. J. Chem.*, **11**, 655-663 (2013).
97. V. A. Montes, R. Pohl, J. Shinar, P. Anzenbacher. *Chem. - A Eur. J.*, **12**, 4523-4535 (2006).
98. I. A. Bagatina, H. E. Toma. *New J. Chem.*, **24**, 841-844 (2000).
99. (a) A. Casnati, F. Sansone, A. Sartori, L. Prodi, M. Montalti, N. Zaccheroni, F. Ugozzoli, R. Ungaro. *Eur. J. Org. Chem.*, 1475-1485 (2003); (b) A. Jäschke, M. Kischel, A. Mansel, B. Kersting. *Eur. J. Inorg. Chem.*, **5**, 894-901 (2017).
100. (a) Y. Ohki, K. Tatsumi. *Eur. J. Inorg. Chem.*, 973-985 (2011); (b) C. A. McQuilken, D. P. Goldberg. *Dalton Trans.*, **41**, 10883-10899 (2012).
101. G. M. Whitesides, B. Grzybowski. *Science*, **295**, 2418-21 (2002).
102. J. Ehrhart. *PhD Thesis* (2009), Université Louis Pasteur de Strasbourg.
103. E. F. Chernova, A. S. Ovsyannikov, S. Ferlay, S. E. Solovieva, I. S. Antipin, A. I. Konovalov, N. Kyritsakas, M. W. Hosseini. *Tetrahedron Lett.*, **59**, 1377-1381 (2018).
104. S. R. Chemler, D. Trauner, S. J. Danishefsky. *Angew. Chem. Int. Ed.*, **40**, 4544-4568 (2001).
105. A. Suzuki. *Proc. Japan Acad. Ser. B.*, **80**, 359-371 (2004).
106. Alexander Ovsyannikov. *PhD thesis* (2009,) Université Louis Pasteur de Strasbourg.
107. A. Spek. *J. Appl. Cryst.* **36**, 7-13 (2003)
108. P. G. Sutariya, N. R. Modi, A. Pandya, B. K. Joshi, K. V. Joshi, S. K. Menon. *Analyst*, **137**, 5491-5494

- (2012).
109. A. Casnati, F. Sansone, A. Sartori, L. Prodi, M. Montalti, N. Zaccheroni, F. Ugozzoli, R. Ungaro. *European J. Org. Chem.*, 1475-1485 (2003).
 110. C. Villa-Pérez, I. C. Ortega, A. Vélez-Macías, A. M. Payán, G. A. Echeverría, D. B. Soria, G. C. Valencia-Uribe. *New J. Chem.*, **42**, 7166-7176 (2018).
 111. A. Furst, R. C. Berlo, S. Hooton. *Chem. Rev.*, **65**, 51-68 (1965).
 112. F. Glasneck, K. Kobalz, B. Kersting. *Eur. J. Inorg. Chem.*, 3111-3122 (2016).
 113. M. Ulzii, K. U. M. Rao, M. Yamada, F. Hamada. *Heterocycles*, **89**, 2554-2561 (2014).
 114. J. Plutnar, J. Rohovec, J. Kotek, Z. Žák, I. Lukeš. *Inorg. Chim. Acta*, **335**, 27-35 (2002).
 115. G. Cao, H. Lee, V. M. Lynch, T. E. Mallouk. *Inorg. Chem.*, **27**, 2781-2785 (1988).
 116. A. B. Arbusov. *Pure Appl. Chem*, **9**, 307-335 (1964).
 117. G. Bhattacharya, A. K. Thyagarajan. *J. Am. Chem. Soc.*, **81**, 415-430 (1981).
 118. G. G. Rajeshwaran, M. Nandakumar, R. Sureshbabu, A. K. Mohanakrishnan. *Org. Lett.*, **13**, 1270-1273 (2010).
 119. J. I. van der Vlugt. *Versatile Phosphorus Ligands: Synthesis, Coordination Chemistry and Catalysis*. (2003).
 120. A. Popa, C. M. Davidescu, P. Negrea, G. Ilia, A. Katsaros, K. D. Demadis. *Ind. Eng. Chem. Res.*, **47**, 2010- 2017 (2008).
 121. a) J. Kim, B. Chen, T. M. Reineke, H. Li, M. Eddaoudi, D. B. Moler, M. O. Keefe and O. M. Yaghi. *J. Am. Chem. Soc.*, **123**, 8239-8247 (2001) ; b) S. Ferlay, S. Koenig, M. W. Hosseini, JA. De Cian and N. Kyritsakas. *Chem. Commun.*, 218-219 (2002).
 122. (a) Y. K. Tang, A. Tasiopoulos, A. J. Teat, S. J. Dubbeldam, D. Rothenberg, S. G. Tanase. *Inorganic Chemistry Frontiers*. **5**, 541-549 (2018); (b) X. X. Wang, X. Q. Niu, X. Y. Hu, T. Ping. *CrystEngComm.*, **18** (39), 7471-7477 (2016).
 123. C. Boskovic, W. Wernsdorfer, K. Folting, J. C. Huffman, D. N. Hendrickson, G. Christou. *Inorg. Chem.*, **41**, 5107-5118 (2002).
 124. M. Soler, W. Wernsdorfer, K. Folting, M. Pink, G. Christou. *J. Am. Chem. Soc.*, **126**, 2156-2165 (2004).
 125. G. Karotsis, S.J. Teat, W. Wernsdorfer, S. Piligkos, S. J. Dalgarno, E. K. Brechin. *Angew. Chem. Int. Ed.*, **48**, 8285-8288 (2009)
 126. a) A. Kornowicz, S. Komorski, Z. Wróbel, I. Justyniak, N. Nedelko, A. Ślawska-Waniewska, J. Lewiński. *Dalton Trans.*, **43**(8), 3048-3051 (2014); b) C. J. Milios, T. C. Stamatatos, P. Kyritsis, A. Terzis, C. P. Raptopoulou, R. Vicente, A. Escuer, S. P. Perlepes. *Eur. J. Inorg. Chem.*, 2885-2901 (2004).
 127. (a) G.E. Kostakis, S.P. Perlepes, V.A. Blatov, D.M. Proserpio, A.K. Powell. *Coord. Chem. Rev.*, **256**, 1246–1278 (2012); (b) S. Zhang, X. Liu, B. Liu, Z. Xia, W. Wang, Q. Yan, H. Ke, Q. Wei, G. Xie, S. Chen, S. Gao. *Science China Chemistry*. **58** (6), 1032-1038 (2015); (c) T. C. Stamatatos, A.K. Boudalis, K. V. Pringouri, C. P. Raptopoulou, A. Terzis, J. Wolowska, E. J. L. McInnes, S.P. Perlepes. *Eur. J. Inorg. Chem.*, 5098-5104 (2007).
 128. Kozlova. PhD Thesis (2008).
 129. M. N. Kozlova, S. Ferlay, N. Kyritsakas, M. W. Hosseini, S. E. Solovieva, I. S. Antipin, A. I. Konovalov. *Chem. Commun.*, 2514-2516 (2009).

130. D. A. Skoog, D. M. West, F. J. Holler. *Fundamentals of Analytical Chemistry, 5th Ed., Saunders: New York*, 525 (1988).
131. P. Bobadova-Parvanova, K. A. Jackson, S. Srinivas, M. Horoi. *J. Chem. Phys.*, **122**, 014310 (2005).
132. L.K. Thompson, O. Waldmann, Z. Xu. *Coordination Chemistry Reviews*, **249**, 2677-2690 (2005).
133. J. I. Martin, J. Nogues, K. Liu, J. L. Vicent, I. K. Schuller. *J. Magn. Magn. Mater.*, **256**, 449 (2003).
134. (a) W. Xia, M.F. Ni, C.H. Yao, X.L. Wang, D.Z. Chen, C. Lin, X.Y. Hu, L.Y. Wang. *Macromolecules*, **48**, 4403 (2015); (b) M.M. Zhang, D.H. Xu, X.Z. Yan, J.Z. Chen, S.Y. Dong, B. Zheng, F.H. Huang. *Angew. Chem. Int. Ed.*, **51**, 7011 (2012); (c) A. Dey, S.K. Mondal, K. Birdha. *CrystEngComm*, **15**, 9769 (2013); (d) M.D. Segarra- Maset, V.J. Nebot, J.F. Miravet, B. Escuder. *Chem. Soc. Rev.*, **42**, 7086 (2013).
135. S. Barman, J.A. Garg, O. Blacque, K. Venkatesan, H. Berke. *Chem. Commun.*, **48**, 11127 (2012).
136. (a) E. Busseron, Y. Ruff, E. Moulin, N. Giuseppone. *Nanoscale*, **5**, 7098 (2013); (b) H.H. Lee, S.H. Jung, S. Park, K.M. Park, J.H. Jung. *New J. Chem.*, **37**, 2330 (2013); (c) Y. Furukawa, T. Ishiwata, K. Sugikawa, K. Kokado, Sada. *Angew. Chem. Int. Ed.*, **51**, 10566 (2012); (d) M. Rodrigues, A.C. Calpena, D.B. Amabilino, M.L. Garduño Ramírez, L. Pérez-García. *J. Mater. Chem. B.*, **2**, 5419 (2014); (e) Y.M. Zhang, W.Q. Zhang, J.Q. Li, J.P. Dang, T.B. Wei. *Materials Letters*, **82**, 227 (2012); (f) S. Sengupta, R. Mondal. *J. Mater. Chem. A*, **2**, 16373 (2014).

Annexes
and
Experimental Part

General information

Solvents and reagents

- Chloroform Riedel-de-Haen ($\geq 99.8\%$)
- Tetrahydrofuran Riedel-de-Haen ($\geq 99.9\%$)
- Ethanol Riedel-de-Haen ($\geq 99.8\%$)
- N,N-Dimethylformamide Alfa Aesar ($\geq 99.0\%$)
- Acetonitrile ($\geq 99.0\%$)
- Acetone ($\geq 99.0\%$)
- Propanol-2 ($\geq 99.7\%$)
- Chloroform ($\geq 99.8\%$)
- Dichloromethane ($\geq 99.5\%$)
- Methanol ($\geq 99.9\%$)
- Ether ($\geq 99.8\%$)

Preparative column chromatography

- Silica gel Si 60 (0.040-0.063 mm) Merck TA1337567 943

Thin-layer chromatography

- TLC Silica gel 60 F254 on aluminium sheets, Merck HX934320

Analyses and characterizations

NMR: ^1H -, ^{13}C - and ^{31}P -NMR spectra were recorded at room temperature on a Bruker AV 300 (300 MHz) and Bruker DRX-500 (500 MHz) spectrometers (Service central de RMN de la Fédération de Recherche de Chimie de l'Université de Strasbourg). Chemical shifts were referenced to the residual proton or carbon peak of the solvent: 1) for ^1H -MNR: CDCl_3 : 7.26 ppm, $(\text{CD}_3)_2\text{SO}$: 2.50 ppm; 2) for ^{13}C -NMR: CDCl_3 : 77.36 ppm, $(\text{CD}_3)_2\text{SO}$: 39.0 ppm.

Spectral data are present as following:

- Chemical shift in ppm;
- Multiplicity of signal: s = singlet, d = doublet, t = triplet, Number of respective atoms;
- Nature of respective atoms.

FT-IR spectra were recorded on a IR Fourier spectrometer IFS 113V (Bruker).

Mass spectra (MALDI TOF and MS(ES+)) were obtained on a MALDI-TOF Dynamo Finnigan mass spectrometer using 1,8,9-trihydroxyanthracene or *p*-nitroaniline as the matrix (“Service commun d’analyse de la Fédération de Recherche Chimie”, Université de Strasbourg, Strasbourg, France).

UV spectra were recorded on a UV-VIS Spectrometer "Lambda 35" Perkin Elmer and UV-vis spectrophotometer SHIMADZU UV-2600.

Elemental analyses were performed by the Service de Microanalyses de la Fédération de Recherche Chimie, Université de Strasbourg, Strasbourg, France.

Melting points were measured in capillar on a Stuart Scientific Melting Point SMP-1 apparatus.

X-ray analyses were performed in our laboratory by Nathalie Kyritsakas-Gruber on a Bruker APEX8 CCD Diffractometer equipped with an Oxford Cryosystem liquid N₂ device at 173(2) K, using graphite-monochromated Mo-K α ($\lambda = 0.71073 \text{ \AA}$) radiation. For all structures, diffraction data were corrected for absorption. Structures were solved using SHELXS-97 and refined by full matrix least-squares on F² using SHELXL-97. The hydrogen atoms were introduced at calculated positions and not refined (riding model).¹

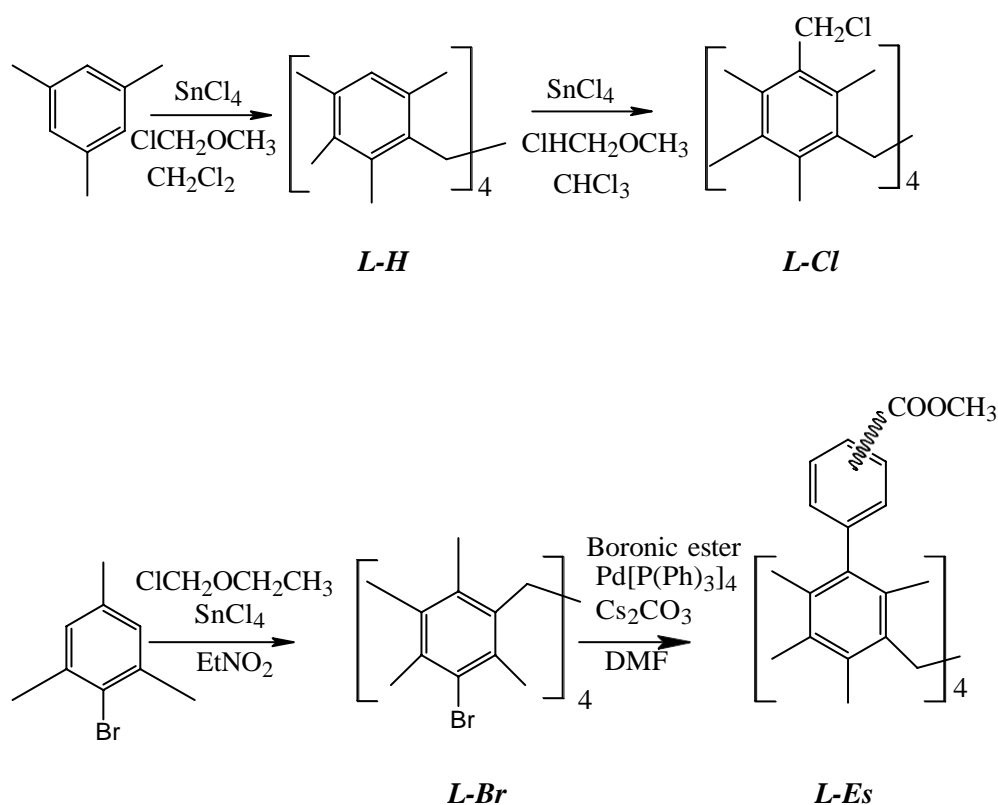
XPRD analysis was realised in A. E. Arbuzov institute of Organic and Physical Chemistry (Kazan, Russia) on a Bruker D8 Advance, source Cu K alpha, bond length 1.5406 Å.

DLS data were collected at 293 K by Malvern NanoZS instrument.

¹ G. M. Sheldrick. *Acta Cryst.*, **71** (2015).

Intermediates used for synthesis

The precursors were synthesized through two steps (both for aliphatic and aromatic spacer compounds): firstly there was performed metacyclophane **L-H** via condensation reaction of mesitylene units² that was further transformed to tetrasubstituted chloromethylmetacyclophane^{II} **L-Cl** – the precursor for the ligands containing aliphatic spacer between aromatic rings and functional groups. The tetrasubstituted bromometacyclophane **L-Br** was synthesized upon condensation of bromo-mesitylene rings³ which was converted to meta-methyl-ester⁴ **L-Es** on the metacyclophane platform containing aromatic spacer in its structure.



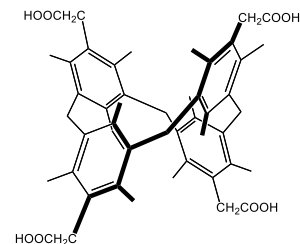
² J. Ehrhart, J-M. Planeix, N. Kyritsakas-Gruber, M. W. Hosseini. *Dalton Trans.*, 2552 (2009);

³ C. Klein, E. Graf, M. W. Hosseini, A. De Cian, N. Kyritsakas. *Eur. J. Org. Chem.*, 802-809 (2002);

⁴ J. Ehrhart, Ph.D. thesis (2009).

Synthesis of targeted ligands

4,11,18,25-tetra(2-(carboxyl)-methylene)-3,5,7,10,12,14,17,19,21,24,26,28-dodecamethyl-[1.1.1]metacyclophane (**L1**)



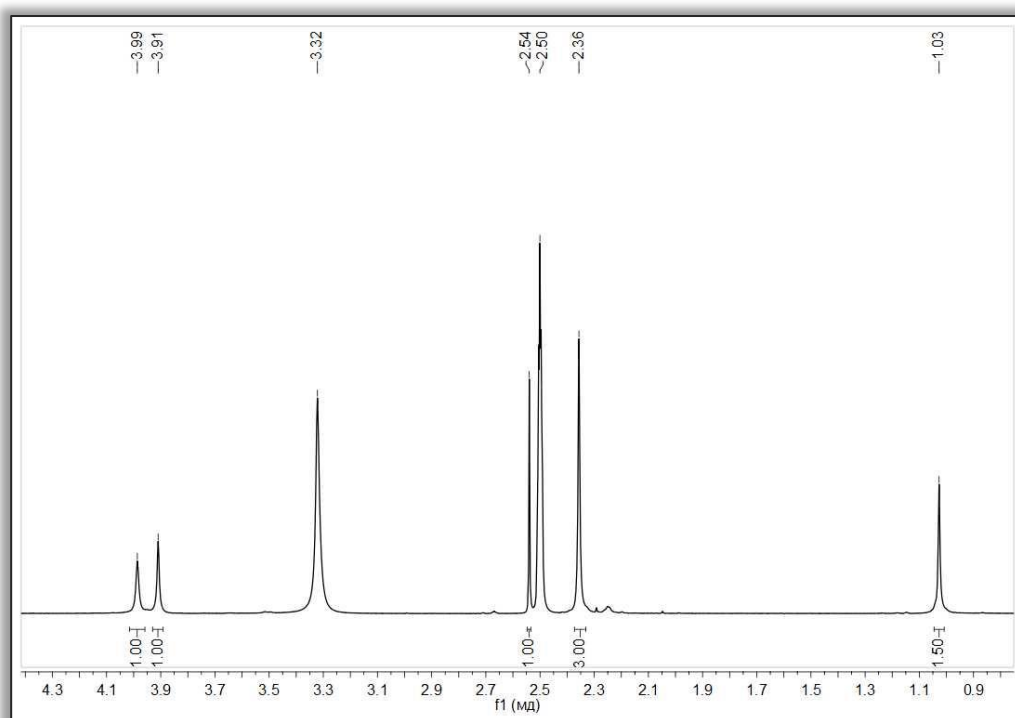
A suspension containing cyano- derivative of metacyclophane (**L9**) (0,35 g, 0,52 mmol), NaOH (0,21 g, 5,2 mmol) in a DMSO:H₂O mixture (5:1) (18 mL) was heated to 120 °C and stirred during 72 h. After cooling, the solvents were evaporated (3/4 of the initial volume) and concentrated HCl (12 M, 5 ml) was carefully added dropwise. After stirring at room temperature during 1 hour, distillate water (100 mL) was added to the mixture and the observed precipitate was collected using centrifugation. **L1** (0,32 g) was obtained with 85% yield as a white powder.

¹H-NMR (DMSO-d₆, 400 MHz, 25 °C): δ(ppm) = 2.36 (s, 24H, *o*-CH₃), 2.54 (s, 12H, *p*-CH₃), 3.91 (s, 8H, Ar-CH₂-Ar), 3.99 (s, 8H, CH₂-COOH);

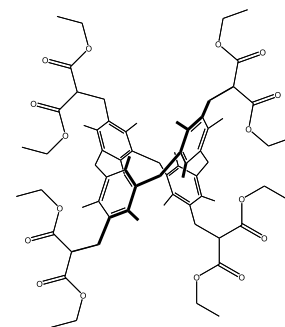
¹³C-NMR (CDCl₃, 125 MHz, 25 °C) δ: 17.82, 18.54, 33.40, 40.79, 131.46, 132.59, 133.63, 137.58, 172.89.

Mp: degradation above 320 °C,

EA for C₄₈H₅₆O₈: C, 75.76 %; H, 7.42 %; found C, 75.81 %; H, 7.49 %.



**4,11,18,25-tetra((diethyl malonate)-methylene)-3,5,7,10,12,14,17,
19,21,24,26,28-dodecamethyl-[1.1.1]Metacyclophane (L2')**



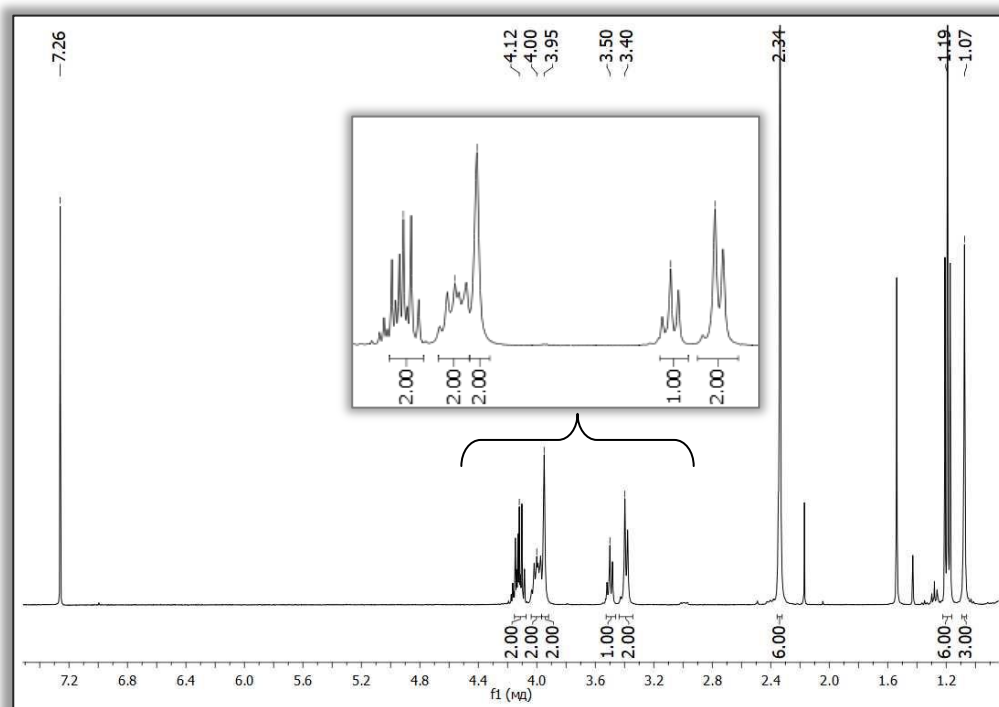
A mixture of sodium diethyl malonate (0.8 g, 4.4 mmol) and **1** (0.32 g, 0.44 mmol) in dry THF (150 mL) was refluxed during 24 h. After cooling, the solvent was evaporated to dryness and the product was purified using column chromatography (SiO₂, eluent EtOAc:Cyclohexane, 2:1). The desired product **L2'** was obtained as a white powder (0.26 g, 48% yield).

¹H-NMR (CDCl₃, 300 MHz, 25 °C): δ(ppm) = 1.07 (s, 12H, *p*-CH₃); 1.19 (t, 24H, RCOOCH₂-CH₃), 2.34 (s, 24H, *o*-CH₃); 3.4 (d, 8H, Ar-CH₂-CH(COOC₂H₅)₂); 3.5 (t, 4H, -CH-(COOC₂H₅)₂); 3.95 (s, 8H, Ar-CH₂-Ar); 4.4, 12 (q, 16H, COO-CH₂-CH₃).

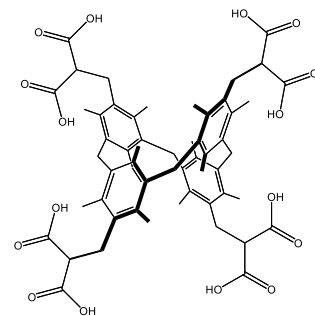
¹³C-NMR (CDCl₃, 125 MHz, 25 °C): δ(ppm) = 14.01, 17.61, 18.11, 29.72, 33.57, 52.40, 61.27, 131.91, 134.08, 138.08, 169.22.

HRMS (ESI): *m/z* calcd. for [M]⁺: 1216,70; found 1216,42; calcd. for [M⁺Na]⁺: 1239,70; found 1239,65.

EA for C₇₂H₉₆O₁₆: C, 71.03 %; H, 7.95 %; found C, 71.07 %; H, 7.93 %.



**4,11,18,25-tetra((malonate)-methylene)-3,5,7,10,12,14,17, 19,
21,24,26,28-dodecamethyl-[1.1.1]metacyclophane (L2)**



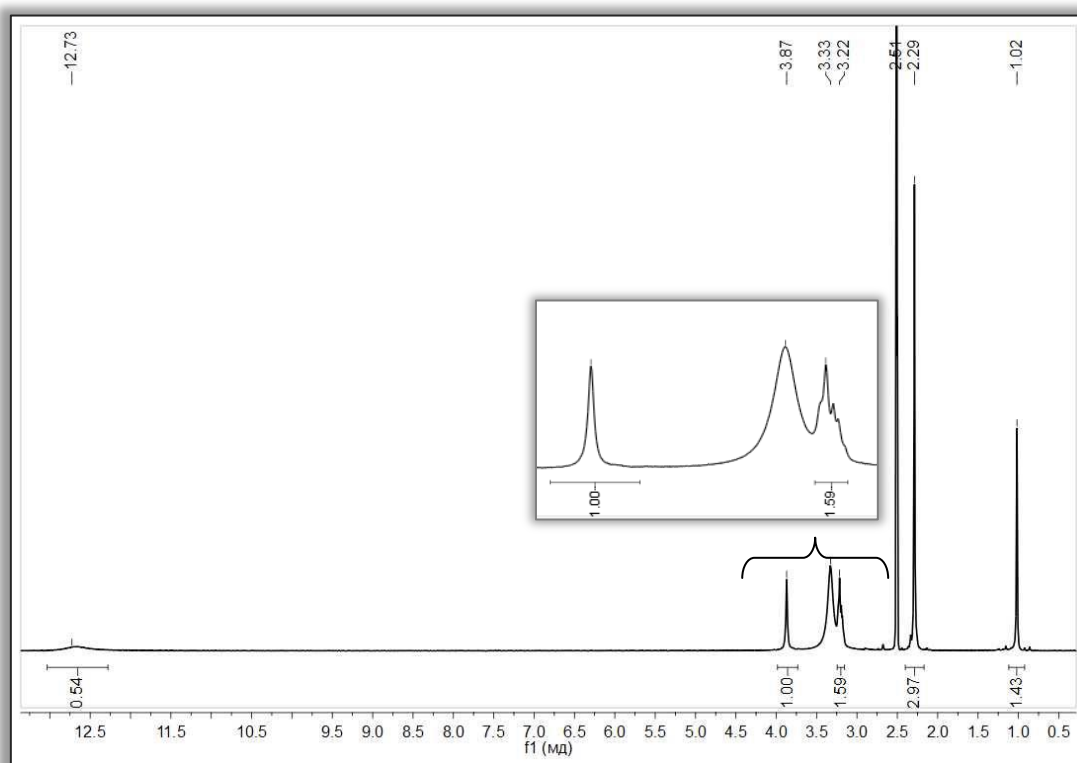
A suspension containing **L2'** (0,26 g, 0,23 mmol), LiOH (0,13 g, 5,2 mmol) in a EtOH:H₂O:THF mixture (2:1:2) (50 mL) was refluxed during 80 h. After cooling, the solvents were evaporated (3/4 of the initial volume) and concentrated HCl (12 M, 5 ml) was carefully added dropwise. After stirring at room temperature during 1 hour, distillate water (100 mL) was added to the mixture and the observed precipitate was collected using centrifugation. **L2** (0,19 g) was obtained with 85% yield as a white powder.

¹H-NMR (DMSO-d₆, 300 MHz, 25°C): δ(ppm) = 1,01 (s, 12H, *p*-CH₃); 2,29 (s, 24H, *o*-CH₃); 3,33 (m, 8H, Ar-CH₂-CH-); 3,87 (s, 8H, Ar-CH₂-Ar-); 12,73 (s, 4H, COOH-).

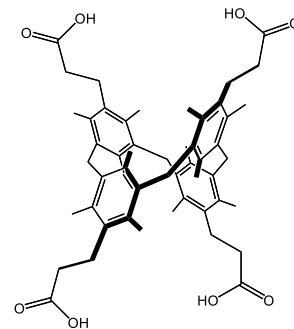
¹³C-NMR (DMSO-d₆, 125 MHz, 25 °C): δ(ppm) = 17.26, 17.70, 29.50, 33.06, 52.64, 79.16, 131.42, 133.04, 137.40, 170.64.

Mp: 325 °C. HRMS (ESI): *m/z* calcd. for [M]⁺:992.40; found: 992.60; calcd for [M+Na⁺] 1015.40 ; found: 1015.59.

EA for C₅₆H₆₆O₁₆: C, 67.59 %; H, 6.68 %; %; found C, 67.74 %; H, 6.47 %.



**4,11,18,25-tetra(2-(carboxyl)-ethylene)-3,5,7,10,12,14,17,
19,21,24,26,28-dodecamethyl-[1.1.1]metacyclophane (L3)**



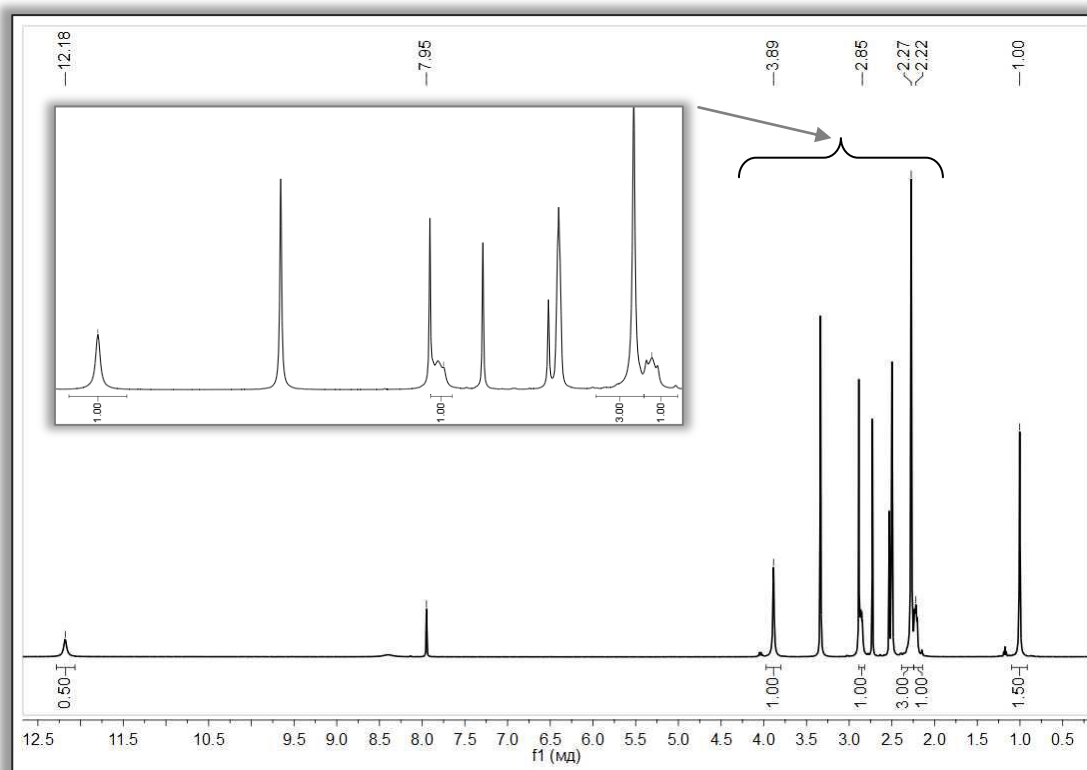
The mixture of **L2** (0,3 g, 0,3 mmol), and concentrated HCl (12 M, 3 mL) was refluxed in dry DMF (15 mL) during 48 h. After solvent evaporation followed by distillate water addition (100 ml), the formed precipitate was collected using centrifugation. **L3** (0,19 g) was obtained as white powder with 78% yield.

$^1\text{H-NMR}$ (DMSO- d_6 , 300 MHz, 25°C): $\delta(\text{ppm}) = 1,00$ (s, 12H, $p\text{-CH}_3$); 2,22 (t, 8H, $\text{CH}_2\text{-COOH}$); 2,27 (s, 24H, $o\text{-CH}_3$); 2,85 (m, 8H, Ar- $\text{CH}_2\text{-}$), 3,89 (s, 8H, Ar- $\text{CH}_2\text{-Ar}$); 12,18 (s, 4H, -COO-H).

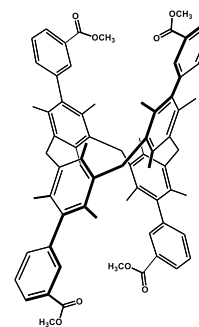
$^{13}\text{C-NMR}$ (DMSO- d_6 , 125 MHz, 25 °C): $\delta(\text{ppm}) = 16.64, 17.90, 30.79, 34.27, 35.81, 130.78, 132.86, 134.50, 137.41, 162.31, 173.90$.

Mp: 330 °C. HRMS (ESI): m/z calcd. for $[\text{M}^+]$: 816.50; found: 816.80; for $[\text{M} + \text{Na}^+]$: 839.40; found 839.63.

EA for $\text{C}_{52}\text{H}_{64}\text{O}_8$: C, 76.44 %; H, 7.90 %; found C, 76,58 %; H, 7,79 %.



4,11,18,25-tetra (3-(methoxycarbonyl) phenyl)-3,5,7,10,12,14,17,19,21,24,26,28-dodecamethyl- [1.1.1]Metacyclophane (L4')

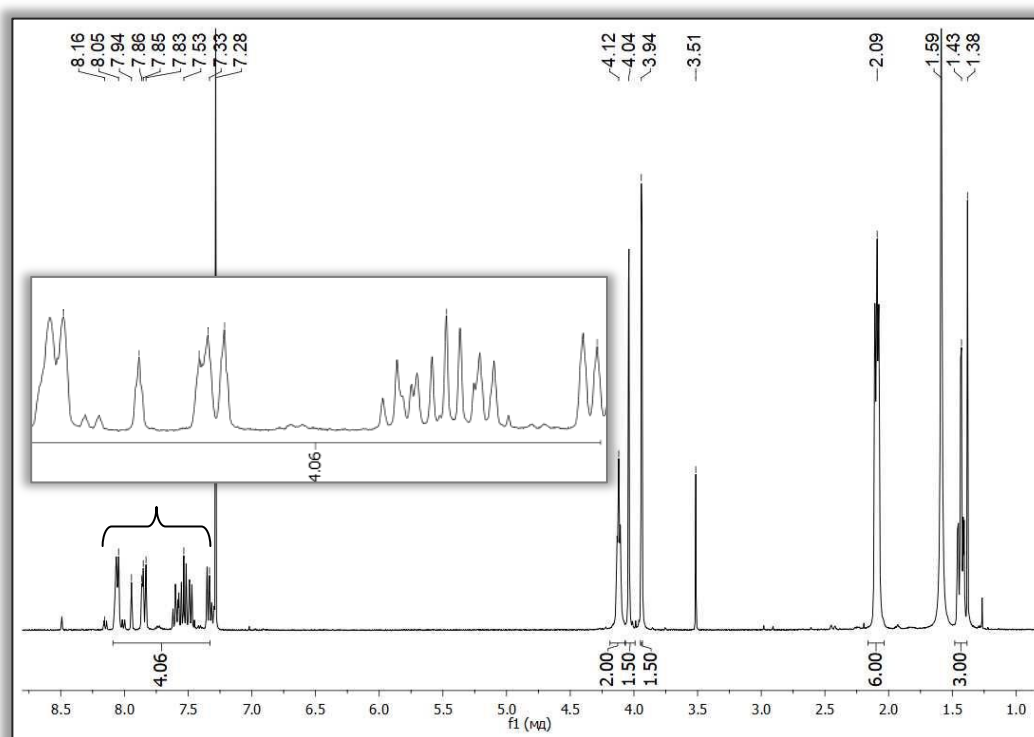


The mixture of **2** (0,3 g, 0,35 mmol), and anhydrous Cs₂CO₃ (0,23 g, 0,7 mmol), in dry DMF (30 mL) was degassed during 20 min using argon. Pd(PPh₃)₄ (0,04 g, 0,035 mmol) and *meta* phenylboronic acid ester (0,28 g, 1,05 mmol), were simultaneously added. The mixture was placed into a microwave reactor (120 W, 130°C, 30 min), then the hot solution was filtered and evaporated. The residue was dissolved in CH₂Cl₂ (40 mL) and washed with NaOH solution (1 M, 40 mL) and then twice by H₂O (40 mL). The organic layer was dried using MgSO₄, filtered and evaporated. The residue was dissolved in a minimum of CH₂Cl₂ and precipitated by slow addition of MeOH (50 mL). The resulting suspension was cooled in an ice bath for 1 hour and then the precipitate was filtered. **L4'** (0,23 g) was obtained as a white powder with 54 % yield.

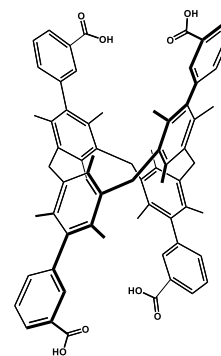
¹H NMR (CDCl₃, 300 MHz, 25°C, δ (ppm) = 1,40 (m, 12H, *p*-CH₃); 2,07 (m, 24H, *o*-CH₃); 3,91 (m, 6H, COOCH₃); 4,02 (m, 6H, COOCH₃); 4,1 (m, 8H, Ar-CH₂-Ar); 7,27-8,04 (m, 16H, Ar-H).

HRMS (ESI): m/z calcd. for [M]⁺: 1064.52, found 1064.38; calcd. for [M+Na]⁺: 1087.51, found 1087.43.

EA for C₇₂H₇₂O₈: C, 81,17%; H, 6,81%; found C, 81,43%; H, 7,05%.



**4,11,18,25-tetra (3-(carboxyl)phenyl)-3,5,7,10,12,14,17,19,21,
24,26,28 -dodecamethyl-[1.1.1]Metacyclophane (L4)**



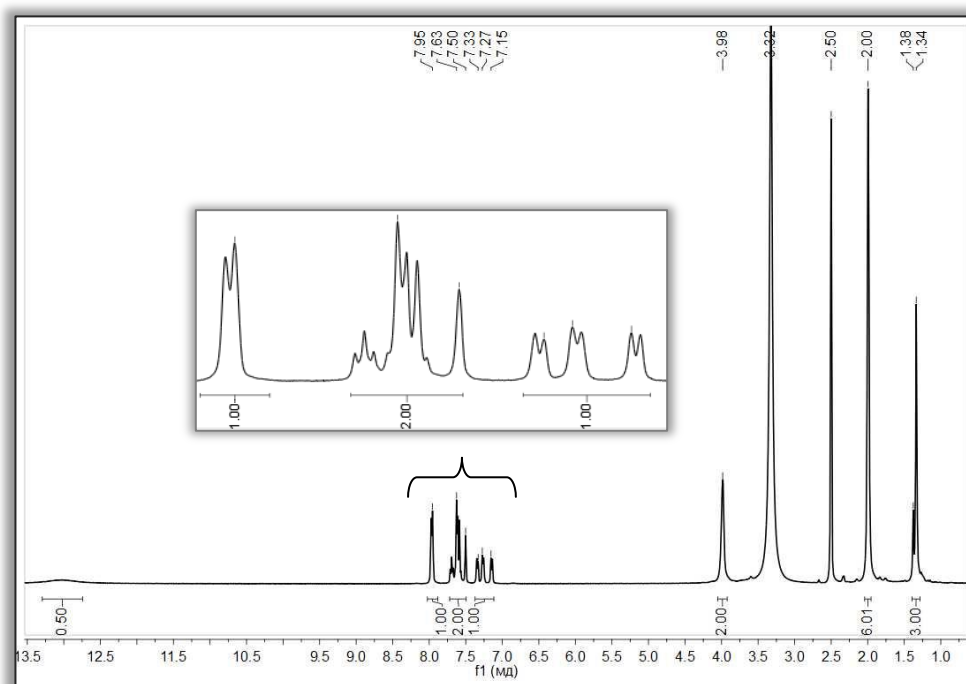
The suspension containing **L4'** (0,32 g, 0,3 mmol), LiOH (0,144 g, 6 mmol) in a EtOH:H₂O:THF mixture (2:1:2) (50 ml) was refluxed during 70 h. After cooling, the solvents were evaporated (3/4 of the initial volume) and concentrated HCl (12 M, 5 ml) was carefully added dropwise. The mixture was stirred for 1 hour and finally distillate water was poured (100 ml) into the solution. **L4** was precipitated, filtrated and dried under vacuum affording a white powder (0,27 g, 88% yield).

¹H NMR (DMSO d₆, 300 MHz, 25 °C, ppm) δ 1,33 (s, 12H, *p*-CH₃); 1,99 (s, 24H, *o*-CH₃); 3,98 (s, 8H, Ar-CH₂-Ar); 7,15-7,33 (m, 4H, Ar-H); 7,5-7,62 (m, 8H, Ar-H); 7,95 (m, 4H, Ar-H); 13,02 (s, 4H, R-COO-H);

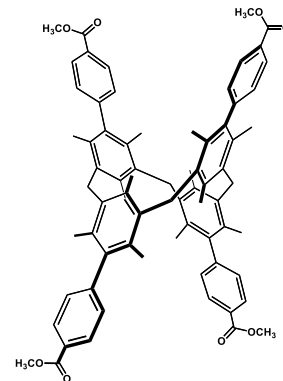
¹³C NMR (DMSO-d₆, 125 MHz, 25 °C) δ: 17.19, 19.00, 32.45, 127.47, 128.86, 129.85, 130.60, 131.03, 133.65, 133.91, 134.67, 137.36, 139.04, 143.76, 167.34;

Mp: degradation above 330-343°C, HRMS (ESI): m/z calcd. for [M]⁺: 1008.23, calcd. for [M⁺Na]⁺; 1031.45, found 1031.428 [M⁺Na]⁺.

EA for C₆₈H₆₄O₈: C, 80.93 %; H, 6.39%; found C, 81.06 %; H, 6.61 %.



4,11,18,25-tetra (4-(methoxycarbonyl) phenyl)-3,5,7,10,12, 14, 17, 19,21,24,26,28 -dodecamethyl-[1.1.1]Metacyclophane (L5'**)**



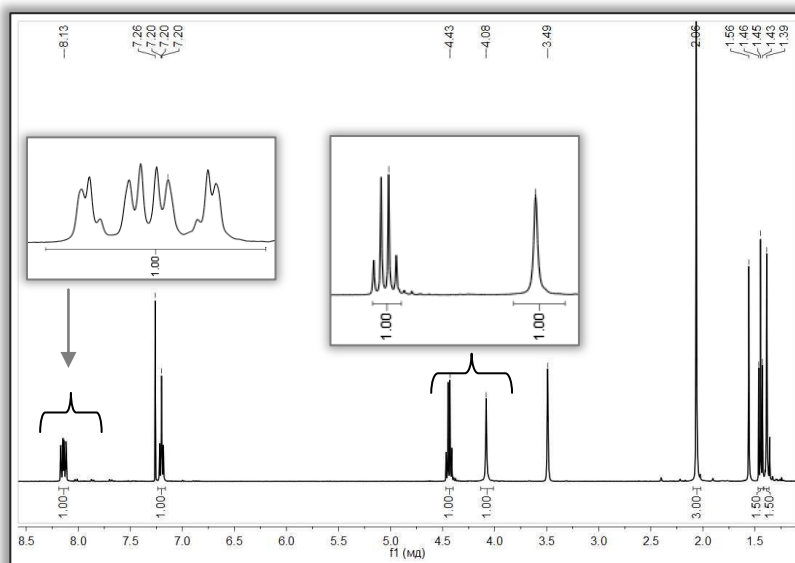
The mixture of **2** (0,3 g, 0,35 mmol), and anhydrous Cs_2CO_3 (0,23 g, 0,7 mmol), in dry DMF (30 mL) was degassed during 20 min using argon. $\text{Pd}(\text{PPh}_3)_4$ (0,04 g, 0,035 mmol) and *para*-phenylboronic acid ester (0,28 g, 1,05 mmol), were simultaneously added. The mixture was placed into a microwave reactor (120 W, 130°C, 30 min), then the hot solution was filtered and evaporated. The residue was dissolved in CH_2Cl_2 (40 mL) and washed with NaOH solution (1 M, 40 mL) and then twice by H_2O (40 mL). The organic layer was dried using MgSO_4 , filtered and evaporated. The residue was dissolved in a minimum of CH_2Cl_2 and precipitated by slow addition of methanol (50 mL). The resulting suspension was cooled in an ice bath for 1 hour and then the precipitate was filtered. **L5'** (0,23 g) was obtained as a white powder with 60 % yield.

$^1\text{H-NMR}$ (CDCl_3 , 300 MHz, 25°C): $\delta(\text{ppm}) = 1,38$ (s, 12 H, *p*- CH_3); 2,06 (s, 24 H, *o*- CH_3); 3,98 (s, 12H, COOCH_3); 4,08 (s, 8H, Ar- CH_2 -Ar); 7,21 (dd, 8H, *H*-Ph); 8,14 (m, 8H, *H*-Ph).

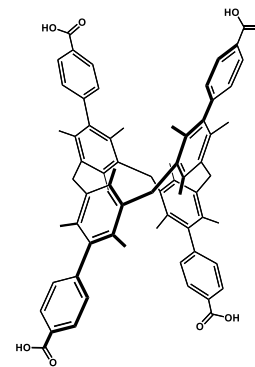
$^{13}\text{C-NMR}$ (CDCl_3 , 125 MHz, 25°C): $\delta(\text{ppm}) = 18,1$; 19,3; 32,9; 52,2; 128,4; 129,7; 129,9; 130,0; 131,0; 135,2; 137,8; 140,0; 149,0; 167,2.

HRMS (ESI): m/z calcd. for $[\text{M}]^+$: 1008.50, found 1008.46; calcd for $[\text{M} + \text{Na}]^+$ 1031.40, found 1031.36.

EA for $\text{C}_{72}\text{H}_{72}\text{O}_8$: C, 81,17%; H, 6,81%; found C, 81,32%; H, 6,99%.



4,11,18,25-tetra(4-(carboxyl)phenyl)-3,5,7,10,12,14,17,19,21, 24,26,28-dodecamethyl-[1.1.1]Metacyclophane (L5)



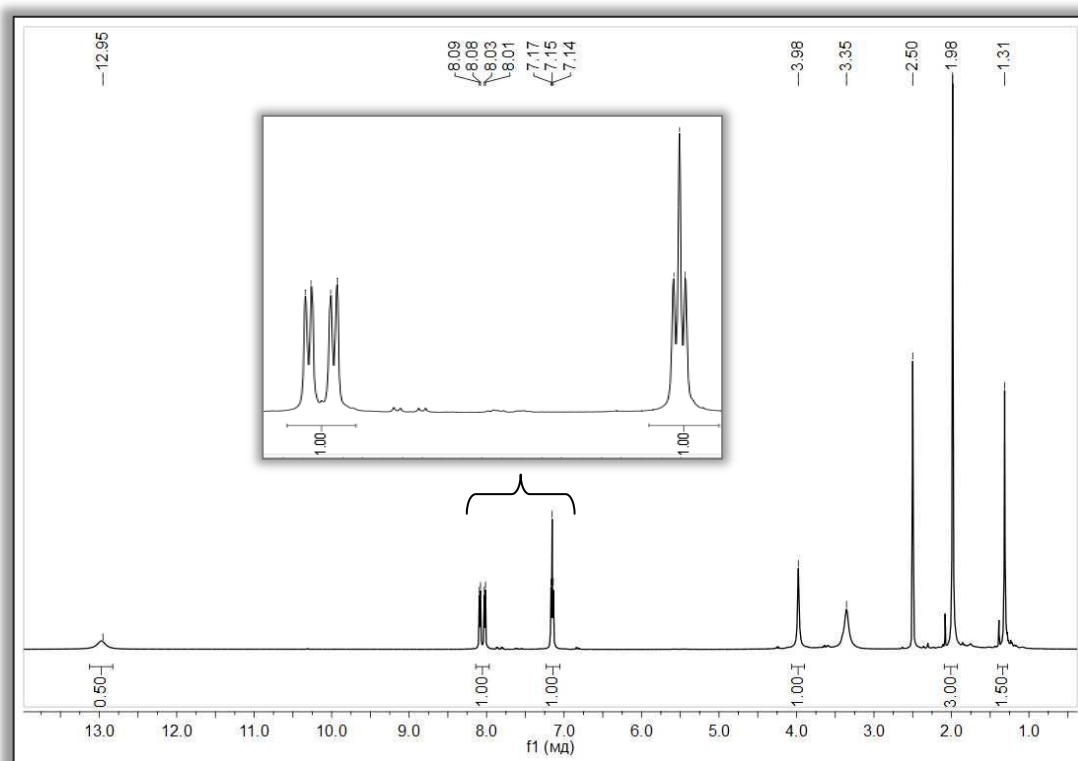
The suspension containing **L5** (0,32 g, 0,3 mmol), LiOH (0,144 g, 6 mmol) in a EtOH:H₂O:THF mixture (2:1:2) (50 ml) was refluxed during 70 h. After cooling, the solvents were evaporated (3/4 of the initial volume) and concentrated HCl (12 M, 5 ml) was carefully added dropwise. The mixture was stirred for 1 hour and finally distillate water was poured (100 ml) into the solution. **L5** was precipitated, filtrated and dried under vacuum affording a white powder (0,26g, 87% yield).

¹H-NMR (DMSO-d₆, 300 MHz, 25°C): δ(ppm) = 1,31 (s, 12H, *p*-CH₃); 1,98 (s, 24H, *o*-CH₃); 3,98 (s, 8H, Ar-CH₂-Ar); 7,15 (m, 8H, Ar-*H*); 8,01 (m, 8H, Ar-*H*); 12,95 (s, 4H, R-COO-*H*). ¹³C-NMR (DMSO-d₆, 125 MHz, 25 °C) : δ(ppm) = 17.63, 19.13, 26.42, 32.56, 129.06, 129.53, 129.65, 129.83, 129.94, 130.23, 134.64, 137.38, 139.35, 148.32, 167.37;

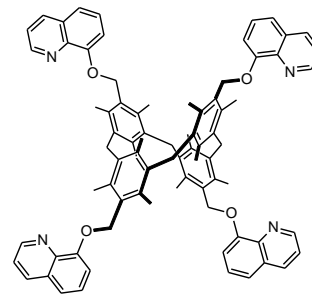
Mp: degradation above 318-350°C;

HRMS (ESI): m/z calcd. for [M]⁺: 1008.50, calcd for [M+ Na]⁺ 1031.40, found 1031.455.

EA for C₆₈H₆₄O₈: C, 80.93 %; H, 6.39%; found C, 80.98 %; H, 6.33 %.



**4,11,18,25-Tetra-8-quinolinomethyl-3,5,7,10,12,14,17,19,
21,24,26,28-dodecamethyl[1.1.1]metacyclophane (L6)**



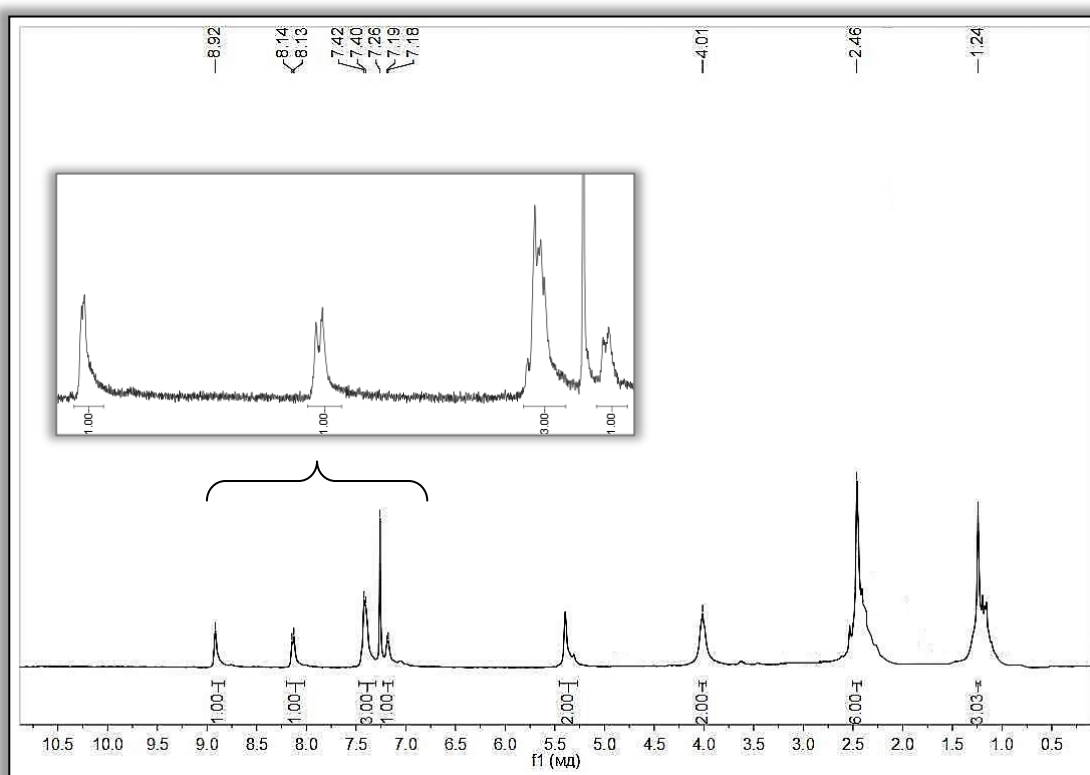
1 (0.5 g, 0.69 mmol) and 8-hydroxyquinoline (0.8 g, 6.9 mmol) were dissolved in 50 ml of DMF. The mixture was refluxed during 48 hours. After cooling and evaporating under vacuum, the residue was washed by 100 ml of CHCl₃:H₂O (1:1), organic layer was dried under MgSO₄, filtrated and evaporated under vacuum. MeOH was added to the residue and filtered precipitation was purified using the chromatography (SiO₂, CH₂Cl₂/Cyclohexane = 1/2) leading to the pure slightly brown product **L6** with 44% yield.

¹H-NMR (CDCl₃, 400 MHz, 25 °C): δ(ppm) = 1.24 (s, 12H, *p*-CH₃), 2.46 (s, 24H, *o*-CH₃), 5.39 (s, 8H, -CH₂-O-quinoline-), 4.01 (s, 8H, Ar-CH₂-Ar); 8.92-7.18 (s,d,m, 12H, H-quinoline).

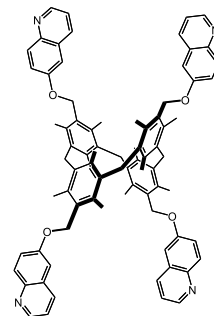
Mp: 208-220 °C, MALDI TOF: m/z = 1157.03 [M⁺] (calculated 1157.48).

Mp: 210 °C, MALDI TOF: m/z = 1157.11 [M⁺] (calculated 1157.48).

EA for C₈₀H₇₆N₄O₄: C, 83.01%; N, 4.84 %; H, 6.62 %; found C, 82.96 %; N, 4.90 %; H, 6.59 %.



**4,11,18,25-Tetra-6-quinolinomethyl-3,5,7,10,12,14,17,19,
21,24,26,28-dodecamethyl[1.1.1]metacyclophane (L7)**



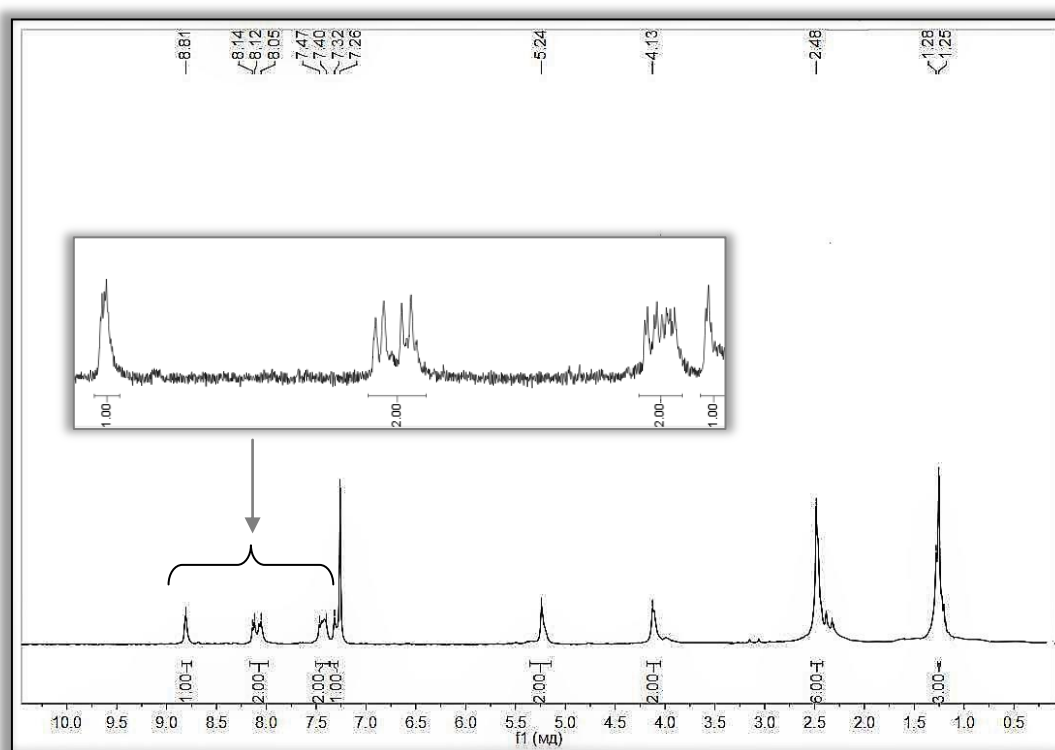
1 (0.5 g, 0.69 mmol) and 6-hydroxyquinoline (0.8 g, 6.9 mmol) were dissolved in 50 ml of DMF. The mixture was refluxed during 48 hours. After cooling and evaporating under vacuum, the residue was washed by 100 ml of CHCl₃:H₂O (1:1), organic layer was dried under MgSO₄, filtrated and evaporated under vacuum. MeOH was added to the residue and filtered precipitation was purified using the chromatography (SiO₂, CH₂Cl₂/Cyclohexane = 1/2) leading to the pure slightly brown product **L7** with 47% yield.

¹H-NMR (CDCl₃, 400 MHz, 25 °C): δ(ppm) = 1.25 (s, 12H, *p*-CH₃), 2.48 (s, 24H, *o*-CH₃), 5.24 (s, 8H, -CH₂-O-quinoline-), 4.13 (s, 8H, Ar-CH₂-Ar); 7.32-8.81 (s,d,m, 12H, H-quinoline)

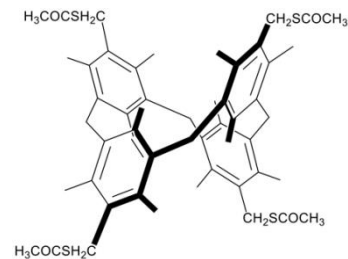
¹³C-NMR (CDCl₃, 125 MHz, 25 °C) δ: 17.20, 18.90, 29.73, 33.14, 66.68, 106.25, 121.49, 122.63, 129.24, 130.49, 130.97, 133.99, 134.86, 138.16, 144.54, 148.10, 157.32.

Mp: 212 °C, MALDI TOF: m/z = 1157. 11 [M⁺] (calculated 1157.48).

EA for C₈₀H₇₆N₄O₄: C, 83.01%; N, 4.84 %; H, 6.62 %; found C, 82.98 %; N, 4.88 %; H, 6.60 %.

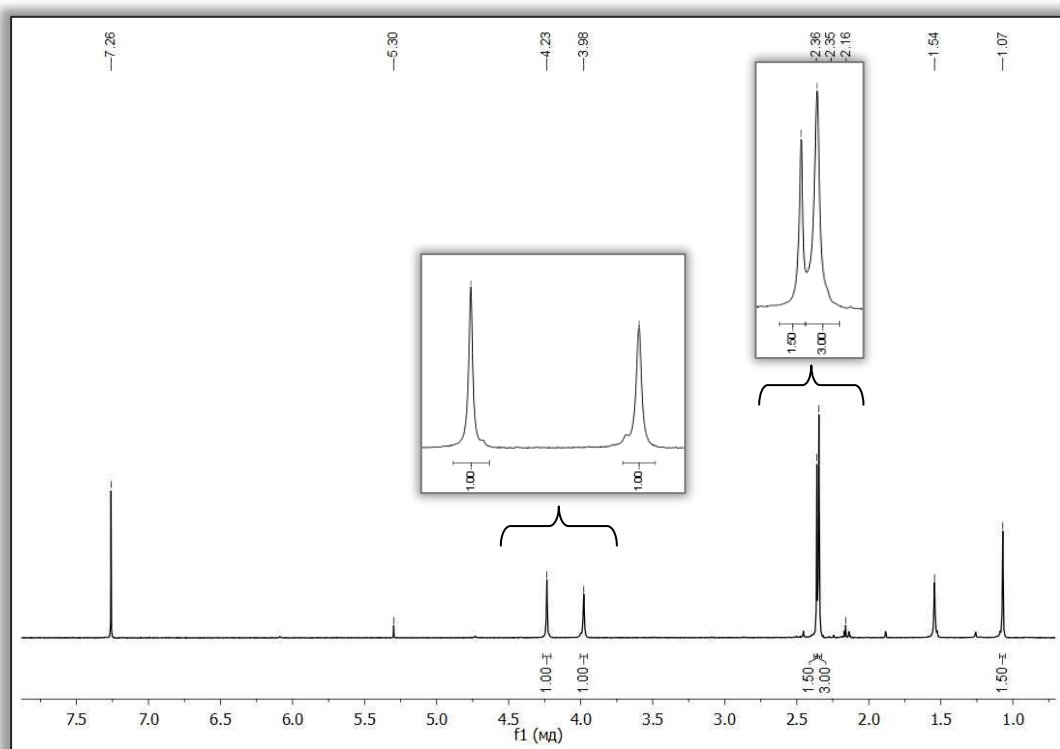


**4,11,18,25-Tetrathioacetylmethyl-3,5,7,10,12,14,17,19,
21,24,26,28-dodecamethyl[1.1.1]metacyclophane (L8')**

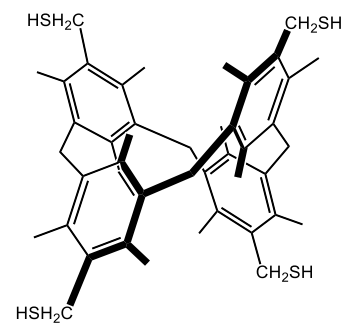


2 g (2,27 mmol) of **1** was suspended in a acetone (50 mL). 0.79 g of potassium thioacetate (27,6 mmol) was added. The reaction mixture was refluxed during 60 hours. After cooling to room temperature, the solvent was evaporated under reduced temperature and the residue was washed by CH₂Cl₂/H₂O (1:1, 100 ml). After organic layer drying under MgSO₄, the solvent was evaporated to dryness. After addition of 30 ml of MeOH to the residue and filtration, the pure compound **L8'** was obtained as a white powder (0.96 g, yield 60%).

¹H-NMR (CDCl₃, 400 MHz, 25 °C): δ(ppm) = 1.07 (s, 12H, *p*-CH₃), 2.35 (s, 24H, *o*-CH₃), 2.36 (s, 12H, -SCO-CH₃), 3.98 (s, 8H, Ar-CH₂-Ar); 4.23 (s, 8H, Ar-CH₂-S-).



**4,11,18,25-Tetramercaptomethyl-3,5,7,10,12,14,17,19,
21,24,26,28-dodecamethyl [1.1.1]metacyclophane (L8)**



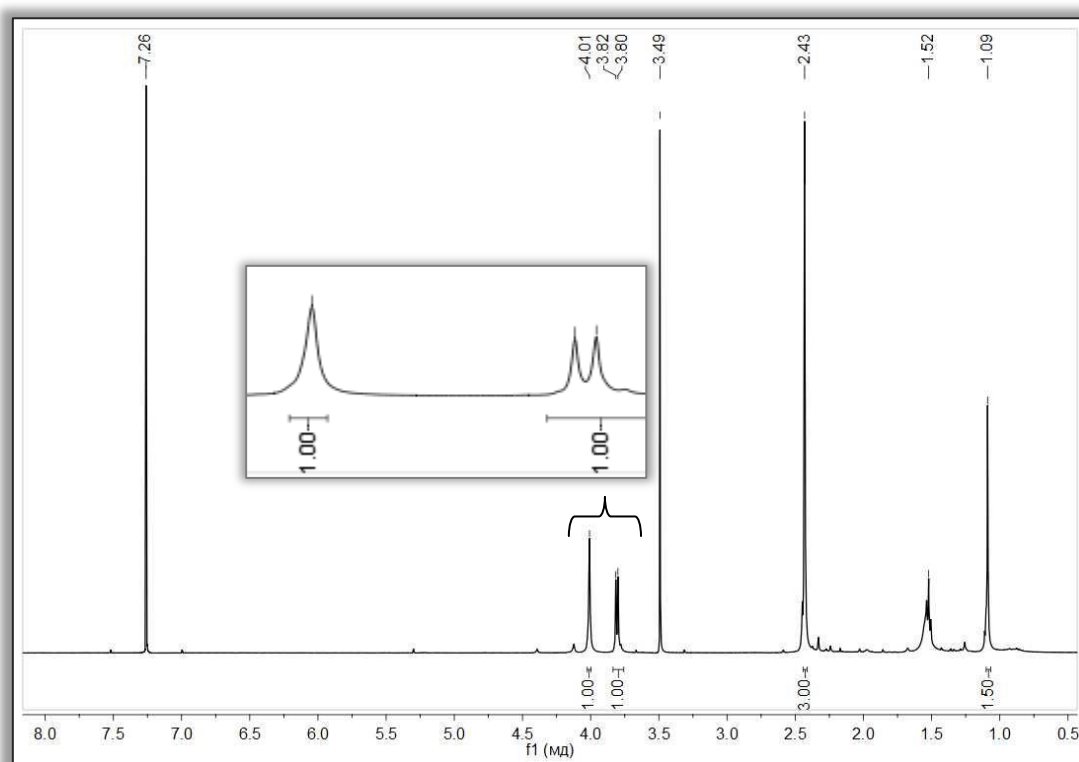
L8' (1.5 g, 1.7 mmol) was dissolved in 50 ml of degassed THF, then NH_2NH_2 (20 ml) was carefully added. The mixture was refluxed during 70 h, after cooling, HCl (12 M) was added dropwise to pH=7, then the solvent was evaporated and extraction ($\text{CHCl}_3/\text{H}_2\text{O}$) was provided. The organic layer was dried under MgSO_4 and the solvent was evaporated under vacuum. Adding MeOH to dry residue and filtration led to **L8** with 58% yield.

$^1\text{H-NMR}$ (CDCl_3 , 400 MHz, 25 °C): δ (ppm) = 1.09 (s, 12H, *p*- CH_3), 2.43 (s, 24H, *o*- CH_3), 3.8 (d, 8H, $-\text{CH}_2\text{-SH}$), 4.01 (s, 8H, Ar- CH_2 -Ar);

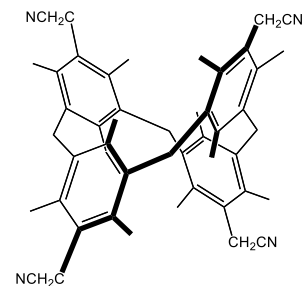
$^{13}\text{C-NMR}$ (CDCl_3 , 125 MHz, 25 °C) δ : 17.04, 18.59, 25.4, 31.08, 33.3, 131.56, 134.81, 138.15.

Mp: 234 °C, MALDI TOF: $m/z = 712.372$ [M^+] (calculated 713.175).

EA for $\text{C}_{44}\text{H}_{56}\text{S}_4$, %, found: C, 75.08 %; H, 8.33 %; calc. : C, 74.10 %; H, 7.92 %.



**4,11,18,25-Tetracyanomethyl-3,5,7,10,12,14,17,19,21,
24,26,28-dodecamethyl[1.1.1]metacyclophane (L9)**



1g (1,38 mmol) of **1** was suspended in a DMF/acetone 3:1 mixture (40 mL). 0.72 g of KCN (720 mg, 11,06 mmol) was added. The reaction mixture was stirred 30 hours under reflux. After cooling to room temperature, the solvent was evaporated under reduced temperature and the residue was treated with 50 ml of CH₂Cl₂. After filtration, the organic solvent was evaporated to dryness. After addition of 50 ml of MeOH to the residue and filtration, **L9** was obtained as a white powder (0.77g, yield 81%).

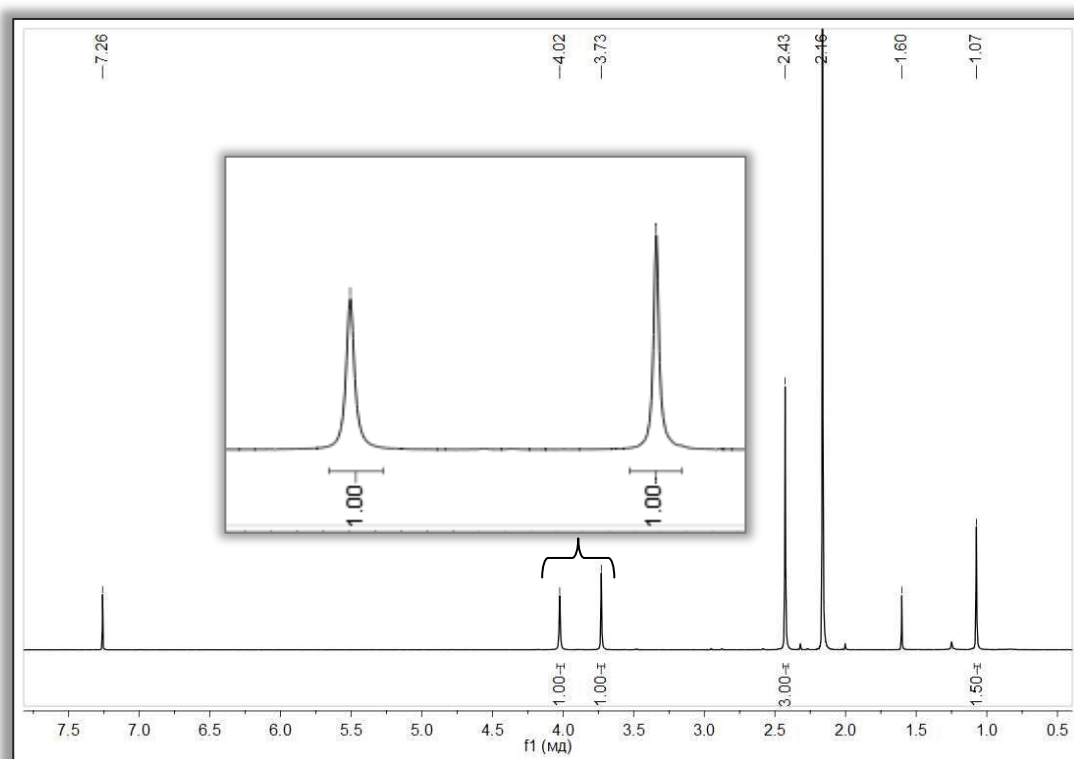
¹H-NMR (CDCl₃, 400 MHz, 25 °C): δ(ppm) = 1.07 (s, 12H, *p*-CH₃), 2.43 (s, 24H, *o*-CH₃), 3.73 (s, 8H, -CH₂-CN), 4.02 (s, 8H, Ar-CH₂-Ar);

¹³C-NMR (CDCl₃, 125 MHz, 25 °C) δ: 17.8, 18.9, 20.1, 33.3, 118.3, 126.1, 132.4, 135.8, 138.2.

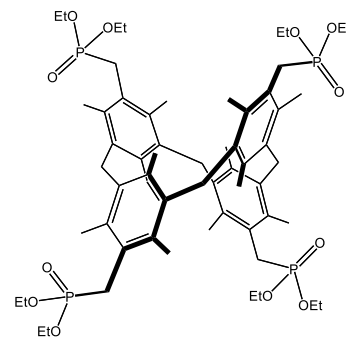
IR, ν (C≡N) = 2246 cm⁻¹. Mp: 246 °C,

MALDI TOF: m/z = 684.24 [M⁺] (calculated 684.96).

EA for C₄₈H₅₂N₄, %, found: C, 84.02; H, 7.62; N, 8.15; calc.: C, 84.17; H, 7.65; N, 8.18; %.



**4,11,18,25-Tetraphosphonomethyl-3,5,7,10,12,14,17,19,
21,24,26,28-dodecamethyl[1.1.1]metacyclophane (L10')**

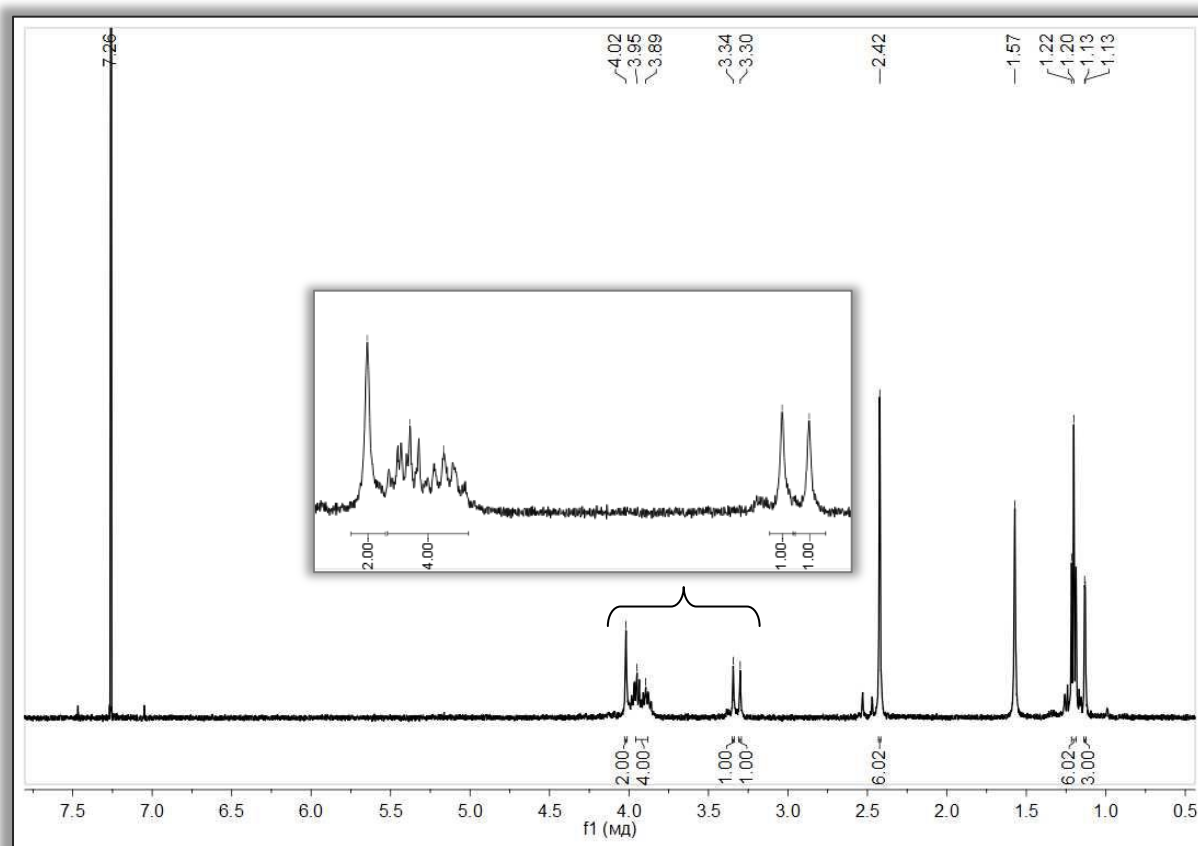


0.15 g (0,21 mmol) of **1** and 0.125g of ZnCl₂ (0.931 mmol) were suspended in (EtO)₃P (0.71 ml, 4.2 mmol) under Ar. After stirring at room temperature during 2 hours, the reaction mixture was heated to 70°C and stirred during 17 hours. After, the ice from distillate water (6g) and concentrated HCl (0.5 ml) were added. After stirring during 1 hour and filtration, the residue was washed by CHCl₃/H₂O, dried under MgSO₄, filtrated and evaporated under vacuum. **L10'** was obtained as a white powder (yield: 0.1 g, 42%)

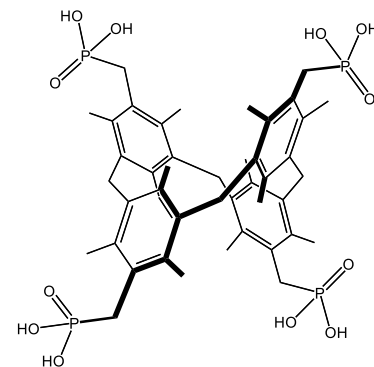
¹H-NMR (CDCl₃, 400 MHz, 25 °C): δ(ppm) = 1.12 (s, 12H, *p*-CH₃), 1.20 (t, 24H, -PO-CH₂-CH₃), 2.42 (s, 24H, *o*-CH₃), 3.30-3.34 (d, 16H, Ar-CH₂-P-), 3.89-3.95 (m, 16H, -PO-CH₂-CH₃), 4.02 (s, 8H, Ar-CH₂-Ar).

³¹P-NMR (CDCl₃, 600 MHz, 25 °C): 27.45

EA for C₆₀H₉₂O₁₂P₄: C, 63.82 %; H, 8.21 %; found C, 63.96 %; H, 8.13 %.



4,11,18,25-Tetraphosphonomethyl-3,5,7,10,12,14,17,19,21,24,26,28-dodecamethyl[1.1.1]metacyclophane (L10)



L10' (0,3 g, 0,27 mmol) was dissolved in the mixture of solvents THF:EtOH 1:1 (20 ml), then NaOH (0,4 g, 10.8 mmol) dissolved in 2,5 ml H₂O was added. Suspension was refluxed during 70 h. After cooling, concentrated HCl was added dropwise (5 ml), the mixture was stirred during 1 hour, after, the solvents were evaporated to the half of volume and distillate water was added (50 ml). The precipitation was filtered and **L10** was obtained with 68% yield.

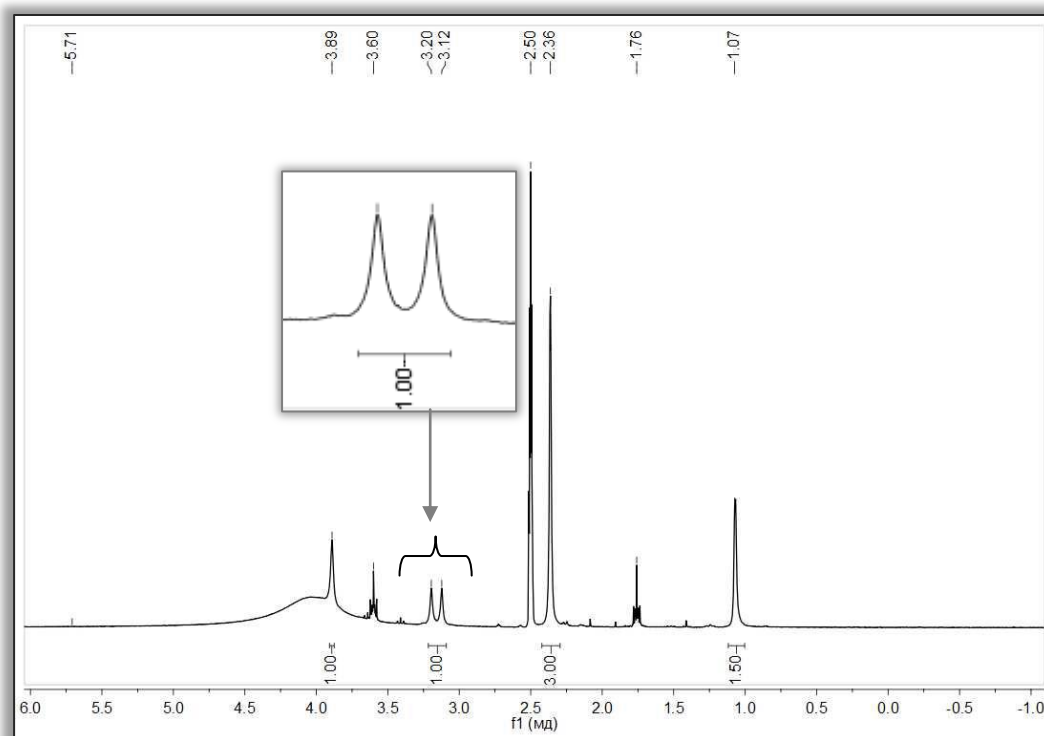
¹H-NMR (CDCl₃, 400 MHz, 25 °C): δ(ppm) = 1.08 (s, 12H, *p*-CH₃), 2.36 (s, 24H, *o*-CH₃), 3.19 (d, 8H, -CH₂-P-), 3.89 (s, 8H, Ar-CH₂-Ar);

³¹P-NMR (CDCl₃, 600 MHz, 25 °C): 28.34

Unfortunately, due to the low solubility in organic solvents, it was impossible to perform ¹³C NMR spectroscopy.

Mp: 228 °C, MALDI TOF: m/z = 904.45 [M⁺] (calculated 904.83).

EA for C₄₄H₆₀O₁₂P₄: C, 58.41 %; H, 6.68 %; found C, 59.01 %; H, 6.17 %;



Crystallisation methods of synthesized ligands and networks

1) *Slow diffusion (liquid/liquid) -binary solvent system in glass sealed tube*

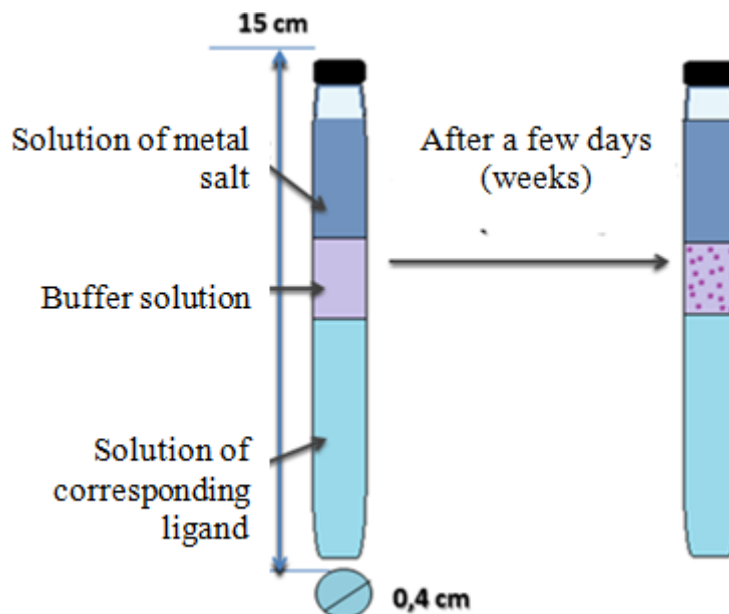


Figure 68. Schematic representation of binary solvent system for slow liquid diffusion

The liquid/liquid diffusion method is a slow diffusion of one solvent into another. A solvent in which the ligand is soluble forms the bottom layer. A solvent, in which the ligand is low soluble (insoluble), forms the top layer. The buffer is the layer between the bottom and top layers which is needed to slow the mixing of the layers.

Solvent 2 gradually diffuses into solvent 1 through the buffer, that could lead to formation of the crystals at the liquid/liquid interface.

Description of the method (all solutions are added by the syringe):

- 1) Solution 1: The ligand is dissolved in the appropriate solvent (solvent 1),
- 2) Solution 2: The metal salt is dissolved in the equal amount of solvent 2
- 3) The buffer: the mixture of solvent 1 and solvent 2 (equal volumes)

4) Solution 1 is carefully added into the glass sealed tube, the buffer solution is carefully added over the top with a syringe, and finally the solution 2 is added on the top of the buffer layer preventing the early mixing of the layers (Figure 67).

2) *Vapour diffusion*

The vapour diffusion method is a slow diffusion of a vapour of one volatile solvent into another, containing the mixture of metal salt and the ligand. A solvent in which the ligand and metal salt are soluble is placed into the small vial for crystallisation. A cap is put on the vial containing the volatile solvent at the bottom (Figure 69).

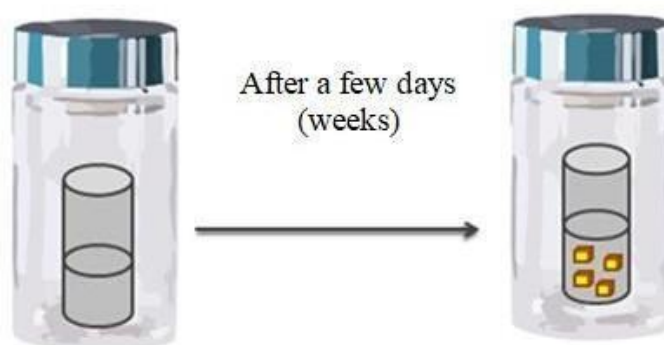


Figure 69. Schematic representation of the system for vapour diffusion

3) *Slow evaporation*

The ligand is dissolved in a suitable solvent and added into a glass flask with a large surface for evaporation and to slow down the process, the flask is covered with a piece of parafilm with the holes into it. The evaporation could occur at room temperature as well as inside the refrigerator at low temperatures (Figure 70).

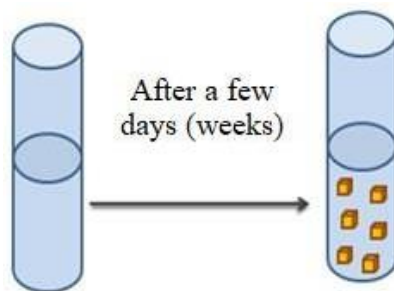


Figure 70. Scheme of slow evaporation process.

4)

Solvothermal synthesis

It is a method for growing single crystals from a solution at high temperature and pressure.

A solution containing the ligand and a metal salt is placed in glass vials resistant to temperature, sealed with an appropriated cap and then subjected to heating under 80-120°C (Figure 71).

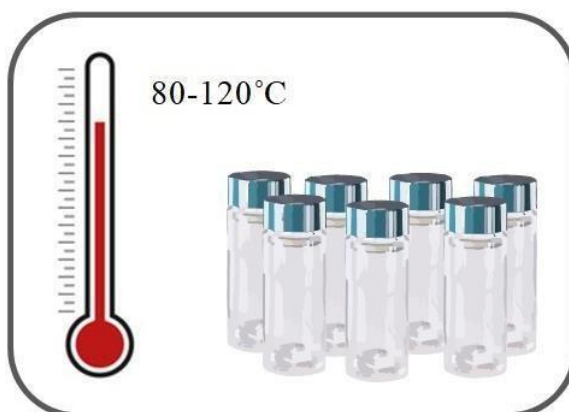
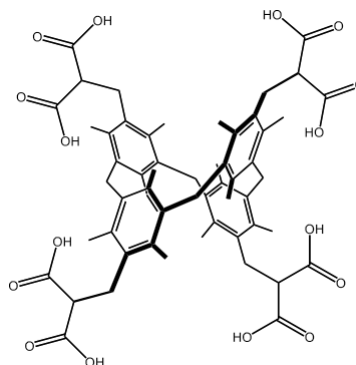
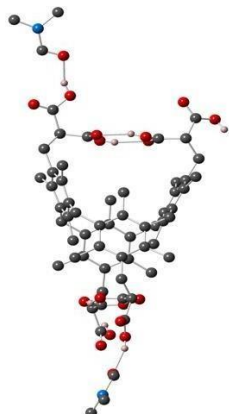


Figure 71. Schematic representation of solvothermal synthesis as one of the crystallization methods.

Crystal data
for synthesized ligands

**4,11,18,25-tetra((malonate)-methylene)-3,5,7,10,12,14,17,
19,21,24,26,28- dodecamethyl- [1.1.1]metacyclophane (L2)**



A vial containing **L2** (5 mg, $5,03 \times 10^{-3}$ mmol) in DMF (1.0 mL) was placed in a closed beaker containing Et₂O. Slow vapour diffusion of Et₂O into the DMF solution produced, and after one week, colourless crystals suitable for X-ray diffraction appeared.

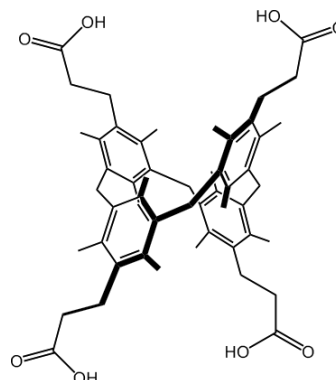
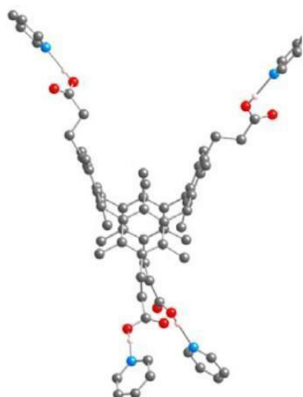
Formula: {C₅₆H₆₆O₁₆•C₃H₇NO}

EA for C₅₉H₇₃O₁₇N: C, 66.34 %; N, 1.31 %; H, 6.89 %; found: C, 66.36 %; N, 1.28 %; H, 6.91 %.

Crystallographic data:

Empirical formula	{C ₅₆ H ₆₆ O ₁₆ •C ₃ H ₇ NO}
Formula weight	1068.21
Temperature	173(2) K
Wavelength	0.71073
Crystal system	Monoclinic
Space group	C 2/c
Unit cell dimensions	a (Å) 39.029(9) α = 90° b (Å) 11.5405(18) β = 107.926(6)° c (Å) 15.809(3) γ = 90°.
Volume	6775.(2) Å ³
Z	4
Density (calculated)	1.061 Mg/m ³
Absorption coefficient	0.078 mm ⁻¹
F(000)	2308
Crystal size	0.05 x 0.06 x 0.07 mm ³
Theta range for data collection	1.85 to 30.09°
Index ranges	-54 ≤ h ≤ 19, -13 ≤ k ≤ 12, -16 ≤ l ≤ 22
Reflections collected	19558
Data / restraints / parameters	8828 / 6 / 358
Goodness-of-fit on F ²	1.103
Final R indices [I > 2σ(I)]	R1 = 0.1041, wR2 = 0.3346
R indices (all data)	R1 = 0.1701, wR2 = 0.4048
Largest diff. peak and hole	1.077 and 0.454 e.Å ⁻³

4,11,18,25-tetra((malonate)-methylene)-3,5,7,10,12,14,17,19,21,24,26,28-dodecamethyl-[1.1.1]metacyclophane (L3)



A vial containing **L3** (5 mg, 6.12×10^{-3} mmol) in pyridine (1 mL) was heated at 120°C under solvothermal conditions. After cooling, slow vapour diffusion of Et₂O into the pyridine solution produced, after one month, colourless crystals suitable for X-ray diffraction.

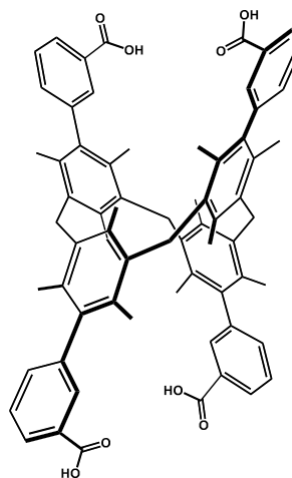
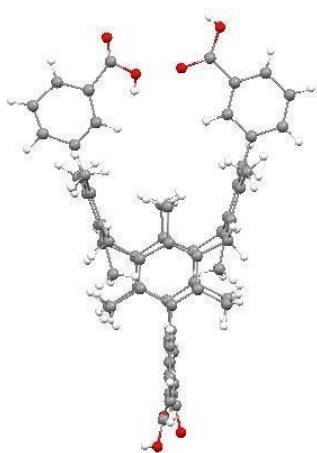
Formula: {C₅₂H₆₄O₈•4(C₅H₅N)}

EA for C₇₂H₈₄O₈N₄: C, 76.3 %; N, 4.94 %; H, 7.47 %; found: C, 76.47 %; N, 4.89 %; H, 7.42 %.

Crystallographic data:

Empirical formula	{C ₅₂ H ₆₄ O ₈ •4(C ₅ H ₅ N)}	
Formula weight	1133.43	
Temperature	173 K	
Wavelength	0.71073	
Crystal system	Monoclinic	
Space group	P 2 ₁ /c	
Unit cell dimensions	a (Å) 17.1048(8)	α = 90°
	b (Å) 24.1178(10)	β = 08.601(2)
	c (Å) 15.6604(8)	γ = 90°
Volume	6122.9(5)	
Z	4	
Density (calculated)	1.230 Mg/m ³	
Absorption coefficient	0.080 mm ⁻¹	
F(000)	2432	
Crystal size	0.07 x 0.08 x 0.1mm ³	
Theta range for data collection	2.28 to 30.14°	
Index ranges	-24 ≤ h ≤ 23, -33 ≤ k ≤ 30, -22 ≤ l ≤ 22	
Reflections collected	54101	
Data / restraints / parameters	17713 / 1 / 771	
Goodness-of-fit on F ²	1.010	
Final R indices	R1 = 0.0703 wR2 = 0.1608	
[I > 2σ(I)]		
R indices (all data)	R1 = 0.1458, wR2 = 0.1987	
Largest diff. peak and hole	0.398 and 0.281 e.Å ⁻³	

**4,11,18,25-tetra (3-(carboxyl)phenyl)-3,5,7,10,12,14,17,19,
21,24,26,28 -dodecamethyl-[1.1.1]Metacyclophane (L4)**



The buffer solution (DMF/MeOH = 1/1, 0.5 mL) was added by syringe into a tube containing **L4** (5 mg, 4.9×10^{-3} mmol) dissolved in DMF (1.0 mL), then a layer of MeOH (1 mL) was carefully added to the top of this solution. The liquid/liquid diffusion produced, after a couple of weeks, colourless crystals suitable for X-ray diffraction.

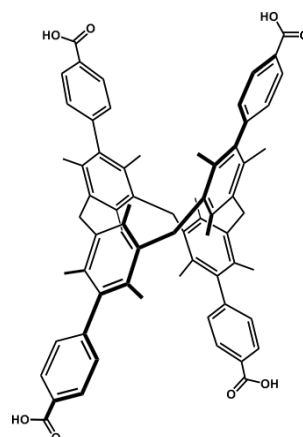
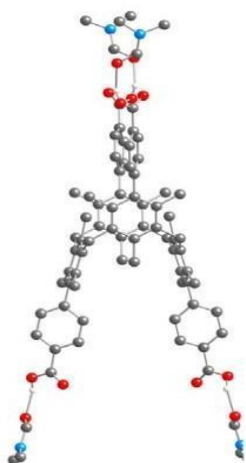
Formula: $\{C_{68}H_{63}O_8 \cdot S\}$

EA for $C_{68}H_{64}O_8$: C, 80.93 %; H, 6.39 %; found: C, 81.06 %; H, 6.61 %.

Crystallographic data:

Empirical formula	$\{C_{68}H_{63}O_8 \cdot S\}$
Formula weight	1008.18 g/mol
Temperature	173 K
Wavelength	0.71073
Crystal system	triclinic
Space group	P 1
Unit cell dimensions	a (Å) 12.417(3) $\alpha = 112.574(6)^\circ$ b (Å) 16.639(3) $\beta = 93.655(4)^\circ$ c (Å) 19.409(5) $\gamma = 111.160(6)^\circ$
Volume	3356.4(13)
Z	2
Density (calculated)	0.998 Mg/m ³
Absorption coefficient	0.996 mm ⁻¹
F(000)	1070
Crystal size	0.070 x 0.060 x 0.070 mm ³
Theta range for data collection	2.169 to 27.528°
Index ranges	-16 ≤ h ≤ 15, -14 ≤ k ≤ 21, -25 ≤ l ≤ 25
Reflections collected	18653
Goodness-of-fit on F ²	1.738
Final R indices	R1 = 0.4697, wR2 = 0.2987
[I > 2σ(I)]	
R indices (all data)	R1 = 0.6788, wR2 = 0.6260
	181

**4,11,18,25-tetra(4-(carboxyl)phenyl)-3,5,7,10,12,14,17,19,
21, 24,26,28-dodecamethyl-[1.1.1]Metacyclophane (L5)**



7 mL of DMF was added to **L5** (5 mg, 4.9×10^{-3} mmol), and upon slow evaporation at room temperature, after two weeks, colourless crystals suitable for X -ray diffraction appeared.

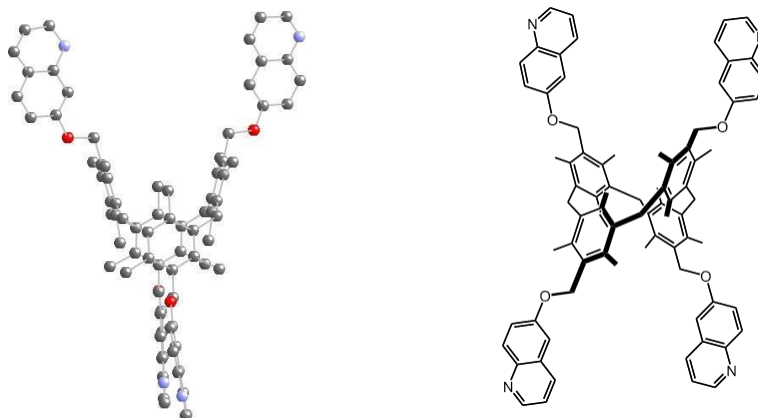
Formula: $\{C_{68}H_{64}O_8 \bullet 4(C_3H_7NO)\}$

EA for $C_{80}H_{92}O_{12}N_4$: C, 73.82 %; N, 4.3 %; H, 7.12 %; found: C, 73.86 %; N, 4.26 %; H, 7.13 %.

Crystallographic data:

Empirical formula	$\{C_{68}H_{64}O_8 \bullet 4(C_3H_7NO)\}$	
Formula weight	1301.57	
Temperature	173 K	
Wavelength	0.71073	
Crystal system	Tetragonal	
Space group	$P 4_2/n$	
Unit cell dimensions	a (Å) 16.1996(7)	$\alpha = 90^\circ$
	b (Å) 16.1996(7)	$\beta = 90^\circ$
	c (Å) 13.7042(8)	$\gamma = 90^\circ$
Volume	3596.4(4)	
Z	2	
Density (calculated)	1.202 Mg/m ³	
Absorption coefficient	0.080 mm ⁻¹	
F(000)	1392	
Crystal size	0.07 x 0.07 x 0.09 mm ³	
Theta range for data	1.95 to 30.00°	
Index ranges	-22 ≤ h ≤ 22, -22 ≤ k ≤ 22, -19 ≤ l ≤ 17	
Reflections collected	30277	
Data / restraints /	4739 / 0 / 223	
Goodness-of-fit on F ²	1.019	
Final R indices	R1 = 0.0747, wR2 = 0.2358	
[I > 2σ(I)]		
R indices (all data)	R1 = 0.1030, wR2 = 0.2579	
Largest diff. peak and hole	0.924 and 0.319 e.Å ⁻³	

4,11,18,25-Tetra-6-quinolinomethyl-3,5,7,10,12,14,17,19,21,24,26,28-dodecamethyl[1.1.1]metacyclophane (L7)



The buffer solution (DMF/MeOH = 1/1, 0.5 mL) was added by syringe into a tube containing **L7** (5 mg, 4.3×10^{-3} mmol) dissolved in CHCl_3 (1.0 mL), then a layer of MeOH (1 mL) was carefully added to the top of this solution. The liquid/liquid diffusion produced, after a couple of days, colourless crystals suitable for X-ray diffraction.

Formula: $\{\text{C}_{80}\text{H}_{76}\text{N}_4\text{O}_4 \bullet 6(\text{H}_2\text{O})\}$

EA for $\text{C}_{80}\text{H}_{88}\text{O}_{10}\text{N}_4$: C, 75.92 %; H, 7.01 %; N, 4.43%; found: C, 75.94 %; H, 7.03 %, N, 4.38 %.

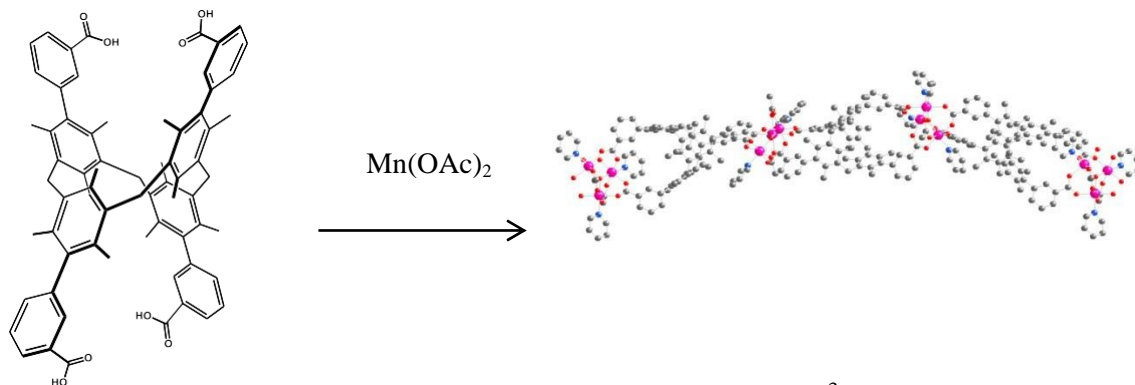
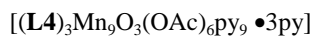
Crystallographic data:

Empirical formula	$\{\text{C}_{80}\text{H}_{76}\text{N}_4\text{O}_4 \bullet 6(\text{H}_2\text{O})\}$	
Formula weight	1265.54 g/mol	
Temperature	173 K	
Wavelength	0.71073	
Crystal system	Tetragonal	
Space group	$I4_1cd$	
Unit cell dimensions	a (Å) 18.1751(11)	$\alpha = 90^\circ$
	b (Å) 18.1751(11)	$\beta = 90^\circ$
	c (Å) 46.792(4) Å	$\gamma = 90^\circ$
Volume	15457.(2)	
Z	8	
Density (calculated)	1.088 Mg/m ³	
Absorption coefficient	0.071 mm ⁻¹	
F(000)	5408	
Crystal size	0.060 x 0.070 x 0.070 mm ³	
Theta range for data collection	1.74 to 30.12°	
Index ranges	-25 ≤ h ≤ 25, -25 ≤ k ≤ 24, -65 ≤ l ≤ 61	
Reflections collected	61541	
Data / restraints / parameters	11276 / 2 / 440	

Goodness-of-fit on F^2	1.102
Final R indices [$I > 2\sigma(I)$]	R1 = 0.1149, wR2 = 0.2988
R indices (all data)	R1 = 0.2077, wR2 = 0.3616
Largest diff. peak and hole	1.143 and -0.467 eÅ ⁻³

**Crystal data for coordination
polymers based on the synthesized
ligands**

4,11,18,25-tetra (3-(carboxyl)phenyl)-3,5,7,10,12,14,17,19, 21,24,26,28 - dodecamethyl- [1.1.1.1]Metacyclophane (L4**) with manganese acetate (1D network)**



In a vial ($V = 4\text{mL}$), a solution of **L4** (5 mg , $4.96 \times 10^{-3}\text{ mmol}$) in pyridine (1.5 mL) was mixed with a solution of $\text{Mn}(\text{NO}_3)_2$ (3.6 mg , $1.98 \times 10^{-3}\text{ mmol}$) also in pyridine (1.5 mL). The mixture was heated at 120°C under solvothermal conditions, and after several days, crystals suitable for X-ray diffraction studies were obtained.

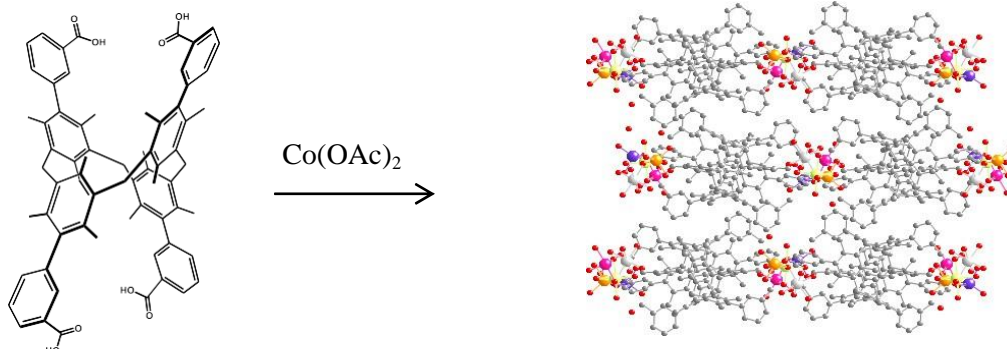
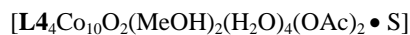
Formula: $\{(\text{C}_{68}\text{H}_{64}\text{O}_8)_3\text{Mn}_9\text{O}_3(\text{CH}_3\text{COO})_6(\text{C}_5\text{H}_5\text{N})_{12}\}$ i.e. $(\mathbf{L4})_3\text{Mn}_9\text{O}_3(\text{OAc})_6\text{py}_9 \bullet 3\text{py}$.

EA for $\text{C}_{276}\text{H}_{270}\text{N}_{72}\text{O}_{39}$: C, 58.00 %; H, 4.77 %; N, 17.66 %; found: C, 58.05 %; H, 4.79 %; N, 17.59 %.

Crystallographic data:

Chemical formula	$\{(\text{C}_{68}\text{H}_{64}\text{O}_8)_3\text{Mn}_9\text{O}_3(\text{CH}_3\text{COO})_6(\text{C}_5\text{H}_5\text{N})_{12}\}$	
Formula weight	4867.44 g/mol	
Temperature	173(2) K	
Wavelength	0.71073 Å	
Crystal system	trigonal	
Space group	R 3 2	
Unit cell dimensions	$a = 20.7486(9)\text{ Å}$	$\alpha = 90^\circ$
	$b = 20.7486(9)\text{ Å}$	$\beta = 120^\circ$
	$c = 55.517(6)\text{ Å}$	$\gamma = 90^\circ$
Volume	$20698.(3)\text{ Å}^3$	
Z	3	
Density (calculated)	1.170 g/cm^3	
Absorption coefficient	0.464 mm^{-1}	
F(000)	7623	
Crystal size	$0.090 \times 0.100 \times 0.120\text{ mm}^3$	
Theta range for data collection	1.85 to 30.14°	
Index ranges	$-28 \leq h \leq 18$, $-27 \leq k \leq 29$, $-78 \leq l \leq 77$	
Reflections collected	67629	
Data / restraints / parameters	13530 / 8 / 494	
Goodness-of-fit on F^2	1.098	
Final R indices	$R1 = 0.1058$, $wR2 = 0.2708$	
$[I > 2\sigma(I)]$		
R indices (all data)	$R1 = 0.2063$, $wR2 = 0.3400$	
Largest diff. peak and hole	0.906 and -1.695 eÅ^{-3}	

4,11,18,25-tetra(4-(carboxyl)phenyl)-3,5,7,10,12,14,17,19,21,24,26,28-dodecamethyl-[1.1.1.1]Metacyclophane (L4) with cobalt acetate (2D network)



In a vial (V= 4mL), a solution of **L4** (5 mg, 4.96×10^{-3} mmol) in DMF (1.5 mL) was mixed with a solution of Co(OAc)₂ (3.6 mg, 1.98×10^{-3} mmol) also in DMF (1.5 mL). The mixture was heated at 120°C under solvothermal conditions, and after several days, there was provided vapour diffusion with MeOH. After one week, crystals suitable for X- ray diffraction studies were obtained.

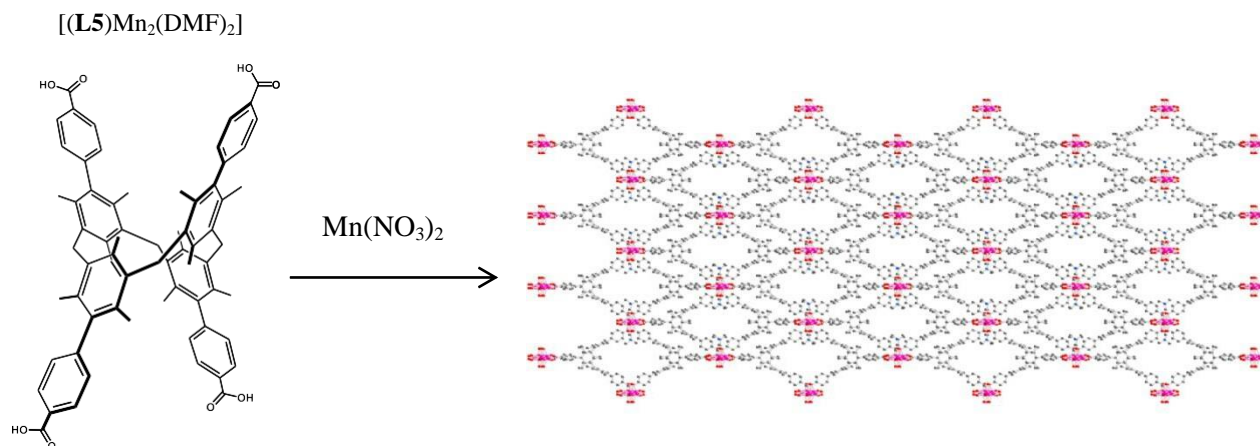
Formula: $\{(C_{68}H_{64}O_8)_4Co_{10}O_4(CH_3OH)_2(H_2O)_4(CH_3COO)_2 \bullet (C_3H_7NO)(H_2O)_7 \bullet S\}$ *i.e* $\{L_4Co_{10}O_2(MeOH)_2(H_2O)_4(OAc)_2 \bullet S\}$

EA for C₂₈₁H₂₇₉Co₁₀NO₅₄: C, 65.87%; H, 5.49 %; N, 0.27 %; found: C,65.91%; H, 5.46%; N, 0.26 %.

Crystallographic data:

Chemical formula	$\{(C_{68}H_{64}O_8)_4Co_{10}O_4(CH_3OH)_2(H_2O)_4(CH_3COO)_2 \bullet (C_3H_7NO)(H_2O)_7 \bullet S\}$
Formula weight	5123.33 g/mol
Temperature	293(2) K
Wavelength	0.80246 Å
Crystal system	monoclinic
Space group	P 1 21/c 1
Unit cell dimensions	a = 23.879(5) Å α = 90° b = 36.386(7) Å β = 106.68(3)° c = 23.144(5) Å γ = 90°
Volume	19263.(7) Å ³
Z	2
Density (calculated)	0.883 g/cm ³
Absorption coefficient	0.655 mm ⁻¹
F(000)	5348
Theta range for data collection	3.21 to 31.03°
Index ranges	-30 ≤ h ≤ 30, -46 ≤ k ≤ 43, -29 ≤ l ≤ 29
Reflections collected	202999
Data / restraints / parameters	42340 / 2 / 1602
Goodness-of-fit on F ²	1.025
Final R indices	R1 = 0.1434, wR2 = 0.3472
[I > 2σ(I)]	
R indices (all data)	R1 = 0.2406, wR2 = 0.4092
Largest diff. peak and hole	1.696 and -0.591 eÅ ⁻³
	188

4,11,18,25-tetra(4-(carboxyl)phenyl)-3,5,7,10,12,14,17,19,21,24,26,28-dodecamethyl-[1.1.1.1]Metacyclophane (L5) with manganese nitrate (3D network)

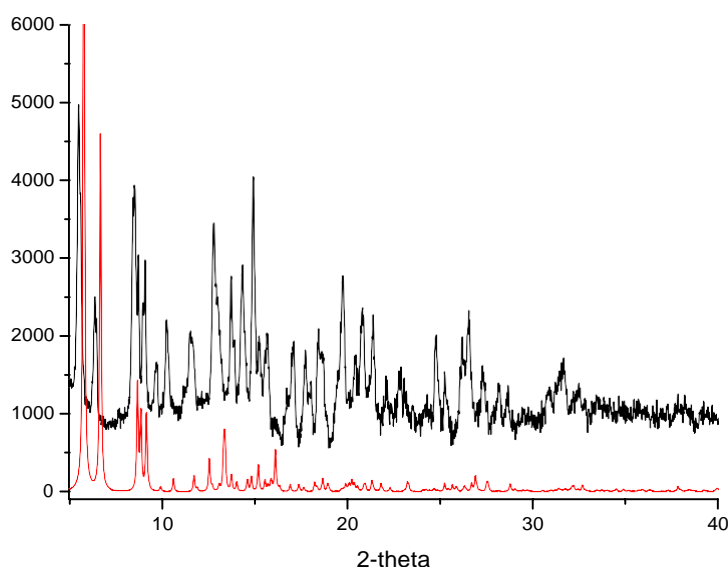


In a vial ($V=4\text{mL}$), a solution of **L5** (5 mg , $4.96 \times 10^{-3}\text{ mmol}$) in DMF (1.5 mL) was mixed with a solution of $Mn(NO_3)_2$ (3.6 mg , $1.98 \times 10^{-3}\text{ mmol}$) also in DMF (1.5 mL). The mixture was heated at 120°C under solvothermal conditions, and after several days there were obtained the crystals suitable for X-ray diffraction studies.

Formula: $\{C_{68}H_{64}O_8\}Mn_2(C_3H_7NO)_2$ *i.e.* $\{(L5)Mn_2(DMF)_2\}$

EA for $C_{37}H_{37}MnNO_5$: C, 70.46 %; H, 5.91 %; N, 2.22 %; found: C, 70.5 %; H, 5.89 %; N, 2.19 %.

XRPD diagram:



Comparison of the simulated (a) and recorded (b) PXRD patterns for **L5- $Mn(NO_3)_2$**

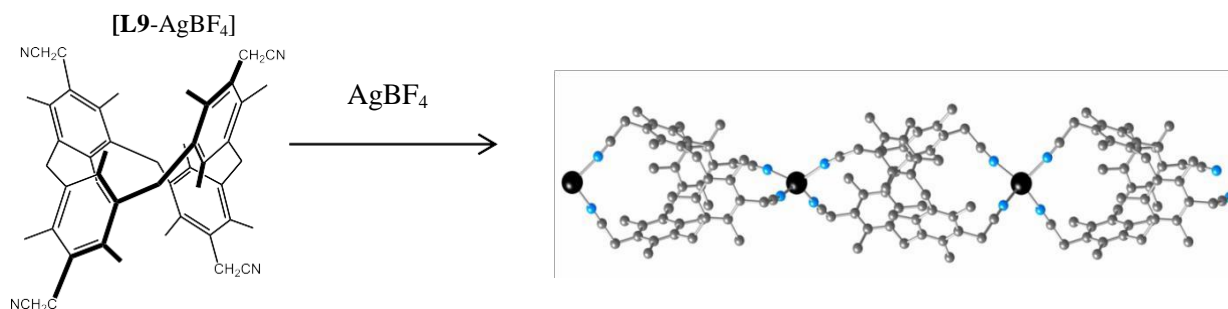
The discrepancy between the simulated pattern using the single crystal data and recorded diagram demonstrates a good match.

a

Crystallographic data:

Chemical formula	{C ₆₈ H ₆₄ O ₈)Mn ₂ (C ₃ H ₇ NO) ₂ }
Formula weight	630.61 g/mol
Temperature	173(2) K
Wavelength	0.71073 Å
Crystal system	monoclinic
Space group	C 1 2/c 1
Unit cell dimensions	a = 20.415(3) Å α = 90° b = 38.697(7) Å β = 125. c = 14.284(2) Å γ = 90°
Volume	9225.(3) Å ³
Z	8
Density (calculated)	0.908 Mg/m ³
Absorption coefficient	0.317 mm ⁻¹
F(000)	2648
Crystal size	0.100 x 0.120 x 0.120 mm ³
Theta range for data collection	2.00 to 27.68°
Index ranges	-26<=h<=26, -50<=k<=50, -18<=l<=18
Reflections collected	58448
Data / restraints / parameters	10515 / 0 / 407
Goodness-of-fit on F ²	1.013
Final R indices	R1 = 0.0794, wR2 = 0.2270
[I>2sigma(I)]	
R indices (all data)	R1 = 0.1396, wR2 = 0.2753
Largest diff. peak and hole	0.929 and -0.837 eÅ ⁻³

4,11,18,25-Tetracyanomethyl-3,5,7,10,12,14,17,19,21,24,26,28-dodecamethyl[1.1.1]metacyclophan (L9) with silver tetrafluoroborate (1D network)



In a crystallization tube (diameter 4 mm, height 15 cm), a solution of **L9** (5 mg, 7.3×10^{-3} mmol) in CHCl_3 (1 mL) was layered with a $\text{CHCl}_3/\text{MeOH}$ (1/1) mixture (1 mL). A solution of AgBF_4 (3.39 mg, 14.6×10^{-3} mmol) in MeOH (1 mL) was carefully added. Upon slow diffusion at room temperature and in the dark, colourless crystals suitable for X-ray diffraction studies were obtained after several days.

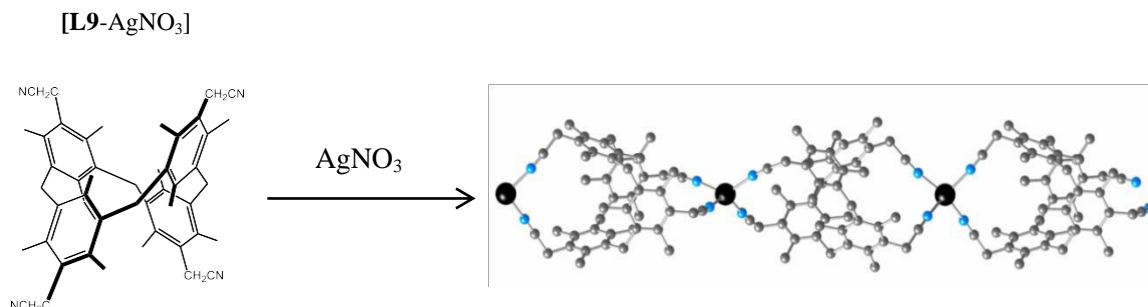
Formula: $\{\text{C}_{144}\text{H}_{156}\text{Ag}_3\text{B}_3\text{F}_{12}\text{N}_{12}\}$ *i.e.* $\{\text{L9-AgBF}_4\}$

EA for $\text{C}_{144}\text{H}_{156}\text{Ag}_3\text{B}_3\text{F}_{12}\text{N}_{12}$: C, 65.54 %; H, 5.96 %; N, 6.37 %; found: C, 65.6 %; H, 5.91 %; N, 6.33 %.

Crystallographic data:

Chemical formula	$\{\text{C}_{144}\text{H}_{156}\text{Ag}_3\text{B}_3\text{F}_{12}\text{N}_{12}\}$	
Formula weight	2638.84 g/mol	
Temperature	173(2) K	
Wavelength	0.71073 Å	
Crystal size	0.050 x 0.050 x 0.060 mm	
Crystal system	cubic	
Space group	$I a - 3 d$	
Unit cell dimensions	$a = 29.4672(11)$ Å	$\alpha = 90^\circ$
	$b = 29.4672(11)$ Å	$\beta = 90^\circ$
	$c = 29.4672(11)$ Å	$\gamma = 90^\circ$
Volume	$25587.(3)$ Å ³	
Z	8	
Density (calculated)	1.370 g/cm ³	
Absorption coefficient	0.529 mm ⁻¹	
F(000)	10944	
Theta range for data collection	1.69 to 30.03°	
Index ranges	$-36 \leq h \leq 21$, $-26 \leq k \leq 27$, $-16 \leq l \leq 41$	
Reflections collected	3125	
Data / restraints / parameters	3125 / 2 / 129	
Goodness-of-fit on F2	1.192	
Final R indices	$R1 = 0.1043$, $wR2 = 0.3306$	
all data	$R1 = 0.1752$, $wR2 = 0.3734$	
Largest diff. peak and hole	1.318 and -0.899 eÅ ⁻³	

4,11,18,25-Tetracyanomethyl-3,5,7,10,12,14,17,19,21,24,26,28-dodecamethyl[1.1.1]metacyclophan (L9) with silver nitrate (1D network)



In a crystallization tube (diameter 4 mm, height 15 cm), a solution of **L9** (5 mg, 7.3×10^{-3} mmol) in CHCl₃ (1 mL) was layered with a CHCl₃/MeOH (1/1) mixture (1 mL). A solution of AgBF₄ (3.39 mg, 14.6×10^{-3} mmol) in MeOH (1 mL) was carefully added. Upon slow diffusion at room temperature and in the dark, colourless crystals suitable for X-ray diffraction studies were obtained after several days.

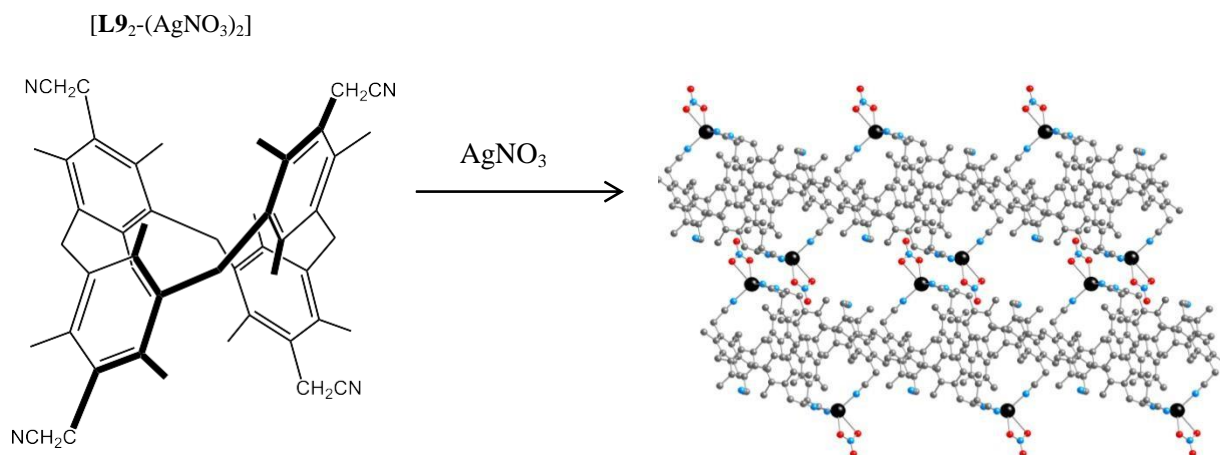
Formula: C₁₄₄H₁₅₆Ag₃B₃F₁₂N₁₂ *i.e.* {**L9**-AgNO₃}

EA for C₁₄₄H₁₅₆Ag₃O₉N₁₅: C, 67.44 %; H, 6.13 %; N, 8.19 %; found: C, 67.5 %; H, 6.11 %; N, 8.16 %;

Crystallographic data:

Chemical formula	{C ₁₄₄ H ₁₅₆ Ag ₃ B ₃ F ₁₂ N ₁₂ }	
Formula weight	2564.44 g/mol g/mol	
Temperature	173(2) K	
Wavelength	0.71073 Å	
Crystal size	0.070 x 0.070 x 0.070 mm	
Crystal system	cubic	
Space group	I a -3 d	
Unit cell dimensions	a = 29.2699(9) Å	α = 90°
	b = 29.2699(9) Å	β = 90°
	c = 29.2699(9) Å	γ = 90°
Volume	25076.(2) Å ³	
Z	8	
Density (calculated)	1.359 g/cm ³	
Absorption coefficient	0.530 mm ⁻¹ mm ⁻¹	
F(000)	10704	
Theta range for data collection	1.70 to 30.02°	
Index ranges	-24 ≤ h ≤ 39, -41 ≤ k ≤ 20, -40 ≤ l ≤ 38	
Reflections collected	3064	
Data / restraints / parameters	3064 / 3 / 137	
Goodness-of-fit on F2	1.074	
Final R indices	R1 = 0.0885, wR2 = 0.2272	
all data	R1 = 0.1526, wR2 = 0.2565	
Largest diff. peak and hole	1.111 and -0.639 eÅ ⁻³	

4,11,18,25-Tetracyanomethyl-3,5,7,10,12,14,17,19,21,24,26,28-dodecamethyl[1.1.1]metacyclophan (L9) with silver nitrate (metallamacrocycle)

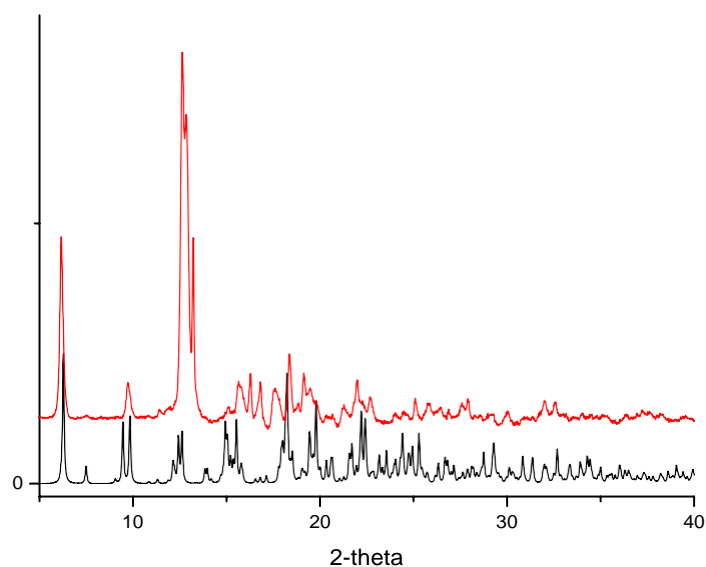


In a crystallization tube (diameter 4 mm , height 15 cm), a solution of **L9** (5 mg, 7.3×10^{-3} mmol) in CHCl₃ (1 mL) was layered with a CHCl₃/MeOH (1/1) mixture (1 mL). A solution of AgNO₃ (5 mg, 29.2×10^{-3} mmol) in MeOH (1 mL) was carefully added. Upon slow diffusion at room temperature and in the dark, colourless crystals suitable for X-ray diffraction studies were obtained after several days.

Formula: {C₉₆H₁₀₄Ag₂N₁₀O₆ •(6CHCl₃)} *i.e.* [L9₂-(AgNO₃)₂ • 6CHCl₃].

EA for C₁₀₂H₁₁₀Ag₂Cl₁₈N₁₀O₆: C, 50.5 %; H, 4.57 %; N, 5.77 %; found: C, 50.62%; H, 4.52 %; N, 5.74 %;

XRPD diagram:



Comparison of the simulated (a) and recorded (b) PXRD patterns for {L9₂- Ag(NO₃)₂}

The discrepancy between the simulated pattern using the single crystal data and recorded diagram demonstrates a good match.

Crystallographic data:

Formula:	{C ₉₆ H ₁₀₄ Ag ₂ N ₁₀ O ₆ •(6CHCl ₃)}	
Formula weight	2425.83 g/mol	
Temperature	173(2) K	
Wavelength	0.71073 Å	
Crystal size	0.050 x 0.060 x 0.060 mm	
Crystal system	triclinic	
Space group	P -1	
Unit cell dimensions	a = 12.7017(9) Å	α = 73.798(3)°
	b = 14.8810(9) Å	β = 69.159(3)°
	c = 15.5594(10) Å	γ = 86.320(4)°
Volume	2637.3(3) Å ³	
Z	1	
Density (calculated)	1.527 g/cm ³	
Absorption coefficient	0.886 mm ⁻¹	
F(000)	1240	
Theta range for data collection	1.46 to 30.35°	
Index ranges	-17<=h<=17, -18<=k<=20, -21<=l<=21	
Reflections collected	78535	
Max. and min. transmission	0.9610 and 0.9410	
Data / restraints / parameters	14260 / 0 / 634	
Goodness-of-fit on F ²	1.020	
Final R indices	1627 data; I>2σ(I) R1 = 0.0706, wR2 = 0.2030	
all data	R1 = 0.1221, wR2 = 0.2340	
Largest diff. peak and hole	2.351 and -1.499 eÅ ⁻³	

**DLS and UV-vis spectroscopy
methods for investigations of ligand
chelating properties and the nature of
forming aggregates.**

I Dynamic light scattering (DLS)

I.1 general information

The method of dynamic light scattering attracts an increasing number of researchers in various fields of science, such as supramolecular, analytical, crystal chemistry, organic, physical and purely preparative synthetic chemistry, physics, as well as studies related to optics etc.

The advantages of this method are mainly the ability to accurately determine the particle size with the aid of an optical device (Figure 1), capable of detecting Brownian motion of particles and their after irradiation with the light (laser device).

With the help of this method, complex compounds, gels, fluids and liquid crystals and other compounds capable to aggregate or form micelles and similar polymeric structures are studied.

In our case, DLS is a particularly useful predictive method since, before engaging in the design and synthesis of crystalline structures, it is quite useful to try to predict the possibility or impossibility of forming aggregates in different supramolecular systems. An important characteristic of this analytical method is the capacity to measure particles **as they exist in solution**. That is, in application to our work, DLS can be described as a method of predicting the ways of self-assembly of supramolecular structures.

The disadvantage of this method can be considered the effect of the presence of any debris in the test solution, so all solvents must be pre-cleaned, and mixtures of solutes must be passed through a special disposable fine-pored filter to avoid contamination of the sample.

Despite the fact that this method has a wide practical application and is a rather fast and convenient analytical method, analyzing the results does not always seem a simple possibility. But this fact does not detract from its usefulness for scientific and practical research, as far as DLS is highly sensitive to aggregation.

I 2. Principle of work

The use of DLS is based on the presence of Brownian motion of nanoparticles in a solvent which are continuously moving along the preset volume. Their distribution occurs in different ways, depending on the size they are. Thus, the influence of the laser light on Brownian motion opens up an opportunities to mathematically analyze the particle size

distribution by the deviation of a light beam by a certain angle (angle θ in Figure 72).

For this purpose, an indicator sensitive to light scattering installed in the device, which provides a signal that captures the real-time correlator, and an initial graph of the correlogram of the particle motion is constructed. After, the mathematical algorithms (by Correlator) are used to determine the real size of aggregates, following from an experimental correlogram.

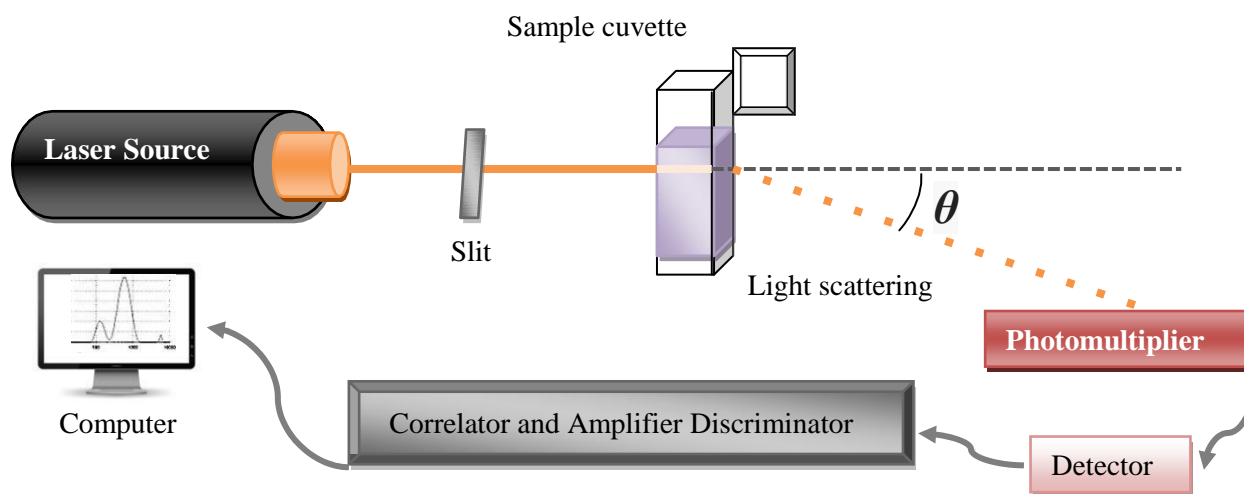


Figure 72: Brief schematic representation of DLS optics.

I 3. Procedure

The source of laser radiation is a He-Ne gas laser with a power of 10 mW and a wavelength of 633 nm. The signals are analyzed by a single-board multi-channel correlator coupled to an IBM PC by a shared computer. The hydrodynamic diameter of the particles is determined by dynamic light scattering. Samples are taken at room temperature 25 ° C at a concentration varying from 0.04 mM for **L4**, and 0.08-25.6 Mm to Mn(OAc), 0.4 mM for **L5** and 0.08-25.6 Mm to Mn(NO₃)₂. All measurements were carried out in DMSO.

II UV-vis titration method for stoichiometry determination

II 1. General information and principle

The second most common method for supramolecular titration experiment is probably UV-Vis spectroscopy. With the right chromophore, host concentration in a in very low concentrations (until 10⁻⁷ M) can be applied. Measuring device supplied with correlator which detects the signal intensity to concentration (Figure 73). This analytical method

requires a colored solution (the presence of chromoforic molecules in measuring solution). According to the basic law of light absorption, the graphical dependence $A = (C)$ is mathematically expressed by a straight line passing through the origin, where A is the light absorption, and C is the concentration. This relationship is called the basic law of light absorption or Lambert-Beer. Under the basic law of light absorption, the optical density of the solution is directly proportional to the molar coefficient of light absorption, the concentration of the absorbing substance, and the thickness of the solution layer.

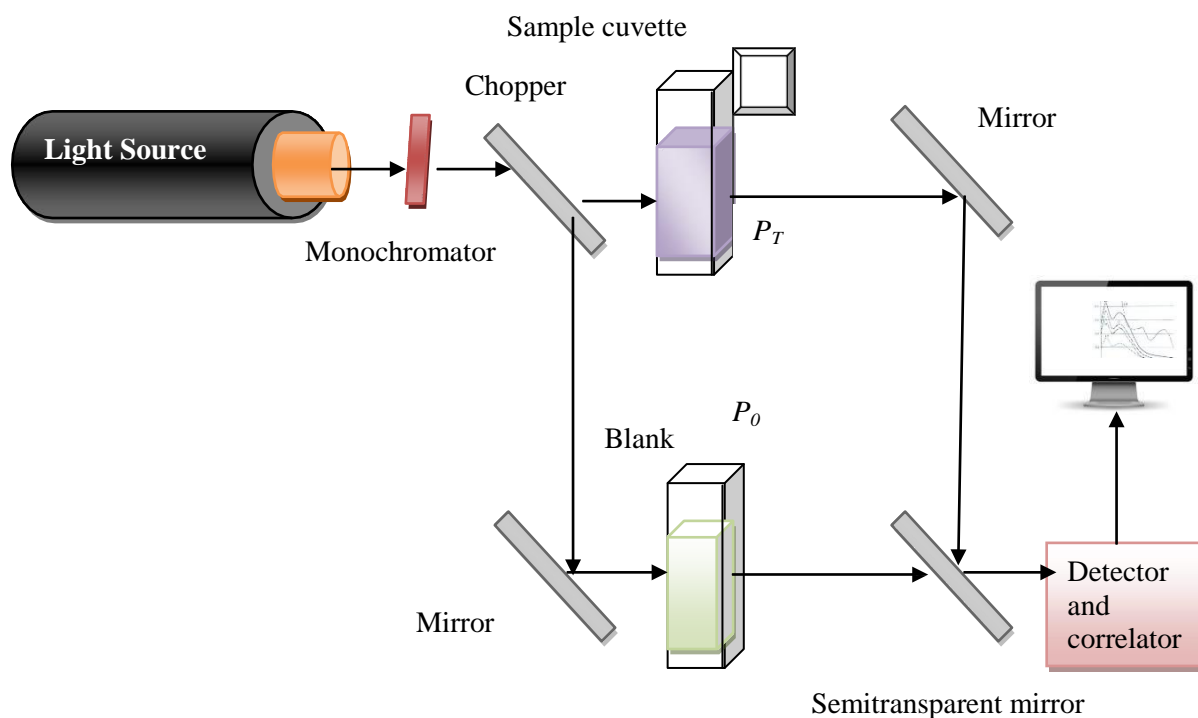


Figure 73: Brief schematic representation of UV-vis optics.

II 2. The procedure

UV-visible spectra were recorded on a spectrometer UV-vis spectrophotometer SHIMADZU UV-2600 at Room temperature. The results were processed using the UVProbe software. A 1 cm cuvette was used. The measurements were carried out at 25 ° C. The working concentration was 0.04 mM. A quartz cell of 0.5 cm path length was used for all measurements. All measurements were carried out in DMSO. The concentration of the ligands was constant, the concentration of the metal was changed.

III Picrate extraction for determination of complexing ability

- UV spectra were recorded on a UV-VIS Spectrometer "Lambda 35" Perkin Elmer.
- The salts of $\text{Cu}(\text{NO}_3)_2 \cdot 6\text{H}_2\text{O}$, $\text{Mn}(\text{NO}_3)_2 \cdot 4\text{H}_2\text{O}$, $\text{Ni}(\text{NO}_3)_2 \cdot 6\text{H}_2\text{O}$, $\text{Co}(\text{NO}_3)_2 \cdot 6\text{H}_2\text{O}$, $\text{Dy}(\text{NO}_3)_3 \cdot 5\text{H}_2\text{O}$, $\text{Pr}(\text{NO}_3)_3 \cdot 6\text{H}_2\text{O}$, $\text{Eu}(\text{NO}_3)_3 \cdot 6\text{H}_2\text{O}$, $\text{Gd}(\text{NO}_3)_3 \cdot 6\text{H}_2\text{O}$, $\text{Er}(\text{NO}_3)_3 \cdot 5\text{H}_2\text{O}$, $\text{Tb}(\text{OTf})_3$, $\text{Er}(\text{NO}_3)_3 \cdot 5\text{H}_2\text{O}$, $\text{Yb}(\text{NO}_3)_3 \cdot 5\text{H}_2\text{O}$ (Aldrich), picric acid brand (HPic). The methylene chloride was purified by the standard method.⁵
- Picrates of transition metals ($C(\text{M}(\text{Pic})_2) = 1 \cdot 10^{-4} \text{ M}$) were obtained by mixing aqueous solutions of picric acid ($C(\text{PicH}) = 1 \cdot 10^{-3} \text{ M}$), the salt of the corresponding metal ($C(\text{M}(\text{NO}_3)_2 \cdot n\text{H}_2\text{O}) = 5 \cdot 10^{-4} \text{ M}$) (pre-titrated with 0.05 M EDTA solution) and Tris buffer ($C = 0.05 \text{ M}$, $\text{pH} = 5.8$). "Idle experiments" were also conducted to test the possibility the transition of the picrate in the absence of metacyclophane, and also the ligand itself into the aqueous phase. The lanthanide picrates ($C(\text{M}(\text{Pic})_3) = 1 \cdot 10^{-5} \text{ M}$) were obtained by mixing aqueous solutions of picric acid ($C(\text{PicH}) = 6 \cdot 4 \text{ M}$), nitrate corresponding about the metal ($C(\text{M}(\text{NO}_3)_3 \cdot n\text{H}_2\text{O}) = 2 \cdot 10^{-4} \text{ M}$) (pre-titrated with 0.05 M EDTA solution) and Tris buffer ($C = 0.05 \text{ M}$, $\text{pH} = 5.8$). "blank experiments" were conducted to verify the possibility of a picrate transition in the absence of metacyclophane, and also of the ligand itself in the aqueous phase.
- Aqueous solutions of picrates (5 ml) and 5 ml of the solution of the test compound in methylene chloride were mixed in a closed flask with an IKA-WERKE RO 15 power magnetic stirrer for 30 minutes at room temperature (20° C). The optical densities A_i and A_0 of the aqueous phase before and after extraction were measured in the wavelength range 300-500 nm with a maximum at 355.67-365.42 nm. The extraction percentage (E%) was calculated by the formula $E\% = 100 \cdot (A_0 - A_i) / A_0$.

⁵ A. Weisberger, E. Proskauer, J. Riddick, E. Tups. Organic solvents, 520 (1958)

Synthèse de nouveaux ligands moléculaires à base de [1111] metacyclophane pour la formation de réseaux de coordination moléculaires

Résumé

En termes de chimie supramoléculaire et de tectonique moléculaire, les métacyclophanes [1111] sont des composés attractifs pour la préparation et l'étude de réseaux moléculaires, car la particularité de ces composés est la stabilité exceptionnelle de la conformation l'encombrement stérique entre les groupes ortho-méthyliques des cycles aryles. Un tel type rigide d'échafaudage moléculaire aussi bien avec la présence de sites de liaison de terminaux est considéré comme un bloc de construction moléculaire très approprié pour la formation de différents types de réseaux moléculaires en utilisant principalement la coordination et la H-bonding. Through ce travail, nous avons étudié le rôle de la nature de la coordination des sites greffés sur le squelette métacyclophane macrocyclique afin d'améliorer leur capacité à former des réseaux de coordination dans la phase cristalline et les systèmes supramoléculaires en solution, une série de nouvelles [1111] métacyclophanes ont été synthétisés et caractérisés en solution et à l'état solide. Leur propension à lier différents cations métalliques dans la phase cristalline ainsi que des complexes en solution ont été étudiés.

Mots-clés: Chimie supramoléculaire, liaison de coordination

Abstract

In terms of supramolecular chemistry and molecular tectonics, [1111]metacyclophanes are attractive compounds for the preparation and study of molecular networks since the particular feature of these compounds is determined by exceptional stability of the 1,3-Alternate conformation of their molecular platform due to the steric hindrance between the ortho-methyl groups of aryl rings. Such rigid type of molecular scaffold both with presence of terminal binding sites is considered as a very suitable molecular building block for formation of different type molecular networks using primarily coordination and H-bonding. Through this work we investigated the role of the nature of the coordinating sites grafted on the metacyclophane macrocyclic backbone in order to enhance their ability to form coordination networks in the crystalline phase and the supramolecular systems in solution, a series of new [1111]metacyclophanes have been synthesized and characterized in solution and in the solid state. Their propensity to bind different metal cations in the crystalline phase as well as complexes in solution have been studied.

Keywords: Supramolecular chemistry, coordination bond.....